AN *ab initio* MOLECULAR ORBITAL STUDY OF SOME BINARY COMPLEXES OF WATER

By

Tankiso Michael Tshehla

A Thesis Submitted to the Faculty of Science, University of Natal, in partial Fulfilment of the Requirements for the degree of Doctor of Philosophy

Durban 1996

Foreword

The research reported in this thesis was carried out at the University of Natal. A portion of the results has been published as "*Ab initio* Molecular Orbital Calculations of the Infrared Spectra of Interacting Water Molecules. 5. Structures, Energetics and Mulliken Charges of the Complexes of Water with Hydrogen Cyanide, Acetylene and Cyanogen" in Bull. Polish Acad. Sci. Chem. **42**, 397-412 (1994) and "*Ab initio* Molecular Orbital Calculations of the Infrared Spectra of Interacting Water Molecules. Part 6. The Infrared Spectra of the Complexes of Water with Hydrogen Cyanide, Acetylene and Cyanogen" in S. Afr. J. Chem. **48**, 127-134 (1995).

Part of the work was presented at the 32nd SACI Convention held at Midrand in January 1994; part at the Sixth International Chemistry Conference in Africa held at Accra, Ghana, August 1995; part at the conference on Fundamentals of Molecular Modelling held at Kruger National Park in August 1995; part at the 33rd SACI Convention held at Cape Town in January 1996 and part at the Fourth World Congress of Theoretically Oriented Chemists (WATOC'96) held at Jerusalem, Israel in July 1996.

Abstract of the Thesis

Ab initio molecular orbital theory has been successful in predicting the stabilities of many weak complexes; typical of these are the complexes formed between water and various small molecules. To account for the correlation effect, Møller-Plesset perturbation theory truncated at the second order level was employed. In order to account for the hydrogen bonding, the 6-31G** basis set was used. The geometry optimisations of the complexes were carried out using the Gaussian-92 suite of programs installed on a Hewlett-Packard 720 computer operating under UNIX.

The interaction energies of the complexes were subjected to further analysis by applying the Morokuma decomposition scheme. The electrostatic interaction component accounts for over 40% of the total stabilisation energy in all the typical hydrogen bonded complexes. Gas phase enthalpies were computed and compared with the experimental values of similar systems. For the systems studied here, the prediction is that all complexes are stable at 25° C.

A second program, Vibra, was used for carrying out a normal coordinate analysis. A third computer program for the graphical representation of molecular and crystallographic models, Schakal-92, was employed to illustrate the predicted equilibrium geometries and the fundamental vibrational modes.

The predicted geometries, interaction energies, charge redistributions, vibrational wavenumbers, infrared intensities and force constants are listed and compared with those in the literature, where applicable. Correlations between the various predicted properties show some interesting chemistry.

Declaration

I declare that this is my own work, unaided. It is being submitted for the degree of Doctor of Philosophy in the University of Natal, Durban. It has not been submitted before for any degree or examination in any other University.

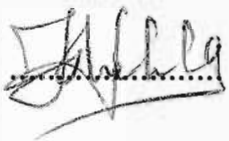

T.M. Tshehla

20:12:1996

Durban, South Africa

Table of Contents

List of Tables

List of Figures

Acknowledgements

I wish to express my sincere thanks to Professor T.A. Ford, under whose supervision this project was carried out, for his guidance and encouragement and for many enlightening discussions during the course of the work. I also wish to thank Dr. M.R. Peterson of the University of Toronto, Canada, for making the Monstergauss program available and for useful communications on the technicalities of the program.

I am grateful to Dr. D. Steele, of Royal Holloway and Bedford New College, University of London, for making available the Vibra program, and many useful communications. Thanks to Messrs B.C. Bricknell and M.G. Govender for their positive criticisms during our discussion sessions and the staff of the Computer Services Division for their assistance.

My sincere gratitude goes to FRD for the funding of the project, to the University of Natal for a graduate assistantship and to the Government of Lesotho for funding my attendance of the ICCA and WATOC'96 conferences and to the National University of Lesotho for granting me study leave.

Last, but not least, I wish to thank my children for their character and understanding, and Miss K. Majara for her support and encouragement. Many thanks go to my father who never stopped supporting me emotionally and who showed me the way.

CHAPTER 1

1.1 Purpose of the project

The aim of this project was to gain some information on the interaction of water with some selected small molecules by means of an ab initio theoretical study. Although a large number of both experimental and theoretical studies has been done on some of the water complexes,[1-7] there is no structured systematic comprehensive study of water complexes as yet.

Water constitutes over 60% of human body mass, and the helix structure of DNA is known to be held together by hydrogen bonds. Intermolecular interaction of the hydrogen bonding type is encountered in catalysis, enzyme activity, dyeing and adsorption.[8a] Because of the importance of the water molecule and its widespread existence in nature, there is a need to study its interactions. To further simplify such a study, only binary complexes are considered here. Since the existence of binary complexes would be very rare in nature, it would appear therefore that a study concentrating on binary complexes only has no real practical parallel. However beside the simplification of such a study as mentioned above, the limitation of the scope of the study to binary systems makes the use of expensive ab initio methods feasible.

Comparison of the computational results for the binary complexes with experimental spectroscopic data shows good correlations. The importance of such correlations is a confirmation of the reliability of the computational techniques employed and inspires confidence in the predictive capabilities of such techniques.

1.2 Structure of the Thesis

The report is divided into parts 1, 2 and 3. Part 1, consisting of chapters 1 to 5, outlines the purpose of the study, the theoretical basis of the project, the computer programs used and the reviews. Part 2, the theme of the thesis, contains chapters 6 to 9 with the results of the research listed and discussed for each group of complexes. Each of these chapters discusses geometrical, energetic, electronic and vibrational properties respectively.

Part 3, which is the last chapter, chapter 10, draws all the results together and discusses general trends among all the complexes. Parallels between the studied complexes and similar studies are made and conclusions are drawn.

1.3 Review of Intermolecular Interactions

As long ago as 1902 Werner revealed that ammonia and water form an adduct[9a]. Pfeiffer in 1914 noted that carboxylic acids dimerise.[9a] In 1919 Huggins studied the hydrogen bifluoride anion, and Latimer and Rodebush in 1920 made the observation that a hydrogen atom held between two octets of electrons forms a weak bond.[9a] They referred to this weak bond as the hydrogen bond. The stage was set by these investigators for the study of the hydrogen bonding problem.

Evidence was required to support the concept of the hydrogen bond. Neutron and X-ray scattering showed that the bridging hydrogen atom is situated along the lone-pair orbital axis of the electron donor (ED). Infrared spectroscopy showed that the stretching frequency of the A-H bond decreases while its intensity increases in the hydrogen bonded complex, indicating an interaction of A-H in the complex. Ultraviolet and visible spectroscopy show a red shift for

the proton donors and blue shift for the proton acceptors.[10a] Nuclear magnetic resonance spectroscopy shows a downfield shift of the bonded proton on complexation.[10b]

While these techniques support the idea of hydrogen bonding, specific interacting sites are hard to probe. Interactions between two molecules, which would give more information on the activities of active sites in most cases are obscured because of the cluster effect. To aid in explaining and understanding this phenomenon, some chemical models have been developed, namely molecular mechanics and electronic structure theory. Both models give basically the same type of information.

The choice of a particular model depends on what type of information and what degree of accuracy one requires within the time constraints and computational resources available. A brief survey of information obtainable from molecular mechanics will be made and compared with that which is obtainable from electronic structure theory. Such a comparison is necessary for the validation of the method chosen in any study.

1.4 Theoretical Model

1.4.1 Molecular Mechanics

Molecular mechanics (MM) models make use of the laws of classical physics to predict the structures and properties of molecules. Some examples of such models are found in applications programs such as HyperChem, Quanta, Sybyl and Alchemy.[11] Molecular mechanics does not treat the electrons in the molecule. The calculations are performed based on nuclear interactions.

Electronic effects are included in the force fields through parametrisation. Because of these approximations, MM methods are relatively inexpensive and can handle far larger molecular systems than can the electronic structure models.

The MM methods are, however, limited to problems which do not require knowledge of electronic effects. There is a lack of generalisation with the MM methods as well.

1.4.2 Electronic Structure Methods

Here the laws of quantum mechanics are used. A solution to the Schrödinger equation is sought. Because of the mathematical rigour involved, the models work well for small molecules. Both semi-empirical and ab initio methods are classified under electronic structure theory models. The semi-empirical methods solve an approximate form of the Schrödinger equation, provided appropriate parameters are available for the type of chemical system in question.

Ab initio methods, unlike semi-empirical and MM methods, use no parameters in their computations. The calculations are based solely on the laws of quantum mechanics.

The ab initio methods provide high quality quantitative predictions for a broad range of molecules. They are more general than MM methods. Although modern computational developments have increased the size of the systems manageable by ab initio methods, they are still very expensive and hence macromolecules like DNA cannot be subjected to ab initio treatment as yet.

1.5 Choice of the Systems

The groupings are based on the presence of isoelectronic molecules, the presence of a common functional group and structural similarities, e.g. HCN and C_2H_2 are isoelectronic but C_2N_2 is not, however all three are linear molecules, therefore they are grouped together. Acetonitrile is placed group 1, due to the fact that it contains a nitrile group, in common with HCN and C_2N_2, and like the rest of the molecules in this group, the CH_3CN molecule contains a triple bond. In Group 2, all three partner molecules are isoelectronic. Group 3 consists of partner molecules containing the carbonyl functional group, while Group 4 contains carboxylic acids and esters.

Table 1.1 shows that most of the compounds forming complexes with the water molecule contain either oxygen or nitrogen atoms which have lone pairs of electrons. In the few cases where there is no oxygen or nitrogen atom, as in ethylene and acetylene, the availability of π-orbitals should be responsible for the interaction.

It is the presence of either lone pairs or π-orbitals, coupled with the limitations on computer resources, which influenced the choice of the systems to be studied.

Table 1.1. The List of the Complexes Studied Grouped by Common Features

Group	Complexes	Characteristics
1	$NCH\text{-}OH_2$ $HCCH\text{-}OH_2$ $NCCN\text{-}OH_2$ $CH_3CN\text{-}HOH$	either a CN or CH group and a triple bond
2	$H_2CO\text{-}HOH$ $H_2CNH\text{-}HOH$ $C_2H_4\text{-}HOH$	isoelectronic components
3	$CH_3CHO\text{-}HOH$ $(CH_3)_2CO\text{-}HOH$	carbonyl group
4	$HCOOH\text{-}HOH$ $CH_3COOH\text{-}HOH$ $HCOOCH_3\text{-}HOH$ $CH_3COOCH_3\text{-}HOH$	carboxylic acids and esters

CHAPTER 2

This chapter gives an overview of the theory underlying ab initio methods. The Schrödinger equation is expanded here in terms of the Born-Oppenheimer approximation; the conversion to atomic units is outlined. Self consistent field (SCF) theory is summarised and the Hartree-Fock (HF) equation defined. The limitations of HF theory are cited and multiple determinant wavefunctions are discussed with the view of introducing higher levels of theory. Pertubation theory to second order level is discussed.

2.1 Theoretical Basis

An attempt to understand the interacting systems invariably calls for the use of the Schrödinger wave equation[12] which provides a quantum mechanical description of molecular properties.
The Schrödinger equation is

$$\hat{H}\psi = E\psi \tag{2.1}$$

where $\hat{H}$ is the Hamiltonian operator, E is the energy of the system and ψ is the wavefunction. Ab initio methods are a set of computational techniques used to find a solution to equation (2.1) as accurately as possible. A brief overview of quantum mechanics will be outlined in order that the importance of equation (2.1) can be appreciated.

2.2 The Born-Oppenheimer Approximation

Electrons are so light compared with nuclei, that the nuclei can be considered

to be stationary while the electrons are moving around rapidly. This is a statement of the Born-Oppenheimer approximation, which allows for the motion of electrons and nuclei to be separated into individual equations.[13] Equation (2.1) can thus be expanded fully into:

$$(T_n(R) + T_e(r) + V_{nn}(R) + V_{ne}(R,r) + V_{ee}(r))\psi(R,r) = E_{tot}\psi(R,r) .$$

(2.2)

$T_n(R)$ and $T_e(r)$ are kinetic energy operators for the nuclei at the R^{th} position and electrons at the r^{th} position with respect to the other nuclei. The subscripts n and e denote the nuclear and electronic motions respectively. The terms $V_{nn}(R)$, $V_{ne}(R,r)$ and $V_{ee}(r)$ are potential operators, describing nuclear-nuclear repulsion, nuclear-electron attraction and electron-electron repulsion.[14a]

Since the motions of the electrons and nuclei are separable, a total wavefunction can be written as a product of the electronic wavefunction $\Phi(R,r)$ and the nuclear wavefunction $\chi(R)$:

$$\psi(R,r) = \Phi(R,r)\chi(R) .$$

(2.3)

The electronic wavefunction $\Phi(R,r)$ depends on the nuclear configuration R and is a solution of the electronic Schrödinger equation

$$(T_e(r) + V_{ne}(R,r) + V_{ee}(r))\Phi(R,r) = E(R)\Phi(R,r) .$$

(2.4)

The nuclear wavefunction $\chi(R)$ is the solution to the nuclear Schrödinger equation

$$(T_n(R) + V_{nn}(R) + E(R))\chi(R) = E_{tot}\chi(R) \ .$$

(2.5)

The variations of the nuclear potential energy, V_{nn}, and of the electronic energy, E, with R, derived from the solution of the Schrödinger equation, constitute what is often referred to as a potential energy surface (PES). The solution of the electronic Schrödinger equation is integral to the use of quantum mechanics for the elucidation of chemical properties. Equation (2.4) can be written more explicitly as:

$$\left(\sum_{i=1}^{n} -\frac{h^2}{8\pi^2 m_e}\nabla_i^2 - \sum_{i=1}^{n}\sum_{\alpha=1}^{N}\frac{Z_\alpha e^2}{4\pi\epsilon_o r_{i\alpha}} + \sum_{i}\sum_{<j}\frac{e^2}{4\pi\epsilon_o r_{ij}}\right)\Phi(R,r) = E(R)\,\Phi(R,r)$$

(2.6)

where

$$\nabla_i^2 = \left(\frac{\partial^2}{\partial x_i^2} + \frac{\partial^2}{\partial y_i^2} + \frac{\partial^2}{\partial z_i^2}\right)$$

and i and α are indices for the electrons and nuclei respectively, m_e is the electron mass, Z_α is the nuclear charge, e is the electron charge, h is Planck's constant, $r_{i\alpha}$ is the distance of the i^{th} electron from nucleus α and r_{ij} is the distance between the i^{th} and j^{th} electrons. The first term of equation (2.6) describes the electronic kinetic energy, while the second term is the nuclear-electron interaction. The third term is the electron-electron repulsion interaction. The exact solution of equation (2.6) is possible only for a one-electron system such as H_2^+. It follows then that some approximations need to be applied in

order to achieve acceptable solutions to equation (2.6). One such approximation is the SCF method.

In discussing the electronic properties, the units in equation (2.6) are often changed to more physically meaningful ones. These are defined as;

$$a_o = \frac{h^2 \epsilon_o}{\pi m_e e^2} \qquad bohr$$
$$E_h = \frac{e^2}{4\pi\epsilon_o a_o} \qquad hartree \tag{2.7}$$

where ϵ_o is the permittivity of free space, a_o is the Bohr radius and e is the electron charge.

Applying equation (2.7) to equation (2.6), an equation which now measures energy in hartrees and atomic separations in bohrs (atomic units, a.u.) is shown below[15,16]

$$\left(\sum_{i=1}^{n} -\frac{1}{2}\nabla_i^2 - \sum_{i=1}^{n}\sum_{\alpha=1}^{N} \frac{Z_\alpha}{r_{i\alpha}} + \sum_{i}\sum_{<j} \frac{1}{r_{ij}} \right) \Phi(R,r) = E(R)\,\Phi(R,r) \,. \tag{2.8}$$

2.3 The Self Consistent Field Method

The theme of the SCF approach is the view that an electron is moving in the average field of the other particles and its properties are due to perturbations of the other particles in equilibrium. The molecular orbital (MO) theory is used to explain electronic structures. The MO theory generally gives accurate molecular properties near the equilibrium configurations. Here a wavefunction appropriate to an independent particle model is used, and the third term in equation (2.8) is omitted, so that equation (2.8) becomes:

$$\left(\sum_i \hat{h}(i)\right)\Phi(R, r_1, \ldots, r_n) = E(R)\,\Phi(R, r_1, \ldots, r_n)$$

(2.9)

where $\hat{h}(i)$ is the one-electron operator given by

$$\hat{h}(i) = -\frac{1}{2}\nabla_i^2 - \sum_{\alpha=1}^{N} \frac{Z_\alpha}{r_{i\alpha}} .$$

(2.10)

Equation (2.10) can be separated into n one-electron equations of the form:

$$\hat{h}(i)\,\phi_i(r_i) = e_i\phi_i(r_i) .$$

(2.11)

For simplification, the electron dependence on the nuclear motion parameter R has been omitted from the one-electron functions $\phi_i(r_i)$. The one-electron wavefunctions are referred to as orbitals and the e_i as orbital energies. One electron is indistinguishable from the other, hence a total wavefunction must display both spatial and spin properties. Electrons have a spin property of magnitude $(1/2)(h/2\pi)$ or $-(1/2)(h/2\pi)$. If one lets $\alpha=(1/2)(h/2\pi)$ and $\beta=-(1/2)(h/2\pi)$ respectively, then equation (2.11) must include the spin property, as shown by equation (2.12):

$$\Phi(r_1, \ldots r_n) = \phi_1(r_1)\,\alpha(1)\,\phi_1(r_2)\,\beta(2)\ldots\phi_{\frac{n}{2}}(r_{n-1})\,\alpha(n-1)\,\phi_{\frac{n}{2}}(r_n)\,\beta(n)$$

(2.12)

for a closed shell system (with an even number of electrons). One other property of electrons is that they must be antisymmetric with respect to exchange.[17] This is a statement of Pauli's principle. A total wavefunction which has spin, antisymmetry and indistinguishability properties can be written as a Slater

determinant, as in equation (2.13) below;

$$\Phi(R,r)=\frac{1}{\sqrt{n!}}\begin{vmatrix} \phi_1(r_1)\alpha & \phi_1(r_1)\beta \ldots \phi_{\frac{n}{2}}(r_1)\beta \\ \phi_1(r_2)\alpha & \phi_1(r_2)\beta \ldots \phi_{\frac{n}{2}}(r_2)\beta \\ \cdot & \cdot & \cdot \\ \cdot & \cdot & \cdot \\ \cdot & \cdot & \cdot \\ \phi_1(r_n)\alpha & \phi_1(r_n)\beta \ldots \phi_{\frac{n}{2}}(r_n)\beta \end{vmatrix} \qquad (2.13)$$

where $1/\sqrt{n!}$ is the normalisation factor.

2.3.1 The Variational Principle

In the derivation of equation (2.13), the interelectronic interaction was neglected, a contribution which is very important to the evaluation of potential energy. To circumvent this shortfall, the variation method is used to calculate the best many-electron wavefunction of the form of equation (2.13), by minimising the electronic energy E given by the expectation value

$$E=\frac{\int \Phi^* \hat{H} \Phi \, d\tau}{\int \Phi^* \Phi \, d\tau} \qquad (2.14)$$

where ϕ^* is the complex conjugate of the wavefunction ϕ and $\hat{H}$ is the Hamiltonian operator defined in equation (2.8), and

$$\int \phi_i \phi_j \, d\tau = \delta_{ij} \quad (=1 \text{ if } i=j)(=0 \text{ if } i \neq j) \qquad (2.15)$$

the integration is over all space for the real electronic wavefunction Φ.

2.3.2 The Roothaan-Hall Equations

For the closed-shell case of n/2 doubly occupied orbitals, the energy, E, is:

$$E = \sum_{i=1}^{n/2} 2h_{ii} + \sum_{i=1}^{n/2}\sum_{j=1}^{n/2} (2J_{ij} - K_{ij}) \tag{2.16}$$

where

$$h_{ii} = \int \phi_i(1) \left(-\frac{1}{2}\nabla_i^2 - \sum_{\alpha=1}^{N} \frac{Z_\alpha}{r_{1\alpha}} \right) \phi_i(1)\, d\tau_1 \tag{2.17}$$

$$J_{ij} = \int \phi_i(1)\phi_j(2) \frac{1}{r_{12}} \phi_i(1)\phi_j(2)\, d\tau_{12} \tag{2.18}$$

$$K_{ij} = \int \phi_i(1)\phi_j(2) \frac{1}{r_{12}} \phi_i(2)\phi_j(1)\, d\tau_{12}. \tag{2.19}$$

Equation (2.18) defines the Coulomb integral, which represents a classical electrostatic interaction between electron densities $\{\phi_i(1)\}^2$ and $\{\phi_j(2)\}^2$ due to the occupancies of orbitals ϕ_i and ϕ_j respectively. Equation (2.19) defines the exchange integral and has no classical counterpart. The energy, E, must be minimised with the condition that the orbitals remain mutually orthogonal; this is a basis of the HF equations, namely:

$$\hat{F}_i(1)\phi_i(1) = \varepsilon_i\phi_i(1) \tag{2.20}$$

where ε_i is the energy of an orbital i and $\hat{F}_i$ is the Fock operator, which is defined as

$$\hat{F}_i(1) = \hat{h}(1) + \sum_j \left(2\hat{J}_j(1) - \hat{K}_j(1)\right) \tag{2.21}$$

where

$$\hat{h}(1) = -\frac{1}{2}\nabla_i^2 - \sum_{\alpha=1}^{N} \frac{Z_\alpha}{r_{1\alpha}} \tag{2.22}$$

and $\hat{J}_j$ and $\hat{K}_j$ are the Coulombic and the exchange operators, similar to equations (2.18) and (2.19). The HF equations are coupled integral differential equations which can be solved iteratively. The second term in equation (2.21) represents the electrostatic field of an electron in orbital ϕ_i due to the electrons in all the other orbitals. The iteration is continued until the effective field remains unchanged (a convergence point is achieved) and hence the method is known as the self consistent field method.

Equation (2.13) is well suited for molecules which have spherical symmetry but not for molecules which lack such symmetry. The modification of equation (2.13) to suit non-spherical systems was done by Hall and Roothaan.[18,19] They expanded the orbitals ϕ_i as linear combinations of m basis functions;

$$\phi_i = \sum_{q=1}^{m} c_{iq}\chi_q$$

(2.23)

where c_i are the coefficients and χ_q are the basis functions. Equation (2.23) is a mathematical representation of the molecular orbital, more generally referred to as a basis. The function of a basis set is to predetermine the location of a particular electron in space. The HF equation then becomes:

$$\hat{F} \sum_q c_{iq}\chi_q = \varepsilon_i \sum_q c_{iq}\chi_q .$$

(2.24)

If equation (2.24) is multiplied on the left hand side by χ_p and integrated, then rearranged, it becomes

$$\sum_q c_{iq}(F_{pq} - S'_{pq}\varepsilon_i) = 0$$

(2.25)

where

$$F_{pq} = \int \chi_p \hat{F} \chi_q d\tau , \quad S'_{pq} = \int \chi_p \chi_q d\tau .$$

(2.26)

Equation (2.26) is analogous to the secular vibrational equation, the solution of which is well detailed by Wilson, Decius and Cross.[20] F_{pq} involves both J and K operators, which in turn depend on the orbitals ϕ_i. By substitution and rearrangement, equation (2.26) can be written as:

$$F_{pq} = h'_{pq} + \sum_j \sum_r \sum_s c_{jr} c_{js} [2(pq|rs) - (ps|rq)]$$

(2.27)

where $(pq|rs)$ is a two-electron integral over the basis functions. The coefficients of equation (2.27) give

$$R_{rs}=\sum_{j} c_{jr}c_{js},$$

the density matrix, which gives information about bond order and charge densities. Solution of equation (2.27) requires first of all the evaluation of two-electron integrals $(pq|rs)$ with respect to the basis set $\{\chi_p\}$. For m basis functions (equation (2.23)) there are m(m+1)/2 one-electron integrals and $m(m+1)(m^2+m+2)/8$ two-electron integrals.[14a] To handle this equation is a very expensive process in terms of central processing unit (cpu) time of the computer, which is one of the reasons why ab initio methods are still restricted to relatively small molecular systems.

HF theory works well for one-electron systems. If this were all, then the application of the theory would be very limited. The motion of one electron relative to the others is not accounted for. This is referred to as the correlation effect. To account for the correlation effect, some other multiple determinant wavefunctions were developed.

2.4 Post-Hartree-Fock Methods

HF theory fails to describe correctly the dissociation of a closed-shell system. This is due to the lack of inclusion of the correlation energy. Trying first one wavefunction and then another is quite an arbitrary approach; there is a need for a systematic theoretical chemical model which can be expected to account for the experimental observations.

The requirements for such a model are:

(a) the method should be well defined and applicable in a continuous manner to any arrangement of nuclei;

(b) the method should demand a reasonable computation time to allow for the investigation of systems of chemical interest;

(c) the method must be size consistent; and

(d) the calculated electronic energies must be variational.

A number of post-HF methods are perfect in principle but hard to achieve in practice. Three of these methods are: full configuration interaction (FCI), limited configuration interaction (LCI) and Møller-Plesset pertubation theory (MPPT). The basics of perturbation theory will be described and then Møller-Plesset theory will be incorporated since this is the level of theory used in this project. The other methods will be briefly described as well for completeness.

2.4.1 Full Configuration Interaction

In this method an attempt to mix all of the possible electronic states of a molecule which, according to quantum mechanical laws, have finite probability of mixing is made. This is the most complete method in the non-relatistivic approach to modelling; it is only constrained by basis set choice. It is, however, very expensive and practical only for very small molecular systems.

2.4.2 Limited Configuration Interaction

In LCI, use is made of FCI, with some cut-off limits to make the FCI of some practical use. Here only a limited set of substitutions is added to the HF configuration. Depending on the level of truncation, there are a number of LCI notations, namely :

(a) CIS (single addition substitution) where a single excitation to the HF determinant is applied;

(b) CISD, where double excitations as well as single ones are made; and

(c) CISDT, triple excitations in addition to single and double ones.

The flaw in these methods of LCI is that they lack size-consistency. Further improvements have been achieved by developing quadratic configuration interaction (QCI) which corrects the size-inconsistency flaw.[11b]

2.4.3 Perturbation Theory

If the Schrödinger equation (2.1) can be solved for a ground state with the Hamiltonian $\hat{H}^{(o)}$, energy $E^{(o)}_n$ and wavefunction $\psi^{(o)}_n$; then for a state which is slightly different from the ground state such an equation can be solved. If V' is such a small perturbation to the system described above that the wavefunction is converted into ψ_n, the system will move from the ground state to some state as a result of such a perturbation. Hence

$$\hat{H} = \hat{H}^0 + V' \tag{2.28}$$

where $\hat{H}$ is the total Hamiltonian and the remaining terms are as defined

above. The perturbed Schrödinger equation then becomes:

$$(\hat{H}^0+\lambda V')\,\psi_n=E_n\psi_n.$$

(2.29)

λ is a parameter measuring the degree of perturbation. The system is unperturbed when λ=0 and the perturbation is fully switched on when λ= 1. Both the wavefunction and energy depend on the parameter λ from equation (2.29), i.e.

$$\psi_n=\psi_n(\lambda, q)$$

$$E_n=E_n(\lambda)$$

(2.30)

where q indicates the spatial coordinates. The perturbation wavefunction ψ_n and energy E_n can be expressed in a Taylor series due to the fact that the total effect can be thought of as a sum of small perturbations. For the k^{th} such perturbation, the resulting wavefunction and energy can be expressed as

$$\psi_n=\psi_n^0+\lambda\psi_n^1+\lambda^2\psi_n^2+\ldots\lambda^k\psi_n^k$$

(2.31)

and the energy becomes

$$E_n=E_n^0+\lambda E_n^1+\lambda^2 E_n^2+\ldots+\lambda^k E_n^k.$$

(2.32)

The series (2.31) and (2.32) are assumed to converge, and due to the nature

of such a series, the higher order terms may, to a good approximation, be dropped without much loss of accuracy. Substituting equations (2.31) and (2.32) into equation (2.29), and collecting like powers of λ, the following expression can be written:

$$\hat{H}^0\psi_n^0+\lambda\,(\hat{H}\psi_n^0+\hat{H}^0\psi_n^1)+\lambda^2\,(\hat{H}^0\psi_n^2+\hat{H}\psi_n^1)+\ldots \quad = \quad E_n^0\psi_n^0+\lambda\,(E_n^1\psi_n^0+E_n^0\psi_n^1)+\lambda^2\,(E_n^2\psi_n^0+E_n^1\psi_n^1+E_n^0\psi_n^2)+\ldots$$

(2.33)

Equating the coefficients of λ^0 together, one can write:

$$\hat{H}^0\psi_n^0=E_n^0\psi_n^0.$$

(2.34)

This is the unperturbed ground state equation. The first order perturbation terms lead to:

$$V'\psi_n^0+\hat{H}^0\psi_n^1=E_n^1\psi_n^0+E_n^0\psi_n^1.$$

(2.35)

Rearrangement of equation (2.35) leads to:

$$(\hat{H}^0-E_n^0)\,\psi_n^1=(E_n^1-V')\,\psi_n^0$$

(2.36)

where $\hat{H}^0$ is a real Hamiltonian. Thus the eigenfunctions of unperturbed systems are a complete set of known functions, so that ψ_n^1 can be expanded in terms of

$$\psi_n^1 = \sum a_j \psi_j^0$$

(2.37)

where a_j is an expansion coefficient. Substituting equation (2.37) into equation (2.36), and multiplying by the complex conjugate wavefunction and integrating over all space leads to

$$\sum a_j (E_j^0 - E_n^0) \int \psi_m^{0*} \psi_j^0 d\tau = E_n^1 \int \psi_m^{0*} \psi_n^0 d\tau - \int^* \psi_n^0 \hat{H} \psi_n^0 d\tau .$$

(2.38)

For unperturbed wavefunctions, which are orthogonal,

$$\int \psi_m^{0*} \psi_j^0 d\tau = \delta_{ij} .$$

(2.39)

In the case of a degenerate state, m=j. Hence the first order correction to the energy becomes:

$$a_m (E_m^0 - E_n^0) = E_n^1 \delta_{ij} - \int \psi_m^{0*} V' \psi_n^0 d\tau$$

which can be expressed as

$$E_n^1 = \int \psi_n^0 V' \psi_n^0 d\tau .$$

(2.40)

Equation (2.40) states that the first order correction to the energy is obtained by averaging the perturbations V′ over the unperturbed wavefunction. Hence the overall correction up to the first order is

$E_n = E_n^0 + E_n^1$.

(2.41)

For a non-degenerate state, m≠n,

$$a_m = \frac{V'}{E_n^0 - E_m^0}$$

(2.42)

and the first order correction to the wavefunction then becomes

$$\psi_n = \psi_n^0 + \sum \frac{|V_{mn}|}{E_n^0 - E_m^0} \psi_m^0$$

(2.43)

so that the wavefunction corrected to the first order term is now:

$$\psi_n = \psi_n^0 + \psi_n^1.$$

(2.44)

To get the second order correction to the wavefunction a similar procedure is followed as above. The total energy corrected for the second order perturbation becomes

$$E_n = E_n^0 + V_{nn} + \sum \frac{|\psi_k^0 V_{nk}|^2}{E_n^0 - E_k^0}.$$

(2.45)

It is important to note that if Ψ_n^o is self-consistent, then there is no first order correction to the energy.

2.4.4 Many Body Perturbation Theory

In many body perturbation theory (MBPT),[14b] the unperturbed Hamiltonian is taken as a sum of Fock operators defined as in equation (2.24). The perturbation V′ is equal to

$$\hat{H}-\sum \hat{F}_j,$$

where j extends over all occupied molecular orbitals.

The HF energy is normally inclusive of first order corrections so that

$$E_{HF}=E_n^0+E_n^1.$$

(2.46)

For a double excitation, in which electrons from spin orbitals i and j are excited to spin orbitals a and b, the summation for such excitation can be written as

$$(ij|ab)=\int \psi_i(1)\,\psi_j(2)\,\frac{1}{r_{12}}\,\psi_a(1)\,\psi_b(2)\,d\tau - \int \psi_i(1)\,\psi_j(2)\,\frac{1}{r_{12}}\,\psi_b(1)\,\psi_a(2)\,d\tau.$$

(2.47)

Hence equation (2.47) becomes:

$$E_n^2=\frac{1}{4}\sum_{i}^{OCC}\sum_{<j}\sum_{a}^{VIRT}\sum_{<b}\frac{(ij|ab)\,(ab|ij)}{(\epsilon_i+\epsilon_j-\epsilon_a-\epsilon_b)}$$

(2.48)

The second order correction to the energy at this level is referred to as MP2 and is size consistent but not variational. The theory gives accurate results where the HF function , Φ_o, is the dominant contributor to the wavefunction. It is not accurate for the bond breaking cases, where a multi-reference configuration is required.[14b]

CHAPTER 3

Since the theme of this project is to investigate molecular interactions, a brief overview of such interactions is presented here. No attempt is made to derive the equations describing the molecular interactions, but they are logically cited to emphasise some of the important physical laws.

3.1 Molecular Interactions

The term "intermolecular interaction" has a broad meaning, implying two or more bodies acting on each other. It will be used here in a narrow sense to indicate the changes brought about when a water molecule comes into close proximity with another molecule without necessarily forming a chemical bond. Such changes are the subject of the project.

3.1.1 Hydrogen Bonding

Many of the complexes are hydrogen bonded; it is therefore necessary to give a conventional hydrogen bond definition as A-H...B, [10b] where B is any σ or π electron donor site and A is an element with electronegativity greater than that of hydrogen.

The degree of interaction is deduced from the magnitude of the interaction energy (stabilisation energy), the length of the association bond (in many instances a hydrogen bond, H...B), the magnitude of the dipole moment change, the wavenumber shifts, infrared intensity ratios, perturbations of the properties of the chemical bonds most closely associated with the interacting centres and the magnitude of the force constants associated with the interaction bond. It is

found that the strength of hydrogen bond depends on the acidity of the proton donor group, A-H, and on the ease with which group B donates electrons.[21,22] In systems which contain hydrogen bonds, typical interaction energies vary between about -8 and -63 kJ mol^{-1}.[23] The attraction is amplified if one of the sub-units is electrically charged, in which case the interaction energy can be as low as -140 kJ mol^{-1}.

3.1.2 Electron Donor-Acceptor Interaction

Although a brief definition of a hydrogen bond has been attempted, it is quite a limited one because the key players in any chemical interaction involve electron redistribution. The term "donation" corresponds to an overall reorganisation of electronic charge, including polarisation, exchange and charge transfer.[24] For donor-acceptor interactions to be important, the acceptor valence orbitals must be sufficiently low in energy and must protrude further into space than the corresponding core orbitals. This configuration allows the n-σ^* interaction to overcome the n-σ repulsion and thus pull the monomers inside the van der Waals contact distance.[25] Electron donor-acceptor complexes can have interaction energies ranging from -4 to -8 kJ mol^{-1} and can be either the hydrogen bonded type or the non-hydrogen bonded type.

3.1.3 van der Waals Interactions

In principle all elements and compounds, when subjected to high pressure and/or low temperature, will form a liquid and then a solid phase. The forces holding noble gas atoms or non-polar molecules together at low temperature are referred to as van der Waals forces.[26] The weakly bound complexes classified as van der Waals complexes are characterised by interaction energies of the order of -2 kJ

mol^{-1}. The study of the interaction energies of these weak complexes by ab initio methods is exceedingly difficult due to basis set superposition error.[27] The role of lone pairs[28] and the overlap of the highest occupied molecular orbital (HOMO) and the lowest unoccupied molecular orbital (LUMO)[29] have been suggested as dominant factors in determining the geometries of van der Waals complexes.[30] The electrostatic energy will not alone determine the structure of a van der Waals complex. The equilibrium configuration is a point of balance between attractive and repulsive forces. Attractive forces arise from dispersion and polarisation energies, while repulsive forces are mainly associated with exchange energies.[30]

3.2 Ab initio MO Calculations of the Properties of Molecular Complexes

3.2.1 Molecular Structures

Use of split-valence basis sets with polarisation functions (e.g. 6-31G**), in conjunction with correlated methods yields geometrical parameters in agreement with experiment.[27] The hydrogen bond angle, A-H...B, is expected to approach 180° in strongly hydrogen bonded complexes.[31,32] Buckingham and Fowler account for the physical justification of the linearity on the basis of electrostatic interaction.[33] The lengthening of the A-H bond on complexation is of interest, in respect of establishing the strength of the hydrogen bonded complex.[34]

The intermolecular distance, A...B, is an important quantity measuring the proximity of interacting sub-units.[35] These are some of the structural properties obtained from ab initio calculations. However their direct comparison with experimental ones must be done with caution.[36]

3.2.2 Interaction Energies

For two interacting molecules A and B, an interaction energy is defined as:

$$\Delta E = E_{AB} - (E_A + E_B) \tag{3.1}$$

where E_{AB} is the energy of the complex (supermolecule) and E_A and E_B are the energies of the individual molecules. The more negative the interaction energy the more stable is the supermolecule.

However, while the energies of the sub-units A and B are determined separately using the same basis set, the energy of a supermolecule AB is determined with all the orbitals of A and B included. The presence of monomer A extends the basis set of B and so does the presence of B on that of A, resulting in a mathematical (non-physical) lowering of the monomer energies which is usually referred to as a basis set superposition error (BSSE).[37] The BSSE is commonly estimated by the full counterpoise method of Boys and Bernardi.[38] In the Boys and Bernardi procedure, the energies of A and B are calculated separately within the basis set of the supermolecule AB. This is achieved by specifying zero nuclear charge at each of the nuclear centres, say of B, when B is a ghost molecule, while omitting the electrons of B; the energy of A calculated in this way is E_A'. When A is a ghost molecule, the energy of B is E_B'. To correct the interaction energy computed from equation (3.1), one then uses the relation:

$$\Delta E' = E_{AB} - (E'_A + E'_B) \tag{3.2}$$

from which the BSSE is evaluated as

$$\text{BSSE} = \Delta E' - \Delta E \tag{3.3}$$

The BSSE defined in equation (3.3) is a positive quantity. The effects of BSSE

on molecular properties are well established.[39-48] Having applied the "full" counterpoise method to various dimers, Johansson[42] came to the conclusion that full counterpoise correction overestimated the BSSE.

Alagona et al.,[46] after detailed analysis of the basis effects on BSSE concluded that full counterpoise procedure was necessary for a consistent description of the interaction energies. Similar conclusions were made by Gutowski et al.[47]. Although the theme of this project was not necessarily to establish the effects of BSSE on the interaction energies, the full counterpoise method was used in this project, following Alagona et al.[46] because of the similarity between the systems considered by Alagona and the ones studied here.

To attach a clearer physical meaning to the interaction energy, it is broken down into different components as follows:

$$\Delta E = \Delta E_{COU} + \Delta E_{EX} + \Delta E_{POL} + \Delta E_{CT} + \ldots \qquad (3.4)$$

where ΔE_{COU} is the classical electrostatic (Coulombic) energy, ΔE_{EX} is the exchange energy, ΔE_{POL} is the polarisation energy and ΔE_{CT} is the charge transfer energy. The first two terms in equation (3.4) are the first order contributions to the interaction energy.

The polarisation and charge transfer terms are second order contributions to the interaction energy. The higher order contributions are normally very small and for the purpose of this project will not be considered. Each of the terms of equation (3.4) will be considered in more detail so as to have a qualitative view of the interaction energy.

3.2.2.1 Electrostatic

This term is obtained directly from the intermolecular geometries and charge distributions of the individual molecules. The classical electrostatic energy for the interaction of two systems consisting of point-charge nuclei and the electronic charges, which are space fixed, can be deduced from equation (2.2). Such an expression has the form:

$$E_{el}^{(1)} = -\sum_a Z_a \int \rho_{mm}^B(j) \frac{1}{r_{aj}} dV_j - \sum_b Z_b \int \rho_{nn}^A(i) \frac{1}{r_{bi}} dV_i + \int \rho_{nn}^A(i)\, \rho_{mm}^B(j) \frac{1}{r_{ij}} dV_i dV_j + \sum_{a,b} \frac{Z_a Z_b}{R_{ab}} \tag{3.5}$$

where Z_a and Z_b are nuclear charges and i and j denote the electrons of molecules A and B respectively. ρ_{nn} and ρ_{mm} are the electron densities of A and B, with dV_i and dV_j denoting the elementary volumes occupied by the electrons belonging to A and B respectively (except the i^{th} and j^{th} electrons). R_{ab} is the nuclear separation distance between A and B.

The first two terms of equation (3.5) are attraction terms between the electron j and the nucleus a, and between the electron i and the nucleus b. These are more physically meaningful terms. The third and fourth terms of equation (3.5) are the repulsion terms between the electrons i and j, and the nuclei a and b respectively. At large internuclear separation distances, there is no overlap between the charge distributions; then the electrostatic energy can be represented to a good approximation in powers of 1/R, which is based on multipole moments of the charge distribution.[49]

The potential due to a system of charges, i.e. the multipole moment potential,

is a function of total charge q, dipole moment vector **q** and quadrupole moments.[49] This potential can be expressed as

$$\vartheta(R) = \sum_i \frac{e_i}{|R - r_i|} = \frac{q}{R} + \frac{dR}{R^3} + \sum_{\alpha,\beta} Q_{\alpha\beta} \frac{X_\alpha X_\beta}{R^5} + \ldots \qquad (3.6)$$

X_α and X_β denote the cartesian components of $\mathbf{r}_i$. The coefficient of the third term of equation (3.6) represents the quadrupole moment. From equation (3.5), it is clear that the dipole moment and the quadrupole component depend on the arrangement of charges. These are the terms which normally dominate the electrostatic component of the interaction energy.[50] The higher terms in equation (3.6) involve octupole and hexadecapole moments and these are normally very weak, hence electrostatic interaction is usually truncated at quadrupole moments. The value of the quadrupole moment, Q_{zz}, is used to indicate the variation of the real charge distribution from its spherical part. If this value is positive, it indicates that the charge is prolate along the z-axis, while a negative value indicates oblate charge distribution.

3.2.2.2 Polarisation

The presence of molecule A in the vicinity of B will cause some perturbation of the electronic configuration of B. The reverse is true. This effect is called polarisation interaction. The two molecules do not have to be very close, i.e. an overlap of the orbitals is not a necessary condition. Thus, this effect is quite a weak one and as such plays a secondary role to the interaction energy.

The polarisation is the sum of induction and dispersion terms as expressed

below:

$$E_{pol}^{(2)} = E_{ind}^{(2)} + E_{disp}^{(2)}. \tag{3.7}$$

The expression for the induction interactions, from second order perturbation theory,[51] is:

$$E_{ind}^{(2)} = -\sum_{m\neq 0} \frac{|\langle \psi_0^A \psi_m^B | \hat{V} | \psi_0^A \psi_0^B \rangle|^2}{E_m^B - E_0^B} - \sum_{n\neq 0} \frac{|\langle \psi_n^A \psi_0^B | \hat{V} | \psi_0^A \psi_0^B \rangle|^2}{E_n^A - E_0^A} \tag{3.8}$$

with n and m quantum numbers not simultaneously corresponding to the ground state of the isolated molecules. The first term of equation (3.8) describes the electrostatic interaction of molecule A in its ground state with the change induced in the electron density distribution of molecule B. The same logic applies for the second term of equation (3.7). In the ground state the induction interaction is always attractive. In excited states the induction can be either attractive or repulsive.

The dispersion energy has no classical meaning. An instantaneous charge distribution, corresponding to an instantaneous dipole moment of one molecule, induces a multipole moment in the other. It is the interaction of these moments which in turn defines the dispersion energy. Just as with induction interaction, the dispersion interaction is always attractive in the ground state of the interacting molecule.

3.2.2.3 Exchange

When two molecules approach each other too closely, short range effects

become predominant. This is a result of the Pauli principle, which demands that permutation of electrons under study must result in a wavefunction which is antisymmetric, i.e. no two electrons can occupy the same spatial and spin wavefunction simultaneously. The energy of the complex is increased because of the repulsions involved; this is termed exchange repulsion.[52-54] The exchange interactions are very effective at short range, even at the van der Waals equilibrium geometry. For closed shell systems, the role played by the exchange term in second order perturbation theory is small.[52-54]

3.2.2.4 Charge Transfer

The charge transfer term comes into play when the interacting systems are close enough for the transfer of charge. This, however, is a more difficult term to define because of the lack of any observable physical quantity with which to associate it. Different formalisms are applied in order to quantify charge transfer, such as the Mulliken population analysis.[55] This is the formalism adopted throughout this work.

3.2.3 Electronic Properties

The charge redistribution calculations in simple hydrogen bonded systems indicate that the polarity of the molecules concerned is increased, as illustrated by the increased dipole moment of the complex compared with the vectorial sum of the monomer dipole moments.[9b] Electron densities at the bridging hydrogens are decreased. These properties can be used as supplementary evidence for hydrogen bonding and are both automatically obtained from the ab initio calculations.

3.2.4 Vibrational Properties

Molecular vibrations, are analysed by infrared and Raman spectroscopy, which are fundamental tools to a chemist. Besides providing intramolecular information, the two techniques can also make available information on the intermolecular force constants in complexes. Theoretical calculations, though operating on the assumption of a harmonic model, do assist to a great extent in this regard. The characteristic vibrational changes of a monomer observed when a typical hydrogen bond forms are:

(a) the A-H stretching mode is red-shifted;

(b) the A-H stretching band is broadened;

(c) the intensity of the A-H stretching mode is greatly enhanced; and

(d) the bending mode of the proton donor is blue-shifted.

Moreover, the formation of the hydrogen bond results in new vibrational degrees of freedom, as a consequence of the restricted rotational and translational motions of the sub-units.[8b,10c] Such new vibrational modes are referred to as intermolecular modes (IMs) and are categorised as:

(a) torsional modes, which are in essence restricted rotation around the H...B bond; and

(b) stretching and bending modes, corresponding to the restricted mutual translation and rotation of the monomers.

These very low frequency vibrational modes are a significant source of information for the hydrogen bond equilibrium constants.

CHAPTER 4

4.1 Computer Programs

The computer programs used in this project, Gaussian-92, Schakal-92, Monstergauss and Vibra, are described. No attempt is made to derive the mathematical equations, but, where such equations clarify the descriptions, they are included, as in the Vibra section.

4.1.1 Gaussian-92

The Gaussian series of computer programs[56-63] are general purpose programs, characterised by a combination of the theoretical procedure and the basis set. Any calculation performed must contain an index of the required level of theory, type of calculation and the molecular system to consider for such a calculation. For example, keywords such as HF, MP2, QCISD, etc., are used to indicate the approximation method used, namely Hartree-Fock, Møller-Plesset perturbation to second order, and Quadratic Configuration Interaction (Singles and Doubles) together with a basis set, a mathematical representation of the molecular orbitals in a molecule, describing the positions of electrons in space to a particular region.[11c] The Gaussian suite of programs has undergone a number of changes, up to the current version, in an attempt to automate the computations for maximum reliability of the results. The earliest member of the Gaussian series, Gaussian-70, was very restrictive, allowing up to and including only p-type orbitals.[56] Gaussian-76 could handle up to d-type orbitals, but with no post-SCF computations.[57] It was replaced by Gaussian-80. The latter could handle electron correlation, a dilemma at the SCF level, and introduction of the use of key

words in specifying the type of optimisation that one sought. Compared with the earlier versions of the Gaussian series, Gaussian-86 also introduced an added feature.[60] The BSSE evaluation is done by using the keyword MASSAGE, which assigns the same basis functions to both monomers and supermolecule prior to determining the number of electrons involved. Gaussian-88, -90 and -92 have similar features, with some finer improvements in the speed of integral handling.

The reports by Swanton et al.[64] on water and Sosa and Schlegel[65] on fluoromethane demonstrate that both basis set and electron correlations influence the infrared intensities. Similar effects of the basis set and the level of theory on the infrared intensities were confirmed by Yamaguchi et al.[66] whereby it was illustrated that the computed infrared intensities were more sensitive to the basis set than frequencies which were in turn less sensitive than geometries. Miller et al.[67] later observed that basis set inadequacies led to defective force constants and hence frequencies. The computation of reasonably accurate interaction potentials requires use of much larger basis sets than typical calculations for isolated systems.[68] Such calculations require significant computation resources and therefore accurate intermolecular potentials are rare.[7,68,69] At the same time such potentials, if available, would be very useful in the interpretation of the large body of spectroscopic and scattering experiments on van der Waals molecules as well as in molecular simulations.[70] A detailed study of successive layers of MPn on geometries and energy prediction by Del Bene[70] demonstrated that MP2 tends to approximate full MP4 rather well. The recent report by Langlet et al.[71] pointed out that current state-of-the-art ab initio calculations are not able to reach the necessary level of accuracy, except of course for very small interacting species. The BSSE is very small for large basis sets.[71] Kim et al.,[72] using very large basis sets, with as many as 262 basis functions in their calculations of the water dimer, including two sets of f functions on O and d

functions on H, reported a BSSE value of 1.38 kJ mol^{-1} at the MP2 level.

The popularity of the use of the moderately sized 6-31G** basis set is based on its ability accurately to describe intermolecular hydrogen bonded complexes;[70,73-75] while the need to account for the electron correlation in interacting species was taken care of by using the MP2 level of theory. Based on the above arguments, all the computations were carried out using second-order Møller-Plesset (MP2) pertubation theory with the 6-31G** split valence polarized basis set,[16] where the inner-shell functions are expanded in terms of six primitive Gaussian functions, the outer valence shells are of split-valence type and a set of p- and d-Gaussian functions is included in the description of the hydrogen or helium atoms and heavy atoms respectively.

For this project part of the results were obtained using Gaussian-90, but for consistency all computations were repeated using Gaussian-92. The BERNY geometry optimisation procedure was used consistently, by citing the keyword OPT, starting at the DEFAULT through the TIGHT to the VERYTIGHT criteria of optimisation. The fully optimised structure was then subjected to frequency calculation using the keyword FREQ, which computes force constants, vibrational wavenumbers and vibrational intensities analytically. Inclusion of polarization functions on the hydrogen atoms is important for bridging hydrogen atoms, as found in hydrogen bonds.

4.1.2 Monstergauss

Monstergauss is a series of programs[77] designed to perform ab initio SCF molecular orbital calculations on organic molecules. Based on parts of Gaussian-82, specifically the integral and derivative routines, Monstergauss is quite

versatile. It features optimisation of geometries analytically, restricted Hartree-Fock open shell SCF, pair-wise multiconfiguration interactions (MCI) and Boys localisation, one-electron properties, direct configuration interaction (CI) and the Morokuma energy decomposition.

For the purpose of this project only the Morokuma energy decomposition was used. Monstergauss is typical of ab initio programs, requiring input in the form of the z-matrix orientation of the converged structure as output by Gaussian-92.

4.1.3 Vibra

Vibra[78] is a general harmonic vibrational analysis program, which allows the calculation of harmonic wavenumbers, cartesian displacement coordinates, force constants and many other properties. The program Vibra was used with the sole purpose of monitoring the changes in the force constants of those bonds which are directly involved in complexation, establishing the force constants of the H...B bond, and determining the potential energy distributions.

The most fundamental information obtained from vibrational spectroscopy is a qualitative knowledge of the interatomic forces within the molecule. The forces holding the atoms together in a molecule determine the vibrational frequencies of the fundamental vibrations. The force constants are in turn determined by the electronic configuration. It follows that, working from the observed or calculated vibrational frequencies, some information about the force constants can be obtained which in turn can be used to describe the electronic structures.[79]

The theoretical basis of Vibra is outlined below. The main equations used for the force constant calculations will be quoted and the application of these

equations will be illustrated.

Let a molecule at equilibrium be defined by a cartesian coordinate position vector R_a[80] as:

$$\boldsymbol{R_a} = (X^e a, Y^e a, Z^e a) \tag{4.1}$$

for a=1, 2, ... N atoms in the molecule of interest. The superscript e denotes the equilibrium position. If an atom, a, shifts instantaneously from the equilibrium position, the deviation from equilibrium in the x-direction is $\Delta X_a = X_a - X_a^e$.

The 3N cartesian displacements are denoted by a column matrix, X, where $X=\{P_1, P_2,..., P_N\}$. The cartesian coordinate system does not have the symmetry properties which are characteristic of the G and F matrices. Hence there is a need for a change to a new coordinate set called symmetry coordinates S.[80] The symmetry coordinate system defines bond stretches, angle bends and torsional motions as basis functions transforming according to each of the irreducible representations spanned by the 3N-6 normal modes of vibration. It is apparent from the above definition that S possesses some symmetry. For a vibrating molecule, $E_T = T + V$, where E_T denotes total energy while T and V denote kinetic and potential energy respectively. The column matrices of momenta conjugate to **x** and **S** may be denoted by $\mathbf{p}_x$ and $\mathbf{P}_S$ respectively; and may be expressed as

$$(\boldsymbol{P_x})_i = \frac{\partial T}{\partial \dot{x}_i} \qquad (\boldsymbol{P_s})_i = \frac{\partial T}{\partial \dot{x}_i} \tag{4.2}$$

where x_i define the cartesian displacements.

Let B be a transformation matrix defined as

$$B_{ij} = \frac{\partial S_i}{\partial x_j} = \frac{\partial \dot{S}_i}{\partial \dot{x}_j}.$$

(4.3)

Equation (4.3) signifies the instantaneous change of the symmetry coordinate, S_i, in the x-direction. The momentum in the x direction becomes

$$(\boldsymbol{P}_x)_i = \sum \frac{\partial T}{\partial S_j} \frac{\partial \dot{S}_j}{\partial \dot{x}_i} = \sum_j (\boldsymbol{P}_s)_j B_{ij},$$

(4.4)

Hence S=BX and

$$\dot{S} = B\dot{X}, \quad \boldsymbol{P}_x = B^+ \boldsymbol{P}_s, \quad \boldsymbol{P}_s = \boldsymbol{P}_x (B^+)^{-1}.$$

(4.5)

The superscript, +, denotes the transpose of the matrix in question.

The G matrix[20] can now be set up in terms of the vibrational kinetic energy as

$$2T = P_x^+ m^{-1} \boldsymbol{P}_x = P_S^+ G \boldsymbol{P}_s.$$

(4.6)

Substitution of equation (4.3) into (4.6) leads to

$$G = B\, m^{-1} B^+.$$

(4.7)

Equation (4.7) holds when P_S are independent coordinates. From the Hamiltonian equations it can be shown that

$$\dot{S}_i = \{\frac{\partial T}{\partial P_S}\}_i = \sum_j G_{ij} = \boldsymbol{GP_s}$$

(4.8)

$$\boldsymbol{P_s = G^{-1}\dot{S}}.$$

(4.9)

For non-redundant symmetry coordinates, S_i, the inverse of G exists; therefore equation (4.9) leads to the kinetic energy function of the form

$$\dot{X}^{+} m\dot{X} = \dot{S}^{+} G^{-1}\dot{S}.$$

(4.10)

Equation (4.10) shows a link between the X and S coordinates. A new matrix can now be defined which leads to a further simplification of the secular equations. This is the matrix A, defined as

$$A_{ij} = \frac{\partial X_i}{\partial S_j}.$$

(4.11)

From equation (4.11), further relationships can be defined, such as

$$X = AS \qquad \dot{X} = A\dot{S} \qquad \boldsymbol{P_s = A^{+} P_X}.$$

(4.12)

From the definition of matrix B, it follows that BA=AB=E; i.e. matrix A is the inverse of matrix B. By substitution of X by S, it can be shown that

$$A^{+}mA=G^{-1}.$$

(4.13)

The relationship shown by equation (4.13) illustrates one of many ways of solving for the G matrix and hence for the kinetic energy term. Applying mass weighted coordinates and following a similar type of logic as for matrices B and A, it can be shown that

$$G=DD^{+}$$

(4.14)

where D is the diagonal matrix whose elements are reciprocal square roots of the atomic masses. The equations (4.1) to (4.13) are kinetic energy equations. The development of the potential energy functions will now be illustrated.

The potential energy can be expressed as

$$2V=Q^{+}\lambda Q$$

(4.15)

where λ is a diagonal matrix, the elements of which are frequency parameters. The important normal coordinate transformation matrix is given by

$$\begin{aligned} S&=LQ \\ \dot{S}&=L\dot{Q} \\ P&=L^{+}P_S \end{aligned}$$

(4.16)

where L is matrix defining a number of independent internal coordinates. As mentioned above, for independent sets of coordinates, the matrix G can be expressed as

$$G=LL^{+}$$
$$\lambda=L^{+}FL.$$

(4.17)

F is the force constant matrix in symmetry coordinates. The symmetry coordinates are linear combinations of the internal coordinates, with the feature that they take full advantage of the symmetry properties. They are defined by

$$S=Us \qquad s=U^{-1}S.$$

(4.18)

Recalling that

$$2V=\sum_{jl} F_{jl}S_jS_l \qquad 2V=s^{+}fs \qquad 2V=S^{+}FS$$

where the f_{ij} denote bond stretching and angle bending internal force constants, which are physically more meaningful than symmetry force constants, F_{ij}.[81] It is usual to solve the secular equations in terms of the F_{ij}, while the terms which are of real interest are the f_{ij}; indeed the program Vibra gives the output in this format. To obtain the f_{ij}, a set of simultaneous equations is solved. The program Vibra requires as input the molecular geometry, in the z-matrix orientation, as output by Gaussian-92, a set of internal coordinates as defined above and the force field from the Gaussian-92 output, first converted from atomic units by FCGMOD (a program for converting force constants from internal units into practical units) and finally the definitions of the symmetry coordinates. All the symmetry coordinates used are defined in the following chapters, along with the corresponding descriptions.

The following symbols are employed for describing the various types of vibrational modes:

(a) ν - bond stretching. In molecular systems where two or more similar modes occur, e.g. the water OH stretching modes, the subscripts s (symmetric) and a (antisymmetric) are used. The abbreviations IP for in-phase and OP (out-of-phase) will also be used for the coupled vibrations in some cases.

(b) δ - bond angle deformation. As in (a) above, the bending can either be symmetric or antisymmetric, so subscripts s and a are used accordingly where appropriate. Again IP or OP may also be used.

(c) γ - distinguishes an out-of-plane bond angle deformation.

(d) τ - torsion. For a molecular fragment A-B-C-D, a torsion may be described as the rotation of the bond A-B, in the opposite direction to the rotation of the bond C-D, about the bond B-C.

4.1.4 Schakal-92

Schakal-92 is a computer program for the graphical representation of molecular and crystallographic models.[82] The package requires a set of Cartesian coordinates in the standard orientation, as output by Gaussian-92. The Schakal-92 package was used throughout this project to represent the equilibrium structures and some of the intermolecular vibrational modes.

CHAPTER 5

5.1 Review of the Structural and Vibrational Properties

A survey of the literature on the complexes and related monomers is presented here. Such a review is necessary if comparisons are to be made. While some systems such as the formaldehyde-water complex, have been extensively studied, some, to the best of our knowledge, have not been investigated so extensively.

5.1.1 Group 1 Complexes

The structures and dynamics of weakly bound molecular complexes are of great interest to chemists and physicists, partly because of their role as intermediates in some chemical reactions, and partly due to the physical nature of the interaction.[83] Coupling matrix isolation infrared spectroscopy with ab initio quantum mechanical calculations for the detection and characterization of weakly bound complexes has proven very useful.[84] Water acts as a proton donor in hydrogen bonding interactions in those complexes with species which are stronger bases than itself, including nitrogen,[85-88] carbon monoxide,[86-88] ammonia[89] and formaldehyde.[86,87,90-97] In complexes which are stronger acids than water, e.g. hydrogen sulphide,[86,87] it acts as an electron donor. Water is also capable of forming complexes which are not of the hydrogen bonding type; the complexes with boron trifluoride,[98] carbon dioxide[99,100] and cyanogen[101] are stabilised by an electron donor-acceptor (EDA) interaction in which the water molecule donates electron density from one of its lone pairs to an orbital on the electropositive site of the partner molecule.

The molecules hydrogen cyanide, acetylene, cyanogen and acetonitrile, provide a set of complexes with water having potentially interesting structures and properties. In the cases of hydrogen cyanide and acetonitrile, water could donate a proton to the axial nitrogen lone pair of the cyano group, or to the C≡N π bonding orbital, or it might accept a proton from the hydrogen cyanide molecule or the methyl group of the acetonitrile molecule respectively. HCN has a pK_a value of 9.31 compared with 15.7 for H_2O[102] (although the pK_a values are measures of acidity in aqueous solution, a rough idea of the ease of proton donation can still be deduced in the gaseous phase), thus a CH...O hydrogen bond is more probable in the hydrogen cyanide-water interaction than either the OH...N or OH...π interaction. Similarly, in the acetylene-water complex, in which there are two equivalent CH bonds and a CC π bond, but no nitrogen atoms, the possible interaction types are OH...π, in which water donates the proton, and CH...O, analogous to the hydrogen cyanide-water complex, in which a proton is donated by the acetylene molecule.

Cyanogen lacks an acidic proton as in the HCN and HCCH cases discussed above, but contains two equivalent C≡N groups; the only hydrogen bonded possibilities are an OH...N or an OH...π hydrogen bonded structure, with water acting as a proton donor, similar to those proposed for NCH-OH_2. In addition there is a possibility of the water oxygen atom interacting with the lowest unoccupied π^* orbitals in cyanogen.[101]

In CH_3CN, there are three possibilities for hydrogen bonding, namely, OH...N, OH...π or CH...O, where one of the methyl group hydrogen atoms interacts with the water oxygen. The last option, of a CH...O bond, is very unlikely on the basis of the low acidities of the methyl hydrogen atoms. The occurrence of an OH...π hydrogen bonded type is unlikely because of steric crowding. The only

remaining option is the OH...N type.

From gas phase microwave spectroscopy,[103,104] a CH...O hydrogen bond is the most favoured for the NCH-OH_2 complex. Gutowsky et al. proposed a pseudoplanar configuration in which the hydrogen of the HCN interacts with either of the oxygen lone pairs.[104] In this type of complex, the water HOH angle bisector was found to make an angle of 20° with the NCH...O axis. Vishveshwara,[105] Hinchliffe[106] and Turi and Dannenberg[107] carried out some ab initio studies of the NCH-OH_2 complex. Vishveshwara found that at the restricted Hartree-Fock (RHF) level, with the STO-3G basis set, a planar structure was more stable.[105] Hinchliffe, using the HF level of theory and Dunning's basis sets, including polarisation functions on all the heavy atoms, identified a C_{2v} structure as having the lowest energy,[106] while Turi and Dannenberg, using larger basis sets, established that both nonplanar and planar structures should be observed.[107]

Peterson and Klemperer studied the gas phase structure of the HCCH-OH_2 complex by the molecular beam electric resonance (MBER) method,[108] while Block et al.[109] and Peterson and Klemperer[108] computed the molecular geometrical parameters with the assumption of a C_{2v} planar structure. Block et al. also proposed a planar structure for the HCCH-OH_2 complex.[109] Engdahl and Nelander,[110] from an infrared study of HCCH-OH_2 trapped in argon matrices, interpreted their work in terms of a C_s structure. Frisch et al. established two structures on the potential energy surface of HCCH-OH_2; the conclusion drawn was that a C_s structure was favoured.[111]

The only work reported in the literature for the NCCN-OH_2 complex is that by Lee et al., who used radiofrequency microwave spectroscopy[101] to determine the

structure of the NCCN-OH_2 complex. Their results supported a planar T-shaped asymmetric top structure with the C_2 axis passing through the water oxygen and bisecting the CC bond. The non-planar isomer was found to be very unlikely due to a high barrier to internal rotation.

A literature search on the CH_3CN-HOH complex showed that no work has been reported on this complex. The few complexes of acetonitrile studied are those with HCN, HF and Cl^-, which will be used as guiding comparisons with the results obtained in this project.[112-116] The far infrared spectroscopic studies by Knözinger and Wittenbeck[112] showed two types of isomers. In one isomer a strong dipole-dipole interacting complex results in a cage-like structure; in the other isomer a linear C_{3v} structure is observed. Legon et al.'s studies on the gas phase microwave spectroscopy of the CH_3CN-HF complex indicated a C_{3v} structure.[113-115] The ab initio molecular orbital calculations on the CH_3CN-Cl^- complex by Jayaraj and Singh, using 3-21G and 6-31+G basis sets, showed that the Cl^- ion interacts preferentially with one of the methyl hydrogens.[116]

5.1.2 Group 2 Complexes

The first ab initio molecular orbital studies of the hydrogen bond in the water dimer with rather small atomic basis sets[117-120] paved the way for the theoretical understanding of hydrogen bond formation, the structures of hydrogen bonded complexes and evaluation of interaction energies.[121]

Formaldehyde is the simplest representative of the carbonyl compounds. It can be used as a model for carbonyl hydration; this signifies the importance of studying the complex. Some theoretical studies[73,96,121,122] predict a non-planar structure for the formaldehyde-water complex, while others[35,86,87,90] predict a

planar form. Mitchell and Price[32] showed that among the complexes of the type NH...O=C, the C=O...H angle approached the expected 120°, consistent with that in the crystal structures of similar types of complex.

Experimental studies on H_2CO-HF,[123,124] H_2CO-HCl[125] and H_2CO-HCN[126] show essentially common features with all three complexes being planar with the hydrogen atom of the proton donor pointing towards a carbonyl oxygen lone pair.

Methyleneimine (a Schiff base) possesses the C=N functional group, which is found in rhodopsin and bacteriorhodopsin. In both instances, it is generally agreed that the Schiff base is protonated during a photochemical reaction.[127-130] This illustrates the biological importance of the C=N group. Properties of a range of imines were studied by ab initio molecular orbital calculations.[131] The interaction of methyleneimine with water is predominantly that between the nitrogen lone pair and one of the water hydrogens, and it has a strong directional effect.[31] The hydrogen bond length and interaction energy obtained for the water-imine systems are of similar magnitude to those in the ammonia-water system.[89] Sreenama and Vishveshwara[132] confirmed the direction of proton approach for Schiff bases and other nitrogen compounds by the ab initio method using the 4-31G basis set. Spectroscopic studies[133] of the solvent dependent reactions of anils of benzaldehyde and salicylaldehyde clearly indicate a strong tendency towards hydrogen bonding.

Binary complexes of water with hydrocarbons have been studied before, particularly those with acetylene,[108] ethylene[134] and methane.[135] Del Bene reported an ethylene-water structure, calculated by the ab initio method, and made the observation that water rotation about the hydrogen bond is almost

free.[136] Matrix isolation studies[137] showed a hydrogen bonded structure consistent with that reported by Del Bene.[136] Microwave studies on the ethylene-water complex and its isotopomers[138] are also consistent with the structure predicted by Del Bene.[136] The formaldehyde-water and methyleneimine-water complexes interact mainly through the oxygen and nitrogen lone pairs, while the ethylene-water complex interacts mainly through the π-orbitals of the ethylene C=C bond. The involvement of the π-orbitals is also demonstrated in the complexes of the hydrogen halides with ethylene, as probed by molecular-beam methods[139,140] and by matrix isolation infrared spectroscopy.[93,141-147]

5.1.3 Group 3 Complexes

Hydrogen bonded complexes are a special case of van der Waals complexes,[148] and the nature of such complexes is primarily electrostatic.[53] The hydrogen bond, which is characteristic of the complexes studied here, is highly directional, and normally projects along the axis of a non-bonding electron pair.[28,34] A wide spectrum of experimental techniques exists for studying these complexes, ranging from gas-phase rotational spectroscopy[139,140] to matrix isolation infrared spectroscopy.[93,141-147]

The solid state and gas phase infrared spectra and normal coordinate analysis of the acetaldehyde molecule were studied by Hollenstein and Günthard.[149] Hollenstein and Winter studied the torsional motion of acetaldyde,[150] while Andrews and Johnson carried out infrared matrix isolation studies of simple carbonyl-hydrogen fluoride complexes, including the CH_3CHO-HF and $(CH_3)_2CO$-HF complexes.[151] The study by Andrews and Johnson indicated large red shifts in the ν(HF) modes. Microwave and double resonance spectroscopy have been used by Baker and Petty to study the torsional motion in

acetaldehyde.[152] Schriver carried out a matrix isolation infrared study of the hydrogen bonded complex of acetone and hydrogen iodide, concluding that the 1:1 species predominates at high dilution[153]. The torsional ground state of acetaldehyde has been analysed by Kleiner et al.[154] Infrared and far infrared spectra of the $(CH_3)_2CO$-HOH complex have been studied in argon matrices.[155] The CO deformation, CC stretching and C=O stretching bands of complexed acetone were significantly shifted compared with the acetone monomer bands, indicating that water was bound to the carbonyl group. Similar work was carried out by Zhang et al.,[156] who also supplemented their experimental data with ab initio SCF calculations.

Detailed ab initio calculations, at the SCF level of theory, for the complexes of the type RCHO...HOH have been performed by Del Bene,[121] and with R=CH_3 the complex was observed to be of C_s symmetry. The vibrational force field of acetaldehyde has been studied by Wiberg et al.[157] Lee and Dyke made a theoretical study of the protonation of acetone monomer and dimer,[158] observing that protonation of the monomer occurs at the carbonyl group. A theoretical study of clusters of protonated acetone was carried out by Aviyente and Vernali.[159] A binary complex of acetone and iodine was studied by Setokuchi and Shimizu at both the SCF and MP2 levels of theory.[160] The conclusion reached by Setokuchi and Shimizu was that, at the SCF level of theory, the complex geometry was not well described, hence to describe the geometry of acetone-iodine fully, a correlated level of theory was necessary. A study of a range of hydrogen bonded complexes, by Scheiner, including those containing some nitrogen and oxygen bases, describes some interesting geometry patterns.[161]

5.1.4 Group 4 Complexes

Formic acid is the simplest of the carboxylic acids and as such its interaction with the water molecule can be used as a model for such interactions. It is expected that the complexes of formic and acetic acids with water will form two hydrogen bonds, deduced from the dissociation constants, 17.7 x 10^{-5} and 1.75 x 10^{-5} mol dm^{-3} for formic and acetic acids respectively.[162] Since the hydroxyl H atom is acidic, it can be easily donated to the water O atom, while one of the water H atoms can interact with the carbonyl O atom as in H_2CO-HOH, discussed in sub-section 5.1.2.

The structure of the carboxylic acid dimers was discovered in 1914.[9a] Coulson used the formic acid dimer as an example in his classical account of the hydrogen bond.[163] Hayashi et al. carried out a theoretical study of the formic acid dimer, elucidating the potential barrier height for the double proton transfer, and the geometry of the dimer.[164] Graf et al. studied the simultaneous hydrogen bond exchange within carboxylic acid dimers by ab initio quantum chemical calculations and by computations of nuclear dynamics.[165] Interaction of formic acid with amines using the STO-3G and 4-31G basis sets have been reported.[166,167] The complex of formic acid with water was studied at the RHF/4-31G level;[168] Williams and Lowrey carried out an ab initio study of the complexes of water with formic and acetic acids and acetone, evaluating both structures and the effect of hydration on the force constants,[169] while the complex of formic acid with methyl chloride at the MP2/6-31+G* level of theory and basis set combination was investigated by Reynolds.[170]

The structure of the formic acid dimer has been determined experimentally by electron diffraction[171-173] and infrared studies[174,175] in a nitrogen matrix. These

studies show the tendency to form strong hydrogen bonded interactions. Ab initio SCF calculations of $(HCOOH)_2$ agree with the general view that two hydrogen bonds occur.[176]

A theoretical study by Berckmans et al.[177] on the integrated intensities of the formic acid dimer justifies the use of a double protonation model in this dimer. Lundell et al. carried out ab initio MO calculations of the formic acid-carbon monoxide complex, at the MP2 level of theory to establish the energetics and structural parameters, and the nature of the complex.[178] The proton transfer in methyleneimine complexed with formic acid was studied by Peeters, at the RHF level of theory and using the 6-31G** basis set,[179] in which formic acid is found to donate its proton to the nitrogen atom of the methyleneimine molecule.

The recent theoretical study on formic acid dimer by Borisenko et al.,[180] at the MP2/6-31G** level of theory and basis set, indicates that the trends in structural changes agree with those implied by the presence of high electron mobility.

The effect of intermolecular hydrogen bond formation on the geometrical parameters in the acetic acid dimer have been carried out by Borisenko et al., using the MP2 level of theory and the 6-31G** split-valence polarised basis set.[180] The double proton donation on dimerisation was noted and compared with that in the formic acid dimer. Turi and Dannenberg[181] carried out similar work on the acetic acid dimer, for which changes in geometry were investigated. Both studies agree fairly well. From the structural similarities between acetic acid and formic acid, it is expected that the complexes of water with both these molecules will also show some similarities. Both complexes have high equilibrium constants for formation, and as mentioned above are capable of double hydrogen bonding.

The structure of methyl formate can assume two configurations, one in which the C=O bond is cis to the methyl group and the other trans.[182] Some infrared studies to establish the most stable configuration have been carried out by Harris et al.[183] They observed that the barrier to internal rotation about the C-O bond is about 36 kJ mol^{-1}, establishing that the cis conformer is more stable than the trans. Microwave studies have shown that there are indeed two forms of methyl formate.[184] Ab initio studies on methyl formate have been carried out by Wennerström et al.[185] to elucidate the nature of the rotational barrier and the s-trans-s-cis conformation. Vibrational conformational analysis of methyl fluoroacetate, by van der Veken et al., shows the presence of two isomers similar to methyl formate.[186] Light-induced isomerism and photochemical transformation of methyl formate in an argon matrix, coupled with normal coordinate analysis, revealed all the fundamental modes of methyl formate.[187] Vanderheyden et al. carried out a matrix isolation infrared spectroscopic study of water complexes with a range of aliphatic esters, including methyl formate.[188] They made the observation that for 1:1 adducts, the hydrogen bond is preferentially formed at the carbonyl oxygen, but more importantly, that the methoxy oxygen also forms a hydrogen bond, although to a limited extent.

Matrix isolation infrared spectra of the complexes between water and methyl acetate have been reported by Maes and Zeegers-Huyskens.[189] They showed that the water molecule hydrogen bonds preferentially to the carbonyl oxygen atom, but an interaction at the methoxy oxygen was not totally excluded. Vanderheyden et al. carried out some infrared studies of the methyl acetate-water complex, along with a series of other esters.[188] Apparently not much computational work has been reported on the complexes of water with the esters, probably due to the relatively large sizes of the complexes, which make such calculations costly in terms of computer resources.

CHAPTER 6

6.1 RESULTS AND DISCUSSION OF THE GROUP 1 COMPLEXES

In this chapter the geometrical parameters, charge redistributions, interaction energies corrected for basis set superposition error and vibrational properties are discussed for the Group 1 complexes, as defined in section 1.5 of chapter 1. The trends within the group are drawn. The predicted properties are compared with the literature ones where such values exist.

6.2 Structural, Energetic and Electronic Properties of the NCH-OH_2, HCCH-OH_2, C_2N_2-OH_2 and CH_3CN-HOH Complexes

6.2.1 Geometrical Parameters

The optimised geometrical parameters of the five monomers together with the experimental values[190] are collected in Table 6.1. The agreement between the calculated and experimental values is indicated by the calculated-experimental differences, and it is consistently not as good for the triple bonds as for the single bonds.

Two forms of the NCH-OH_2 complex were identified. The C_s isomer has a lower absolute energy and the frequency calculation proved this form to be a true minimum.[11] The planar form, forced into C_{2v} symmetry, has a higher absolute energy and one negative frequency. Thus the C_{2v} isomer is a transition state. Figure 6.1 is a Schakal-92 plot of the two isomers.

Table 6.1. Optimised and Experimental Structural Parameters of the Water, Hydrogen Cyanide, Acetylene, Cyanogen and Acetonitrile Monomers and the Calculated-Experimental Differences

Molecule	Parameter	Calculated	Experimental[a]	Difference[b]
H_2O	r(OH)/pm	96.1	95.8	0.3
	HOH/deg	103.8	104.5	-0.7
HCN	r(CH)/pm	106.5	106.5	0.0
	r(CN)/pm	117.8	115.3	2.5
C_2H_2	r(CH)/pm	106.2	106.1	0.1
	r(CC)/pm	121.7	120.3	1.4
C_2N_2	r(CN)/pm	118.7	115.4	3.3
	r(CC)/pm	138.3	138.9	-0.6
CH_3CN	r(CH)/pm	108.7	110.4	-1.7
	r(CN)/pm	118.0	115.7	2.3
	r(CC)/pm	146.2	145.8	0.4
	HCC/deg	110.0	109.5	0.5

[a] Ref. 190. [b] Difference = calculated - experimental parameter.

A structure in which the water H5 or H6 atoms (see Figure 6.1) interact with the lone pair of the N1 atom is less favoured compared with the C_s structure, as indicated by the fact that an optimisation starting with such a geometry collapsed to the C_s form. The values of the geometrical parameters of the more stable of the two isomers are shown in Table 6.2, together with the complex-monomer differences, and the atom numbering is adopted from Figure 6.1.

The column headed Diff. shows the changes occurring on complexation. The hydrogen bonded C2H3 bond length is extended by 1.0 pm (see Figure 6.1). The H5O4H6 angle of the water molecule opens out somewhat by 0.8°,

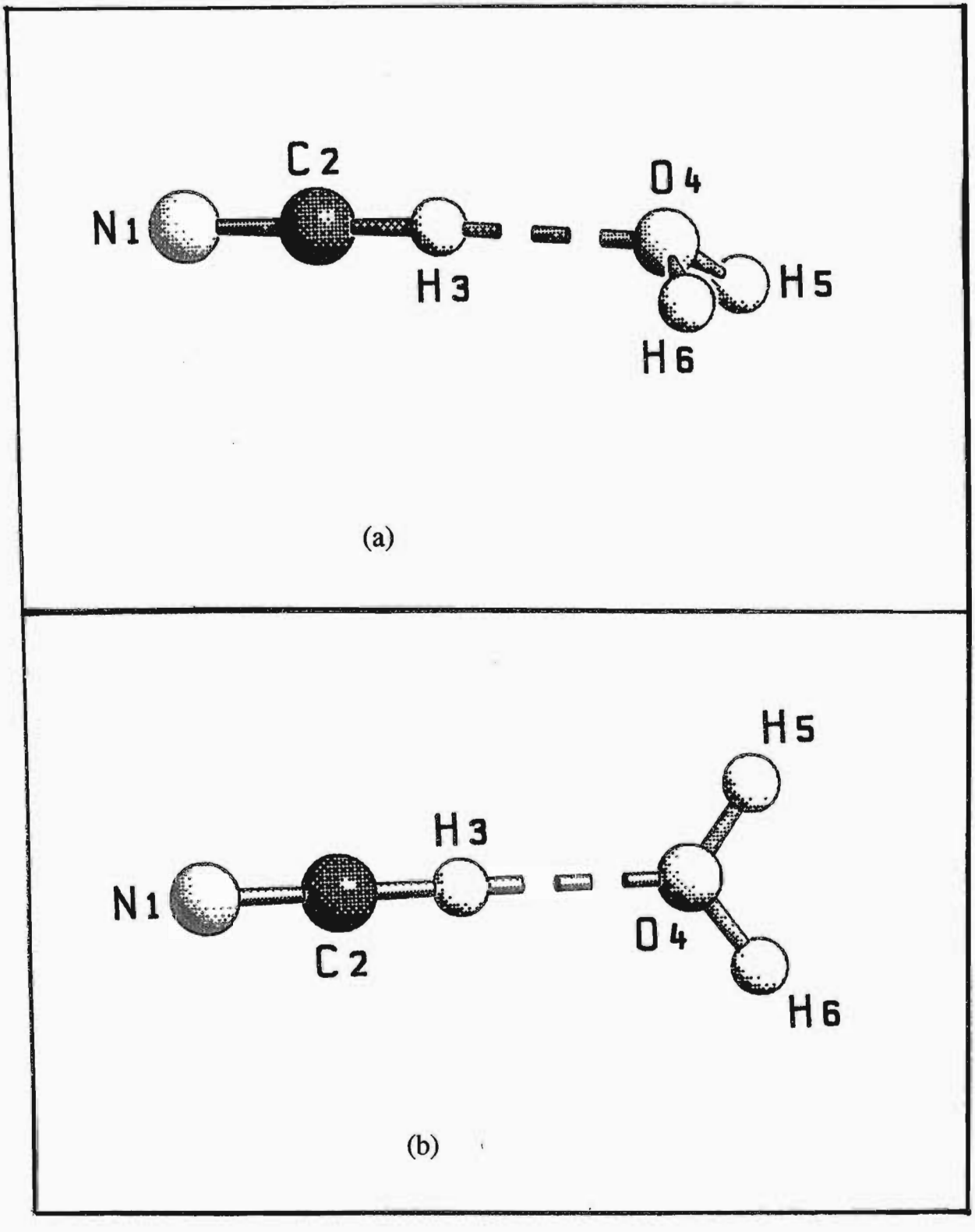

Figure 6.1. Numbering of atoms of the two configurations of the NCH-OH_2 complex: (a) C_s structure; (b) C_{2v} structure.

Table 6.2. Optimised Structural Parameters of the Complexes of Water with Hydrogen Cyanide, Acetylene, Cyanogen and Acetonitrile and the Complex-Monomer Differences

		Value	
Complex	Parameter[a]	Calc.	Diff.
$NCH\text{-}OH_2$	r(C2N1)/pm	117.8	0.0
	r(C2H3)/pm	107.5	1.0
	r(O4H5),r(O4H6)/pm	96.2	0.1
	r(H3..O4)/pm	202.5	-
	r(C2...O4)/pm	310.0	-
	H3C2N1/deg	179.7	-0.3
	H5O4H6/deg	104.6	0.8
	C2H3...O4/deg	176.6	-
	N1C2H3...O4/deg	0.0	-
	C2H3..O4H5,C2H3..O4H6/deg	117.7	-
$HCCH\text{-}OH_2$	r(C1H3)/pm	106.2	0.0
	r(C1C2)/pm	122.0	0.3
	r(C2H4)/pm	106.8	0.6
	r(O5H6), r(O5H7)/pm	96.3	0.2
	r(H4...O5)/pm	220.5	-
	r(C2...O5)/pm	326.2	-
	H3C1C2/deg	179.9	-0.1
	H4C2C1/deg	179.8	-0.2
	H6O5H7/deg	104.1	0.3
	C2H4...O5/deg	170.1	-
	H3C1C2H4/deg	180.0	-
	C1C2H4...O5/deg	0.0	-
	C2H4...O5H6,C2H4...O5H7/deg	126.4	-
$C_2N_2\text{-}OH_2$	r(C1N3),r(C4N5)/pm	118.6	-0.1
	r(C1C4)/pm	138.5	0.2
	r(O2H6),r(O2H7)/pm	96.2	0.1
	r(O2...C1C4)/pm	273.4	-
	N3C1C4,C1C4N5/deg	176.0	-4.0
	H6O2H7/deg	104.7	0.9
	N5C4C1N3/deg	0.0	-

Table 6.2 (continued)

CH_3CN-HOH	r(C1C2)/pm	146.1	0.1
	r(C1H3)/pm	108.7	0.0
	r(C1H4),r(C1H5)/pm	108.7	0.0
	r(C2N6)/pm	117.8	-0.2
	r(H7...N6)/pm	214.2	-
	r(O8...N6)/pm	310.2	-
	r(O8H7)/pm	96.5	0.4
	r(O8H9)/pm	96.1	0.0
	C1C2H3/deg	109.9	-0.1
	C1C2H4/deg	109.9	-0.1
	C1C2H5/deg	109.9	-0.1
	C2C1N6/deg	179.9	-0.1
	C1N6...H7/deg	166.5	-
	O8H7...N6/deg	173.1	-
	H9O8H7/deg	103.2	-0.6
	H3C1C2N6/deg	0.0	0.0
	H4C1C2N6,H5C1C2N6/deg	120.0	0.0
	C2N6...H7O8/deg	0.0	-

[a] Atom numbering is as in Figures 6.1 to 6.4.

Calc. : calculated. Diff. : difference.

while the HCN linearity is distorted by 0.3°, with the NCH...O fragment in a cis configuration. The hydrogen bond angle differs from 180° by 3.4°. The structure is consistent with the CH...O hydrogen bond being directed along the axis of one of the lone pair orbitals, rather than along the direction of the water dipole moment vector, which would be the case if the minimum energy geometry were found to be planar.[31] The hydrogen bond length, H3...O4, is 202.5 pm and the internuclear separation distance, C2...O4, is 310.0 pm.

The most probable structure for the acetylene-water complex was also found to

be non-planar with C_s symmetry. An attempt to optimise a structure in which one of the water hydrogens interacted with the π-orbitals of the acetylene molecule always resulted in such a structure collapsing to a C_s configuration, as shown in Figure 6.2, as was the case with the NCH-OH_2 complex. The forced C_{2v} planar structure is a transition state, as confirmed by the frequency calculations. Figure 6.2 shows both the preferred and the constrained structures. Table 6.2 shows the optimised structural parameters of the preferred HCCH-OH_2 complex. The water OH bonds remain virtually unperturbed, as was found in the case of the NCH-OH_2 complex.

The non-bonded C1H3 bond length remains the same on complexation, while the hydrogen bonded C2H4 bond length is extended by 0.6 pm (see Figure 6.2). The HOH bond angle is slightly increased in the HCCH-OH_2 complex, but much less than it was in the NCH-OH_2 complex. The HCCH fragment is hardly distorted from linearity, while the C2H4...O5 hydrogen bond angle deviates from linearity by 9.9°, i.e. three times the deviation from linearity calculated for the NCH-OH_2 complex. The HCC angles are distorted in a trans fashion, while the CCH...O arrangement is cis, as for the NCH...O fragment in the NCH-OH_2 complex. The interaction is again lone pair, rather than dipole, directed.[31] The predicted H4...O5 and C2...O5 distances, 220.5 pm and 326.2 pm, are both longer than those of the NCH-OH_2 complex, implying a weaker complex.

Table 6.2 also presents the optimised geometrical parameters of the energetically preferred cyanogen-water complex. The preferred structure is planar with C_{2v} symmetry, with the water oxygen interacting with the mid-point of the C-C bond. A second optimised perpendicular C_{2v} configuration was found to be a

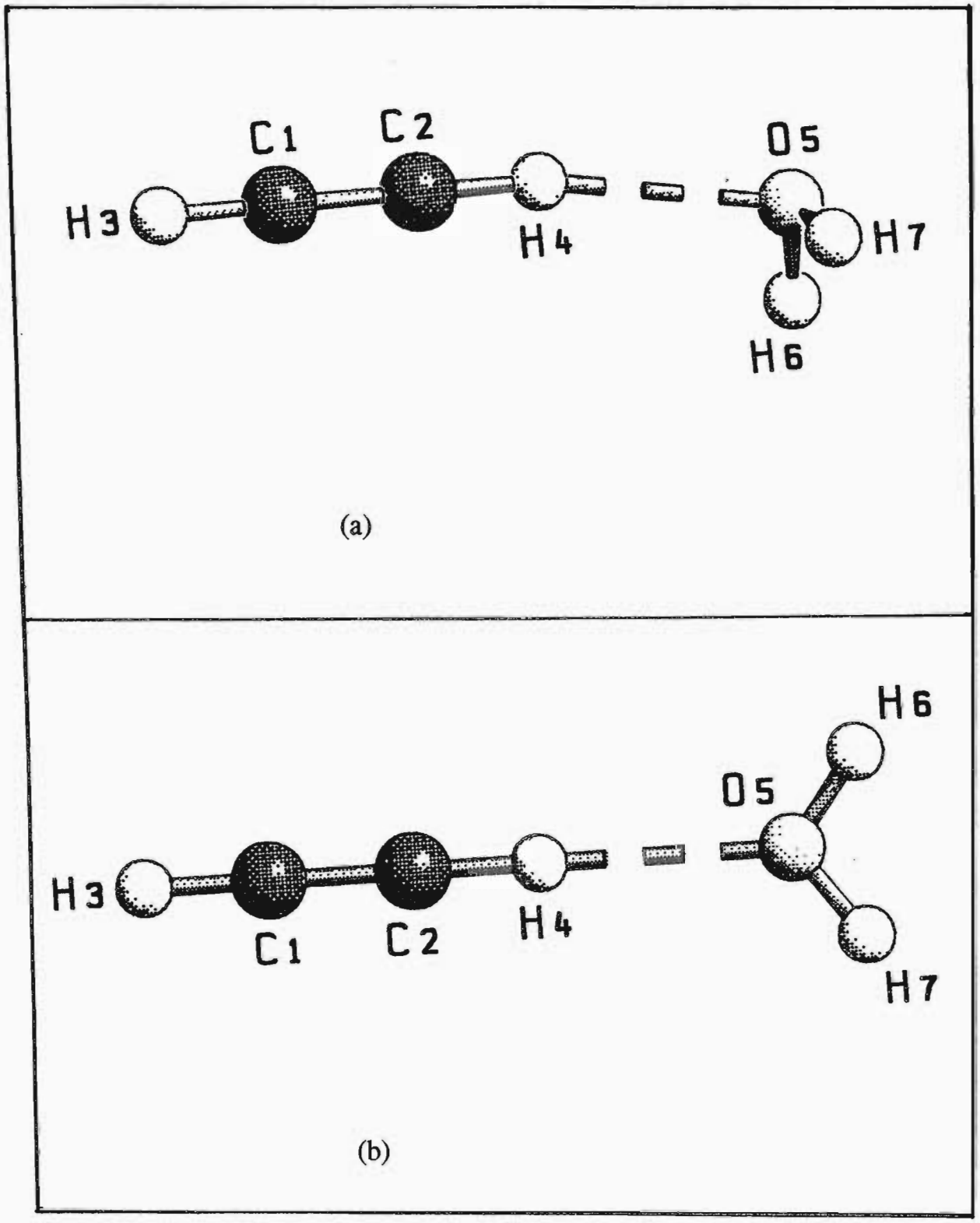

Figure 6.2. Numbering of atoms of the two configurations of the HCCH-OH_2 complex: (a) C_s structure; (b) C_{2v} structure.

saddle point. An attempt to optimise a complex NCCN...HOH always resulted in the final structure collapsing to C_{2v}. Figure 6.3 is a graphical representation of both the planar and the perpendicular C_{2v} structures. Once again the water OH bond length is hardly perturbed, as was observed for the NCH-OH_2 and HCCH-OH_2 complexes. The CC and CN bond lengths also remain virtually the same. The NCC angles are distorted from 180° by about 4°, away from the water OH bonds. The interaction in this case is between the dipole moment of the water and the quadrupole moment of the cyanogen molecule.

The optimised structural parameters of the preferred structure of the CH_3CN-HOH complex are presented in Table 6.2 and Figure 6.4 shows the two conformers of the complex. The preferred structure is the one in which the non-bonded water hydrogen, H9, is eclipsed by the H3 atom of the methyl group (see Figure 6.4). The other isomer is generated by a 180° rotation of the water sub-unit about the CCN axis, and is a transition state. The changes on complexation are minimal. The bonded OH bond length is increased by 0.4 pm, while the HOH angle is decreased by 0.6°. The heavy atom distances, A...B, are predicted to be 310.0, 326.2 and 310.2 pm for the NCH-OH_2, HCCH-OH_2 and CH_3CN-HOH complexes. The hydrogen bond angle, O8H7...N6, deviates from linearity by about 7° for the CH_3CN-HOH complex (see Figure 6.4), compared with 3.4° and 9.9° in the cases of the NCH-OH_2 and HCCH-OH_2 complexes (Figures 6.1 and 6.2). The A...B lengths, excluding that of the C_2N_2-OH_2 complex, confirm the order of complex stability indicated above. It is important to note that the four complexes are not all hydrogen bonded, hence stability comparisons must be made with some caution.

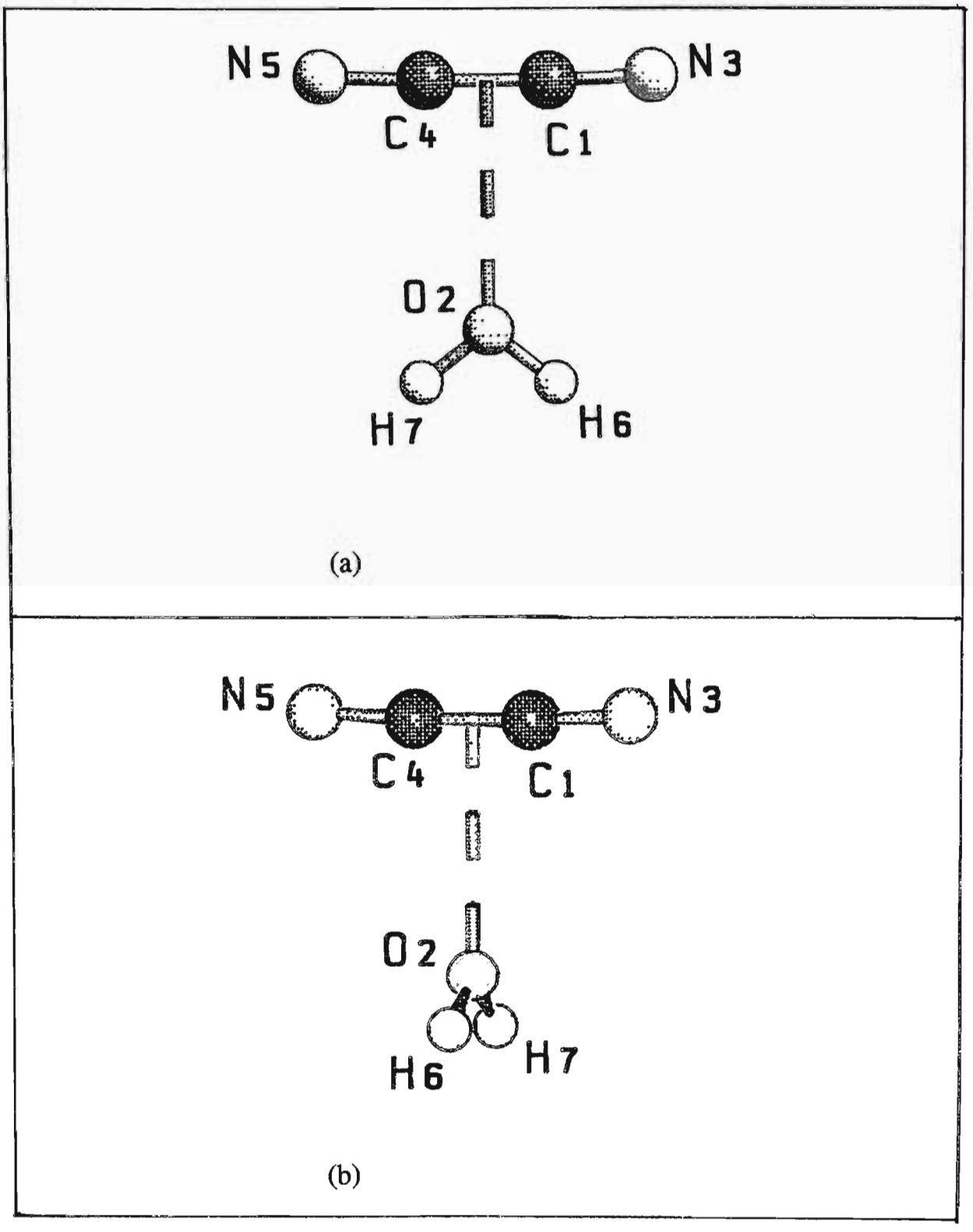

Figure 6.3. Numbering of atoms of the two configurations of the NCCN-OH_2 complex: (a) C_{2v} planar structure; (b) C_{2v} non-planar structure.

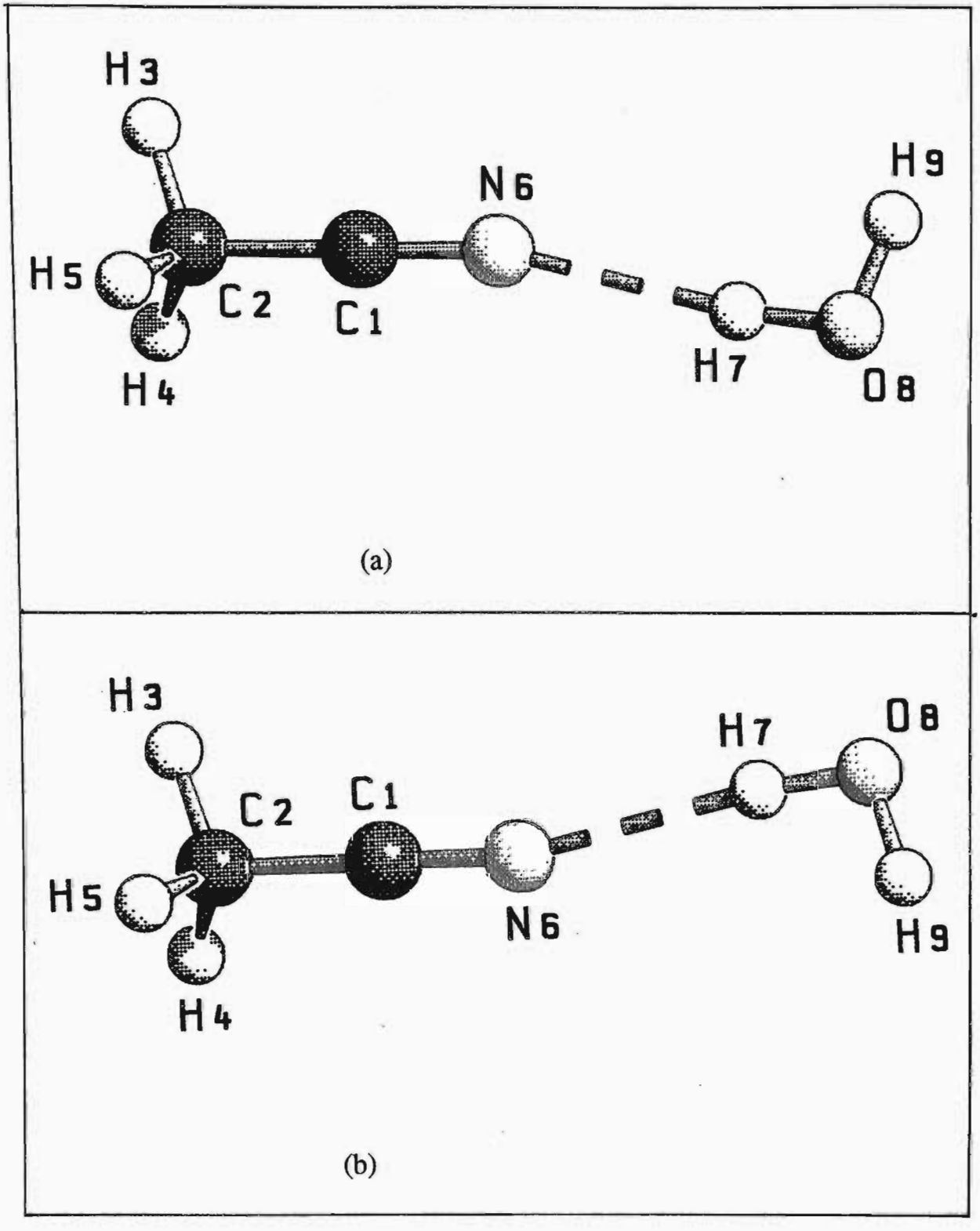

Figure 6.4. Numbering of atoms of the two configurations of the CH_3CN-HOH complex: (a) C_s structure I; (b) C_s structure II.

6.2.2 Interaction Energies and the Morokuma Energy Components

The computed interaction energies of the four complexes are presented in Table 6.3, before and after correcting for BSSE, at both the MP2 and RHF levels of theory. In both cases, the NCH-OH_2 complex is found to be the most strongly bound of the four. Although the C_2N_2-OH_2 and HCCH-OH_2 complexes are more stable than the CH_3CN-HOH complex before correction at the correlated level, the order is reversed after correction. Other computed values of the interaction energies of the C_s structures are in the range -15.86[106] to -27.89[105] kJ mol^{-1} for the NCH-OH_2 and -9.16[106] to -14.58[105] kJ mol^{-1} for the HCCH-OH_2 complexes[136] at comparable levels of theory and using similar basis sets. Thus the computed interaction energies are consistent with most of those reported earlier.

The barriers to internal rotation for all four complexes, computed by taking the energy differences between the structures shown in Figures 6.1(a) and 6.1(b), 6.2(a) and 6.2(b), 6.3(a) and 6.3(b), and 6.4(a), and 6.4(b) are listed in Table 6.4. For the NCH-OH_2 adduct, the rotational barrier of 530 J mol^{-1} is comparable with the value of 690 J mol^{-1} determined experimentally by Gutowsky et al.,[104] but agrees less well with their computed value of 1.20 kJ mol^{-1}. Turi and Dannenberg concluded that the barrier to internal rotation for HCCH-OH_2 is insignificant on the basis of their computations.[107] Lee and co-workers derived a value of 3.41 kJ mol^{-1} as the barrier to internal rotation for the C_2N_2-OH_2 complex.[101] This is significantly higher than our computed value of 2.65 kJ mol^{-1}. The very low barriers to inversion at the oxygen atom in the C_s species confirm the experimental results that the potential energy surfaces are extremely flat, that the complexes are effectively planar, and that a large amplitude wagging motion of the water molecule interconverts the two equivalent non-planar structures through a planar transition state.[103,104,108,109]

Table 6.3. Computed MP2 and RHF Interaction Energies of the Complexes of Water with Hydrogen Cyanide, Acetylene, Cyanogen and Acetonitrile

Complex	Energy /kJ mol^{-1}		
	Uncorrected	BSSE	Corrected
		MP2	
$NCH\text{-}OH_2$	-28.91	6.62	-22.29
$HCCH\text{-}OH_2$	-18.68	6.42	-10.26
$C_2N_2\text{-}OH_2$	-18.25	6.03	-12.22
$CH_3CN\text{-}HOH$	-17.91	2.50	-15.41
		RHF	
$NCH\text{-}OH_2$	-25.74	2.81	-22.93
$HCCH\text{-}OH_2$	-12.42	3.07	-9.34
$C_2N_2\text{-}OH_2$	-13.83	4.29	-9.54
$CH_3CN\text{-}HOH$	-17.91	2.50	-15.41

In $C_2N_2\text{-}OH_2$, internal rotation is much more hindered than in the other two cases discussed above. The rotation of the water component about the CN bond in $CH_3CN\text{-}HOH$ is almost free.

Table 6.4. Computed MP2 Energies and Barriers to Internal Rotation of the Complexes of Water with Hydrogen Cyanide, Acetylene, Cyanogen and Acetonitrile

Complex	Energy/Hartree		Rotational barrier /J mol^{-1}
	Structure I	Structure II	
$NCH\text{-}OH_2$	-169.39697193941	-169.39676857329	530.0
$HCCH\text{-}OH_2$	-153.30856791902	-153.30786451501	1850.0
$C_2N_2\text{-}OH_2$	-261.38425204579	-261.38324276737	2650.0
$CH_3CN\text{-}HOH$	-208.58959381310	-208.58959356401	0.653

The results of the Morokuma energy decomposition scheme[191,192] implemented in the computer program Monstergauss are shown in Table 6.5.

The full interpretation of the energy components has been dealt with by Morokuma.[12] The electrostatic term contributes between 47 and 53% to the total interaction energy in all four complexes. This is the highest stabilising factor. The charge transfer term is the next most significant contributor to the stabilisation energy, ranging from 9 to 17%. The exchange term is repulsive and, as such, is a destabilising component to the interaction energy.

For all four complexes the partitioning of the interaction energy leads to the result that the five components have roughly equal importance, irrespective of whether the interaction is of the hydrogen bonded or EDA type. The implication of this is that there is nothing fundamentally different in the mode of interaction between hydrogen bonded and EDA complexes.

6.2.3 Atomic Charge Redistributions

The electronic populations of the five monomers (water included), and in the four complexes, are reported in Table 6.6. This table also shows the differences, expressed as the charge on an atom in the complex minus its value in the monomer, and the absolute shift of charge from one sub-unit in the complex to the other. Thus positive differences for individual atoms represent decreases of negative charge, or electron density.

Table 6.5. The Uncorrected and Corrected Components of the Interaction Energies of the Complexes of Water with Hydrogen Cyanide, Acetylene, Cyanogen and Acetonitrile, Computed according to the Morokuma Decomposition Scheme

		Energy/kJ mol^{-1}		
Complex	Component	Uncorrected	Corrected	%Contribution
NCH-OH_2	El	-36.58	-36.58	53
	Pl	-3.08	-3.08	5
	Ex	21.12	22.01	31
	Ct	-8.03	-7.13	12
	Mix	0.23	1.96	0.3
	Total	-26.34	-22.82	-
HCCH-OH_2	El	-17.98	-17.98	47
	Pl	-1.24	-1.24	3
	Ex	12.21	13.11	32
	Ct	-6.51	-5.15	17
	Mix	0.30	1.91	0.8
	Total	-13.22	-9.35	-
C_2N_2-OH_2	El	-21.03	-21.03	48
	Pl	-2.05	-2.05	5
	Ex	15.98	17.02	36
	Ct	-4.53	-3.61	10
	Mix	0.41	2.05	0.9
	Total	-11.22	-7.62	-
CH_3CN-HOH	El	-26.12	-26.12	53
	Pl	-2.88	-2.88	6
	Ex	15.81	16.07	32
	Ct	-4.50	-3.83	9
	Mix	0.30	1.36	0.6
	Total	-17.43	-15.41	-

Note :The abbreviations El, Pl, Ex, Ct and Mix stand for electrostatic, polarisation, exchange, charge transfer and mixing terms.

Table 6.6. The Predicted MP2 Atomic Charge Redistributions of the HCN, C_2H_2, C_2N_2 and CH_3CN Monomers and the Corresponding Complexes along with the Differences between the Complex and the Monomer Charges

		Mulliken Charge/e			
Complex	Atom	Complex	Monomer	Difference	Fragment
$NCH\text{-}OH_2$	N1	-0.4485	-0.3863	-0.0622	
	C2	0.1034	0.1124	-0.0090	
	H3	0.3163	0.2740	0.0423	-0.0288
	O4	-0.6804	-0.6738	-0.0066	
	H5,H6	0.3546	0.3369	0.0177	0.0288
$HCCH\text{-}OH_2$	C1	-0.3062	-0.2374	-0.0688	
	C2	-0.2336	-0.2374	0.0038	
	H3	0.2338	0.2374	-0.0036	
	H4	0.2793	0.2374	0.0419	-0.0267
	O5	-0.6666	-0.6738	0.0072	
	H6,H7	0.3466	0.3369	0.0097	0.0266
$C_2N_2\text{-}OH_2$	C1,C4	0.4144	0.3920	0.0224	
	N3,N5	-0.4194	-0.3920	-0.0274	-0.0100
	O2	-0.6870	-0.6738	-0.0132	
	H6,H7	0.3486	0.3369	0.0117	0.0102
$CH_3CN\text{-}HOH$	C1	0.3286	0.2919	0.0367	
	C2	-0.3721	-0.3728	0.0007	
	H3	0.1876	0.1822	0.0054	
	H4,H5	0.1891	0.1822	0.0069	
	N6	-0.5063	-0.4656	-0.0407	0.0160
	O7	-0.7179	-0.6738	-0.0441	
	H8	0.3791	0.3369	0.0422	
	H9	0.3226	0.3369	-0.0143	-0.0162

In the $NCH\text{-}OH_2$ complex, the bridging H3 atom has lost an appreciable amount of charge on complexation, while the nitrogen atom gains some negative charge. The water oxygen unexpectedly gains a small amount of negative charge; this can be attributed to its higher electronegativity compared with the hydrogens which, although they are fairly remote from the active interacting region, still lose some electron density. The fragment charges show that the water

component is positively charged overall in the complex, while HCN is negatively charged, hence water is the electron donor (ED) and proton acceptor (PA), as expected.

In the case of the HCCH-OH_2 complex, the most striking feature is that of the charge depletion on the bridging H4 atom, as in the NCH-OH_2 complex. The other atoms are affected to a relatively small extent. The overall charge distribution shows that the water molecule is again the ED and PA.

The extent of charge transfer associated with the C_2N_2-OH_2 complex is much less than in the other two complexes. There is, however, a marked charge increase on the nitrogen atoms, while the carbon atoms lose charge density. The water fragment is again an electron donor but not a proton acceptor as with the NCH-OH_2 and HCCH-OH_2 complexes. The CH_3CN-HOH complex shows strikingly similar features to those shown by the NCH-OH_2 complex. The nitrogen atom gains some electron density on complexation, while the methyl carbon loses electron density to the nitrile carbon. This charge rearrangement is a result of the methyl hydrogens being slightly acidic. As noted above, the bridging hydrogen has again lost an appreciable amount of charge density. Unlike any of the cases studied so far, this complex provides the feature that the water sub-unit acts as the EA and PD.

6.3 Vibrational Properties of the NCH-OH_2, HCCH-OH_2, C_2N_2-OH_2 and CH_3CN-HOH Complexes

In this section, the predicted vibrational wavenumbers and their shifts, potential

energy distributions, band assignments, infrared intensities and their ratios and the changes in force constants are reported. Comparisons of the parameters among the complexes are made.

6.3.1 Intra- and Intermolecular Wavenumbers

The computed wavenumbers of the water, hydrogen cyanide, acetylene, cyanogen and acetonitrile monomers are listed in Table 6.7, along with their experimental[193,194] counterparts and the calculated/experimental ratios. These ratios are typical for molecules of this complexity calculated at this level of theory with a basis set of the size we have used[84,85,88,89,99,195-203] with the exception of the stretching modes of the multiply bonded groups and the bending vibrations of their associated angles. In these cases the extent of overestimation of the wavenumbers is lower than that normally observed for such vibrations of monomeric species and, indeed, in six cases the computed wavenumbers are actually lower than those determined experimentally. This anomaly is clearly associated with the fact that, in the HCN, C_2H_2, C_2N_2 and CH_3CN monomers, the predicted CN and CC bond lengths were found to be substantially larger than those determined experimentally. In Table 6.8 are collected the local symmetry coordinates, S_i, describing the vibrational modes. The calculated wavenumbers and the complex-monomer wavenumber shifts, together with the percentage potential energy distributions (%PED) and assignments, are reported in Table 6.9.

Table 6.7. Computed and Experimental Wavenumbers of the Water, Hydrogen Cyanide, Acetylene, Cyanogen and Acetonitrile Monomers, and Calculated/Experimental Wavenumber Ratios

Molecule	Symmetry species	Mode	$\tilde{\nu}/cm^{-1}$		$\tilde{\nu}_{calc.}/\tilde{\nu}_{exp.}$
			Calc.	Exp.	
H_2O[a]	a_1	ν_1	3891	3657	1.06
		ν_2	1682	1595	1.06
	b_1	ν_3	4030	3756	1.07
HCN[a]	Σ^+	ν_1	3533	3311	1.07
		ν_2	2039	2097	0.97
	π	ν_3	725	712	1.02
C_2H_2[a]	Σ_g^+	ν_1	3597	3374	1.07
		ν_2	2008	1974	1.02
	Σ_u^+	ν_3	3510	3289	1.07
	π_g	ν_4	435	612	0.71
	π_u	ν_5	746	730	1.02
C_2N_2[b]	Σ_g^+	ν_1	2257	2330	0.97
		ν_2	868	851	1.02
	Σ_u^+	ν_3	2061	2158	0.96
	π_g	ν_4	526	507	1.04
	π_u	ν_5	237	233	1.02
CH_3CN[a]	a_1	ν_1	3150	2954	1.07
		ν_2	2232	2267	0.98
		ν_3	1462	1385	1.06
		ν_4	944	920	1.03
	e	ν_5	3251	3009	1.08
		ν_6	1535	1448	1.06
		ν_7	1089	1041	1.05
		ν_8	355	362	0.98

Calc. : calculated. Exp. : experimental. parameter. [a] Ref. 193. [b] Ref. 194.

Table 6.8. Local Symmetry Coordinate Definitions and Descriptions of the Vibrational Modes for the Binary Complexes of Water with HCN, C_2H_2, C_2N_2 and CH_3CN

Complex	Symmetry Coordinate		Description
NCH-OH_2	S_1	$\{\Delta r_{4,5} + \Delta r_{5,6}\}/\sqrt{2}$	OH_2 s-stretch
	S_2	$\Delta r_{2,3}$	CH stretch
	S_3	$\Delta r_{1,2}$	C≡N stretch
	S_4	$\{2\Delta\delta_{5,4,6} - \Delta\delta_{6,4,3} - \Delta\delta_{5,4,3}\}/\sqrt{6}$	OH_2 bend
	S_5	$\Delta\delta_{1,2,3}$	HCN ip bend
	S_6	$\{\Delta\delta_{6,4,3} + \Delta\delta_{5,4,3}\}/\sqrt{2}$	OH_2 wag
	S_7	$\Delta r_{3,4}$	H...O stretch
	S_8	$\Delta\delta_{2,3,4}$	CH..O ip bend
	S_9	$\Delta\{\Delta r_{4,5} - \Delta r_{5,6}\}/\sqrt{2}$	OH_2 a-stretch
	S_{10}	$\Delta\gamma_{1,2,3,4}$	HCN op bend
	S_{11}	$\{\Delta\delta_{6,4,3} - \Delta\delta_{5,4,3}\}/\sqrt{2}$	OH_2 twist
	S_{12}	$\Delta\tau_{2,3,4,5}$	torsion about H...O axis

Table 6.8 (continued)

$HCCH\text{-}OH_2$	S_1	$\{\Delta r_{5,6} + \Delta r_{5,7}\}/\sqrt{2}$	OH_2 s-stretch
	S_2	$\{\Delta r_{1,3} + \Delta r_{2,4}\}/\sqrt{2}$	CH s-stretch
	S_3	$\{\Delta r_{1,3} - \Delta r_{2,4}\}/\sqrt{2}$	CH a-stretch
	S_4	$\Delta r_{1,2}$	C≡C stretch
	S_5	$\Delta\delta_{6,5,7}$	HOH bend
	S_6	$\{\Delta\delta_{3,1,2} - \Delta\delta_{4,2,1}\}/\sqrt{2}$	HCC ip bend out-of-phase
	S_7	$\{\Delta\delta_{3,1,2} + \Delta\delta_{4,2,1}\}/\sqrt{2}$	HCC ip bend in-phase
	S_8	$\{\Delta\delta_{4,5,6} + \Delta\delta_{4,5,7}\}/\sqrt{2}$	OH_2 wag
	S_9	$\Delta r_{4,5}$	H...O stretch
	S_{10}	$\Delta\delta_{2,4,5}$	CH...O ip bend
	S_{11}	$\{\Delta r_{5,6} - \Delta r_{5,7}\}/\sqrt{2}$	OH_2 a-stretch
	S_{12}	$\{\Delta\gamma_{3,1,2,4} + \Delta\gamma_{4,2,1,3}\}/\sqrt{2}$	HCC op bend in-phase
	S_{13}	$\{\Delta\delta_{4,5,6} - \Delta\delta_{4,5,7}\}/\sqrt{2}$	OH_2 twist
	S_{14}	$\{\Delta\tau_{7,5,4,2} + \Delta\tau_{6,5,4,2}\}/\sqrt{2}$	torsion about H...O axis
	S_{15}	$\Delta\gamma_{5,4,2,1}$	CH...O op bend

Table 6.8 (continued)

C_2N_2-OH_2	S_1	$\{\Delta r_{2,6} + \Delta r_{2,7}\}/\sqrt{2}$	OH_2 s-stretch
	S_2	$\{\Delta r_{1,3} + \Delta r_{4,5}\}/\sqrt{2}$	C≡N s-stretch
	S_3	$\{2\Delta\delta_{6,2,7} - \Delta\delta_{1,2,6} - \Delta\delta_{4,2,7}\}/\sqrt{6}$	OH_2 bend
	S_4	$\Delta r_{1,4}$	CC stretch
	S_5	$\{\Delta\delta_{3,1,4} + \Delta\delta_{5,4,1}\}/\sqrt{2}$	NCC ip bend in-phase
	S_6	$\{\Delta r_{1,2} + \Delta r_{2,4}\}/\sqrt{2}$	O...C s-stretch
	S_7	$\{\Delta\tau_{6,2,1,3} + \Delta\tau_{7,2,4,5}\}/\sqrt{2}$	torsion in-phase
	S_8	$\{\Delta\gamma_{6,2,4,5} + \Delta\gamma_{7,2,1,3}\}/\sqrt{2}$	OH_2 wag
	S_9	$\{\Delta r_{2,6} - \Delta r_{2,7}\}/\sqrt{2}$	OH_2 a-stretch
	S_{10}	$\{\Delta r_{1,3} - \Delta r_{4,5}\}/\sqrt{2}$	C≡N a-stretch
	S_{11}	$\{\Delta\delta_{3,1,4} - \Delta\delta_{5,4,1}\}/\sqrt{2}$	C_2N_2 libration
	S_{12}	$\{\Delta\tau_{6,2,1,3} - \Delta\tau_{7,2,4,5}\}/\sqrt{2}$	torsion out-of-phase
	S_{13}	$\{\Delta\delta_{1,2,6} - \Delta\delta_{4,2,7}\}/\sqrt{2}$	OH_2 rock
	S_{14}	$\{\Delta\gamma_{6,2,4,5} - \Delta\gamma_{7,2,1,3}\}/\sqrt{2}$	OH_2 twist
	S_{15}	$\{\Delta r_{1,2} - \Delta r_{2,4}\}/\sqrt{2}$	O...C a-stretch

Table 6.8 (continued)

CH_3CN-HOH	S_1	$\{\Delta r_{7,8} - \Delta r_{8,9}\}/\sqrt{2}$	OH_2 a-stretch
	S_2	$\{\Delta r_{7,8} + \Delta r_{8,9}\}/\sqrt{2}$	OH_2 s-stretch
	S_3	$\{2\Delta r_{1,3} - \Delta r_{1,4} - \Delta r_{1,5}\}/\sqrt{6}$	CH_3 d-stretch
	S_4	$\{\Delta r_{1,3} + \Delta r_{1,4} + \Delta r_{1,5}\}/\sqrt{3}$	CH_3 s-stretch
	S_5	$\Delta r_{1,2}$	CC stretch
	S_6	$\Delta\delta_{7,8,9}$	HOH bend
	S_7	$\{2\Delta\delta_{4,1,5} - \Delta\delta_{3,1,4} - \Delta\delta_{3,15}\}/\sqrt{6}$	CH_3 d-deform
	S_8	$\{\Delta\delta_{3,1,4} + \Delta\delta_{3,1,5} + \Delta\delta_{4,1,5} - \Delta\beta_{3,1,2} - \Delta\beta_{4,1,2} - \Delta\beta_{5,1,2}\}/\sqrt{6}$	CH_3 s-deform
	S_9	$\{2\Delta\beta_{3,1,2} - \Delta\beta_{4,1,2} - \Delta\beta_{5,1,2}\}/\sqrt{6}$	CH_3 ip rock
	S_{10}	$\Delta r_{2,6}$	C≡N stretch
	S_{11}	$\Delta\delta_{1,2,6}$	CCN ip bend
	S_{12}	$\Delta\delta_{6,7,8}$	O-H...N ip bend
	S_{13}	$\Delta r_{6,7}$	H...N stretch
	S_{14}	$\Delta\delta_{2,6,7}$	C≡N...H ip bend
	S_{15}	$\{\Delta r_{1,4} - \Delta r_{15}\}/\sqrt{2}$	CH_3 d-stretch
	S_{16}	$\{\Delta\delta_{3,1,4} - \Delta\delta_{315}\}/\sqrt{2}$	CH_3 d-deform
	S_{17}	$\{\Delta\beta_{4,1,2} - \Delta\beta_{512}\}/\sqrt{2}$	CH_3 op rock
	S_{18}	$\Delta\gamma_{6,2,1,3}$	CCN op bend
	S_{19}	$\Delta\gamma_{7,6,1,2}$	C≡N...H op bend
	S_{20}	$\Delta\tau_{8,7,6,1}$	torsion about H...N bond
	S_{21}	$\Delta\gamma_{9,8,7,6}$	HOH hindered rotation

a : antisymmetric, s : symmetric, deform. : deformation, ip : in-plane, op : out-of-plane, d : degenerate.

Table 6.9. Computed Wavenumbers of the Complexes of Water with HCN, C_2H_2, C_2N_2 and CH_3CN and the Complex-Monomer Wavenumber Shifts

Complex	Symmetry species	Mode	Wavenumber /cm^{-1}	Shift /cm^{-1}	%PEDs
NCH-OH_2	a'	ν_1	3887	-4	$100S_1$
		ν_2	3390	-143	$93S_2$
		ν_3	2039	0	$93S_3$
		ν_4	1676	-6	$93S_4$
		ν_5	872	147	$66S_5 + 19S_8$
		ν_6	209	IM	$53S_6 + 45S_4$
		ν_7	165	IM	$91S_7$
		ν_8	118	IM	$47S_6 + 41S_4$
	a"	ν_9	4020	-10	$100S_9$
		ν_{10}	929	204	$76S_{10} + 20S_{12}$
		ν_{11}	292	IM	$86S_{11} + 13S_{10}$
		ν_{12}	122	IM	$79S_{12} + 13S_{11}$

Table 6.9 (continued)

C_2H_2-OH_2	a'	ν_1	3880	-11	$100S_1$
		ν_2	3564	-33	$81S_2 + 13S_3$
		ν_3	3441	-69	$85S_3 + 12S_2$
		ν_4	1990	-18	$93S_4$
		ν_5	1677	-5	$97S_5$
		ν_6	835	89	$80S_6 + 14S_{10}$
		ν_7	493	58	$73S_7 + 14S_6 + 11S_{10}$
		ν_8	215	IM	$88S_8$
		ν_9	131	IM	$91S_9$
		ν_{10}	91	IM	$65S_{10} + 18S_8 + 10S_7$
	a"	ν_{11}	4016	-14	$100S_{11}$
		ν_{12}	873	127	$46S_{12} + 32S_{15} + 18S_{14}$
		ν_{13}	516	81	$58S_{12} + 30S_{15}$
		ν_{14}	242	IM	$79S_{13} + 20S_{15}$
		ν_{15}	99	IM	$63S_{14} + 23S_{13} + 13S_{15}$

Table 6.9 (continued)

C_2N_2-OH_2	a_1	ν_1	3886	-5	$100S_1$
		ν_2	2267	10	$71S_2 + 28S_4$
		ν_3	1672	-10	$98S_3$
		ν_4	868	0	$73S_4 + 26S_2$
		ν_5	245	8	$89S_5 + 10S_7$
		ν_6	122	IM	$94S_6$
	a_2	ν_7	533	7	$85S_7 + 14S_8$
		ν_8	117	IM	$50S_8 + 49S_7$
	b_1	ν_9	246	9	$97S_{12}$
		ν_{10}	39	IM	$50S_{14} + 49S_{12}$
	b_2	ν_{11}	4024	-6	$100S_9$
		ν_{12}	2069	8	$100S_{10}$
		ν_{13}	519	-7	$92S_{11}$
		ν_{14}	174	IM	$87S_{13} + 12S_{15}$
		ν_{15}	24	IM	$51S_{15} + 48S_{13}$

Table 6.9 (continued)

CH_3CN-HOH	a'	ν_1	4005	-25	$94S_1$
		ν_2	3868	-23	$93S_2$
		ν_3	3254	3	$46S_3 + 43S_9$
		ν_4	3152	2	$56S_4 + 39S_8$
		ν_5	2244	12	$65S_5 + 19S_4$
		ν_6	1709	27	$94S_6$
		ν_7	1532	-3	$71S_7 + 13S_9$
		ν_8	1462	0	$47S_8 + 29S_4 + 12S_5$
		ν_9	1089	0	$52S_9 + 46S_3$
		ν_{10}	948	4	$39S_{10} + 39S_5 + 15S_4$
		ν_{11}	354	-1	$60S_{11} + 20S_9 + 17S_3$
		ν_{12}	254	IM	$78S_{12} + 10S_6$
		ν_{13}	131	IM	$94S_{13}$
		ν_{14}	29	IM	$76S_{14} + 22S_{12}$
	a"	ν_{15}	3255	4	$46S_{15} + 43S_{17}$
		ν_{16}	1532	-3	$71S_{16} + 15S_{15} + 13S_{17}$
		ν_{17}	1088	-1	$51S_{17} + 45S_{15}$
		ν_{18}	417	IM	$69S_{21} + 18S_{20}$
		ν_{19}	350	-5	$48S_{19} + 29S_{18}$
		ν_{20}	34	IM	$65S_{20} + 33S_{21}$
		ν_{21}	2	IM	$56S_{21} + 31S_{20}$

The intramolecular H_2O shifts in the NCH-OH_2 complex are negligible. The HCN fragment modes show quite substantial shifts, -143 cm^{-1} for the C2H3 stretching vibration and 147 cm^{-1} and 204 cm^{-1} for the a' and a" components of the HCN bending mode respectively.

These shifts are consistent with a hydrogen bonded structure of moderate strength with the HCN molecule donating a proton to H_2O.[8b] In the C_2H_2-OH_2 complex, the water OH stretching modes are perturbed slightly more than those in the NCH-OH_2 adduct, but the shifts of the acetylene sub-unit are significantly smaller, as shown in Table 6.9. The lower of the two CH stretching modes, which is derived from the antisymmetric vibration of the monomer, but which involves a greater contribution from the bonded CH group, is red-shifted by -69 cm^{-1} and the second CH stretching vibration, which correlates with the symmetric CH mode and is dominated by the non-bonded CH group, by -33 cm^{-1} in the same direction.

Of the two degenerate CCH bending modes of the free C_2H_2 molecule, the higher frequency (π_u) vibration splits into an a' (ν_6, blue-shifted by 89 cm^{-1}) and an a" mode (ν_{12}, shifted to higher wavenumber by 127 cm^{-1}), while the corresponding motions derived from the π_g mode are shifted towards the blue by 58 cm^{-1} (ν_7, a') and 81 cm^{-1} (ν_{13}, a") respectively. The CC stretching vibration in the complex undergoes a slight shift of -18 cm^{-1} relative to the monomer (compared with the CN mode in NCH-OH_2 which is unshifted from its value in free HCN). The smaller perturbations of the vibrational spectrum of C_2H_2, compared with HCN, are consistent with a lower hydrogen bond energy for C_2H_2-OH_2 (ca. 12 kJ mol^{-1} lower).

The vibrational spectrum of the C_2N_2-OH_2 complex indicates that there is a

significant difference in the mode of bonding in C_2N_2-OH_2 from that observed in the NCH-OH_2 and HCCH-OH_2 complexes, since none of the vibrational wavenumbers of this complex is displaced by more than 10 cm^{-1}. This precludes a hydrogen bonding interaction, for which some of the modes, at least, should suffer much larger shifts on complexation.[8b] The vibrational data therefore confirm the electron donor-acceptor nature of the interaction deduced from the gas-phase radiofrequency and microwave spectra.[101] It is important to note that, despite the vibrational wavenumber shifts being markedly smaller than those in HCCH-OH_2, the computed interaction energy is nevertheless slightly greater, by about 2 kJ mol^{-1}; this illustrates the fact that, while interaction energies are good predictors of hydrogen bond wavenumber shifts for interactions of the same type, the use of such energies when comparing different modes of interaction should be used with caution.

The CH_3CN-HOH complex shows vibrational wavenumber shifts less than those shown by the NCH-OH_2 and C_2H_2-OH_2 complexes respectively, but greater than those predicted for the C_2N_2-OH_2 complex. Unlike any of the cases discussed above, it is the water sub-unit which undergoes the most significant shifts on complexation. The antisymmetric stretching vibration mode of H_2O is red shifted by -25 cm^{-1} and the symmetric stretching mode by about a similar magnitude (-23 cm^{-1}) in the same direction. The water bend is blue shifted, by 27 cm^{-1}, while it suffers small red-shifts of 5, 6 and 10 cm^{-1} for the NCH-OH_2, HCCH-OH_2 and C_2N_2-OH_2 complexes.

The vibrational wavenumber changes, in particular those of the water component, indicate yet a different type of hydrogen bonding. Figure 6.4(a) illustrates the case of a hydrogen bonded complex with water donating a proton to the acetonitrile molecule. This is further confirmed by a slight blue shift of the CN

vibrational wavenumber (by 12 cm^{-1}). The rest of the modes are hardly perturbed.

The forms of the complex modes which correlate with the intramolecular vibrations of the monomer fragments are very little changed from those in the free monomers and for that reason they will not be illustrated graphically. The intermolecular modes are heavily coupled, and include substantial contributions from both monomer sub-units. The forms of the intermolecular modes are illustrated by means of Schakal-92 plots in Figures 6.5 and 6.6, which also include the orientations of the Cartesian axes used to describe these vibrations.

Only the graphical representations of the intermolecular modes (IMs) corresponding to the NCH-OH_2 and C_2N_2-OH_2 complexes are presented here, because of the fact that the forms of the HCCH-OH_2 IM modes are very similar to those of NCH-OH_2, while the C_2N_2-OH_2 complex has a different structure and thus a different pattern of vibrational modes is anticipated. Here too, illustrations of the IMs are presented. The IMs of CH_3CN-HOH are not included, because the forms of the modes are fairly simple, and a pictorial illustration will not make the descriptions any clearer.

The assignments of the intermolecular modes of each complex were made with the aid of the Vibra and Vibram programs.[204] In the NCH-OH_2 and HCCH-OH_2 complexes, which have C_s symmetry, the intermolecular modes transform in each case as 3a'+ 2a", with the wagging motion of the water components occurring at 209 and 215 cm^{-1} respectively. The ν(H...B) hydrogen bond stretching mode occurs at 165 and 131 cm^{-1} and is 91% pure in the NCH-OH_2 and HCCH-OH_2 complexes respectively.

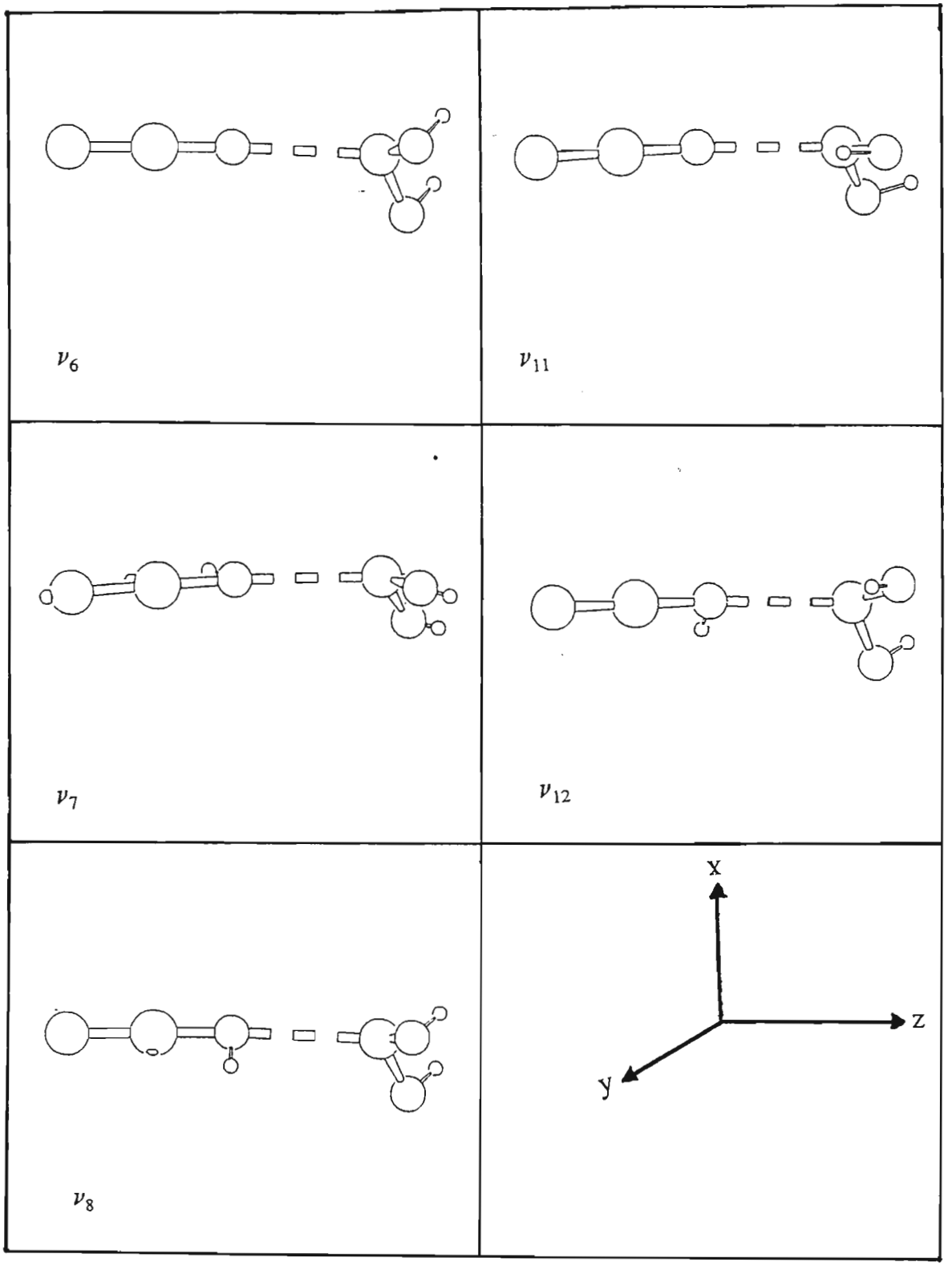

Figure 6.5. Pictorial representations of the intermolecular modes of the NCH-OH_2 complex.

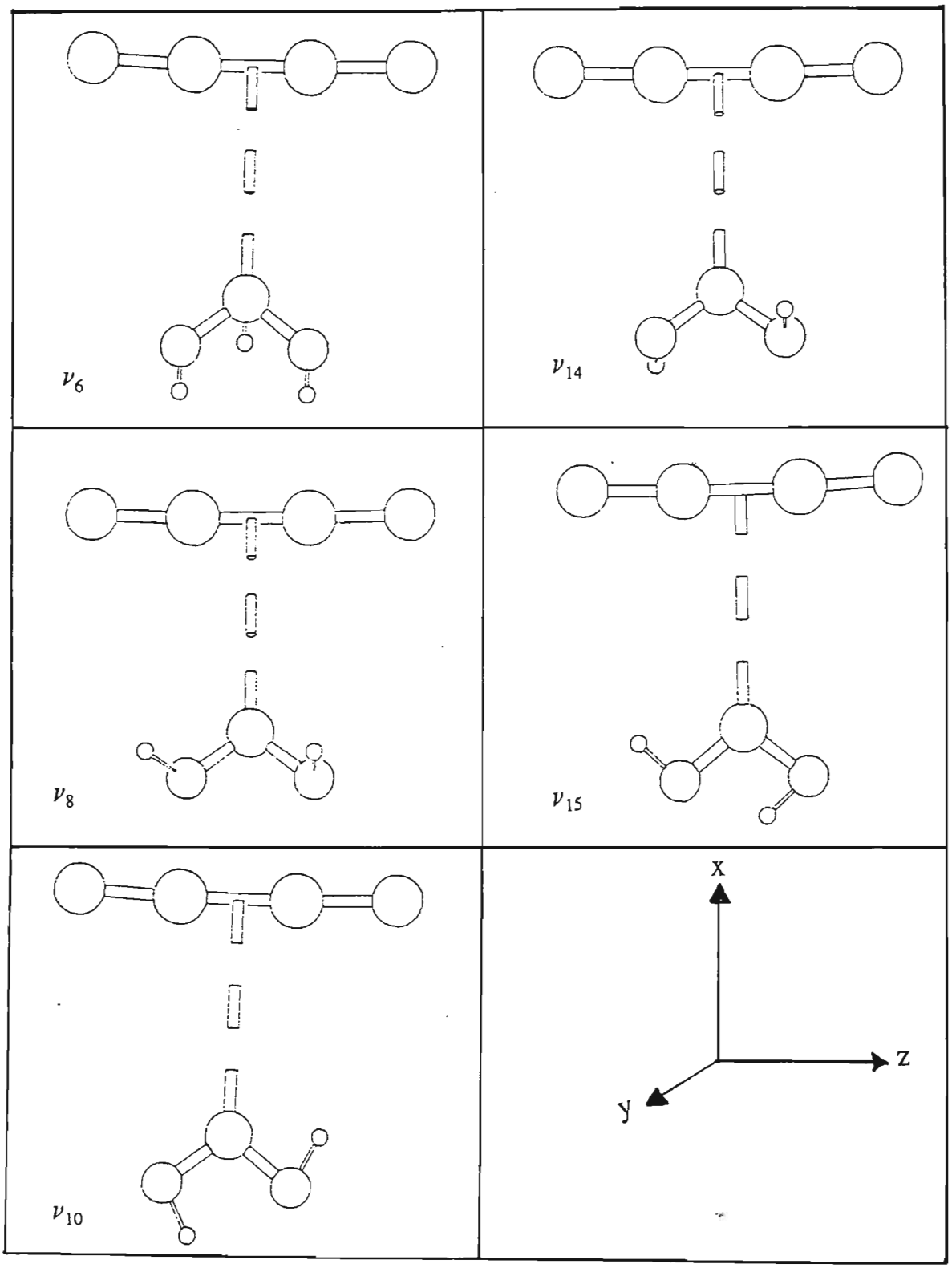

Figure 6.6. Pictorial representations of the intermolecular modes of the $NCCN\text{-}OH_2$ complex.

The in-plane bending, δ(A-H...B), motion is observed at 118 cm^{-1} for the NCH-OH_2 complex coupling heavily with both the water sub-unit wagging and the HOH deformation vibrational modes, as shown in Table 6.9. For the HCCH-OH_2 complex, δ(A-H...B) occurs at 91 cm^{-1} with 65% purity, coupled with 18% water wagging and 10% in-phase bending of the HCC angles. The wavenumber corresponding to the ν(H...B) motion indicates that of the two complexes, NCH-OH_2 is the stronger.

The two out-of-plane motions in the NCH-OH_2 and HCCH-OH_2 complexes correspond to the OH_2 twisting and hydrogen bond torsional modes, where the twisting vibration occurs at a higher wavenumber, 292 cm^{-1}, for the stronger complex (NCH-OH_2) and at 242 cm^{-1} for the weaker adduct (HCCH-OH_2).

In the C_2N_2-OH_2 complex, which has C_{2v} symmetry, the IMs are distributed as $a_1 + a_2 + b_1 + 2b_2$, with the ν(O...CC) mode occurring at 122 cm^{-1}, a fairly low wavenumber in comparison with the NCH-OH_2 and HCCH-OH_2 complexes. The a_2 symmetry mode at 117 cm^{-1} is a 50% in-phase coupling of water wagging with 49% hydrogen bond torsion (see Figure 6.6) and the b_1 mode at 39 cm^{-1} is an out-of-phase combination of 50% twisting and 49% hydrogen bond torsion.

The water rocking motion at 174 cm^{-1} is 87% pure, with a 12% contribution from the antisymmetric stretching of the C1...O2 and C4...O2 bonds defining the ν(O...CC) mode (see Figure 6.6). The lowest of the IMs, of b_2 type, is observed at 24 cm^{-1}, and is 51% ν(O...CC) and 48% H_2O rocking.

The six intermolecular modes of the CH_3CN-HOH complex span 3a' + 3a", instead of the usual sum of five IMs for complexes involving a linear sub-unit. While in the cases of the NCH-OH_2 and HCCH-OH_2 complexes, C-H...O type

of hydrogen bonding was observed and O...CC bonding was found in the case of C_2N_2-OH_2, in the complex of water with acetonitrile an O-H...N hydrogen bonding interaction occurs, and as such some differences in the IMs are expected. Of all the IMs of the NCH-OH_2 and HCCH-OH_2 complexes, the a' wagging motion of the water sub-unit occurs with the largest vibrational frequency. However in the CH_3CN-HOH complex, the a' bending of the C1N6...H7 angle has the highest wavenumber, 254 cm^{-1}, with a purity of 78% and with a 10% contribution from the HOH deformation. The ν(H7...N6) mode is observed at 131 cm^{-1}, and is lower than the corresponding IM in the NCH-OH_2 complex, while it is equal to that of the HCCH-OH_2 complex. The mode at 29 cm^{-1} is a combination of 76% C1N6...H7 and 22% O8H7...N6 angle bends.

All the a" motions are associated with the attempted rotation of the water sub-unit about the N6...H7 bond. The band at 417 cm^{-1} corresponds to 69%S_{21} and 18%S_{20}, hindered HOH rotation coupled with torsional motion about the H7...N6 bond, while the band at 34 cm^{-1} is described by the same coordinates but with differing contributions. The vibrational mode with a wavenumber of 2 cm^{-1} is a rotation of both sub-units in opposite directions with heavy coupling from torsion about the hydrogen bond axis.

The similarities between the IM vibrational properties of the complexes NCH-OH_2 and HCCH-OH_2 are remarkable. In each case the highest frequency vibration is the H_2O twisting, followed by the wagging, then the inter-monomer stretching mode. The actual magnitudes of these wavenumbers are also fairly similar. The in-plane hydrogen bond bending is the lowest frequency mode, with the out-of-plane counterpart only slightly higher. For the C_2N_2-OH_2 adduct, the pattern is different due to the different structure, with the H_2O rocking mode coupled with the librational motion of the C_2N_2 molecule having the highest

vibrational frequency. Next is the inter-monomer stretching mode, followed by the wagging of the water component.

The forms of the IMs of the acetonitrile-water complex do not show the patterns of those of either NCH-OH_2 or HCCH-OH_2, but instead the highest frequency mode corresponds to the H9O8H7..N6 out-of-plane bending, followed by the in-plane bending of the same angle, then the inter-monomer stretching at 131 cm^{-1}, with 94% purity.

It has been observed that the wavenumbers of the highest IMs correlate well with the strength of the interaction;[205] this is also true of the complexes of water with HCN, C_2H_2 and CH_3CN. In all four binary complexes the ν(H...B) mode is the least strongly coupled, thus enhancing the potential of using this band as a probe of hydrogen bond strength.

6.3.2 Intra- and Intermolecular Intensities

Table 6.10 shows the computed infrared band intensities of the five monomers H_2O, HCN, C_2H_2, C_2N_2 and CH_3CN and the experimental intensities reported in the literature.[206-212] The intensities of infrared absorption bands cover a wide range of orders of magnitude. As a result, it is more meaningful to compare the calculated and experimental intensities through their ratios rather than their differences. Table 6.10 thus shows the calculated/experimental ratios for the five monomers. Most ratios lie in a range corresponding to a factor of 2 difference on either side of the experimental intensity value; this level of agreement is considered acceptable.[213] Notable exceptions are the C≡N stretching mode of

Table 6.10. Computed and Experimental Band Intensities of the Water, Hydrogen Cyanide, Acetylene, Cyanogen and Acetonitrile Monomers, and the Calculated/Experimental Intensity Ratios

Molecule	Symmetry species	Mode	A/km mol^{-1}		$A_{Calc.}/A_{Exp.}$
			Calc.	Exp.	
H_2O	a_1	ν_1	4.2	2.2[a]	1.9
		ν_2	77.7	53.6[a]	1.5
	b_1	ν_3	33.8	44.6[a]	0.8
HCN	Σ^+	ν_1	66.0	62.3[b]	1.1
		ν_2	0.21	0.03[b]	7.0
	π	ν_3	36.1	57.7[c]	0.6
C_2H_2	Σ_g^+	ν_1	0.0	-	-
		ν_2	0.0	-	-
	Σ_u^+	ν_3	87.2	26.25[d]	3.3
	π_g	ν_4	0.0	-	-
	π_u	ν_5	80.5	177.1[e]	0.5
C_2N_2	Σ_g^+	ν_1	0.0	-	-
		ν_2	0.0	-	-
	Σ_u^+	ν_3	12.6	4.55[f]	2.8
	π_g	ν_4	0.0	-	-
	π_u	ν_5	18.8	36.28[f]	0.5
CH_3CN[g]	a_1	ν_1	3.2	2.74	1.2
		ν_2	0.3	2.52	0.1
		ν_3	1.5	1.14	1.3
		ν_4	1.6	2.52	0.6
	e	ν_5	1.3	3.01	0.4
		ν_6	9.0	23.02	0.4
		ν_7	1.7	3.13	0.5
		ν_8	0.8	1.68	0.5

Calc. : calculated. Exp. : experimental. [a] Ref. 206. [b] Ref. 207. [c] Ref. 208. [d] Ref. 209. [e] Ref. 210. [f] Ref. 211. [g] Ref. 212.

HCN and the antisymmetric CH and C≡N stretching modes[207,209,211] of C_2H_2 and C_2N_2 respectively. The principal error is not necessarily associated with the

theoretically determined intensities, however, since the difficulties inherent in their experimental determination are notorious. The computed intensities of the four binary complexes of water with HCN, C_2H_2, C_2N_2 and CH_3CN are presented in Table 6.11, with the complex/monomer intensity ratios for the intramolecular bands. In the NCH-OH_2 complex, the major change is in the intensity of the C≡N stretching mode, ν_3, but the ratio is overestimated in this case because of the expected error associated with the very low value calculated for the monomer intensity. The CH stretching intensity, ν_2, increases by a factor of over 5, consistent with normal expectation,[214] since this is the mode most affected by hydrogen bonding. The symmetric OH_2 stretching vibration, ν_1, also shows a noticeable intensity increase, but those of the other bands are hardly affected by the hydrogen bonding interaction.

Table 6.11 shows that the perturbation of the monomer intensities is small for the HCCH-OH_2 complex. The intensity ratios of those complex modes derived from the infrared inactive vibrations are not included in this discussion. The bonded C2H4 stretching band increases in intensity (see Figure 6.2), as was the case for the C2H3 bond of the NCH-OH_2 complex, but by a factor of only 2.83 compared with 5.56 for the NCH-OH_2 complex. This is consistent with the weaker hydrogen bonding interaction in the HCCH-OH_2 complex. The two OH_2 stretching modes of the water sub-unit increase in intensity, again as found for the NCH-OH_2 adduct, and again the change is greater for the symmetric than for the antisymmetric mode. The bending intensity in HCCH-OH_2 remains unchanged, having increased very little in the NCH-OH_2 complex.

Table 6.11. Computed Band Intensities of the Complexes of H_2O with HCN, C_2H_2, C_2N_2 and CH_3CN and the Complex/Monomer Intensity Ratios

Complex	Symmetry species	Mode	A/km mol^{-1} Complex	A_c/A_m
NCH-OH_2	a'	ν_1	17.1	4.07
		ν_2	366.8	5.56
		ν_3	11.8	53.33
		ν_4	73.8	0.95
		ν_5	42.1	1.17
		ν_6	263.0	IM
		ν_7	7.0	IM
		ν_8	44.2	IM
	a"	ν_9	62.6	1.85
		ν_{10}	41.6	1.15
		ν_{11}	48.5	IM
		ν_{12}	3.6	IM
C_2H_2-OH_2	a'	ν_1	12.7	3.02
		ν_2	0.24	*
		ν_3	246.5	2.83
		ν_4	5.9	*
		ν_5	77.7	1.00
		ν_6	74.9	0.93
		ν_7	5.8	*
		ν_8	271.0	IM
		ν_9	22.4	IM
		ν_{10}	42.6	IM
	a"	ν_{11}	49.3	1.46
		ν_{12}	66.4	0.82
		ν_{13}	8.1	*
		ν_{14}	4.5	IM
		ν_{15}	2.2	IM

Table 6.11 (continued)

C_2N_2-OH_2	a_1	ν_1	10.4	2.48
		ν_2	0.12	*
		ν_3	76.8	0.99
		ν_4	0.04	*
		ν_5	29.0	1.54
		ν_6	0.02	IM
	a_2	ν_7	0	*
		ν_8	0	IM
	b_1	ν_9	34.8	1.85
		ν_{10}	277.4	IM
	b_2	ν_{11}	51.4	1.52
		ν_{12}	8.8	0.70
		ν_{13}	0.01	*
		ν_{14}	52.5	IM
		ν_{15}	18.5	IM
CH_3CN-HOH	a'	ν_1	120.7	3.6
		ν_2	161.1	38.4
		ν_3	0.45	0.35
		ν_4	1.70	0.52
		ν_5	0.07	0.28
		ν_6	93.1	1.20
		ν_7	9.8	1.09
		ν_8	1.3	0.89
		ν_9	2.0	1.20
		ν_{10}	3.5	2.22
		ν_{11}	2.0	3.45
		ν_{12}	89.7	IM
		ν_{13}	2.3	IM
		ν_{14}	5.6	IM
	a"	ν_{15}	0.38	0.29
		ν_{16}	9.8	1.09
		ν_{17}	2.0	1.20
		ν_{18}	170.9	IM
		ν_{19}	2.0	3.4
		ν_{20}	56.7	IM
		ν_{21}	29.3	IM

* : division by zero.

A similar pattern of intensity behaviour is found for the C_2N_2-OH_2 complex, as shown in Table 6.11. Of the infrared active counterparts of the cyanogen modes, the antisymmetric C≡N stretching band loses intensity, while the two bending modes increase, but by a larger factor than in either NCH-OH_2 or HCCH-OH_2. The antisymmetric stretching intensity, ν_{11}, of the C_2N_2-OH_2 complex increases substantially by about 50% and the bending mode remains virtually unchanged.

The major intensity changes of the CH_3CN-HOH complex occur in the water sub-unit, with the symmetric stretching intensity increasing by a factor of 38, about 11 times more than the average intensity ratio of the NCH-OH_2, HCCH-OH_2 and C_2N_2-OH_2 complexes.

The huge change in the intensity ratio of $\nu_s(OH_2)$ for the CH_3CN-HOH complex is consistent with the observation that the water molecule is a PD in this complex as opposed to NCH-OH_2 and HCCH-OH_2, where the water molecule acted as a PA, and still further, in C_2N_2-OH_2 where the H_2O molecule acted neither as a PA nor a PD. The antisymmetric stretching intensity ratio of the water component is about twice the average value of structures NCH-OH_2, HCCH-OH_2 and C_2N_2-OH_2 for the same vibrational mode, again confirming the view that with CH_3CN-HOH the interaction is of a different type from any of the other types mentioned above. The intensity ratio of the water HOH deformation mode is slightly increased, but is still comparable with those of NCH-OH_2, HCCH-OH_2 and C_2N_2-OH_2. The patterns of the intensity changes confirm the conclusion that the nature of the participation of the water molecule is almost identical in the NCH-OH_2 and HCCH-OH_2 complexes, and fairly different in the C_2N_2-OH_2 complex and in CH_3CN-HOH. The differences between the extent of perturbation of the spectra of HCN, C_2H_2, C_2N_2 and CH_3CN and H_2O, however, serve to illustrate the different modes of bonding in

9NCH-OH_2, HCCH-OH_2, C_2N_2-OH_2 and CH_3CN-HOH.

With no corresponding experimental intensities available for the IMs, the comparisons will be made between the complexes. The IM intensities are included in Table 6.11, referred to as IM. The water wagging motion, ν_6, has the highest intensity for the three complexes NCH-OH_2, HCCH-OH_2 and C_2N_2-OH_2. This is in accord with other complexes containing water.[84,199] Moreover the intensity value is almost identical in all three complexes. The in-plane bending mode of the CH...O angle in NCH-OH_2 and HCCH-OH_2 show essentially identical intensities, while the inter-monomer stretching intensity is 7.0 and 22.4 km mol^{-1} in NCH-OH_2 and HCCH-OH_2 respectively, and has an intensity of virtually zero in C_2N_2-OH_2. The twisting mode of OH_2 shows no consistency for the structures NCH-OH_2 and HCCH-OH_2.

In the CH_3CN-HOH complex, the highest intensity corresponds to the out-of-plane motion of the bonded water hydrogen (restricted water wagging motion) coupled with a torsion about the H7...N6 axis, ν_{18}, followed by the C≡N...H bending (ν_{12}). The inter-monomer stretching mode, ν_{13}, appears with a low intensity of 2.3 km mol^{-1}. The remaining modes show moderate intensities, but are still much higher than those in NCH-OH_2 and HCCH-OH_2 and certainly more so than in C_2N_2-OH_2.

6.3.3 Intra- and Intermolecular Force Constants

Table 6.12 presents the computed force constants of the H_2O, HCN, C_2H_2, C_2N_2 and CH_3CN monomers and the corresponding literature[215-218] values for the first four molecules respectively. No literature force constants were found for acetonitrile, but the computed force constants are listed for consistency and in

Table 6.12. Calculated and Literature Force Constants of H_2O, HCN, C_2H_2, C_2N_2 and CH_3CN Monomers and the Ratios of the Computed/Literature Force Constants

Molecule	Parameter	Value		Ratio
		Calculated	Literature	
H_2O[a]	f(OH)/N m^{-1}	877.7	943.9	0.9
	f(HOH)/N m rad^{-2}	73.9	76.5	1.0
HCN[b,c]	f(CH)/N m^{-1}	662.8	580.0	1.1
	f(CN)/N m^{-1}	1703.9	1837.5	0.9
	fHCN/N m rad^{-2}	19.4	26.0	0.7
C_2H_2[b]	f(CH)/N m^{-1}	674.6	592.0	1.1
	f(CC)/N m^{-1}	1618.8	1580.0	1.0
	f(HCC)/N m rad^{-2}	17.8	12.0	1.5
C_2N_2[c,d]	f(CC)/N m^{-1}	731.8	1299.0	1.2
	f(CN)/N m^{-1}	1533.5	685.2	1.1
	f(NCC)/N m rad^{-2}	33.4	32.9	1.0
CH_3CN	f(CC)/N m^{-1}	533.8	-	-
	f(CN)/N m^{-1}	1687.4	-	-

[a] Ref. 216. [b] Ref. 217. [c] Ref. 218. [d] Ref. 219.

order to compare them with the complex force constants in Table 6.13. The force constant numbering is adopted from the optimised equilibrium structures.

The ratio of the calculated/literature values is usually close to unity, indicating the good correlation between the calculated and the literature force constants. In Table 6.13 are shown the computed values and the differences between the complex and monomer force constants. Only the force constants which are most closely associated with the complexation or those which assist in clarifying certain trends are listed here. In the NCH-OH_2 and HCCH-OH_2 complexes, the stretching force constant of the CH bond is reduced by about 36 and 14 N m^{-1}

Table 6.13. Computed Force Constants and the Differences between Complex and Monomer Force Constants of the Adducts of H_2O with HCN, C_2H_2, C_2N_2 and CH_3CN

		Value	
Complex	Parameter	Calculated	Difference
NCH-OH_2	f(C2H3)/N m^{-1}	627.2	-35.6
	f(C2N1)/N m^{-1}	1708.8	5.3
	f(H3...O4)/N m^{-1}	17.2	IM
	f(O4H5)/N m^{-1}	874.5	-3.2
	f(N1C2H3)/N m rad^{-2}	27.8	8.4
	f(C2H3...O4)/N m rad^{-2}	5.0	IM
C_2H_2-OH_2	f(C2H4)/N m^{-1}	660.2	-14.4
	f(C1C2)/N m^{-1}	1595.0	-23.8
	f(O5H6)/N m^{-1}	871.9	-5.8
	f(H5...O4)/N m^{-1}	10.7	IM
	f(C2H4...O5)/N m rad^{-2}	4.0	IM
C_2N_2-OH_2	f(C1N3)/N m^{-1}	1547.3	13.8
	f(C1C4)/N m^{-1}	732.1	0.3
	f(O2H6)/N m^{-1}	875.3	-2.4
	f(C1..O2),		
	f(C4....O2)/N m^{-1}	6.6	IM
	f(N3C1C4)/N m rad^{-2}	35.1	IM
CH_3CN-HOH	f(C1N6)/N m^{-1}	1705.2	17.8
	f(C1C2)/N m^{-1}	562.3	28.5
	f(O7H8)/N m^{-1}	868.6	-9.1
	f(H7...N6)/N m^{-1}	12.7	IM
	f(O8H7...N6)/N m rad^{-2}	3.2	IM

respectively, and the C≡N force constant in the NCH-OH_2 adduct is slightly increased while the C≡C force constant in the HCCH-OH_2 complex is remarkably reduced, but the C≡N force constant in the C_2N_2-OH_2 adduct is increased by about 14 N m^{-1}. The OH stretching force constant is reduced by 3, 6 and 2 N m^{-1} in the complexes of water with the NCH, C_2H_2 and C_2N_2 molecules, and by 9 N m^{-1} in the CH_3CN-HOH adduct.

There is no noticeable consistency in the intramolecular force constant perturbations which reflects the trends in the strengths of the interactions. The intermolecular force constants of interest are those for inter-monomer stretching and the bending, f(H...B) and f(A-H...B) respectively,[8b,10c,219]. The inter-monomer stretching force constant, f(H...B), of the NCH-OH_2 complex is 17.2 N m^{-1} followed by 12.3 N m^{-1} for the CH_3CN-HOH adduct and 10.7 N m^{-1} for the HCCH-OH_2 adduct.

The descending order of the f(H...B) values coincides with the descending order of the stabilities of the adducts. The exception is the C_2N_2-OH_2 complex which, although it has a lower inter-monomer stretching force constant than the HCCH-OH_2 complex, has a higher interaction energy than the HCCH-OH_2 adduct. This is due to the fact that, in the C_2N_2-OH_2 complex, the complexation is of the EDA type, while in HCCH-OH_2 it is of the hydrogen bond type.

The values of the A-H...B bending mode force constants are 5, 4 and 3 N m rad^{-2} for the NCH-OH_2, HCCH-OH_2 and CH_3CN-HOH complexes respectively; again the magnitudes of the bending force constants do not correlate with the ordering of the stabilities of the complexes.

CHAPTER 7

7.1 RESULTS AND DISCUSSION OF THE GROUP 2 COMPLEXES

The geometrical parameters, stabilisation energies, charge redistributions and vibrational properties of the three isoelectronic binary complexes of water with formaldehyde, methyleneimine and ethylene are reported. Some parallels are drawn among the complexes. Literature values are used as a test of the quality of the results where such values exit.

7.2 Structural, Energetic and Electronic Properties of the H_2CO-HOH, CH_2NH-HOH and C_2H_4-HOH Complexes

7.2.1 Geometrical Parameters

In Table 7.1 are presented the geometrical parameters of the optimised equilibrium structures of H_2CO, CH_2NH and C_2H_4, along with the corresponding experimental values and the differences between the computed and the literature parameters. The agreement between the computed and the experimental work is reasonable in general, with an absolute average difference of 0.1 pm for all the bond lengths and 0.3° for the angles.

The fully optimised geometrical parameters of the H_2CO-HOH, CH_2NH-HOH and C_2H_4-HOH complexes are shown in Table 7.2. The atom numbering is adopted from the Schakal-92 plots for the lowest energy structures illustrated in Figures 7.1(a), 7.2(a) and 7.3(a).

Table 7.1. Optimised Structural Parameters of the Formaldehyde, Methyleneimine and Ethylene Monomers Compared with the Corresponding Literature Parameters

		Monomer		
Monomer	Parameter	Calculated	Experimental[a]	Difference[b]
H_2CO	r(C1O2)/pm	122.0	120.8	1.2
	r(C1H3)/pm	110.0	110.8	-0.8
	r(C1H4)/pm	110.0	110.8	-0.8
	H3C1O2/deg	122.2	121.7	0.5
	H4C1O2/deg	122.2	121.7	0.5
CH_2NH	r(C1N2)/pm	128.1	127.3	0.8
	r(C1H3)/pm	108.5	110.3	-1.8
	r(C1H4)/pm	109.0	108.1	0.9
	r(N2H5)/pm	102.2	102.3	-0.1
	H3C1N2/deg	118.4	119.7	-1.3
	H4C1H3/deg	116.7	116.9	-0.2
	H3C1N2/deg	125.4	123.4	-2.0
	H5N2C1/deg	109.3	110.5	-1.2
C_2H_4	r(C1H3)/pm	108.0	108.0	0.0
	r(C1C2)/pm	133.3	133.3	0.0
	H3C1C2/deg	121.6	121.1	0.5

[a] Ref. 190. [b] Difference = calculated - experimental value.

On complexation the bond lengths and angles are minimally perturbed, as is expected for weak complexes.[31,35] In the H_2CO-HOH complex, the C1O2 and O6H5 bonds are both extended by 0.6 pm on complexation (see Table 7.2). Of interest is the shortening of the C1H4 bond on complexation, which is part of the distorted 5-membered ring. The C1H4 bond shortening is due to back donation from the water oxygen. The ring formation leads to a decrease in the H4C1O2 angle by 0.8°.

Table 7.2. Optimised Structural Parameters of the Complexes of Water with Formaldehyde, Methyleneimine and Ethylene together with the Complex - Monomer Differences

Complex	Parameter	Calculated	Difference
H_2CO-HOH	r(C1O2)/pm	122.6	0.6
	r(C1H3)/pm	109.8	-0.2
	r(C1H4)/pm	109.5	-0.5
	r(O6H5)/pm	96.7	0.6
	r(O6H7)/pm	96.1	0.0
	r(H5...O2)/pm	203.3	-
	r(H4...O6)/pm	255.3	-
	r(O2...O6)/pm	289.4	-
	H3C1O2/deg	121.3	0.1
	H5O6H7/deg	104.1	0.3
	H4C1O2/deg	121.4	-0.8
	C1O2...H5/deg	97.3	-
	O6H5...O2/deg	147.3	-
	C1H4...O6/deg	109.5	-
	H5O6...H4/deg	36.0	-
	H7O6H5...O2/deg	116.0	-
CH_2NH-HOH	r(C1N2)/pm	128.2	0.1
	r(C1H3)/pm	108.4	-0.1
	r(C1H4)/pm	108.9	-0.1
	r(N2H5)/pm	102.1	-0.1
	r(H6...N2)/pm	201.5	-
	r(H3...O7)/pm	261.2	-
	r(O7...N2)/pm	289.5	-
	r(O7H6)/pm	97.1	1.0
	r(O7H8)/pm	96.1	0.0
	H3C1N2/deg	117.6	-0.8
	H4C1H3/deg	117.7	1.0
	H3C1N2/deg	124.7	-0.7
	H5N2C1/deg	110.8	1.5
	C1N2...H6/deg	99.2	-
	O7H6...N2/deg	149.7	-
	H6O7...H3/deg	28.0	-
	H8O7H6/deg	104.8	0.0
	H8O7H6...N2/deg	106.7	-

Table 7.2 (continued)

C_2H_4-HOH	r(C1H2)/pm	108.1	0.5
	r(C1H3)/pm	108.1	-
	r(C1C5)/pm	133.8	0.5
	r(H4...C1C5)/pm	244.7	-
	r(O8...C1C5)/pm	341.0	-
	r(O8H4)/pm	96.3	0.2
	r(O8H9)/pm	96.1	0.0
	H2C1C5/deg	121.5	-0.1
	H3C1C5/deg	121.6	-
	H9O8H4/deg	103.8	0.0

The computed H5...O2 hydrogen bond length is 203.3 pm, which compares quite well with that of Ventura et al.,[96] Kumpf and Damewood[73] and Ha et al.,[92] but not so well with that of Del Bene,[35] who used a smaller basis set. The hydrogen bond angle, O6H5...O2, is expected to be around 180° for strong hydrogen bonds[31]. In Table 7.2 the O6H5...O2 angle is 147.3°, deviating from linearity by 32.7°. Kumpf and Damewood[73] obtained a value of 146.7°. For the formaldehyde-water complex, the linearity effect is overshadowed by the lone pair directionality effect.[31] The linearity is also affected by the weak secondary hydrogen bonding interaction between the water O6 atom and the formaldehyde H4 atom. The secondary hydrogen bond contributing to the non-linearity of the O6H5...O2 angle has a length 255.3 pm, and the secondary hydrogen bond angle, C1H4...O6, is 109.5°. The intermolecular distance, O2...O6, is 289.4 pm and the non-bonded water O6H7 bond lies 116.0° out of the heavy atom plane. The C1O2...H5 angle is 97.3°, which is close to the value of 100.9° obtained by Kumpf and Damewood.[73] This angle indicates the fact that the hydrogen bond forms along the axis of the lone pair, conforming to rule I of Legon and Millen.[31] These findings are consistent with the experimental results.[124,220,221]

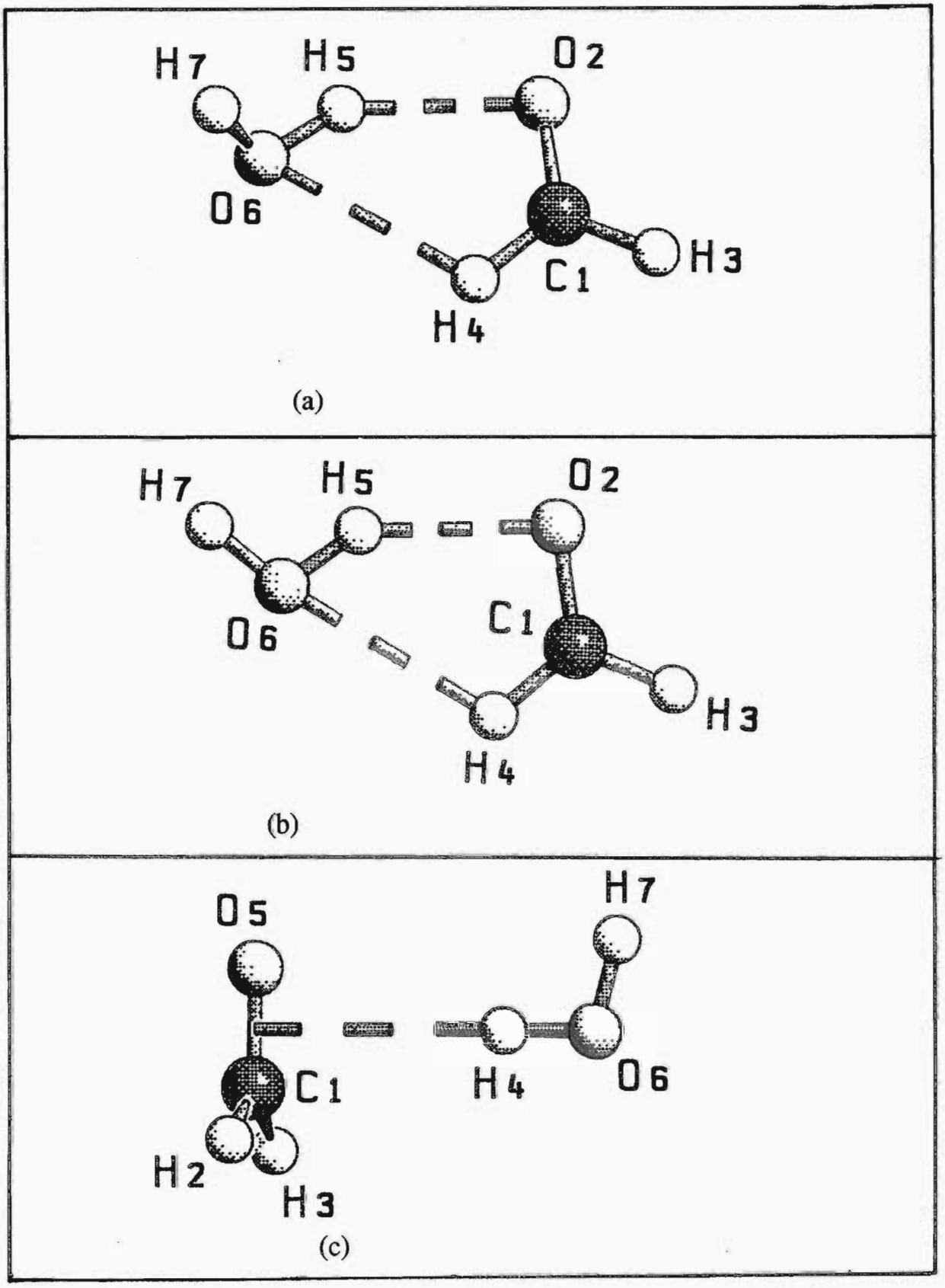

Figure 7.1. Graphical representations of the three conformers of the H_2CO-HOH complex and atom numbering: (a) C_1 planar structure; (b) C_1 planar (TS) structure; (c) π-bonded structure.

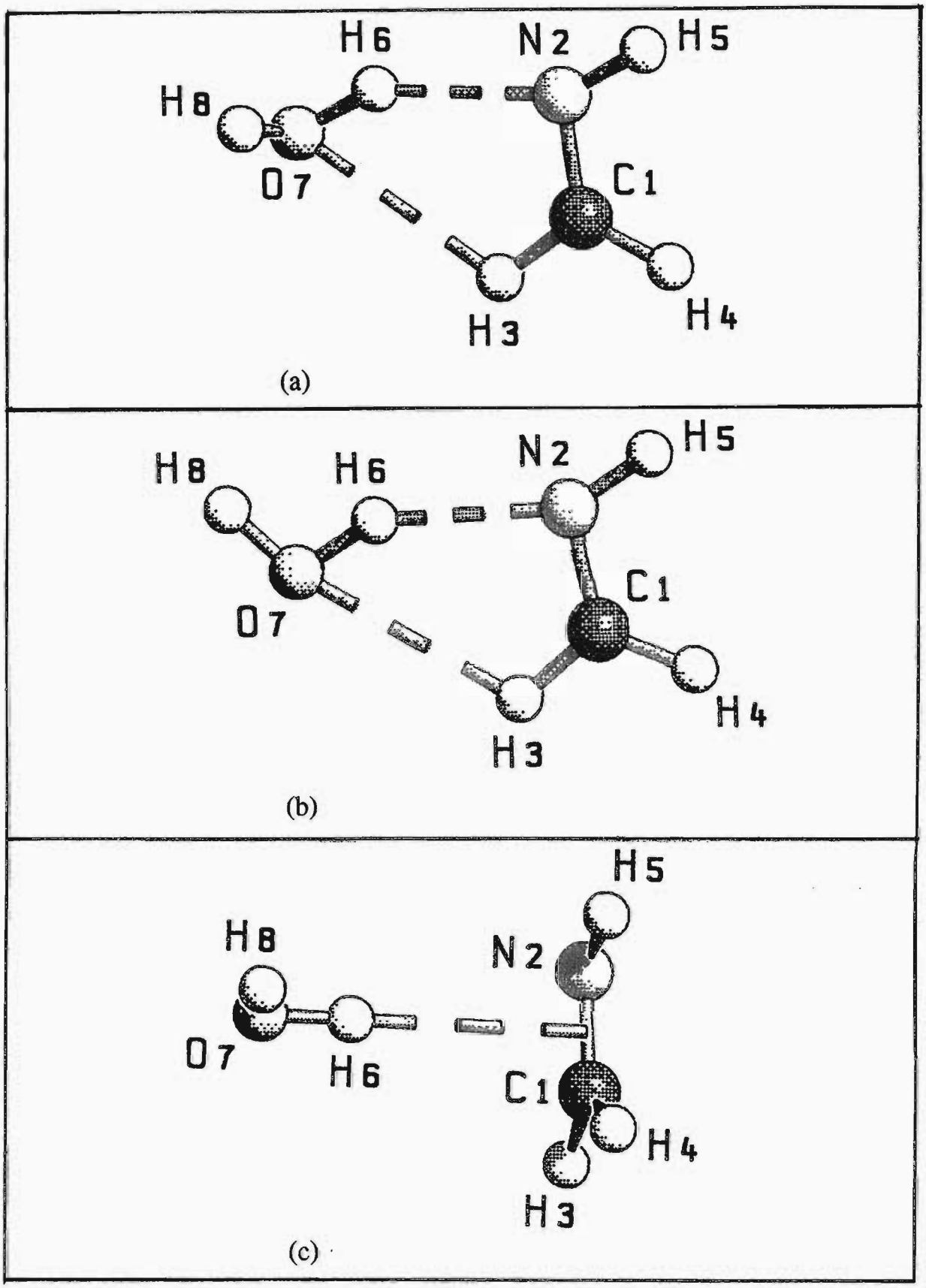

Figure 7.2. Graphical representations of the three conformers of the CH_2NH-HOH complex and atom numbering: (a) C_1 non-planar structure; (b) C_s planar (TS) structure; (c) C_1 π-bonded structure.

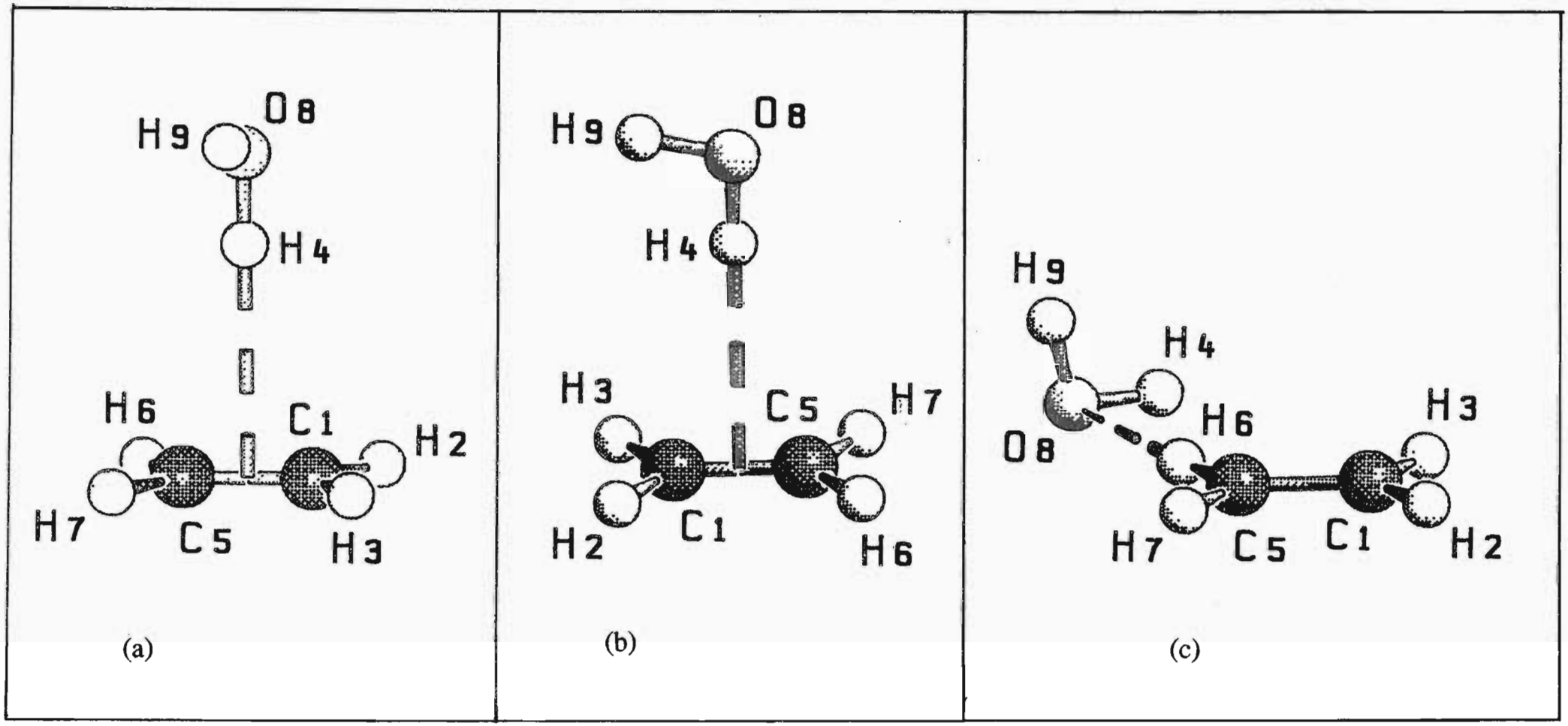

Figure 7.3. Graphical representations of the three conformers of the C_2H_4-HOH complex and the atom numbering: (a) C_s structure I; (b) C_s structure II; (c) C_1 structure.

Unlike the formaldehyde-water complex discussed above, the methyleneimine-water complex forms a primary hydrogen bond of the type O-H...N, but, like the formaldehyde-water complex, there are dramatic geometrical distortions. There is a noticeable increase of the O7H6 bond length, and the H5N2C1 bond angle opens up by 1.5°, as shown in Table 7.2. The H5N2C1 angle increase indicates a reduced lone pair effect on complexation. The H3 atom interacts rather strongly with the water oxygen atom forming a distorted 5-membered ring. From the column of differences in Table 7.2, it is clear that the C=N bond length is rather insensitive to the H6...N2 bond formation. Yeo and Ford[89] computed the H...N bond length of the ammonia-water complex and found a value of 198.9 pm, compared with 201.5 pm determined in this project.

C_2H_4-HOH is a π-bonded complex, a fairly weak type of interaction. The H...CC bond length is 244.5 pm, which compares well with the 248.0 pm determined experimentally.[134] The O8H4 bond is perpendicular to the C=C bond, while the H9O8H4 plane bisects the CC axis. This is the structure generally agreed upon.[134,139] Table 7.3 presents the absolute energies of the three possible conformers of the H_2CO-HOH, CH_2NH-HOH and C_2H_4-HOH complexes along with the differences between the most stable and the less stable conformers. Rotation of the water molecule by 90° about the O8H4 axis of C_2H_4-HOH led to an alternative structure which is 0.50 kJ mol^{-1} higher in energy (see Figure 7.3(b)). This implies that the rotation of the water molecule about the O8H4 bond is almost free, consistent with an observation made by Del Bene.[136] Bemish et al.[222] have demonstrated that the complex of C_2H_4 with CO_2 shows a similar feature in that the C atom of CO_2 lies above the centre of mass of C_2H_4, and that there is no fixed angular configuration, implying the ability of the CO_2 molecule to rotate freely about the axis joining the carbon dioxide C atom and the C=C mid-point.

Table 7.3. The Absolute Energies and their Diferences at the MP2 Level of the Optimised H_2O Complexes with H_2CO, CH_2NH and C_2H_4, for the three possible Configurations

		Differences[a]	
Complex	Absolute Energy/a.u	/a.u	/kJ mol^{-1}
H_2CO-HOH			
(a)	-190.41411442669		
(b)	-190.41357112872	0.0054329797	14.26
(c)	-190.40542671794	0.0086877087	22.81
CH_2NH-HOH			
(a)	-170.57321486268		
(b)	-170.57225774646	0.0009571162	2.51
(c)	-170.56298949237	0.0102253703	26.85
C_2H_4-HOH			
(a)	-154.54187731947		
(b)	-154.54168787737	0.0001894421	0.50
(c)	-154.54072427262	0.0011530469	3.03

[a] Differences are between the absolute energies of the most stable structure and of each of the alternative structures.

Figures 7.1(a), 7.2(a) and 7.3(a) illustrate the equilibrium structures with the lowest absolute energies, at the MP2 level of theory. Formaldehyde, methyleneimine and ethylene each have a π-bond, which is nucleophilic. A search was made for structures in which one of the water hydrogens interacts with the double bonds of formaldehyde and methyleneimine; the results were the unstable structures shown in Figures 7.1(c) and 7.2(c) respectively, showing that the configurations depicted in Figures 7.1(a) and 7.2(b) are preferred. Figures 7.1(b) and 7.2(b) show the planar intermediate complexes for both H_2CO-HOH and CH_2NH-HOH, while Figure 7.3(c) illustrates the case of the water molecule acting as the ED and PA, in the ethylene-water complex. As

shown in Table 7.3, the possibility of water being the EA is energetically unfavourable for the ethylene-water complex.

7.2.2 Interaction Energies and Morokuma Energy Components

The formaldehyde-water complex has an interaction energy of -15.04 kJ mol^{-1}, at the MP2 level, as shown in Table 7.4. The geometrical parameter changes were fairly small for the H_2CO-HOH adduct when compared with those of the CH_2NH-HOH complex, which turns out to be the strongest adduct among the Group 2 complexes, with an interaction energy of -21.00 kJ mol^{-1}.

Table 7.4. Uncorrected and Corrected Interaction Energies of the Complexes of Water with Formaldehyde, Methyleneimine and Ethylene

	Energy/kJ mol^{-1}		
Complex	Uncorrected	BSSE	Corrected
		MP2	
H_2CO-HOH	-28.43	13.39	-15.04
CH_2NH-HOH	-32.86	11.86	-21.00
C_2H_4-HOH	-12.63	5.75	-6.88
		RHF	
H_2CO-HOH	-21.09	5.64	-15.45
CH_2NH-HOH	-24.11	5.58	-18.53
C_2H_4-HOH	-8.00	3.27	-4.73

Migchels et al.[131] computed a stabilisation energy of -34.39 kJ mol^{-1} (uncorrected for BSSE) for the H_2CO-HOH complex. Yeo and Ford[89] obtained -26.90 kJ mol^{-1} for the interaction energy of the ammonia-water complex. The predicted interaction energy for the methyleneimine-water complex is in this range.

The ethylene-water complex has a fairly long separation distance. It turns out to be the weakest of the three complexes, as expected. Engdahl and Nelander computed an interaction energy of -10.04 kJ mol^{-1} using the STO-3G level of theory.[137] The ethylene-water complex has an interaction energy of -6.88 kJ mol^{-1} (see Table 7.4), which is fairly small in comparison with those of the rest of the group, consistent however with the very low perturbation of the values of the geometrical parameters, as depicted in Table 7.2 above.

The cyclic complexes can exist in two forms, with one of the water OH groups projecting above or below the molecular plane. The transition state, which for these complexes is planar, was determined. The energy differences between the (planar) transition states and the (non-planar) true minima were evaluated. The planar form of the formaldehyde-water complex is less stable by 14.26 kJ mol^{-1} compared with the non-planar configuration, while the planar form of the methyleneimine-water complex is 2.51 kJ mol^{-1} less stable compared with the corresponding non-planar form, as shown in Figures 7.1(b) and 7.2(b) (see Table 7.3).

For the three complexes the forces behind dimerisation are qualitatively the same, as shown in Table 7.5. The dominating factor in all three complexes is the electrostatic energy. This shows that not only are the O-H...O and O-H...N hydrogen bonds controlled by electrostatic forces but that the O-H...π system also obeys the same rule. While the electrostatic term is dominant in stabilising the complexes of H_2O with H_2CO and CH_2NH, in the C_2H_4-HOH complex the charge transfer term significantly contributes 21% of the total energy, contrary to the values of 12% and 16% found in the typically hydrogen bonded H_2CO-HOH and CH_2NH-HOH complexes.

Table 7.5. Morokuma Decomposed Energy Components

		Decomposed Interaction Energy/kJ mol^{-1}		
Component		Uncorrected	Corrected	%Contribution
H_2CO-HOH	El	-31.93	-31.93	45
	Pl	-2.94	-2.94	4
	Ex	23.91	25.07	34
	Ct	-11.08	-8.90	16
	Mix	-1.21	3.24	1
	Total	-23.25	-15.46	-
CH_2NH-HOH	El	-41.57	-41.57	46
	Pl	-4.83	-4.83	5
	Ex	32.84	33.86	36
	Ct	-11.26	-9.14	12
	Mix	-0.39	3.16	0.4
	Total	-25.21	-18.52	-
C_2H_4-HOH	El	-12.82	-12.82	38
	Pl	-1.14	-1.14	3
	Ex	12.57	13.01	37
	Ct	-7.26	-5.87	21
	Mix	0.11	2.10	0.3
	Total	-8.54	-4.72	-

7.2.3 Atomic Charge Redistributions

Table 7.6 shows the atomic charges of the three isoelectronic monomers and their corresponding water complexes. The last column of this table shows the charge difference between the complex and the monomer. A negative change in this column indicates a gain in charge density, while a positive change indicates a loss of charge.

The atoms directly involved in the H_2CO-HOH complex formation are O2, H4, O6 and H5, as depicted in Figure 7.1(a). These are the atoms which show the

Table 7.6. The Predicted MP2 Atomic Charge Distributions of the H_2CO-HOH, CH_2NH-HOH and C_2H_4-HOH Complexes together with the Differences between the Complex and Monomer Charges and the Fragment Charges

		Charge/e			
Species	Atom	Monomer	Complex	Difference	Fragment
H_2CO-HOH	C1	0.2448	0.2403	-0.0045	
	O2	-0.4524	-0.4899	-0.0375	
	H3	0.1038	0.1184	0.0146	
	H4	0.1038	0.1441	0.0403	0.0129
	H5	0.3369	0.3695	0.0326	
	O6	-0.6738	-0.7139	-0.0401	
	H7	0.3369	0.3315	-0.0054	-0.0129
CH_2NH-HOH	C1	0.0043	0.0260	0.0217	
	N2	-0.5111	-0.5779	-0.0668	
	H3	0.1322	0.1645	0.0323	
	H4	0.1127	0.1237	0.0110	
	H5	0.2619	0.2771	0.0152	0.0133
	H6	0.3369	0.3841	0.0472	
	O7	-0.6738	-0.7211	-0.0473	
	H8	0.3369	0.3237	-0.0132	-0.0133

Table 7.6 (continued)

C_2H_4-HOH	C1	-0.2568	-0.2713	-0.0144	
	H2	0.1284	0.1468	0.0185	
	H3	0.1284	0.1387	0.0102	
	H6	0.1284	0.1468	0.0185	
	C5	-0.2568	-0.2713	-0.0144	
	H7	0.1284	0.1387	0.0102	0.0286
	H7	0.3369	0.3423	0.0053	
	O8	-0.6738	-0.6981	-0.0243	
	H9	0.3369	0.3273	-0.0096	-0.0286

most significant charge redistributions. O2 gains a charge of 0.0375 e on complexation. The formaldehyde H4 atom loses 0.0403 e, while the H3 atom, which is not even part of the five-membered ring, loses about a third of this charge. The discrepancy between the two equivalent atoms of the formaldehyde molecule can be attributed to the fact that H4 loses part of its electron density to the C1 atom and is in turn stabilised by charge transfer from the water O6 atom.The C1H4 bond is shortened by the increased charge separation between C1 and H4. The bridging water hydrogen H5 atom loses 0.0326 e on complexation. The water O6 atom gains 0.0401 e, comparable with the 0.0375 e gained by the formaldehyde O2 atom and also comparable with the charge lost by the H4 atom.

In the CH_2NH-HOH complex, the atoms directly involved in complexation are O7, H6, N2 and H3; they also show significant charge redistributions. The N2 atom gains a charge of 0.0668 e, while the H3 atom (like the H4 atom in the formaldehyde-water complex) loses a charge of 0.0323 e to the C1 atom. The water H6 atom loses an appreciable amount of charge as a result of the H6...N2 bond formation, comparable with the charge lost by H5 in the H_2CO-HOH complex. The water O7 atom gains a charge of 0.0473 e while the N2 atom gains 0.0688 e. No significant charge redistributions are observed in the C_2H_4-HOH complex, because of its very weak nature and due to the fact that H4 interacts with the π-bond and not directly with a specific atom. The redistribution is thus spread over all the atoms in the complex. It is worthwhile to note, however, that the water O8 atom has gained about half the charge density of the O6 and O7 atoms in the H_2CO-HOH and CH_2NH-HOH complexes. Table 7.6 shows an interesting pattern among the three complexes; the bridging water hydrogen invariably loses charge, while the free water hydrogen on the other hand consistently gains charge.

The calculations predict cyclic C_1 structures for the H_2CO-HOH and CH_2NH-HOH complexes, and an open C_s structure for the C_2H_4-HOH complex. Of the three complexes, CH_2NH-HOH is the most stable one, with an interaction energy of -21.00 kJ mol^{-1} and C_2H_4-HOH is the weakest with an interaction energy of -6.88 kJ mol^{-1}. Both the geometrical distortions and the Mulliken charge analysis support the notion of formation of a secondary hydrogen bond in the cyclic complexes.

7.3 Vibrational Properties of the H_2CO-HOH, CH_2NH-HOH and C_2H_4-HOH Complexes

7.3.1 Intra- and Intermolecular Wavenumbers

The computed wavenumbers of the formaldehyde, methyleneimine and ethylene monomers are shown in Table 7.7, along with the experimental[193,223-227] values and the calculated/experimental ratios. These ratios are close to unity in all the Group 2 complexes, indicating that the calculated and experimental wavenumbers correlate fairly well. The symmetry coordinates describing the vibrational modes of the complexes are presented in Table 7.8. No symmetry coordinates are listed for the monomers, since the intramolecular vibrational modes of the monomer are basically the same in both complex and monomer. The predicted wavenumbers, the complex-monomer wavenumber shifts and the %PEDs of the three complexes are listed in Table 7.9. Significant changes in vibrational wavenumbers are observed in both the water and formaldehyde sub-units in the H_2CO-HOH complex. The ν_1 and ν_2 modes, corresponding to $\nu_a(OH_2)$ and $\nu_s(OH_2)$ of the H_2CO-HOH adduct are red shifted by -37 and -61 cm^{-1} respectively; the ν_2 mode red shift compares favourably with the -55 cm^{-1} and -55.2 cm^{-1} shifts observed by Ha et al.[92] and Lewell et al.[97] respectively.

Table 7.7. The Computed and Experimental Wavenumbers of Formaldehyde, Methyleneimine and Ethylene and the Calculated/Experimental Wavenumber Ratios

Molecule	Symmetry species	Mode	$\tilde{\nu}$/cm^{-1} Calc.	$\tilde{\nu}$/cm^{-1} Exp.	$\tilde{\nu}_{cal.}/\tilde{\nu}_{exp.}$
H_2CO[a]	a_1	ν_1	3026	2783	1.09
		ν_2	1792	1746	1.03
		ν_3	1587	1500	1.06
	b_1	ν_4	3104	2843	1.09
		ν_5	1296	1249	1.04
	b_2	ν_6	1218	1167	1.04
CH_2NH[b,c,d,e,f]					
	a'	ν_1	3523	3538	1.00
		ν_2	3262	3021	1.08
		ν_3	3145	2914	1.08
		ν_4	1712	1638	1.05
		ν_5	1526	1452	1.05
		ν_6	1397	1344	1.04
		ν_7	1090	1058	1.03
	a"	ν_8	1193	1127	1.06
		ν_9	1106	1061	1.04
C_2H_4[a]	a_g	ν_1	3256	3026	1.08
		ν_2	1726	1623	1.06
		ν_3	1412	1342	1.05
	a_u	ν_4	1089	1023	1.06
	b_{1g}	ν_5	3333	3103	1.07
		ν_6	1266	1236	1.02
	b_{1u}	ν_7	992	949	1.05
	b_{2g}	ν_8	938	943	0.99
	b_{2u}	ν_9	3356	3106	1.08
		ν_{10}	846	826	1.02
	b_{3u}	ν_{11}	3237	2989	1.08
		ν_{12}	1522	1444	1.05

[a] Ref. 193. [b] Ref. 223. [c] Ref. 224. [d] Ref. 225. [e] Ref. 226. [f] Ref. 227.

Table 7.8. Symmetry Coordinates of the Vibrational Motions for the Complexes of Water with Formaldehyde, Methyleneimine and Ethylene

Complex	Symmetry Coordinate		Description
H_2CO-HOH	S_1	$\{\Delta r_{5,6} - \Delta r_{6,7}\}/\sqrt{2}$	OH_2 a-stretch
	S_2	$\{\Delta r_{5,6} + \Delta r_{6,7}\}/\sqrt{2}$	OH_2 s-stretch
	S_3	$\{\Delta r_{1,3} - \Delta r_{1,4}\}/\sqrt{2}$	CH_2 a-stretch
	S_4	$\{\Delta r_{1,3} + \Delta r_{1,4}\}/\sqrt{2}$	CH_2 s-stretch
	S_5	$\Delta r_{1,2}$	CO stretch
	S_6	$\Delta\delta_{5,6,7}$	OH_2 bend
	S_7	$\{2\Delta\delta_{3,1,4} - \Delta\delta_{2,1,3} - \Delta\delta_{214}\}/\sqrt{6}$	CH_2 bend
	S_8	$\{\Delta\delta_{2,1,3} - \Delta\delta_{2,1,4}\}/\sqrt{2}$	CH_2 rock
	S_9	$\Delta\gamma_{1,2}$	CO op bend
	S_{10}	$\Delta\delta_{2,5,6}$	O-H...O ip bend
	S_{11}	$\Delta\tau_{6,5,2,1}$	torsion about H...O axis
	S_{12}	$\Delta\delta_{1,2,5}$	C=O...H ip bend
	S_{13}	$\Delta r_{2,5}$	H...O stretch
	S_{14}	$\Delta\gamma_{2,5,6}$	O-H...O op bend
	S_{15}	$\Delta\tau_{7,6,5,2}$	hindered rotation about H...O axis

Table 7.8 (continued)

CH_2NH-HOH	S_1	$\{\Delta r_{6,7} - \Delta r_{7,8}\}/\sqrt{2}$	OH_2 a-stretch
	S_2	$\{\Delta r_{6,7} + \Delta r_{7,8}\}/\sqrt{2}$	OH_2 s-stretch
	S_3	$\Delta r_{2,5}$	NH stretch
	S_4	$\{\Delta r_{1,3} - \Delta r_{1,4}\}/\sqrt{2}$	CH_2 a-stretch
	S_5	$\{\Delta r_{1,3} + \Delta r_{1,4}\}/\sqrt{2}$	CH_2 s-stretch
	S_6	$\Delta\delta_{6,7,8}$	HOH bend
	S_7	$\Delta r_{1,2}$	C=N stretch
	S_8	$\{\Delta\delta_{3,1,2} + \Delta\delta_{4,1,2}\}/\sqrt{2}$	CH_2 bend
	S_9	$\Delta\delta_{1,2,5}$	C=N-H ip bend
	S_{10}	$\Delta\gamma_{5,4,1,2}$	C=N-H op bend
	S_{11}	$\Delta\gamma_{3,2,1,4}$	H-C=N op bend
	S_{12}	$\{\Delta\delta_{3,1,2}-\Delta\delta_{4,1,2}\}/\sqrt{2}$	CH_2 rock
	S_{13}	$\Delta\delta_{2,6,7}$	O-H...N ip bend
	S_{14}	$\Delta\gamma_{6,2,1,4}$	O-H...N op bend
	S_{15}	$\Delta\gamma_{7,6,1,5}$	torsion about CN
	S_{16}	$\Delta r_{2,6}$	H...N stretch
	S_{17}	$\Delta\tau_{7,6,2,5}$	torsion about H...N
	S_{18}	$\Delta\delta_{1,2,6}$	C=N...H ip bend

Table 7.8 (continued)

C_2H_4-HOH	S_1	$\{\Delta r_{4,8} - \Delta r_{8,9}\}/\sqrt{2}$	OH_2 a-stretch
	S_2	$\{\Delta r_{4,8} + \Delta r_{8,9}\}/\sqrt{2}$	OH_2 s-stretch
	S_3	$\{\Delta r_{1,2} - \Delta r_{1,3} + \Delta r_{5,6} - \Delta r_{5,7}\}/2$	CH_2 a-stretch
	S_4	$\{\Delta r_{1,2} + \Delta r_{1,3} + \Delta r_{5,6} + \Delta r_{5,7}\}/2$	CH_2 s-stretch
	S_5	$\Delta r_{1,5}$	CC stretch
	S_6	$\Delta \delta_{4,8,9}$	HOH bend
	S_7	$\{\Delta \delta_{2,1,5} + \Delta \delta_{3,1,5} + \Delta \delta_{6,5,1} + \Delta \delta_{7,5,1}\}/2$	CH_2 bend
	S_8	$\{\Delta \gamma_{1,6,5,7} - \Delta \gamma_{5,2,1,3}\}/\sqrt{2}$	CH_2 twist
	S_9	$\{\Delta \delta_{2,1,5} - \Delta \delta_{3,1,5} + \Delta \delta_{6,5,1} - \Delta \delta_{7,5,1}\}/2$	CH_2 rock
	S_{10}	$\{\Delta \tau_{8,4,5,7} + \Delta \tau_{1,4,8,9}\}/\sqrt{2}$	torsion about H...CC
	S_{11}	$\{\Delta r_{1,4} + \Delta r_{4,5}\}/\sqrt{2}$	H...CC s-stretch
	S_{12}	[a]	librational motion of H2CCH2
	S_{13}	$\{\Delta r_{1,2} - \Delta r_{1,3} - \Delta r_{5,6} + \Delta r_{5,7}\}/2$	CH_2 a-stretch
	S_{14}	$\{\Delta r_{1,2} + \Delta r_{1,3} - \Delta r_{5,6} - \Delta r_{5,7}\}/2$	CH_2 s-stretch
	S_{15}	$\{\Delta \delta_{2,1,5} + \Delta \delta_{3,1,5} - \Delta \delta_{6,5,1} - \Delta \delta_{7,5,1}\}/2$	CH_2 bend
	S_{16}	$\{\Delta \delta_{2,1,5} - \Delta \delta_{3,1,5} - \Delta \delta_{6,5,1} + \Delta \delta_{7,5,1}\}/2$	CH_2 rock
	S_{17}	$\{\Delta \tau_{6,5,1,3} + \Delta \tau_{7,5,1,2}\}/\sqrt{2}$	CH_2 wag
	S_{18}	$\{\Delta \gamma_{5,1,2,3} + \Delta \gamma_{1,5,6,7}\}/\sqrt{2}$	CH_2 wag
	S_{19}	$\{\Delta \delta_{5,4,8} - \Delta \delta_{1,4,8}\}/\sqrt{2}$	O-H...C deformation
	S_{20}	$\{\Delta r_{1,4} - \Delta r_{4,5}\}/\sqrt{2}$	H...CC a-stretch
	S_{21}	$\{\Delta \tau_{9,8,4,5} + \Delta \tau_{9,8,4,1}\}/\sqrt{2}$	torsion of HOH...C

[a] - No suitable symmetry coordinate could be found.

Table 7.9. The Computed Wavenumbers of the Complexes of H_2O with H_2CO, CH_2NH and C_2H_4, the Complex-Monomer Shifts and the %PEDs

Complex	Mode	Wavenumber /cm^{-1}	Shift /cm^{-1}	%PED[a]
H_2CO-HOH	ν_1	3993	-37	$89S_1 + 10S_2$
	ν_2	3830	-61	$87S_2 + 11S_1$
	ν_3	3169	58	$97S_3$
	ν_4	3062	36	$96S_4$
	ν_5	1767	-25	$74S_5 + 25S_7$
	ν_6	1703	21	$90S_6$
	ν_7	1574	-13	$81S_7 + 18S_5$
	ν_8	1300	4	$99S_8$
	ν_9	1233	15	$95S_9$
	ν_{10}	592	IM	$58S_{10} + 17S_{12} + 13S_{13}$
	ν_{11}	329	IM	$47S_{11} + 20S_{14} + 19S_{15}$
	ν_{12}	227	IM	$48S_{11} + 40S_{14}$
	ν_{13}	195	IM	$65S_{13} + 26S_{12}$
	ν_{14}	163	IM	$87S_{15} + 4S_{11}$
	ν_{15}	158	IM	$46S_{12} + 39S_{10}$

Table 7.9 (continued)

CH_2NH-HOH	ν_1	3980	-50	$80S_1 + 19S_2$
	ν_2	3769	-122	$76S_2 + 21S_1$
	ν_3	3543	20	$100S_3$
	ν_4	3294	32	$90S_4 + 9S_5$
	ν_5	3162	17	$89S_5 + 9S_4$
	ν_6	1709	-3	$83S_6 + 5S_{15} + 3S_{17}$
	ν_7	1704	22	$62S_7 + 35S_8$
	ν_8	1519	-7	$68S_8 + 31S_7$
	ν_9	1401	4	$58S_9 + 38S_{12} + 3S_7$
	ν_{10}	1188	-5	$72S_{10} + 24S_{11}$
	ν_{11}	1120	9	$54S_{11} + 42S_{10}$
	ν_{12}	1093	3	$57S_{12} + 42S_9$
	ν_{13}	680	IM	$64S_{13} + 16S_{18} + 14S_{15}$
	ν_{14}	337	IM	$45S_{15} + 34S_{17} + 11S_{14}$
	ν_{15}	221	IM	$58S_{15} + 37S_{14}$
	ν_{16}	206	IM	$74S_{16} + 22S_{18}$
	ν_{17}	171	IM	$58S_{17} + 19S_{15} + 18S_{14}$
	ν_{18}	141	IM	$62S_{18} + 35S_{13}$

Table 7.9 (continued)

C_2H_4-HOH	ν_1	4014	-16	$98S_1$
	ν_2	3879	-12	$98S_2$
	ν_3	3357	1	$100S_3$
	ν_4	3254	-2	$98S_4$
	ν_5	1719	-7	$55S_5 + 44S_7$
	ν_6	1693	11	$95S_6$
	ν_7	1411	-1	$57S_7 + 40S_5$
	ν_8	1004	12	$100S_8$
	ν_9	847	1	$100S_9$
	ν_{10}	218	IM	$93S_{10}$
	ν_{11}	107	IM	$100S_{11}$
	ν_{12}	60	IM	[b]
	ν_{13}	3334	1	$99S_{13}$
	ν_{14}	3238	1	$100S_{14}$
	ν_{15}	1523	1	$100S_{15}$
	ν_{16}	1268	2	$100S_{16}$
	ν_{17}	1089	0	$100S_{17}$
	ν_{18}	945	7	$100S_{18}$
	ν_{19}	332	IM	$69S_{19} + 26S_{20}$
	ν_{20}	64	IM	$77S_{21} + 12S_{19}$
	ν_{21}	40	IM	$47S_{20} + 30S_{19} + 21S_{21}$

[a] See Table 7.8. [b] The symmetry coordinate for the band at 60 cm^{-1} has been omitted.

The carbonyl stretching mode, ν_5, is red shifted by -25 cm^{-1}, indicating the active involvement of the carbonyl bond in the interaction. The ν_3 and ν_4 modes, $\nu_a(CH_2)$ and $\nu_s(CH_2)$, are blue shifted by 58 and 36 cm^{-1} respectively. The HOH angle bend is blue shifted by 21 cm^{-1}, in agreement with the observation of Ha et al.[92] A dramatic red shift of -122 cm^{-1} is observed for the ν_2 mode in the CH_2NH-HOH adduct, which is twice that of its counterpart, H_2CO-HOH, while the ν_1 mode is shifted by -50 cm^{-1}. The large shifts in vibrational wavenumbers are consistent with the higher interaction energy of CH_2NH-HOH, -21 kJ mol^{-1}, while H_2CO-HOH, with a smaller interaction energy of -15.04 kJ mol^{-1}, shows moderate shifts, as observed above. The HOH angle bend is blue shifted by 22 cm^{-1}, a fairly similar shift compared with that in the formaldehyde-water complex. The symmetric and antisymmetric CH_2 bond stretches of the CH_2NH component in the CH_2NH-HOH complex are blue shifted by 17 and 32 cm^{-1} respectively. A similar pattern of shifts was observed for the formaldehyde-water complex. The ν_6 mode (HOH bend) is essentially unaffected by the hydrogen bonded interaction, as shown by the very low wavenumber shift.

In the C_2H_4-HOH adduct, the ν_1 and ν_2 modes are shifted towards lower wavenumbers by -16 and -12 cm^{-1} respectively, while the HOH angle bend mode, ν_6, is shifted to higher wavenumber by 11 cm^{-1}. The rest of the vibrational wavenumbers remain unshifted. These small wavenumber shifts are fitting for such a weak complex (interaction energy of -6.88 kJ mol^{-1}).

The intermolecular modes are heavily coupled, and include substantial contributions from both monomer fragments. The forms of the intermolecular modes are illustrated by means of Schakal-92 plots, in Figures 7.4 and 7.5. The assignments of the intermolecular modes were carried out by means of the

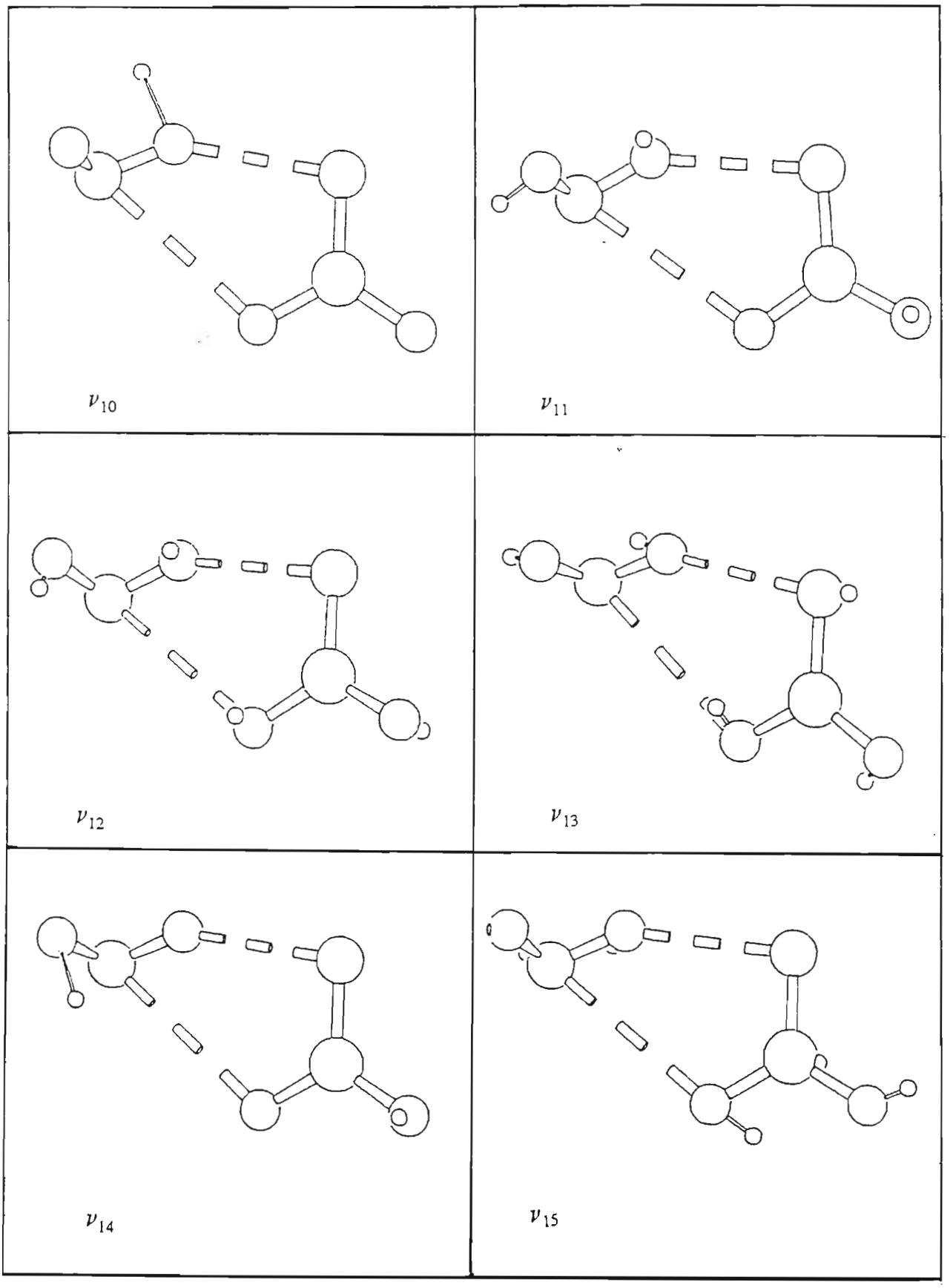

Figure 7.4. The six intermolecular modes of the H_2CO-HOH complex.

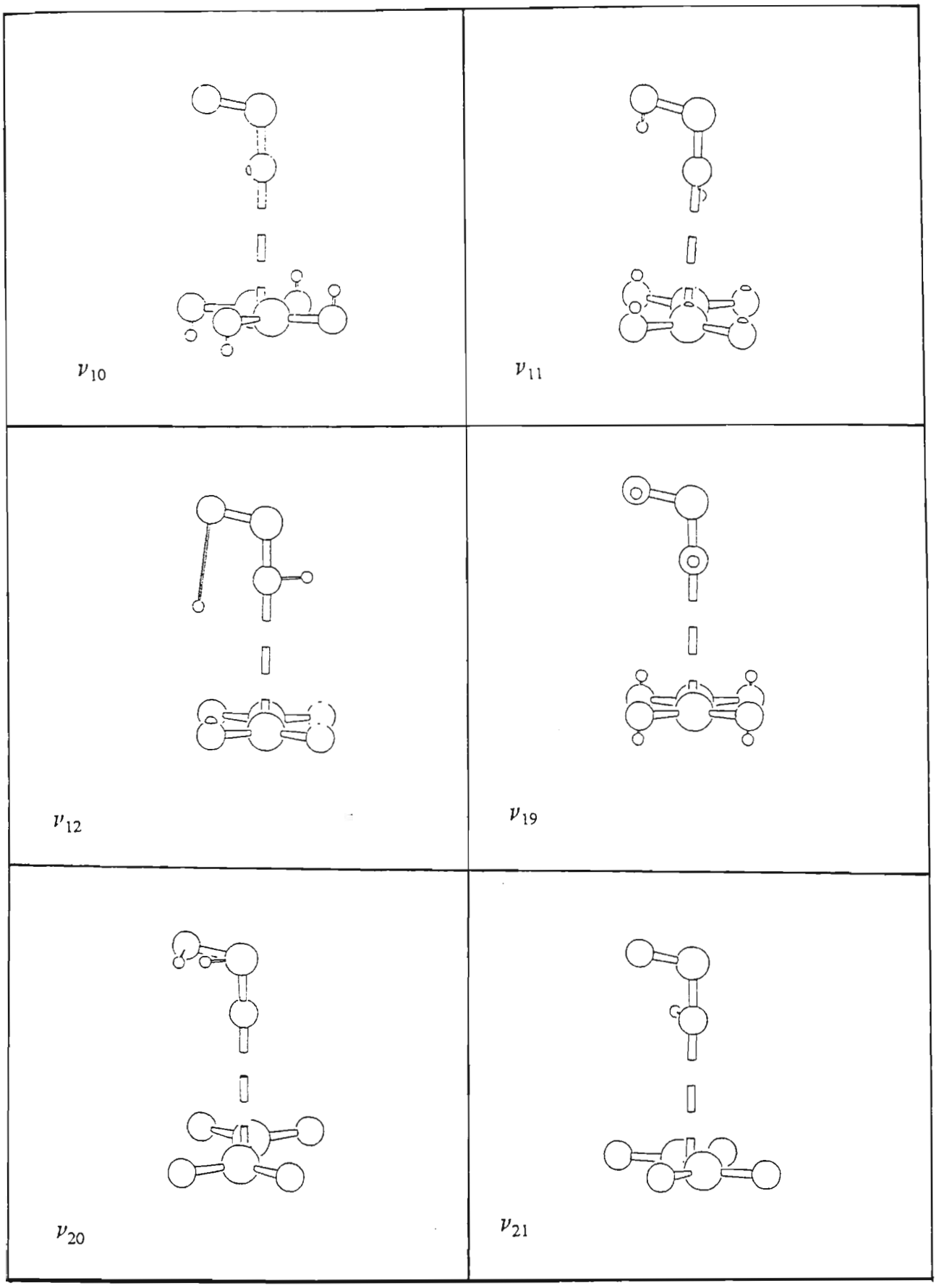

Figure 7.5. The six intermolecular modes of the C_2H_4-HOH complex.

programs Vibram and Vibra. In the H_2CO-HOH and CH_2NH-HOH complexes, which have C_1 symmetry, the intermolecular modes are very similar both in local symmetry description and in the wavenumber ranges spanned; only the IMs of the H_2CO-HOH complex are graphically presented in Figure 7.4, while those of C_2H_4-HOH are shown separately in Figure 7.5, since they exhibit quite a different pattern.

The O6H5...O2 bending motion in the formaldehyde-water complex occurs at 592 cm^{-1} and is coupled with the C1O2...H5 bending and to a small extent with the O2...H5 stretching, while the O7H6...N2 bending mode in the methyleneimine-water adduct occurs at 680 cm^{-1} and is also coupled with the C1N2...H6 bending mode and the motion of the water O7 atom out of the plane of the five-membered ring.

The characteristic H...O(N) stretching vibrational mode is located at 195 and 206 cm^{-1} for the formaldehyde- and methyleneimine-water complexes respectively (see Table 7.9). The remaining IM modes are heavily coupled, mainly between the restricted water sub-unit rotation and the A-H...B in-plane or out-of-plane bending. The ν_{11} mode of C_2H_4-HOH, corresponding to the intermonomer separation motion, is observed at 107 cm^{-1} and its wavenumber is half the magnitude of that of the corresponding mode in either H_2CO-HOH or CH_2NH-HOH. The librational motion, ν_{12}, depicted in Figure 7.5 could not be reproduced due to mixing. The ν_{19} mode, associated with the out-of-plane motion of the H4 atom, occurs at 332 cm^{-1} and this is the only IM with such a large wavenumber for the C_2H_4-HOH complex. The last two IM modes, ν_{20} and ν_{21}, are associated with the antisymmetric stretch of the H4...C1 and H4...C5 bonds and the torsion of the water component about the CC axis.

7.3.2 Intra- and Intermolecular Intensities

Table 7.10 shows the computed infrared intensities of the H_2CO, CH_2NH and C_2H_4 monomers and the reported experimental intensities.[228,229] The correlation between the computed and the experimental values, illustrated in Table 7.10 by the ratio of the calculated/experimental intensities, is variable. The CH_2NH intensities are also in good agreement with those calculated by Komornicki and Mclver [230]. The most notable trend observed in Table 7.10 is that the intensities calculated in this work are almost always lower than the experimental ones, with the exception of the b_2 vibrational modes of H_2CO, where the computed intensities are higher. The computed intensities of the binary complexes of water with H_2CO, CH_2NH and C_2H_4 are presented in Table 7.11, where the ratios of the complex/monomer intensities are also shown for both the intramolecular and intermolecular vibrational modes.

In the H_2CO-HOH complex, the intensities of the ν_1 and ν_2 modes are increased by factors 2 and 23 on complexation respectively. The intensity of the carbonyl stretching mode, ν_5, is slightly decreased, as is the intensity of the water bending mode, ν_6. The CH_2 bending motion, ν_7, is twice as intense in the H_2CO-HOH complex compared with the monomer, providing further evidence of the involvement of the H4 atom in forming part of the ring structure in H_2CO-HOH. The CH_2NH-HOH adduct shows similar intensity ratios to those of the H_2CO-HOH complex. The intensities of the ν_1 and ν_2 modes are increased 2-fold and 51-fold on complexation, while the intensity of the ν_6 mode associated with the water HOH bend is increased 5-fold.

Table 7.10. The Calculated Intensities of the Formaldehyde, Methyleneimine and Ethylene Monomers, the Literature Intensities and the Calculated/Experimental Intensity Ratios

Molecule	Symmetry species	Mode	A/km mol^{-1}		$A_{calc.}/A_{exp.}$
			Calculated	Experimental	
H_2CO[a]	a_1	ν_1	52.6	75.5	0.70
		ν_2	57.5	74.0	0.77
		ν_3	5.0	11.2	0.45
	b_1	ν_4	1.9	6.5	0.29
	b_2	ν_5	140.7	87.6	1.61
		ν_6	11.6	9.9	1.17
CH_2NH	a'	ν_1	2.5	-	-
		ν_2	35.7	-	-
		ν_3	36.5	-	-
		ν_4	13.2	-	-
		ν_5	2.6	-	-
		ν_6	37.8	-	-
		ν_7	40.1	-	-
	a"	ν_8	52.0	-	-
		ν_9	8.6	-	-
C_2H_4[b]	a_g	ν_1	0.0	-	-
		ν_2	0.0	-	-
		ν_3	0.0	-	-
	a_u	ν_4	0.0	-	-
	b_{1g}	ν_5	0.0	-	-
		ν_6	0.0	-	-
	b_{1u}	ν_7	82.1	84.4	0.97
	b_{2g}	ν_8	0.0	-	-
	b_{2u}	ν_9	24.5	26.0	0.44
		ν_{10}	0.4	0.03	13.33
	b_{3u}	ν_{11}	11.4	14.3	0.80
		ν_{12}	3.9	10.4	0.38

[a] Ref. 228. [b] Ref. 229.

Table 7.11. Computed Infrared Intensities of the H_2CO-HOH, CH_2NH-HOH and C_2H_4-HOH Complexes and the Corresponding Monomers with the Complex/Monomer Intensity Ratios

		A/km mol^{-1}		
Species	Mode	Complex	Monomer	A_c/A_m
H_2CO-HOH	ν_1	77.8	33.8	2.3
	ν_2	98.0	4.2	23.3
	ν_3	60.7	140.7	0.4
	ν_4	56.9	52.6	1.2
	ν_5	43.5	57.5	0.8
	ν_6	73.4	77.7	0.9
	ν_7	10.9	5.0	2.2
	ν_8	5.5	11.6	0.5
	ν_9	3.4	1.9	1.8
	ν_{10}	224.4	IM	IM
	ν_{11}	79.1	IM	IM
	ν_{12}	38.0	IM	IM
	ν_{13}	50.0	IM	IM
	ν_{14}	99.8	IM	IM
	ν_{15}	32.3	IM	IM
CH_2NH-HOH	ν_1	65.0	33.8	1.9
	ν_2	214.6	4.2	51.1
	ν_3	0.7	2.5	0.3
	ν_4	9.9	35.7	0.3
	ν_5	35.4	36.5	1.0
	ν_6	67.1	13.2	5.1
	ν_7	7.3	77.7	0.1
	ν_8	5.9	2.6	2.3
	ν_9	36.0	37.8	1.0
	ν_{10}	62.1	52.0	1.2
	ν_{11}	2.7	8.6	0.3
	ν_{12}	49.1	40.1	1.2
	ν_{13}	204.1	IM	IM
	ν_{14}	111.8	IM	IM
	ν_{15}	37.8	IM	IM
	ν_{16}	21.8	IM	IM
	ν_{17}	102.2	IM	IM
	ν_{18}	15.5	IM	IM

Table 7.11 (continued)

C_2H_4-HOH	ν_1	94.5	33.8	2.8
	ν_2	65.3	4.2	15.5
	ν_3	15.2	24.5	0.6
	ν_4	0.2	0.0	*
	ν_5	5.2	0.0	*
	ν_6	65.8	11.4	5.8
	ν_7	0.4	0.0	*
	ν_8	0.0	3.9	0.0
	ν_9	0.5	0.0	*
	ν_{10}	84.8	IM	IM
	ν_{11}	1.0	IM	IM
	ν_{12}	0.0	IM	IM
	ν_{13}	0.0	82.1	0.0
	ν_{14}	6.8	0.0	*
	ν_{15}	5.2	0.0	*
	ν_{16}	0.0	0.0	*
	ν_{17}	0.0	0.0	*
	ν_{18}	0.5	0.0	*
	ν_{19}	80.0	IM	IM
	ν_{20}	85.1	IM	IM
	ν_{21}	41.8	IM	IM

A_c : complex intensity, A_m : monomer intensity,

* : Division by zero.

As was observed with H_2CO-HOH, the intensity of the CH_2 bending motion, ν_8, is increased by a similar order of magnitude. Again, as with the C=O stretch of the H_2CO-HOH complex, the intensity of the C=N stretching mode, ν_7, of CH_2NH-HOH is decreased, though much more drastically in this complex than in H_2CO-HOH. It is interesting to note such a dramatic intensity decrease in the CH_2NH-HOH complex while its C=N bond length was hardly changed on complexation. The intensities of the rest of the modes are unaffected.

In the C_2H_4-HOH complex, only ν_1 and ν_2 show appreciable increases in intensity, with factors of 3 and 16 respectively. Again the ν_6 mode shows a 5-fold intensity increase, as in the case of CH_2NH-HOH. The rest of the modes remain unaffected. In all three complexes of Group 2, the intensity of the water symmetric stretching mode is most enhanced, the enhancement being in the order 15.5, 23.3 and 51.1 for the complexes C_2H_4-HOH, H_2CO-HOH and CH_2NH-HOH respectively; and the water antisymmetric stretching mode is enhanced by a factor of 2 to 3, for H_2CO-HOH, CH_2NH-HOH and C_2H_4-HOH.

Among the IMs the ν_{10} mode of H_2CO-HOH has the highest intensity, which is comparable with that of ν_{13} in the CH_2NH-HOH complex. There is no mode in C_2H_4-HOH with such a high intensity. The intensities of the other IM modes of the H_2CO-HOH complex are in the range 32 to 100 km mol^{-1}; while those of CH_2NH-HOH are in the range 16 to 112 km mol^{-1}. It is interesting to note that ν_{12}, the librational mode, in the C_2H_4-HOH complex has zero intensity, and this is the only IM mode in this series which is predicted to be so weak.

7.3.3 Intra- and Intermolecular Force Constants

Both computed and literature[223,231,232] force constants are collected in Table 7.12, together with the calculated/literature force constant ratios. The last column of Table 7.12 shows that the correlation between the computed force constants and those appearing in the literature is satisfactory.

Table 7.12. Computed Force Constants of the Formaldehyde, Methyleneimine and Ethylene Monomers together with the Literature Values and the Computed/Literature Force Constant Ratios

Molecule	Force constant	Value		Ratio
		Calculated	Literature	
H_2CO[a]	f(C1O2)/N m^{-1}	1297.96	1228.5	1.1
	f(C1H3)/N m^{-1}	518.54	436.5	1.2
	f(H3C1H4)/N m rad^{-2}	161.84	78.8	2.1
CH_2NH[b]	f(C1N2)/N m^{-1}	1115.47	1039.0	1.1
	f(C1H3)/N m^{-1}	561.64	485.0	1.2
	f(N2H5)/N m^{-1}	688.04	450.0	1.5
	f(C1N2H5)/N m rad^{-2}	87.81	61.0	1.4
C_2H_4[c]	f(C1C2)/N m^{-1}	991.3	890.7	1.1
	f(C1H3)/N m^{-1}	596.7	513.8	1.2
	f(H3C1C2)/N m rad^{-2}	59.2	54.4	1.1

[a] Ref. 231. [b] Ref. 223. [c] Ref. 232.

Table 7.13 presents the corresponding computed force constants of the complexes along with the differences between the complex and monomer, in an attempt to establish the extent of perturbation of the force constants on complexation.

The stretching force constant of the C=O bond, f(C1O2), of H_2CO-HOH is reduced by about 5 N m^{-1}, while the f(C1H4) force constant increases by 16.6 N m^{-1} and the water hydrogen bonded OH force constant is reduced by 13.6 N m^{-1}. The changes are consistent with the notion that with an increase in the electron density in the bonding region, the bond is strengthened and vice versa. In the case of the CH_2NH-HOH adduct, the stretching force constant of

Table 7.13. Computed Force Constants of the Complexes of H_2O with H_2CO, CH_2NH and C_2H_4 and the Differences between the Complex and Monomer Force Constants

Complex	Force Constant	Value	
		Calculated	Difference
H_2CO-HOH	f(C1O2)/N m^{-1}	1284.1	-4.9
	f(C1H4)/N m^{-1}	535.1	16.6
	f(O6H5)/N m^{-1}	864.1	-13.6
	f(O2...H5)/N m^{-1}	20.9	IM
	f(O6H5...O2)/N m rad^{-2}	10.6	IM
CH_2NH-HOH	f(C1N2)/N m^{-1}	1123.1	7.6
	f(N2H5)/N m^{-1}	695.7	7.7
	f(C1H3)/N m^{-1}	573.1	12.1
	f(O7H6)/N m^{-1}	853.0	-24.7
	f(H6..N2)/N m^{-1}	22.1	IM
	f(O7H6..N2)/N m rad^{-2}	11.1	IM
C_2H_4-HOH	f(C1C5)/N m^{-1}	991.0	-0.3
	f(C1H5)/N m^{-1}	596.9	0.2
	f(O8H4)/N m^{-1}	871.8	-5.9
	f(H4..C1)/N m^{-1}	5.6	IM

the C=N bond, f(C1N2), is increased by 7.6 N m^{-1}, as is f(N2H5), by 7.7 N m^{-1}. The increase in the stretching force constant of the C1N2 bond is hard to explain, but is consistent with the observation made for the C≡N bond in the CH_3CN-HOH complex (see section 6.3.3). The stretching force constant of the C1H3 bond forming the secondary hydrogen bond is increased by 12.1 N m^{-1}, a similar increase to that in the formaldehyde-water complex. Again the water f(O7H6) force constant is reduced by 24.7 N m^{-1}, compared with 13.6 N m^{-1} for the H_2CO-HOH complex.

There are practically no changes to the intramolecular force constants in the

C_2H_4-HOH complex. The intermonomer stretching force constant, f(H...B), has a value of 20.9 N m^{-1} and the in-plane bending force constant, f(A-H...B), has a value of 10.6 N m rad^{-2} in this complex. In the CH_2NH-HOH complex the ν(H...B) mode has a force constant of 22.9 N m^{-1} and the δ(A-H...B) mode has a force constant of 11.1 N m rad^{-2}. In the latter case both the force constants are higher, expectedly so because the CH_2NH-HOH adduct is the stronger complex of the two. The intermonomer stretching force constant of C_2H_4-HOH is 5.6 N m^{-1}, which is quite small compared with those of H_2CO-HOH and CH_2NH-HOH. It is not surprising to observe such a low force constant for a complex almost half as stable as the H_2CO-HOH complex and approximately one third of the stability of the CH_2NH-HOH complex.

CHAPTER 8

8.1 RESULTS AND DISCUSSION OF THE GROUP 3 COMPLEXES

The structural parameters, energetics, charge redistributions and vibrational properties of the binary complexes of water with acetaldehyde and acetone are reported. The results are compared with those of the formaldehyde-water complex, section 7.2, and parallels drawn.

8.2 Structural, Energetic and Electronic Properties of the CH_3CHO-HOH and $(CH_3)_2CO$-HOH Complexes

8.2.1 Geometrical Parameters

Figure 8.1(a) illustrates the optimised equilibrium structure for the acetaldehyde-water complex, which contains a distorted 5-membered ring. Table 8.1 gives a listing of all the geometrical parameters of the CH_3CHO and $(CH_3)_2CO$ monomers, according to the atom numbering used in Figure 8.1. The last column shows the differences between the calculated and experimental[190] values. In general the correlation is good. Table 8.2 presents the computed structural parameters of both the CH_3CHO-HOH and $(CH_3)_2CO$-HOH complexes, with the last column showing the differences between the calculated complex parameters and those of the corresponding monomers. In the CH_3CHO-HOH complex, there are in general no dramatic geometrical distortions on complexation. However, a few significant changes which will be singled out for comment are the C2O3, C2H4 and O9H8 bond lengths and the C1C2O3, H4C2C1 and O3C2H4 angles.

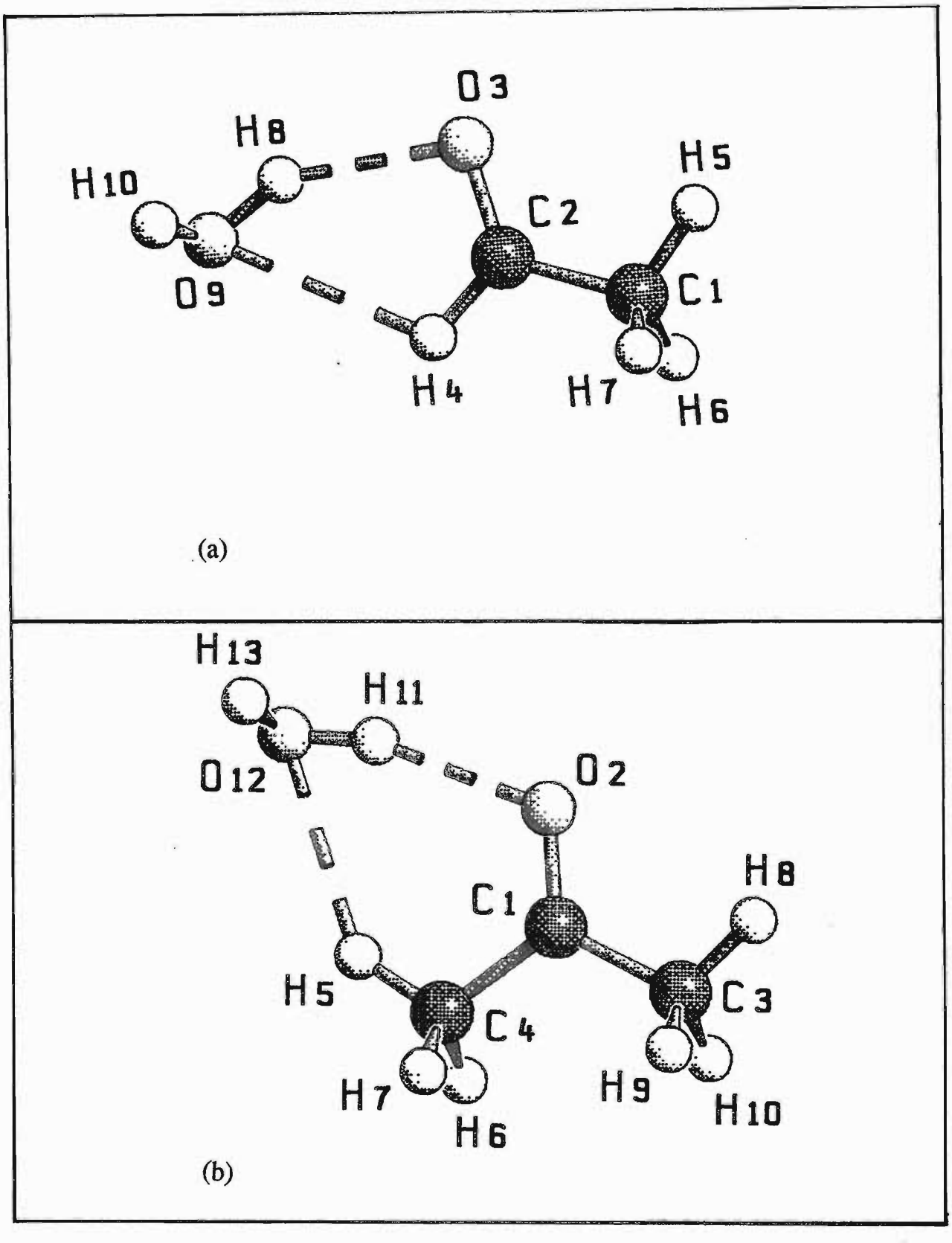

Figure 8.1. Graphical representations of the equilibrium structures and the atom numbering: (a) CH_3CHO-HOH; (b) $(CH_3)_2CO$-HOH.

Table 8.1. The Calculated and Experimental Geometrical Parameters of Acetaldehyde and Acetone together with the Differences between the Calculated and Experimental Parameters

		Value		
Molecule	Parameter	Calculated	Experimental (Ref. 190)	Difference
CH_3CHO	r(C1C2)/pm	150.2	150.4	0.2
	r(C2O3)/pm	122.3	121.7	-0.6
	r(C1H5)/pm	108.6	107.4	-1.2
	r(C1H6)/pm	109.1	107.4	-1.7
	r(C1H7)/pm	109.1	107.4	-1.7
	r(C2H4)/pm	110.5	111.4	0.9
	r(O9H8)/pm	96.1	96.5	0.4
	r(O9H10)/pm	96.1	96.5	0.4
	O3C2C1/deg	124.3	124.0	-0.3
	C2C1H5/deg	109.9	110.6	0.7
	O3C2H4/deg	120.5	121.1	0.6
	C2C1H6/deg	109.7	109.3	-0.4
	C2C1H7/deg	109.7	110.3	0.6
$(CH_3)_2CO$	r(C1O2)/pm	122.7	119.2	-3.5
	r(C1C3)/pm	151.3	151.3	0.0
	r(C1C4)/pm	151.3	151.3	0.0
	r(C3H8)/pm	108.6	108.1	-0.5
	r(C3H9)/pm	109.0	108.6	-0.4
	r(C3H10)/pm	109.0	108.6	-0.4
	r(C2H4)/pm	108.6	108.1	-0.5
	r(C4H5)/pm	109.0	108.6	-0.4
	r(C4H7)/pm	109.0	108.6	-0.4
	r(O12H11)/pm	96.1	94.3	-1.8
	r(O12H13)/pm	96.1	94.3	-1.8
	C3C1O2/deg	121.8	121.7	-0.1
	H8C3C1/deg	109.6	109.8	0.2
	H9C3C1/deg	110.2	110.3	0.1
	H10C3C1/deg	110.2	110.3	0.1
	H5C4C1/deg	109.6	109.8	0.2
	H7C4C1/deg	110.2	110.3	0.1
	H6C4C1/deg	110.2	110.2	0.0

Table 8.2. The Geometrical Parameters of the Acetaldehyde- and Acetone-Water Complexes and the Differences between the Complex and Monomer Parameters

Complex Difference	Parameter	Value Calculated	Value
CH_3CHO-HOH	r(C1C2)/pm	149.8	-0.4
	r(C2O3)/pm	122.9	0.6
	r(C1H5)/pm	108.6	0.0
	r(C1H6)/pm	109.0	-0.1
	r(C1H7)/pm	109.1	0.0
	r(C2H4)/pm	110.0	-0.5
	r(O8...O3)/pm	199.7	-
	r(O3...O9)/pm	288.1	-
	r(H4...O9)/pm	258.1	-
	r(O9H8)/pm	96.8	0.7
	r(O9H10)/pm	96.1	0.0
	C1C2O3/deg	123.5	-0.8
	C2C1H5/deg	110.2	0.3
	H4C2C1/deg	116.8	1.6
	O3C2H4/deg	119.6	-0.9
	C2C1H6/deg	109.5	-0.2
	C2C1H7/deg	109.6	-0.1
	C2O3....H8/deg	98.4	-
	O9H8...O3/deg	150.0	-
	H8O9...H4/deg	62.6	-
	C2H4...O9/deg	72.0	-
	H8O9H10/deg	103.9	0.1
	H10O9H8...O3/deg	112.0	-

Table 8.2 (continued)

$(CH_3)_2CO$-HOH	r(C1O2)/pm	123.2	0.5
	r(C1C3)/pm	150.9	-0.4
	r(C1C4)/pm	150.9	-0.4
	r(C3H8)/pm	108.6	0.0
	r(C3H9)/pm	109.0	0.0
	r(C3H10)/pm	109.1	0.1
	r(C4H5)/pm	108.6	0.0
	r(C4H6)/pm	109.0	0.0
	r(C4H7)/pm	109.0	0.0
	r(H11...O2)/pm	198.1	-
	r(O2...O12)/pm	292.7	-
	r(H5...O12)/pm	243.2	-
	r(O12H11)/pm	96.9	0.8
	r(O12H13)/pm	96.1	0.0
	C3C1O2/deg	120.8	1.0
	C4C1O2/deg	122.2	0.4
	H8C3C1/deg	110.1	0.5
	H9C3C1/deg	109.7	-0.5
	H10C3C1/deg	109.6	-0.6
	H5C4C1/deg	109.8	0.2
	H6C4C1/deg	110.0	-0.2
	H7C4C1/deg	110.0	-0.2
	C1O2...H11/deg	114.9	-
	O12H11...O2/deg	163.4	-
	H11O12...H5/deg	51.1	-
	C4H5...O12/deg	104.4	-
	H11O12H13/deg	103.9	0.5
	H8C3C1O2/deg	121.4	0.5
	H9C3C1O2/deg	121.1	0.2
	H13O12H11...O2/deg	107.7	-

It is comforting to note that four of these parameters are directly involved in the formation of the 5-membered ring, while the C1C2O3 and H4C2C1 angles are related to the O3C2H4 angle which is directly involved in the ring formation. The C2O3 bond is extended by 0.6 pm while the C2H4 bond is shortened by 0.5

pm. One would have expected a bond extension, but here back donation from the water oxygen atom, O9, occurs, which interacts with the H4 atom of the acetaldehyde sub-unit. The O9H8 bond is extended by 0.5 pm. This is an important distortion illustrating the fact that the water H8 atom is actually displaced towards the carbonyl oxygen.

The angle O3C2H4 decreases by 0.9°. The angle H4C2C1 opens up by 1.6°, while the C1C2O3 angle decreases by 0.8° (see Table 8.2). This allows a more favourable orbital overlap for the H8...O3 and H4...O9 interactions, with predicted lengths of 199.7 and 258.1 pm respectively. Indeed it is the formation of the secondary hydrogen bond, H4..O9, which explains the large deviation, by 30°, of the O9H8...O3 hydrogen bond angle from linearity. The intermolecular A...B separation distance, O9...O3, is 288.1 pm, which compares favourably with the value of 286.0 pm obtained by Del Bene[35]. The corresponding primary O9H8...O3 and secondary C2H4...O9 bond angles are 150° and 72° respectively with the weaker hydrogen bond showing a greater deviation from linearity.

Figure 8.1(b) is a graphical representation of the optimised equilibrium structure of the acetone-water complex, together with the atom numbering which will be used throughout whenever reference to any parameter concerning this structure is made. The complex features a distorted 6-membered ring. The geometrical parameters directly involved in complexation are C1O2, C1C4, C4H5, O12H11, H5C4C1 and C4C1O2, as illustrated and listed in Figure 8.1(b) and Table 8.2 respectively. The C1O2 bond is extended by 0.5 pm as expected. The C1C4 bond is however shortened by 0.4 pm; this is due to the positive inductive effect of the methyl groups. The O12H11 bond is extended by 0.8 pm, indicating an even stronger proton donating tendency than in the acetaldehyde-water complex, in the absence of any other factors.

It is interesting to note that, although it forms part of the six-membered ring, the C4H5 bond length does not seem to be perturbed at all on complexation. The apparent constancy of the C4H5 bond length is perhaps due to the inductive and steric effects of the methyl groups. The calculated primary H...B bond length (H11...O2) is 198.1 pm, which compares fairly well with the 205.8 pm computed by Parnis et al.[156] at the SCF level. The results of this work are in good agreement with those of Lee and Dyke,[158] who used both the RHF and MP2 levels of theory to investigate the geometry of the protonated acetone molecule. The secondary H...B bond length (H5...O12) found in this work is 243.2 pm, which is considerably shorter than the 255.3 and 258.1 pm values for the H_2CO-HOH (see section 7.2) and CH_3CHO-HOH complexes respectively and, furthermore, the A...B separation distances are 292.7, 288.1 and 289.4 pm for the $(CH_3)_2CO$-HOH, CH_3CHO-HOH and H_2CO-HOH complexes respectively. The two bond angles, O12H11...O2 and C4H5...O12, in the $(CH_3)_2CO$-HOH complex, are increased slightly compared with the corresponding angles O9H8...O3 and C2H4...O9 respectively in the CH_3CHO-HOH complex.

The angle increases can be attributed to the decreased steric strain present in the six-membered ring, compared with that in the five-membered ring. The C=O...H angles are 98.4° and 114.9° for the acetaldehyde- and acetone-water complexes respectively. In these two cases the angle approaches the ideal[31] value of 120° more effectively than in the H_2CO-HOH complex, in which it has a value of 97.3°.

8.2.2 Interaction Energies and the Morokuma Energy Components

Table 8.3 presents the interaction energies before and after BSSE correction. It is interesting to note that the interaction energies of the Group 3 (including H_2CO-HOH) complexes are all in the same range; expectedly so due to the fact that all the EDs have a carbonyl group which is the dominant centre of interaction.

Table 8.3. Interaction Energies with and without BSSE Correction, at both MP2 and RHF Theory Levels

	ΔE/kJ mol^{-1}		
Complex	Uncorrected	BSSE	Corrected
		MP2	
H_2CO-HOH	-28.43	13.39	-15.06
CH_3CHO-HOH	-30.53	13.93	-16.60
$(CH_3)_2CO$-HOH	-33.70	18.22	-16.48
		RHF	
H_2CO-HOH	-21.09	5.64	-15.45
CH_3CHO-HOH	-22.57	5.47	-17.10
$(CH_3)_2CO$-HOH	-24.79	5.88	-18.91

Of the three complexes (including H_2CO-HOH), the acetaldehyde- and acetone-water complexes are very similar in strength, while the formaldehyde-water complex is slightly weaker. Table 8.4 presents the energy components from the Morokuma decomposition scheme. The energy decomposition analysis[191,192] confirms that hydrogen bonding is basically electrostatic in nature, constituting over 40% of the total interaction energy. The secondary stabilisation effect arises from the charge transfer term, contributing about 15% for each complex.

The polarization energy is fairly small in both the CH_3CHO-HOH and the $(CH_3)_2CO$-HOH complexes, but is certainly more pronounced than the mixing term. The most important destabilisation component of the interaction energy is that which arises from exchange repulsion, which can be associated with the tendency to contravene the Pauli exclusion principle.[26]

Table 8.4. Energy Components from the Morokuma Decomposition Scheme

		Decomposed Interaction Energies /kJ mol^{-1}		
Complex	Component	Uncorrected	Corrected	%Contribution
CH_3CHO-HOH	El	-39.27	-39.27	44
	Pl	-3.90	-3.90	4
	Ex	30.77	32.00	35
	Ct	-13.07	-10.45	15
	Mix	-1.96	2.69	2
	Total	-25.04	-17.10	-
$(CH_3)_2CO$-HOH	El	-34.91	-34.91	45
	Pl	-3.33	-3.33	4
	Ex	26.29	27.43	34
	Ct	-11.54	-9.29	15
	Mix	-1.56	3.00	2
	Total	-27.44	-18.93	-

As with the complexes of Groups 1 and 2 (sections 6.2 and 7.2), the Gaussian-92 RHF interaction energies corrected for the counterpoise effect are identical with those from the Monstergauss output. This reaffirms the expectation that at the SCF level, if the decomposition is applied at the true converged geometry, the stabilisation energy must be the same.

8.2.3 Atomic Charge Redistributions

Table 8.5 gives the atomic charges in both the monomers and the complexes. The penultimate column shows the difference between the complex and the monomer atomic charges. From Table 8.5, it is seen that the acetaldehyde O3 atom gains 0.0405 e. This is quite a significant charge redistribution, with part of this electron density being used for the hydrogen bond formation. The acetaldehyde H4 atom loses 0.0414 e. This again shows the involvement of this atom in the complexation and supports the view that the deviation from linearity of the hydrogen bond angle is due to the formation of the secondary hydrogen bond. The H8 atom of the water molecule loses a significant amount of charge towards the formation of the hydrogen bond, while the water oxygen gains a charge of 0.0432 e.

The fragment charge on the water sub-unit is negative implying that the water component has gained charge density on complexation while acetaldehyde has lost a similar amount of charge. The acetaldehyde sub-unit is an ED and a PA while the water molecule is an EA and PD, as shown in Table 8.5. In short, the charge redistributions support the geometrical distortion arguments, in that the atoms most significantly affected are the ones directly involved in the complexation.

The acetone-water complex shows a very similar pattern. The analysis of the charge redistribution again confirms the involvement of H5 of the acetone molecule in complexation. The overall charge analysis shows that the water molecule in the acetone-water complexes becomes negatively charged, while the

Table 8.5. The Predicted MP2 Charge Distributions of the H_2O, CH_3CHO and $(CH_3)_2CO$ Monomers and their Complexes, with the Changes in Charges between Complex and Monomer, and the Fragment Charges

		Charge/e			
Complex	Atom	Monomer	Complex	Change	Fragment[a]
CH_3CHO-HOH	C1	-0.4307	-0.4309	-0.0002	
	C2	0.3810	0.3805	-0.0005	
	O3	-0.4981	-0.5386	-0.0405	
	H4	0.1000	0.1414	0.0414	
	H5	0.1629	0.1654	0.0025	
	H6	0.1424	0.1502	0.0078	
	H7	0.1424	0.1470	0.0045	
					0.0150
	H8	0.3369	0.3733	0.0364	
	O9	-0.6738	-0.7170	-0.0432	
	H10	0.3369	0.3287	-0.0082	
					-0.0150

Table 8.5 (continued)

$(CH_3)_2CO$-HOH[a]	C1	0.5042	0.5218	0.0176	
	O2	-0.5398	-0.5768	-0.0370	
	C3	-0.4172	-0.4162	0.0010	
	C4	-0.4172	-0.4395	-0.0223	
	H5	0.1621	0.1950	0.0329	
	H6	0.1365	0.1419	0.0054	
	H7	0.1365	0.1364	-0.0001	
	H8	0.1621	0.1653	0.0032	
	H9	0.1365	0.1411	0.0046	
	H10	0.1365	0.1433	0.0068	
					0.0121
	H11	0.3369	0.3782	0.0413	
	O12	-0.6738	-0.7166	-0.0428	
	H13	0.3369	0.3259	-0.0110	-0.0125

[a] Note that due to round-off error the fragment charges in the acetone-water complex do not add up to zero.

acetone sub-unit loses an amount of charge equal to that gained by the water molecule. In both the CH_3CHO-HOH and $(CH_3)_2CO$-HOH complexes, the H_2O component is the EA and PD with strong evidence of secondary hydrogen bond formation. The systems studied indicate the presence of cyclic complexes. The stabilities of the complexes are enhanced by electrostatic interactions.

8.3 Vibrational Properties of the CH_3CHO-HOH and $(CH_3)_2CO$-HOH Complexes

8.3.1 Intra- and Intermolecular Wavenumbers

The computed wavenumbers of the acetaldehyde and acetone monomers are listed in Table 8.6, along with their experimental counterparts[193] and the computed/experimental ratios. The computed wavenumbers of water were listed in Table 6.7 of chapter 6. The calculated/experimental ratios approximate unity with the exception of ν_{13} in the CH_3CHO molecule, where the vibrational wavenumber is overestimated by 1.34 times compared with the experimental value. In the acetone molecule, the very low vibrational wavenumbers, namely those of the ν_{12} and ν_{17} modes, are not so well reproduced theoretically. This is not unusual for very low vibrational frequencies.

The local symmetry coordinates of both the intramolecular and intermolecular vibrations in the complexes of water with acetaldehyde and acetone are collected in Table 8.7, and Table 8.8 presents the wavenumbers and wavenumber shifts along with the potential energy distributions. In this set of complexes the stretching vibrations most intimately associated with the complexation are significantly perturbed. There are five such major wavenumber shifts observed for the acetaldehyde-water complex. The $\nu_s(OH_2)$ and $\nu_a(OH_2)$ vibrational modes

are red shifted by -80 and -42 cm^{-1} respectively while the HOH bending mode is blue shifted by 25 cm^{-1}. The ν(CO) bond stretch is red shifted by -20 cm^{-1}. It is important to note that in the H_2CO-HOH and CH_3CHO-HOH complexes, the C1H4 and C2H4 bonds were shortened to the same extent, 0.5 pm (see Tables 7.2 and 8.2). The stretching vibrational wavenumbers of these bonds are both blue shifted, by 74 and 58 cm^{-1} respectively.

Table 8.6. The Computed and Experimental Wavenumbers of Acetaldehyde and Acetone and the Calculated/Experimental Ratios

Complex	Symmetry species	Mode	$\tilde{\nu}/cm^{-1}$ Calculated	$\tilde{\nu}/cm^{-1}$ Experimental	$\tilde{\nu}_{calc.}/\tilde{\nu}_{exp}$
CH_3CHO	a'	ν_1	3265	3005	1.09
		ν_2	3129	2917	1.07
		ν_3	3010	2822	1.07
		ν_4	1799	1743	1.03
		ν_5	1522	1441	1.06
		ν_6	1466	1400	1.05
		ν_7	1431	1352	1.06
		ν_8	1163	1113	1.04
		ν_9	921	919	1.00
		ν_{10}	511	509	1.00
	a"	ν_{11}	3216	2967	1.08
		ν_{12}	1533	1420	1.08
		ν_{13}	1164	867	1.34
		ν_{14}	795	763	1.04
		ν_{15}	149	150	1.00

Table 8.6 (continued)

$(CH_3)_2CO$	a_1	ν_1	3265	3019	1.08
		ν_2	3132	2937	1.07
		ν_3	1794	1731	1.04
		ν_4	1529	1435	1.07
		ν_5	1435	1364	1.05
		ν_6	1111	1066	1.04
		ν_7	814	777	1.05
		ν_8	382	385	1.00
	a_2	ν_9	3213	2963	1.08
		ν_{10}	1526	1426	1.07
		ν_{11}	915	877	1.04
		ν_{12}	56	105	0.53
	b_1	ν_{13}	3219	3019	1.07
		ν_{14}	1547	1410	1.08
		ν_{15}	1147	1091	1.05
		ν_{16}	488	484	1.01
		ν_{17}	142	109	1.30
	b_2	ν_{18}	3264	2972	1.10
		ν_{19}	3127	2937	1.06
		ν_{20}	1523	1454	1.05
		ν_{21}	1442	1364	1.06
		ν_{22}	1281	1216	1.05
		ν_{23}	923	891	1.04
		ν_{24}	534	530	1.01

The wavenumber shift patterns of $(CH_3)_2CO$-HOH are very similar to those of CH_3CHO-HOH. The symmetric stretching mode of the water molecule is red shifted by -94 cm^{-1}, about 1.2 times that of the shift in the acetaldehyde-water complex. The antisymmetric stretching mode of the water molecule is again shifted to lower wavenumber by -48 cm^{-1}, in a similar fashion to the shift of the corresponding mode in the CH_3CHO-HOH complex. While the ν(CO) mode is red shifted, this shift is lower in the acetone-water adduct than in the acetaldehyde-water complex and still lower than in the formaldehyde-water complex.

Table 8.7. Local Symmetry Coordinates of the Acetaldehyde- and Acetone-Water Complexes and the Descriptions of each Coordinate

Complex	Symmetry Coordinate		Description
CH_3CHO-HOH	S_1	$\{\Delta r_{8,9} - \Delta r_{9,10}\}/\sqrt{2}$	OH_2 a-stretch
	S_2	$\{\Delta r_{8,9} + \Delta r_{9,10}\}/\sqrt{2}$	OH_2 s-stretch
	S_3	$\{2\Delta r_{1,5} - \Delta r_{1,6} - \Delta r_{1,7})/\sqrt{6}$	CH_3 d- stretch
	S_4	$\{\Delta r_{1,6} - \Delta r_{1,7})/\sqrt{2}$	CH_3 d-stretch
	S_5	$\{\Delta r_{1,5} + \Delta r_{1,6} + \Delta r_{1,7})/\sqrt{3}$	CH_3 s-stretch
	S_6	$\Delta r_{2,4}$	CH stretch
	S_7	$\Delta r_{2,3}$	CO stretch
	S_8	$\Delta\delta_{8,9,10}$	OH_2 bend
	S_9	$\{\Delta\delta_{5,1,6} - \Delta\delta_{5,1,7}\}/\sqrt{2}$	CH_3 d-deformation
	S_{10}	$\{2\Delta\delta_{6,1,7} - \Delta\delta_{5,1,6} - \Delta\delta_{5,1,7}\}/\sqrt{3}$	CH_3 d-deformation
	S_{11}	$\Delta\delta_{3,2,4}$	O=C-H bend
	S_{12}	$\{\Delta\delta_{5,1,6} + \Delta\delta_{5,1,7} + \Delta\delta_{6,1,7}$ $- \Delta\beta_{5,1,2} - \Delta\beta_{6,1,2} - \Delta\beta_{7,1,2}\}/\sqrt{6}$	CH_3 s-deformation
	S_{13}	$\Delta\gamma_{3,1,2,4}$	CO op bend
	S_{14}	$\{2\Delta\beta_{5,1,2} - \Delta\beta_{6,1,2} - \Delta\beta_{7,1,2}\}/\sqrt{6}$	CH_3 rock
	S_{15}	$\Delta r_{1,2}$	CC stretch
	S_{16}	$\{\Delta\beta_{6,1,2} - \Delta\beta_{7,1,2}\}/\sqrt{2}$	CH_3 rock
	S_{17}	$\Delta\delta_{3,8,9}$	O-H...O bend
	S_{18}	$\Delta\delta_{1,2,3}$	CCO bend
	S_{19}	$\Delta\tau_{2,3,8,9}$	torsion about H...O bond
	S_{20}	$\Delta r_{3,8}$	O...H stretch

Table 8.7 (continued)

	S_{21}	$\Delta\tau_{3,8,9,10}$	restricted rotation about O...H bond
	S_{22}	$\Delta\tau_{5,1,2,4}$	torsion about CC bond
	S_{23}	$\Delta\delta_{2,3,8}$	C=O...H ip bend
	S_{24}	$\Delta\gamma_{3,8,9}$	O-H..O op bend
$(CH_3)_2CO$-HOH	S_1	$\{\Delta r_{11,12} - \Delta r_{12,13}\}/\sqrt{2}$	OH_2 a-stretch
	S_2	$\{\Delta r_{11,12} + \Delta r_{12,13}\}/\sqrt{2}$	OH_2 s-stretch
	S_3	$\{\Delta r_{4,5} + \Delta r_{3,8}\}/\sqrt{2}$	CH s-stretch
	S_4	$\{\Delta r_{4,5} - \Delta r_{3,8}\}/\sqrt{2}$	CH a-stretch
	S_5	$\{\Delta r_{4,6} - \Delta r_{4,7} + \Delta r_{3,9} - \Delta r_{3,10}\}/2$	CH_3 d-stretch
	S_6	$\{\Delta r_{4,6} - \Delta r_{4,7} + \Delta r_{3,9} - \Delta r_{3,10}\}/2$	CH_3 d-stretch
	S_7	$\{\Delta r_{4,6} + \Delta r_{4,7} + \Delta r_{3,10} + \Delta r_{3,9}\}/2$	CH_3 s-stretch
	S_8	$\{\Delta r_{4,6} + \Delta r_{4,7} - \Delta r_{3,10} - \Delta r_{3,9}\}/2$	CH_3 d-stretch
	S_9	$\Delta r_{1,2}$	CO stretch
	S_{10}	$\Delta\delta_{11,12,13}$	OH_2 bend
	S_{11}	$\{\Delta\delta_{5,4,6} - \Delta\delta_{547} + \Delta\delta_{8,3,10} - \Delta\delta_{8,3,9}\}/2$	CH_3 d-deformation
	S_{12}	$\{\Delta\delta_{5,4,6} + \Delta\delta_{547} + \Delta\delta_{8,3,10} + \Delta\delta_{8,3,9}\}/2$	CH_3 s-deformation
	S_{13}	$\{\Delta\delta_{5,4,6} - \Delta\delta_{547} - \Delta\delta_{8,3,10} + \Delta\delta_{8,3,9}\}/2$	CH_3 d-deformation
	S_{14}	$\{\Delta\delta_{5,4,6} + \Delta\delta_{547} - \Delta\delta_{8,3,10} - \Delta\delta_{8,3,9}\}/2$	CH_3 d-deformation
	S_{15}	$\{\Delta\beta_{6,4,1} + \Delta\beta_{741} - \Delta\beta_{10,3,1} - \Delta\beta_{9,3,1}\}/2$	CH_3 rock
	S_{16}	$\{\Delta\beta_{6,4,1} + \Delta\beta_{741} + \Delta\beta_{10,3,1} + \Delta\beta_{9,3,1}/2$	CH_3 rock
	S_{17}	$\{\Delta r_{1,3} - \Delta r_{1,4}\}/\sqrt{2}$	CC a-stretch
	S_{18}	$\{\Delta\beta_{6,4,1} - \Delta\beta_{7,4,1} + \Delta\beta_{10,3,1} - \Delta\beta_{9,3,1}/2$	CH_3 rock
	S_{19}	$\{\Delta\beta_{8,3,1} + \Delta\beta_{5,4,1}\}/\sqrt{2}$	CH_3 rock

Table 8.7 (continued)

S_{20}	$\{\Delta\beta_{8,3,1} - \Delta\beta_{5,4,1}\}/\sqrt{2}$	CH_3 rock
S_{21}	$\{\Delta\beta_{6,4,1} - \Delta\beta_{7,4,1} - \Delta\beta_{10,3,1} + \Delta\beta_{9,3,1}/2$	CH_3 rock
S_{22}	$\{\Delta r_{1,3} + \Delta r_{1,4}\}/\sqrt{2}$	CC s-stretch
S_{23}	$\Delta\delta_{2,11,12}$	O-H..O ip bend
S_{24}	$\Delta\{\Delta\delta_{3,1,2} - \Delta\delta_{4,1,2}\}/\sqrt{2}$	CCO bend oop
S_{25}	$\Delta\tau_{2,3,1,4}$	torsion
S_{26}	$\Delta\{\Delta\delta_{3,1,2} + \Delta\delta_{4,1,2}\}/\sqrt{2}$	CCO bend in-phase
S_{27}	$\Delta\tau_{1,2,11,12}$	torsion about
S_{28}	$\Delta\tau_{13,12,11,2}$	hindered rotation H...O
S_{29}	$\Delta r_{2,11}$	O...H stretch
S_{30}	$\{\Delta\tau_{5,4,1,2} - \Delta\tau_{8,3,1,2}\}/\sqrt{2}$	torsion about CC oop
S_{31}	$\Delta\delta_{12,11}$	C=O..H ip bend
S_{32}	$\Delta\{\Delta\tau_{5,4,12} + \Delta\tau_{8,3,12}\}/\sqrt{2}$	torsion about CC in-phase
S_{33}	$\Delta\gamma_{11,2,1}$	O-H...O op bend

Table 8.8. The Predicted Wavenumbers of the Acetaldehyde and Acetone-Water Complexes together with the Wavenumber Shifts and the %PEDs

		$\tilde{\nu}/cm^{-1}$		
Complex	Mode	Calculated	Shift	%PED
CH_3CHO-HOH	ν_1	3988	-42	$86S_1 + 13S_2$
	ν_2	3812	-80	$83S_2 + 14S_1$
	ν_3	3267	2	$98S_3$
	ν_4	3217	1	$100S_4$
	ν_5	3130	1	$97S_7$
	ν_6	3084	74	$99S_6$
	ν_7	1779	-20	$81S_7$
	ν_8	1707	25	$88S_8$
	ν_9	1531	-2	$91S_9$
	ν_{10}	1520	-2	$91S_{10}$
	ν_{11}	1468	2	$79S_{11}$
	ν_{12}	1432	1	$82S_{12} + 10S_{11}$
	ν_{13}	1177	13	$60S_{13} + 30S_{16}$
	ν_{14}	1171	8	$40S_{14} + 27S_{15} + 19S_{19}$
	ν_{15}	931	10	$53S_{15} + 33S_{14}$
	ν_{16}	816	21	$52S_{16} + 38S_{13}$
	ν_{17}	629	IM	$60S_{17} + 18S_{23} + 10S_{20}$
	ν_{18}	520	9	$65S_{18} + 19S_{14}$

Table 8.8 (continued)

	ν_{19}	319	IM	$59S_{19} + 28S_{21}$
	ν_{20}	183	IM	$62S_{20} + 21S_{21}$
	ν_{21}	178	IM	$45S_{21} + 35S_{20}$
	ν_{22}	147	-2	$52S_{22} + 13S_{21}$
	ν_{23}	108	IM	$66S_{23} + 25S_{17}$
	ν_{24}	88	IM	$56S_{24} + 21S_{21} + 14S_{19}$
$(CH_3)_2CO$-HOH	ν_1	3982	-48	$84S_1 + 15S_2$
	ν_2	3798	-94	$81S_2 + 16S_1$
	ν_3	3270	5	$41S_3 + 39S_4 + 10S_7$
	ν_4	3267	3	$42S_4 + 39S_3 + 10S_8$
	ν_5	3220	1	$88S_5 + 11S_6$
	ν_6	3213	0	$88S_6 + 11S_5$
	ν_7	3133	1	$70S_7 + 18S_3$
	ν_8	3127	0	$70S_8 + 16S_4 + 10S_8$
	ν_9	1782	-12	$74S_9$
	ν_{10}	1712	30	$71S_{10} + 15S_{27} + 10S_{28}$
	ν_{11}	1556	9	$81S_{11}$
	ν_{12}	1531	2	$63S_{12} + 13S_{13}$
	ν_{13}	1529	3	$56S_{13} + 25S_{12}$
	ν_{14}	1523	0	$78S_{14}$
	ν_{15}	1451	9	$37S_{15} + 26S_{15} + 10S_{17}$
	ν_{16}	1441	6	$34S_{16} + 25S_{12} + 11S_{15} + 10S_{14}$
	ν_{17}	1299	18	$35S_{17} + 37S_{20} + 20S_{24}$
	ν_{18}	1154	7	$63S_{18} + 22S_{25}$
	ν_{19}	1123	12	$47S_{19} + 39S_{16}$

Table 8.8 (continued)

ν_{20}	937	14	$36S_{20} + 41S_{15} + 16S_{17}$
ν_{21}	921	6	$94S_{21}$
ν_{22}	823	9	$91S_{22}$
ν_{23}	634	IM	$55S_{23} + 26S_{30}$
ν_{24}	553	19	$64S_{24} + 10S_{20}$
ν_{25}	495	7	$74S_{25} + 20S_{18}$
ν_{26}	397	15	$68S_{26} + 16S_{19} + 12S_{17}$
ν_{27}	336	IM	$57S_{27} + 35S_{28}$
ν_{28}	197	IM	$56S_{28} + 18S_{30}$
ν_{29}	160	IM	$86S_{29}$
ν_{30}	137	-5	$59S_{30} + 12S_{25} + 10S_{28}$
ν_{31}	122	IM	$66S_{31} + 14S_{23}$
ν_{32}	88	31	$43S_{32} + 18S_{28} + 11S_{30}$
ν_{33}	32	IM	$29S_{33} + 38S_{32} + 10S_{27}$

As in the CH_3CHO-HOH complex, the water HOH angle bend wavenumber is shifted to higher wavenumber, by about 1.2 times greater than in the formaldehyde-water complex, compared with about 1.4 times for the $(CH_3)_2CO$-HOH complex. The ν(C4H5) stretching vibrational mode is slightly perturbed in the $(CH_3)_2CO$-HOH complex (see Table 8.2), and as such it presents evidence of involvement of the H5 atom interacting with the water oxygen. The magnitudes of the wavenumber shifts in the two binary complexes suggest complexes of similar stability, and indeed their interaction energies are very close to one another.

The intermolecular vibrational modes are characterised by heavy coupling involving both the monomer sub-units. Both the binary complexes of water with acetaldehyde and acetone are of C_1 symmetry, and show strongly correlated intermolecular modes. The highest intermolecular wavenumber, 629 cm^{-1}, for the CH_3CHO-HOH adduct has a 60% contribution from the in-plane bending of the O9H8...O3 angle, 18% from the in-plane bending of the C=O...H angle and 10% from the intermonomer stretching, as shown in Table 8.8. The band at 319 cm^{-1} is about 60% torsion about the intermolecular bond axis and 30% restricted rotation of the water sub-unit about the carbonyl bond. The characteristic intermonomer stretching, ν(H...O), occurs at 183 cm^{-1}, with a purity of 62% and with a 21% contribution from the restricted water rotation about the carbonyl bond. It is worth noting that the purity of the ν(H...O) mode is highly contaminated in the cyclic complexes compared with the non-cyclic ones, as seen in section 6.3 (see the IMs of the NCH-OH_2 and HCCH-OH_2 complexes). Of the remaining modes, that at 178 cm^{-1} is 45% S_{21} and 35% S_{20}, while that at 108 cm^{-1} is 66% S_{23} and 25% S_{17} and the 88 cm^{-1} mode is composed of 56% S_{24}, 21% S_{21} and 14% S_{19}; in short there is heavy coupling among the intermolecular modes, partly because of the low symmetry of the CH_3CHO-HOH complex.

The δ(O12H11...O2) intermolecular mode of $(CH_3)_2CO$-HOH is observed at the highest vibrational wavenumber, 634 cm^{-1}, with a purity of 55% and with fairly low coupling from the out-of-phase torsion about the CC bonds. The torsion about the O...H axis at 336 cm^{-1} contains a 35% contribution from the restricted rotation of the water sub-unit about the carbonyl bond, while the 197 cm^{-1} mode is mainly the restricted water rotation about the carbonyl bond, with 56% from the H13O12H11...O2 torsion and a fairly small contribution from the CC bond torsion as well. The intermonomer stretching vibrational mode, ν(H...O), occurs at 160 cm^{-1}, with the highest purity among the complexes forming cyclic structures encountered so far. The purity of the ν(H11...O2) mode in the $(CH_3)_2CO$-HOH adduct demonstrates the very weak nature of the secondary H5...O12 bond, in comparison with CH_3CHO-HOH and H_2CO-HOH. Again the remaining intermolecular vibrations are heavily coupled, e.g. the band at 122 cm^{-1} is 66% in-plane C=O...H bend and 14% in-plane O12H11...O2 bend. The lowest wavenumber observed in the $(CH_3)_2CO$-HOH complex corresponds to the O12H11...O2 out-of-phase torsion and the torsional mode about the H...O axis of the C=O...H-O fragment, with a 38% contribution from the in-phase torsion about the CC bonds.

8.3.2 Intra- and Intermolecular Intensities

The computed and experimental[233] intensities of the CH_3CHO monomer are listed in Table 8.9. The computed intensities of the $(CH_3)_2CO$ molecule are included, but there are no literature intensities available. In Table 8.10 both the computed complex and monomer intensities are tabulated together with the ratios of the complex to the monomer intensities. The major changes are in the antisymmetric and symmetric water stretching modes for both complexes of water with acetaldehyde and acetone.

Table 8.9. The Computed and Experimental Intensities of Acetaldehyde and the Calculated/Experimental Intensity Ratios, together with the Calculated $(CH_3)_2CO$ Intensities

Molecule	Symmetry species	Mode	Calculated	Experimental[a]	$A_{calc.}/A_{exp.}$
CH_3CHO	a'	ν_1	6.9	25.4	0.3
		ν_2	2.1	-	-
		ν_3	122.8	123.8	1.0
		ν_4	97.3	159.5	0.6
		ν_5	14.9	28.8	0.5
		ν_6	11.9	21.2	0.6
		ν_7	14.9	21.2	0.7
		ν_8	21.9	28.4	0.8
		ν_9	6.0	5.2	0.2
		ν_{10}	13.2	16.6	0.8
	a"	ν_{11}	7.0	25.4	0.3
		ν_{12}	8.6	-	-
		ν_{13}	0.5	28.4	0.0
		ν_{14}	0.5	3.5	0.1
		ν_{15}	0.5	-	-

Table 8.9 (continued)

$(CH_3)_2CO$	a_1	ν_1	6.2	-	-
		ν_2	0.0	-	-
		ν_3	89.1	-	-
		ν_4	20.7	-	-
		ν_5	11.4	-	-
		ν_6	0.0	-	-
		ν_7	0.9	-	-
		ν_8	0.8	-	-
	a_2	ν_9	0.0	-	-
		ν_{10}	0.0	-	-
		ν_{11}	0.0	-	-
		ν_{12}	0.0	-	-
	b_1	ν_{13}	17.1	-	-
		ν_{14}	18.3	-	-
		ν_{15}	2.0	-	-
		ν_{16}	0.0	-	-
		ν_{17}	0.5	-	-
	b_2	ν_{18}	8.0	-	-
		ν_{19}	1.6	-	-
		ν_{20}	0.3	-	-
		ν_{21}	59.8	-	-
		ν_{22}	61.0	-	-
		ν_{23}	4.3	-	-
		ν_{24}	15.5	-	-

[a] Ref. 233.

Table 8.10. The Computed Band Intensities of CH_3CHO-HOH, $(CH_3)_2CO$-HOH, CH_3CHO and $(CH_3)_2CO$ along with the Complex/Monomer Intensity Ratios

		A/km mol^{-1}		
Complex	Mode	Complex	Monomer	A_c/A_m
CH_3CHO-HOH	ν_1	80.3	33.8	2.4
	ν_2	148.6	4.2	35.4
	ν_3	5.6	6.8	0.8
	ν_4	4.8	7.0	0.7
	ν_5	1.6	2.1	0.8
	ν_6	39.9	122.8	0.3
	ν_7	97.2	97.3	1.0
	ν_8	69.0	77.7	0.9
	ν_9	9.1	8.6	1.1
	ν_{10}	17.4	14.9	1.2
	ν_{11}	6.0	11.9	0.5
	ν_{12}	17.7	14.9	1.2
	ν_{13}	0.3	0.5	0.6
	ν_{14}	20.0	21.9	0.9
	ν_{15}	3.0	6.0	0.5
	ν_{16}	1.2	0.5	2.4
	ν_{17}	236.7	IM	IM
	ν_{18}	52.9	13.2	4.0
	ν_{19}	106.8	IM	IM
	ν_{20}	49.2	IM	IM
	ν_{21}	60.3	IM	IM
	ν_{22}	21.9	0.5	*
	ν_{23}	16.4	IM	IM
	ν_{24}	5.3	IM	IM

Table 8.10 (continued)

$(CH_3)_2CO$-HOH	ν_1	89.6	33.8	2.7
	ν_2	213.9	4.2	50.9
	ν_3	1.6	6.2	0.3
	ν_4	5.8	8.0	0.7
	ν_5	11.3	17.1	0.7
	ν_6	1.7	0.0	*
	ν_7	7.5	6.0	1.3
	ν_8	3.8	1.6	2.4
	ν_9	118.1	89.1	1.3
	ν_{10}	64.0	77.7	0.8
	ν_{11}	16.4	18.3	0.9
	ν_{12}	13.5	20.7	0.7
	ν_{13}	5.1	0.0	*
	ν_{14}	4.6	0.3	15.3
	ν_{15}	42.5	59.8	0.7
	ν_{16}	27.1	11.4	2.4
	ν_{17}	59.8	61.0	1.0
	ν_{18}	2.0	2.0	1.0
	ν_{19}	0.0	0.0	*
	ν_{20}	2.5	4.3	0.6
	ν_{21}	0.1	0.0	*
	ν_{22}	0.3	0.9	0.3
	ν_{23}	229.6	IM	IM
	ν_{24}	20.0	1.5	13.3
	ν_{25}	1.3	0.5	2.6
	ν_{26}	5.9	0.9	7.4
	ν_{27}	103.0	IM	IM
	ν_{28}	74.3	IM	IM
	ν_{29}	4.2	IM	IM
	ν_{30}	42.1	0.0	*
	ν_{31}	0.0	IM	IM
	ν_{32}	6.5	0.0	*
	ν_{33}	1.8	IM	IM

* Division by zero.

There is a two-fold increase in the intensity of the antisymmetric water stretching mode in the CH_3CHO-HOH complex, while a three-fold increase is observed for the corresponding mode in the $(CH_3)_2CO$-HOH complex. A similar order of increase was observed in the formaldehyde-water and methyleneimine-water complexes.

The intensities of the symmetric stretching mode of the water sub-unit show 35- and 51-fold increases for the acetaldehyde- and acetone-water complexes respectively; again a marked increase in the intensity of the stretching mode of the water sub-unit was noted in the formaldehyde-water complex and an identical ratio for the methyleneimine-water and acetone-water complexes is observed. The changes in the intensity ratios are fairly similar in both complexes, confirming the fact that the stabilities of the CH_3CHO-HOH and $(CH_3)_2CO$-HOH complexes are fairly similar. Indeed the interaction energies of the Group 3 complexes, as discussed in section 8.2.2, are very similar, consistent with the intensity ratios noted above.

Reference to the ratios of Table 8.10 shows that except for the antisymmetric and symmetric water stretching modes, the rest of the vibrational modes of the acetaldehyde- and acetone-water complexes have insignificant perturbations to their intensities. Comparison of the intensities of the IM modes of the two complexes, given in Table 8.10, reveals the common feature that in each complex the in-plane bending of the O-H...O angle has the highest intensity. This is consistent with the formaldehyde- and methyleneimine-water complex intensity changes dealt with in the Group 2 complexes, section 7.2.2. The intensity of the torsional mode about the H...O bond is the next highest in both complexes and spans a similar range of magnitude in either complex. The inter-monomer stretching mode spans the same range of intensity in both the

formaldehyde-water and acetaldehyde-water complexes, and is 12 times higher in the acetaldehyde-water complex than in the acetone-water complex. The marked deviation from the expected pattern for the inter-monomer stretching mode can be attributed to the fact that in the acetone-water complex a six-membered ring is formed, which reduces the ring strain, compared with the five-membered ring complexes in H_2CO-HOH and CH_3CHO-HOH, where such strain is quite significant. The out-of-plane bending of the O-H...O angle has quite a low intensity, 5.3 and 1.8 km mol^{-1}, in the acetaldehyde- and acetone-water complexes respectively, but a significantly higher intensity is observed for this mode in the formaldehyde-water complex.

8.3.3 Intra- and Intermolecular Force Constants

Some selected force constants of the acetaldehyde and acetone monomers are collected in Table 8.11.

Table 8.11. Some Selected Computed Force Constants of the Acetaldehyde and Acetone Monomers

Molecule	Parameter	Force constant
CH_3CHO	f(C2O3)/N m^{-1}	1289.6
	f(C2H4)/N m^{-1}	500.1
	f(O3C2H4)/N m rad^{-2}	138.3
$(CH_3)_2CO$	f(C1O2)/N m^{-1}	1267.3
	f(C1C4)/N m^{-1}	452.4
	f(C4H5)/N m^{-1}	578.0
	f(O2C1C4)/N m rad^{-2}	195.4
	f(C1C4H5)/N m rad^{-2}	127.9

Wiberg et al.,[234] using the 4-31G and 6-31G* basis sets, evaluated the force field of acetaldehyde. Their computed force constants are slightly lower (f(C2O3) and f(C2H4) have values of 1227 N m^{-1} and 499 N m^{-1}) than the ones arising from this work. In the $(CH_3)_2CO$ monomer, the computed force constants are again, in general, higher than those of Dellepiane and Overend,[235] who applied the Urey-Bradley potential function[236] to evaluate the force constants. The computed force constants are believed to be reliable.

In Table 8.12 are shown the predicted force constants of the complexes of water with acetaldehyde and acetone, together with the corresponding differences between the complex and monomer force constants. The stretching force constant of the ν(C=O) mode is decreased by 18.5 N m^{-1}, while the ν(CH) stretching force constant increases by 24.0 N m^{-1} in the CH_3CHO-HOH adduct. In the acetone-water complex, the CO bond stretching force constant is lowered by 9.5 N m^{-1}, about half the lowering of the corresponding force constant in the CH_3CHO-HOH complex. The stretching force constant of the water OH bond forming part of the cyclic fragment of the complex is lowered by 17.0 and 21.4 N m^{-1} in the CH_3CHO-HOH and $(CH_3)_2CO$-HOH adducts respectively. The hydrogen bonded C4H5 bond of the acetone molecule does not a show dramatic change in the force constant, unlike the C1H4 bonds in both acetaldehyde and formaldehyde (see Tables 7.12 and 8.12).

The two complexes have a small range of relative magnitudes of the hydrogen bond stretching force constants, namely 22.2 and 19.6 N m^{-1} for acetaldehyde- and acetone-water respectively. The order of the magnitudes is reversed in the case of the in-plane hydrogen bond bending force constants, with the acetone-water complex having a value of 12.2 N m rad^{-2} and the acetaldehyde-water complex 10.9 N m rad^{-2}.

Table 8.12. The Predicted Force Constants of the Complexes of Water with Acetaldehyde and Acetone together with the Differences between Complexes and Monomers

Complex	Parameter	Calculated	Difference
CH_3CHO-HOH	f(C2O3)/N m^{-1}	1271.8	-18.5
	f(C2H4)/N m^{-1}	524.1	24.0
	f(O9H8)/N m^{-1}	860.7	-17.0
	f(H8...O3)/N m^{-1}	22.2	IM
	f(O3C2H4)/N m rad^{-2}	136.6	0.0
	f(O9H8...O3)/N m rad^{-2}	10.9	IM
$(CH_3)_2CO$-HOH	f(C1O2)/N m^{-1}	1257.8	-9.5
	f(O12H11)/N m^{-1}	870.3	-21.4
	f(C4H5)/N m^{-1}	578.9	0.9
	f(H11...O2)/N m^{-1}	19.6	IM
	f(O2C1C4)/N m rad^{-2}	135.5	-59.7
	f(O12H11...O)2/N m rad^{-2}	12.2	IM
	f(C1C4H5)/N m rad^{-2}	133.9	6.0

The magnitudes of the hydrogen bond stretching force constants are quite similar, consistent with the predicted stabilities of these complexes. The inter-monomer stretching force constant of the formaldehyde-water complex, f(H...O), is about 21 N m^{-1} and the f(O6H5...O2) force constant of H_2CO-HOH has a value of about 11 N m rad^{-2} (see Table 7.12). The values spanned by the ν(H...O) and δ(O-H...O) force constants are very similar in all three complexes of water with the H_2CO, CH_3CHO and $(CH_3)_2CO$ monomers.

CHAPTER 9

9.1 RESULTS AND DISCUSSION OF THE GROUP 4 COMPLEXES

Chapter 9 deals with the changes of the structural and vibrational properties of complexes of water with formic and acetic acids, methyl formate and methyl acetate. Numerous similarities are expected for the esters, because they are derivatives of carboxylic acids.

9.2 Structural, Energetic and Electronic Properties of the HCOOH-HOH and CH_3COOH-HOH Complexes

9.2.1 Geometrical Parameters

Table 9.1 presents the calculated structural parameters of formic and acetic acids together with the corresponding experimental values.[190,237] The last column shows the difference between the computed and the experimental parameters (see Figure 9.1). The differences are fairly small, indicating that the experimental parameters are fairly well reproduced.

In Table 9.2 the geometrical parameters of the complexes are collected and compared with the corresponding parameters in the monomers in the column labelled Difference. Figure 9.1 is a Schakal-92 plot illustrating the equilibrium structures of the formic and acetic acid-water complexes, and the atom numbering used in Figure 9.1 applies to both Tables 9.1 and 9.2.

Table 9.1. Computed and Experimental Structural Parameters of Formic and Acetic Acids together with the Differences between Calculated and Experimental Parameters

		Value		
Molecule	Parameter	Calculated	Experimental	Difference
HCOOH[a]	r(C1O2)/pm	120.7	120.2	0.5
	r(C1H3)/pm	110.0	109.2	0.8
	r(C1O4)/pm	135.7	134.3	1.4
	r(O4H5)/pm	96.7	97.2	-0.5
	H3C1O2/deg	124.0	124.6	-0.6
	H3C1O4/deg	113.5	110.8	2.7
	O2C1O4/deg	122.5	124.6	-2.1
	C1O4H5/deg	108.3	106.3	2.0
CH_3COOH[b]				
	r(C1C2)/pm	150.2	149.7	0.5
	r(C2O3)/pm	121.7	124.5	-2.8
	r(C1H6)/pm	108.4	108.0	0.4
	r(C1H7),			
	r(C1H8)/pm	108.8	108.0	0.8
	r(C2O4)/pm	136.2	131.2	5.0
	r(O4H5)/pm	97.1	95.0	2.1
	H6C1C2/deg	109.3	-	-
	H7C1C2,			
	H8C1C2/deg	109.6	-	-
	C1C2O3/deg	126.3	119.2	7.1
	C1C2O4/deg	111.0	-	-
	O3C2O4/deg	122.7	-	-
	C2O4H5/deg	105.3	107.5	-2.2

[a] Ref. 190. [b] Ref. 237.

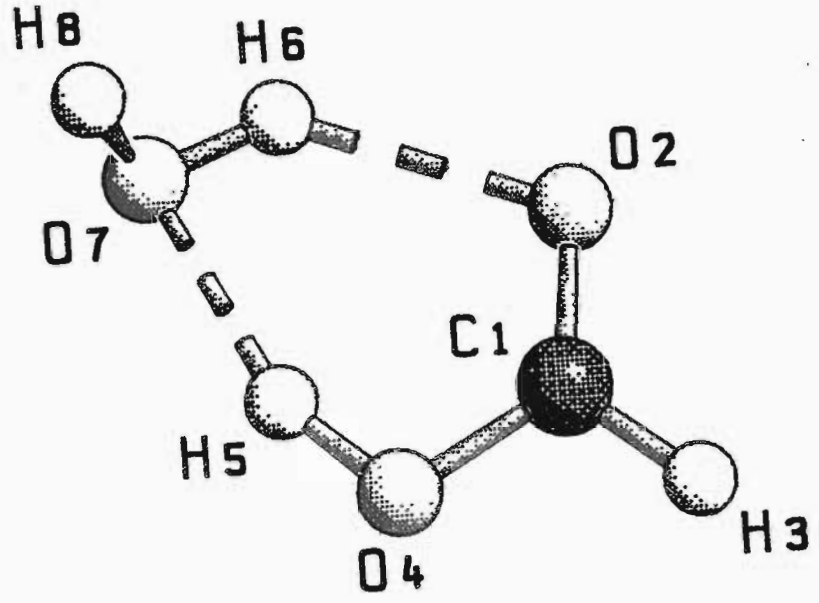

HCOOH-HOH complex

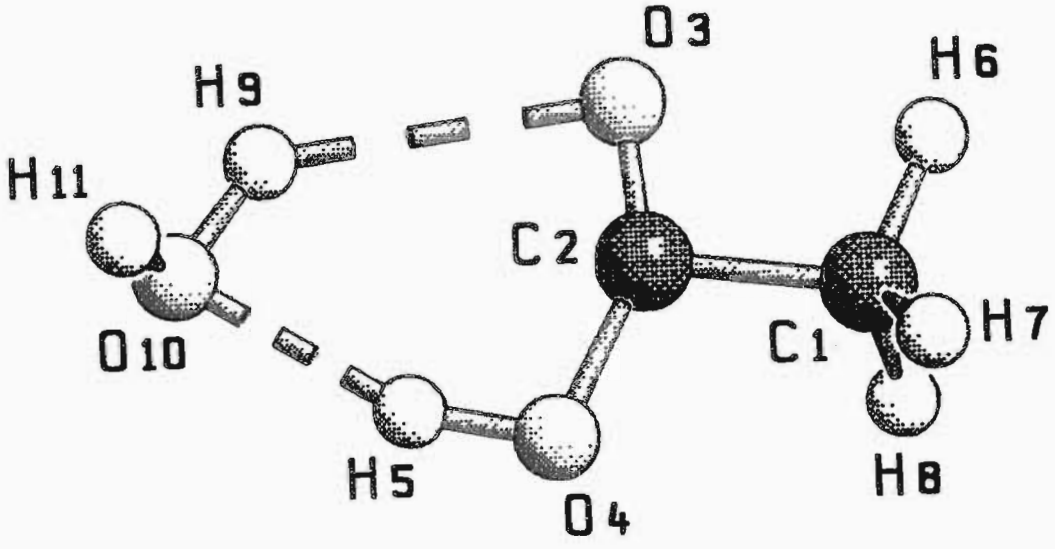

CH_3COOH-HOH complex

Figure 9.1. Graphical representations of the equlibrium structures of the HCOOH-HOH and CH_3COOH-HOH complexes and atom numbering.

Table 9.2. Optimised Geometrical Parameters of the Complexes of Water with Formic and Acetic Acids, together with the Differences between the Complex and Monomer Parameters

Species	Parameter	Calculated	Difference
HCOOH-HOH	r(C1O2)/pm	122.5	1.8
	r(C1H3)/pm	109.3	-0.7
	r(C1O4)/pm	133.1	-2.6
	r(O4H5)/pm	99.1	2.4
	r(H6...O2)/pm	202.4	-
	r(H5...O7)/pm	176.4	-
	r(O2...O7)/pm	281.0	-
	r(O4...O7)/pm	271.1	-
	r(O7H6)/pm	97.2	1.1
	r(O7H8)/pm	96.3	0.2
	H3C1O2/deg	123.2	0.0
	H3C1O4/deg	110.6	-2.9
	O2C1O4/deg	126.2	3.7
	C1O4H5/deg	107.3	-1.0
	O7H6...O2/deg	136.5	-
	C1O2...H6/deg	105.3	-
	O4H5...O7/deg	158.6	-
	H6O7H8/deg	105.1	1.3
	H8O7H6...O2/deg	115.2	-

Table 9.2 (continued)

CH_3COOH-HOH	r(C1C2)/pm	150.2	0.0
	r(C2O3)/pm	123.0	1.3
	r(C2O4)/pm	134.1	-2.1
	r(O4H5)/pm	98.9	1.8
	r(C1H6)/pm	108.4	0.0
	rC1H7,rC1H8/pm	108.8	0.0
	r(H9...O3)/pm	197.1	-
	r(H5...O10)/pm	177.7	-
	r(O3...O10)/pm	278.4	-
	r(O4...O10)/pm	272.4	-
	r(O10H9)/pm	97.4	1.3
	r(O10H11)/pm	96.3	0.2
	H9O10H11/deg	104.9	1.1
	O10H9...O3/deg	139.5	-
	C2O3...H9/deg	106.8	-
	O4H5...O10/deg	158.9	-
	H6C1C2/deg	107.3	-2.0
	H7C1C2,H8C1C2/deg	109.5	0.2
	C1C2O3/deg	124.1	-2.6
	O3C2O4/deg	123.9	-1.2
	C2O4H5/deg	107.3	2.0
	H7C1C2O3/deg	121.1	-
	H11O10H9...O3/deg	113.2	-

Figure 9.1(a) shows that there are two bonds of the formic acid molecule directly involved in complexation with the water molecule, the C1O2 and O4H5 bonds. Table 9.2 shows that in the HCOOH-HOH complex, the C1O2 bond is extended by 1.8 pm, while the O4H5 bond is extended by 2.4 pm. The O4H5 bond extension is quite significant, indicating that the H5 atom of the formic acid molecule is fairly acidic and is strongly attracted to the water oxygen atom. The C1O4 bond, though not directly associated with the hydrogen bonding interaction in the HCOOH-HOH complex, is dramatically shortened by 2.6 pm.

In the HCOOH-HOH complex, the water O7H6 bond is extended by 1.1 pm, while the non-bonded O7H8 bond is hardly perturbed. The water H6O7H8 angle opens by 1.3° on complexation and the formic acid O2C1O4 angle opens even further by 3.7°. Furthermore, the angle H3C1O4 decreases by 2.6°, while the angle C1O4H5 closes by 1.0°. It is interesting to note that the same angle, C1O4H5, increased on dimerisation of formic acid, as was reported by Borisenko.[180]

The association distances H6...O2 and H5...O7, are 202.4 and 176.4 pm respectively. The primary and secondary intermolecular distances, O4...O7 and O2...O7, are 271.1 and 281.0 pm respectively. The computed primary and secondary hydrogen bond angles, O4H5...O7 and O7H6...O2, are 158.6° and 136.5° respectively. Both deviate quite dramatically from linearity. The HCOOH-HOH complex has C_1 symmetry (see Figure 9.1(a)).

The structural parameters of the acetic acid-water complex are also collected in Table 9.2. The differences between the complex and monomer parameters are listed as well. The parameter identification is that adopted from the Schakal-92 plot, Figure 9.1(b), of the equilibrium structure of the acetic acid-water complex. As in the case of the formic acid-water complex, the acetic acid-water adduct shows double hydrogen bond formation with a distorted six-membered ring. The C2O3 bond is extended by 1.3 pm on complexation in CH_3COOH-HOH; a similar feature was observed in the formic acid-water complex.

The C2O4 bond, though not directly participating in the hydrogen bonding interaction, is shortened by a value of 2.1 pm. A similar observation was made by Borisenko et al.[180] of the acetic acid dimer. The CH_3COOH molecule H5 atom is again shifted towards the water oxygen atom as was the case with the

formic acid-water complex. The extent of the H5 atom shift, in the CH_3COOH-HOH complex, is slightly lower (1.8 pm compared with 2.4 pm) than that of the HCOOH-HOH complex. The latter observation is consistent with the fact that formic acid is indeed a stronger acid than acetic acid; it is thus expected from the degree of proton shift towards the water oxygen atom, that formic acid will form a stronger complex with water in the absence of any other factors. The C2O4H5 angle opens by 2.0° on complexation.

In CH_3COOH-HOH, the primary and secondary hydrogen bonds formed, H5...O10 and H9...O3, are 177.7 and 197.1 pm long respectively. These hydrogen bonds are of a similar order of magnitude to those formed between water and formic acid. The hydrogen bond angles, O4H5...O10 and O10H9...O3, corresponding to the two hydrogen bonds formed, have values of 158.9° and 139.5° respectively. There is a marked deviation from linearity. However, the primary hydrogen bond angle is closer to 180° than its counterpart secondary hydrogen bond angle. In both the formic and acetic acid-water complexes, the non-bonded water OH bond protrudes out of the molecular plane by 115.2° and 113.2° respectively; this is the optimal configuration for an acidic proton to attack the water oxygen lone pair forming a cyclic doubly hydrogen bonded structure.

9.2.2 Interaction Energies and the Morokuma Energy Components

Table 9.3 presents the interaction energies of the complexes, before and after basis set superposition error correction, at the MP2 and the RHF levels.

Table 9.3. Uncorrected and Corrected Interaction Energies together with the BSSE Values for the Complexes of Water with Formic and Acetic Acids

	Energy/kJ mol^{-1}		
Complex	Uncorrected	BSSE	Corrected
		MP2	
HCOOH-HOH	-81.68	41.01	-40.67
CH_3COOH-HOH	-57.99	16.86	-40.13
		RHF	
HCOOH-HOH	-67.10	29.09	-38.01
CH_3COOH-HOH	-41.39	4.39	-37.20

Both the interaction energies are consistent in predicting that the formic acid-water complex is the more stable structure. The difference in stability, however, is very marginal. In the formic acid-water complex about 50% of the MP2 interaction energy is attributed to the BSSE, while in the CH_3COOH-HOH complex, only 30% of the interaction energy is attributed to the BSSE.

The corrected interaction energies of the formic and acetic acid-water complexes are -40.67 and -40.13 kJ mol^{-1} at the correlated level and -38.01 and -37.20 kJ mol^{-1} at the SCF level respectively. Table 9.4 presents the Morokuma energy components. The distribution of the energy components depicts very similar patterns in both complexes, with the usual observation that the electrostatic and charge transfer components are the main stabilising factors in the water complexes, while the exchange repulsions are the most destabilising factors (see Tables 6.5, 7.5 and 8.4).

Table 9.4. Interaction Energies Decomposed according to the Morokuma Scheme

		Decomposed Interaction Energy/kJ mol^{-1}		
Complex	Component	Uncorrected	Corrected	%Contribution
HCOOH-HOH	El	-85.72	-85.72	43
	Pl	-10.42	-10.42	5
	Ex	75.28	76.94	38
	Ct	-23.14	-20.77	12
	Mix	-4.60	1.96	2
	Total	-48.60	-38.01	-
CH_3COOH-HOH	El	-87.00	-87.00	43
	Pl	-10.39	-10.39	5
	Ex	78.06	79.74	38
	Ct	-23.84	-21.48	12
	Mix	-4.89	1.92	2
	Total	-48.05	-37.20	-

The interaction energies calculated by the Monstergauss program with counterpoise corrections are identical with the RHF interaction energies corrected for BSSE, from Gaussian-92. This correlation is expected for the interaction energies at the RHF level, i.e. since the Morokuma decomposition scheme is carried out at the SCF level, the computed energies should agree with those computed at the same level of theory, and indeed such agreement is observed as shown in Tables 9.3 and 9.4.

9.2.3 Atomic Charge Redistributions

In Table 9.5 are shown the atomic charges of both the monomers and the complexes of water with formic and acetic acids. The atomic numbering used

Table 9.5. The Predicted MP2 Atomic Charge Distributions for the Formic and Acetic Acid-Water Complexes, and the Monomers, the Complex - Monomer Differences and the Fragment Charges

			Charge/e			
Complex	Molecule	Atom	Monomer	Complex	Changes	Fragment
HCOOH-HOH	HCOOH	C1	0.6037	0.6206	0.0169	
		O2	-0.5042	-0.5949	-0.0907	
		H3	0.1117	0.1450	0.0333	
		O4	-0.5730	-0.6157	-0.0427	
		H5	0.3619	0.4222	0.0603	
						-0.0229
	H_2O	H6	0.3369	0.3881	0.0512	
		O7	-0.6738	-0.7172	-0.0434	
		H8	0.3369	0.3519	0.0150	
						0.0228
CH_3COOH-HOH	CH_3COOH	C1	-0.4097	-0.4062	0.0035	
		C2	0.7357	0.7573	0.0216	
		O3	-0.5712	-0.6310	-0.0598	
		O4	-0.6080	-0.6382	-0.0302	
		H5	0.3684	0.4183	0.0499	
		H6	0.1639	0.1606	-0.0033	
		H7	0.1605	0.1583	-0.0022	
		H8	0.1605	0.1614	0.0009	
						-0.0196

Table 9.4 (continued)

	H_2O	H9	0.3369	0.3909	0.0540
		O10	-0.6738	-0.7199	-0.0461
		H11	0.3367	0.3486	0.0117
					0.0196

is that shown in Figure 9.1. The differences between the complex and monomer atomic charges are reflected in the table as changes. The last column of Table 9.5 indicates the overall charge of a fragment.

The C1 atom of the formic acid molecule loses 0.0169 e on complexation, while the carbonyl O2 atom gains a remarkable amount of electron density, 0.0907 e. The O4 atom of the formic acid component gains charge density of 0.0427 e; it is about half the value of the O2 atom charge density in the same complex. The non-bonded H3 atom of formic acid loses a fairly small amount of charge. The acidic proton, H5, loses a dramatic amount of charge density, second only to the amount of charge density gained by the carbonyl oxygen atom, O2, consistent with the nature of H5 as a bridging hydrogen atom.[9b]

The bridging water H6 atom loses a marked degree of electron density. The water oxygen atom gains some charge on complexation. The water component is positively charged while the formic acid component is negatively charged. Hence, although the complex is doubly hydrogen bonded, overall the formic acid component gains electron density and the water component loses electron density. Formic acid is the EA and PD, whereas water is the ED and PA in the HCOOH-HOH complex.

In the CH_3COOH-HOH adduct, the carbonyl O3 atom gains 0.0598 e, comparable with that gained in the formic acid-water complex. The hydroxyl O4 atom gains some electron density in this complex, although to a lesser degree compared with the corresponding atom in the HCOOH-HOH complex. In the acetic acid-water complex, the charge redistribution along the C2O3 and the C2O4 bonds is subjected to methyl group inductive effects. This results in the depletion of charge density in the C2O3 bond being slightly lower than that for

the formic acid-water complex. The H5 atom of the acetic acid molecule has lost a significant charge density on complexation; this is the acidic proton, which is being donated towards the water O10 atom. The methyl group hydrogens are fairly far from the effective sites of interaction and as such remain generally unaffected. The H9 atom of the water molecule has lost a significant amount of charge, a norm for bridging hydrogens. The water oxygen, as was the case with the formic acid-water complex, has gained a significant charge on complexation. The acetic acid component is negatively charged overall, whereas the water molecule is positively charged. Acetic acid is the EA and PD, while water is the ED and PA in the CH_3COOH-HOH complex, in a similar fashion to the HCOOH-HOH complex.

9.3. Structural, Energetic and Electronic Properties of the $HCOOCH_3$-HOH and CH_3COOCH_3-HOH Complexes

The calculated structural parameters of the methyl formate and methyl acetate monomers, together with their experimental values, are reported as well as the differences between the calculated and experimental values. The changes in the structural parameters, charge distributions on complexation and interaction energies are discussed. A number of similarities can be expected between the $HCOOCH_3$-HOH adduct and the corresponding homologous CH_3COOH-HOH complex.

9.3.1 Geometrical Parameters

The structural parameters of the methyl formate and methyl acetate monomers are collected in Table 9.6. The differences between the computed and experimentally[190,238] determined parameters are also shown in this table.

Table 9.6. The Optimised Geometrical Parameters of Methyl Formate and Methyl Acetate and the Differences between the Calculated and Literature Parameters

		Value		
Molecule	Parameter	Calculated	Experimental	Difference[a]
$HCOOCH_3$[b]	r(C1O2)/pm	121.5	120.0	1.5
	r(C1O4)/pm	134.7	133.4	1.3
	r(C5O4)/pm	134.7	143.7	-9.0
	r(C1H3)/pm	109.4	108.6	0.8
	r(C5H6)/pm	108.7	108.6	0.1
	r(C5H7)/pm	108.7	108.6	0.1
	r(C5H8)/pm	108.7	108.6	0.1
	H3C1O2/deg	125.3	124.8	0.5
	O2C1O4/deg	125.7	125.9	-0.2
	H3C1O4/deg	109.0	109.3	-0.3
	C5O4C1/deg	113.8	114.8	-1.0
	H6C5O4/deg	110.3	109.3	1.0
	H7C5O4/deg	105.2	-	-

Table 9.6 (continued)

CH_3COOCH_3[c]	r(C1C2)/pm	150.4	150.4	0.0
	r(C2O3)/pm	121.9	118.8	3.1
	r(C2O7)/pm	135.8	132.7	3.1
	r(C1H4)/pm	108.5	108.0	0.5
	r(C1H5)/pm	108.8	108.4	0.4
	r(C1H6)/pm	108.8	108.4	0.4
	r(C8O7)/pm	143.9	141.7	2.2
	r(C8H9)/pm	108.4	-	-
	r(C8H10)/pm	108.7	-	-
	r(C8H11)/pm	108.7	-	-
	C1C2O3/deg	126.0	125.2	0.8
	O3C2O7/deg	123.5	123.4	0.1
	C8O7C2/deg	113.9	116.9	-3.0
	H4C1C2/deg	109.2	109.6	-0.4
	H5C1C2/deg	109.8	109.7	0.1
	H6C1C2/deg	105.2	-	-
	H9C8O7/deg	110.5	-	-

[a] Difference = calculated - experimental value. [b] Ref. 190. [c] Ref. 238.

The difference in the r(C5O4) parameter of $HCOOCH_3$ (-9.0 pm) is the largest recorded in this work so far, as indicated in Table 9.6. The calculated structural parameters of the complexes of water with methyl formate and methyl acetate are presented in Table 9.7. The atom numbering of the monomers is also shown in Figure 9.2, which shows the optimised equilibrium structures of the methyl formate and methyl acetate-water complexes. The parameter distortions suffered by the monomers on complexation are shown by the differences between the complex and the monomer parameter. Both complexes are of C_1 symmetry, just as was the case with the HCOOH-HOH and CH_3COOH-HOH complexes.

Table 9.7. The Optimised Geometrical Parameters for the Methyl Formate- and Methyl Acetate-Water Complexes and the Differences between the Complex and the Monomer Parameters

Complex	Parameter	Calculated	Difference
$HCOOCH_3$-HOH	r(C1O2)/pm	122.2	0.7
	r(C1O4)/pm	133.9	0.5
	r(C5O4)/pm	144.3	0.6
	r(C1H3)/pm	109.1	-0.3
	r(C5H6)/pm	108.7	0.0
	r(C5H7)/pm	108.7	0.0
	r(C5H8)/pm	108.3	-0.4
	r(H9...O2)/pm	203.8	-
	r(H3...O10)/pm	257.1	-
	r(O2...O10)/pm	289.7	-
	r(C1...O10)/pm	306.3	-
	r(O10H9)/pm	96.7	0.6
	r(O10H11)/pm	96.1	0.0
	H3C1O2/deg	124.3	-1.0
	O4C1O2/deg	125.0	-0.7
	H3C1O2/deg	110.7	1.7
	C1O4C5/deg	114.2	0.4
	H6C5O4/deg	110.2	-0.1
	H7C5O4/deg	105.1	-0.1
	H8C5O4/deg	105.1	-
	C1O2...H9/deg	96.9	-
	O10H9....O2/deg	147.0	-
	C1H3...O10/deg	96.1	-
	H9O10H11/deg	104.0	0.2
	H8C5O4C1, H7C5O4C1/deg	60.4	-0.4
	H11O10H9...O2/deg	111.5	-

Table 9.7 (continued)

CH_3COOCH_3-HOH	r(C1C2)/pm	150.1	-0.3
	r(C2O3)/pm	122.6	0.7
	r(C2O7)/pm	135.0	-0.8
	r(C1H4)/pm	108.5	0.0
	r(C1H5)/pm	108.8	0.0
	r(C1H6)/pm	108.8	0.0
	r(C8O7)/pm	144.1	0.2
	r(C8H9)/pm	108.8	0.4
	r(C8H10)/pm	108.3	-0.4
	r(C8H11)/pm	108.7	0.0
	r(H12...O3)/pm	198.5	-
	r(H4...O13)/pm	243.9	-
	r(O3...O13)/pm	292.1	-
	r(O13H12)/pm	96.9	0.8
	r(O13H14)/pm	96.2	0.1
	C1C2O3/deg	126.0	0.0
	C1C2O7/deg	122.6	0.9
	C2O7C8/deg	114.4	0.5
	H4C1C2/deg	109.2	0.0
	H5C1C2/deg	109.2	-0.6
	H6C1C2/deg	105.1	-0.1
	H9C8O7/deg	110.4	-0.1
	C2O3...H12/deg	112.9	-
	O13H12...O3/deg	161.7	-
	C1H4...O13/deg	141.1	-
	H12O13H14/deg	103.9	-0.1
	H14O13H12...O3/deg	106.7	-

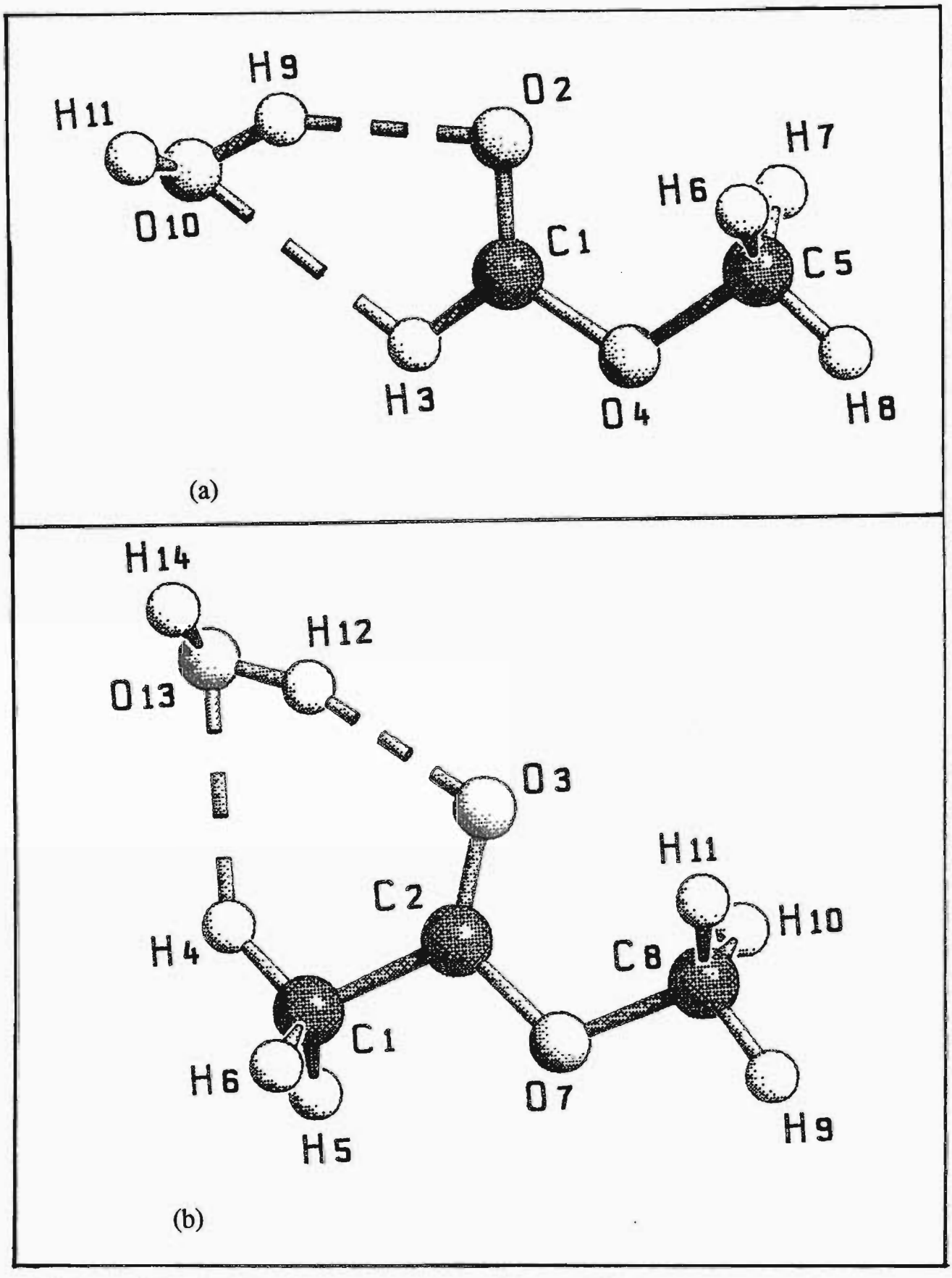

Figures 9.2. Graphical representations of the equilibrium structures of the $HCOOCH_3$-HOH and CH_3COOCH_3-HOH complexes: (a) $HCOOCH_3$-HOH; (b) CH_3COOCH_3-HOH.

As shown in Figure 9.2(a), the $HCOOCH_3$-HOH complex forms a distorted five-membered ring with two hydrogen bonds. The C1O2 bond is slightly extended when the complex forms. The C1O4 and C5O4 bonds are both extended more or less by the same order of magnitude. The C1H3 bond is shortened by 0.3 pm. A similar feature was observed for the H_2CO-HOH, CH_3CHO-HOH and CH_3COCH_3-HOH complexes (see sections 7.2.1 and 8.2.1). The primary and secondary hydrogen bonds formed, H9...O2 and H3...O10, are 203.8 and 257.1 pm long respectively.

The corresponding primary and secondary intermolecular distances, O10...O2 and C1...O10, are 289.7 and 306.3 pm respectively, following the trend in the primary and secondary hydrogen bond distances, while the hydrogen bond angles, O10H9..O2 and C1H3...O10, corresponding to these hydrogen bonds, are 147.0° and 96.1° respectively. The angle C1O2...H9, with a value of 96.9°, defines the optimum angle at which the bridging water hydrogen can approach the lone pair on the O2 atom of the $HCOOCH_3$-HOH complex. The angles H3C1O2 and O2C1O4 close up, by the same amount by which the angle H3C1O4 opens. The O10H9 bond length increases quite significantly by 0.6 pm, indicating that the water component is donating a proton to the O2 atom of methyl formate.

The interaction of water with the CH_3COOCH_3 molecule results in formation of a distorted six-membered ring structure, as illustrated in Figure 9.2(b). The extension of the C2O3 bond, the counterpart of the C1O2 bond in the $HCOOCH_3$-HOH complex, is 0.7 pm, as it was in the methyl formate-water complex. The hydrogen bonds arising from this complexation are H12...O3 and H4...O13, and are 198.5 and 243.9 pm long respectively. The hydrogen bond angles corresponding to these hydrogen bonds are O13H12...O3 and

C1H4...O13, with values of 161.7° and 141.1°. In both the $HCOOCH_3$-HOH and CH_3COOCH_3-HOH complexes, the angle of the primary hydrogen bond is larger than that of the secondary hydrogen bond. The angle C2O3...H12 in the CH_3COOCH_3-HOH complex approaches the expected[239] value of 120° and compares reasonably well with the corresponding angle in the $HCOOCH_3$-HOH complex. The formic and acetic acid-water complexes possess very similar features, in contrast to the $HCOOCH_3$-HOH and CH_3COOCH_3-HOH complexes, which not only do not compare well with the acid-water complexes, but fail to compare reasonably between themselves. The methyl formate-water complex, for instance, has quite a small CH...O angle compared with the rest of the complexes. The C=O...H angle for the $HCOOCH_3$-HOH complex is again fairly small when compared with the other complexes, in which this angle ranges from 105.3° to 112.9°. It is noted here that while the secondary hydrogen bond angle for the methyl formate complex is small, the corresponding secondary hydrogen bond length is conspicuously longer than those of the other complexes.

9.3.2 Interaction Energies and the Morokuma Energy Components

Table 9.8 is a collection of the interaction energies before and after basis set superposition error correction. It is apparent from Table 9.8 that the methyl formate-water complex is less stable than the methyl acetate-water complex. The same predictions are made from the correlated level of theory as from the SCF level. The energy components evaluated by the Morokuma decomposition scheme are presented in Table 9.9. From the energy components, it is observed that electrostatic and charge transfer processes are primarily responsible for the stabilisation of the ester-water complexes. Polarisation effects contribute minimally to the stabilisation, so too does the coupling term.

Table 9.8. The Uncorrected and Corrected Interaction Energies at both the RHF and MP2 levels of Theory for the Ester-Water Complexes

	Energy/kJ mol^{-1}		
Complex	Uncorrected	BSSE	Corrected
		MP2	
$HCOOCH_3$-HOH	-29.45	13.48	-15.97
CH_3COOCH_3-HOH	-33.77	13.00	-20.77
		RHF	
$HCOOCH_3$-HOH	-22.75	6.36	-16.39
CH_3COOCH_3-HOH	-24.66	6.42	-18.24

Table 9.9. Interaction Energy Components derived from the Morokuma Scheme

		Interaction Energy Components/kJ mol^{-1}		
Complex	Component	Uncorrected	Corrected	%Contribution
$HCOOCH_3$-HOH	El	-33.84	-33.84	46
	Pl	-2.92	-2.92	4
	Ex	24.84	25.99	34
	Ct	-10.68	-8.41	14
	Mix	-1.42	2.87	2
	Total	-24.02	-16.31	-
CH_3COOCH_3-HOH	El	-38.84	-38.84	45
	Pl	-3.77	-3.77	4
	Ex	30.42	31.42	35
	Ct	-12.55	-10.00	14
	Mix	-1.58	2.74	2
	Total	-26.31	-18.24	-

The exchange repulsions are the main destabilising forces in both the methyl formate- and methyl acetate-water complexes. The total energies corrected for counterpoise effects in the Morokuma scheme are -16.39 and -18.24 kJ mol^{-1} for the $HCOOCH_3$-HOH and CH_3COOCH_3-HOH complexes respectively; these values are identical with those from the RHF Gaussian calculation but slightly different from those at the MP2 level, again an illustration of good agreement for the energies evaluated using both programs at the same level of theory.

9.3.3 Atomic Charge Redistributions

The atomic charge redistributions of the $HCOOCH_3$-HOH and CH_3COOCH_3-HOH complexes are collected in Table 9.10, wherein the differences between the complex and monomer atomic charges are presented as changes. Although some atoms do not show any significant charge changes on complexation, they are nevertheless cited for completeness of the description. In the $HCOOCH_3$-HOH complex, a few atoms show some significant changes, namely O2, H3, H9, and O10. The O2 atom gains 0.0418 e on complexation. The H3 atom loses 0.0331 e, and the bridging H9 atom loses a similar amount of charge (0.0350 e). The O10 atom gains 0.0392 e. The O4 atom is hardly perturbed throughout these changes, partly because of the inductive effect of the methyl group and perhaps due to the fact that the hydrogen bonding is occurring at a relatively distant site. It should be recalled that the C1H3 bond was shortened by 0.3 pm on complexation, and the C1H4 bond of the formaldehyde-water complex suffered the same shortening (refer to section 7.2.1). The overall charge redistributions predict that the ester component is the ED and PA while the water component is the EA and PD in the $HCOOCH_3$-HOH complex.

Table 9.10. The Predicted MP2 Atomic Charge Distributions for the H_2O, $HCOOCH_3$ and CH_3COOCH_3 Monomers and the $HCOOCH_3$-HOH and CH_3COOCH_3-HOH Complexes along with the Complex - Monomer Charge Changes and the Fragment Charges

		Charge/e			
Species	Atom	Monomer	Complex	Changes	Fragment[a]
HCOOCH3-HOH	C1	0.6188	0.6289	0.0101	
	O2	-0.5480	-0.5898	-0.0418	
	H3	0.1453	0.1784	0.0331	
	O4	-0.6017	-0.5991	0.0026	
	C5	-0.0366	-0.0388	-0.0022	
	H6	0.1425	0.1429	0.0005	
	H7	0.1425	0.1456	0.0032	
	H8	0.1425	0.1419	-0.0006	
					0.010
	H9	0.3369	0.3719	0.0350	
	O10	-0.6738	-0.7130	-0.0392	
	H11	0.3369	0.3312	-0.0057	
					-0.010

Table 9.10 (continued)

CH_3COOCH_3-HOH	C1	-0.4039	-0.4256	-0.0217	
	C2	0.7616	0.7831	0.0215	
	O3	-0.5826	-0.6228	-0.0402	
	H4	0.1568	0.1915	0.0347	
	H5	0.1568	0.1607	0.0039	
	H6	0.1568	0.1552	-0.0016	
	O7	-0.6278	-0.6197	0.0081	
	C8	-0.0288	-0.0313	-0.0025	
	H9	0.1321	0.1371	0.0050	
	H10	0.1381	0.1425	0.0044	
	H11	0.1381	0.1395	0.0014	
					0.013
	H12	0.3369	0.3799	0.0430	
	O13	-0.6738	-0.7158	-0.0420	
	H14	0.3369	0.3267	-0.0102	
					-0.010

[a] The rounding off error causes the differences in fragment charges.

In CH_3COOCH_3-HOH, the C1 atom gains charge density of 0.0217 e, while the C2 atom loses a similar amount of charge, 0.0215 e. The O3 atom gains a significant amount of charge, 0.0402 e, which compares well with that gained by the O2 atom in the $HCOOCH_3$-HOH complex (see Figure 9.3). The bridging hydrogen atoms H12 and H4 atoms lose remarkable amounts of charge density, 0.0430 e and 0.0347 e respectively, typical of hydrogen bonded hydrogen atoms.[9b] The O3 atom gains 0.0402 e of electron density compared with 0.0418 e gained by its O2 counterpart in the $HCOOCH_3$-HOH complex. Again, as in the $HCOOCH_3$-HOH complex, the ester component is the ED and PA whereas the water component is the EA and PD. In both the $HCOOCH_3$-HOH and CH_3COOCH_3-HOH complexes, the fragment charge on the ester sub-unit is about 0.01 e, about half of the fragment charge on the acid component in the acid-water complexes (see Tables 9.5 and 9.10). The ester-water complexes are about half as strong as the acid-water complexes.

9.4 Vibrational Properties of the HCOOH-HOH and CH_3COOH-HOH Complexes

9.4.1 Intra- and Intermolecular Wavenumbers

The computed vibrational wavenumbers of the formic and acetic acid monomers are collected in Table 9.11, along with their experimental counterparts[193] and their calculated/experimental ratios. The ratios are close to unity in both monomers, indicating a good correlation between the calculated and experimentally determined wavenumbers.

The few exceptions to the observed trend are the vibrational modes at the low end of the vibrational spectrum, where the anharmonicity effects are not well

Table 9.11. Computed and Experimental Wavenumbers of the Formic and Acetic Acid Monomers and the Calculated/Experimental Ratios

Molecule	Symmetry species	Mode	$\tilde{\nu}/cm^{-1}$ Calculated	$\tilde{\nu}/cm^{-1}$ Experimental[a]	$\tilde{\nu}_{Calc.}/\tilde{\nu}_{Exp.}$
HCOOH	a'	ν_1	3869	3570	1.08
		ν_2	3077	2943	1.05
		ν_3	1876	1770	1.06
		ν_4	1470	1387	1.06
		ν_5	1297	1229	1.06
		ν_6	1144	1109	1.03
		ν_7	655	625	1.05
	a"	ν_8	1052	1035	1.02
		ν_9	525	638	0.82
CH_3COOH	a'	ν_1	3817	3583	1.07
		ν_2	3285	3051	1.08
		ν_3	3154	2944	1.07
		ν_4	1858	1788	1.04
		ν_5	1533	1430	1.07
		ν_6	1463	1382	1.06
		ν_7	1380	1264	1.09
		ν_8	1231	1182	1.04
		ν_9	1030	989	1.04
		ν_{10}	886	847	1.05
		ν_{11}	583	657	0.89
		ν_{12}	425	581	0.73
	a"	ν_{13}	3246	2996	1.08
		ν_{14}	1537	1430	1.07
		ν_{15}	1096	1048	1.05
		ν_{16}	688	642	1.07
		ν_{17}	552	534	1.03
		ν_{18}	90	93	0.97

[a] Ref. 193.

accounted for by the ab initio method in the harmonic approximation; as a result the predicted wavenumbers of the ν_9 mode of HCOOH and the ν_{11}, ν_{12} and ν_{18}

modes of CH_3COOH are underestimated. This underestimation of the wavenumbers can be attributed to the basis set shortcomings.

In Table 9.12 are collected the definitions of the local symmetry coordinates. The predicted wavenumbers and the complex-monomer wavenumbers shifts are presented in Table 9.13, together with the %PEDs for the formic and acetic acid-water complexes. Both the water and acid sub-units show dramatic shifts in their vibrational wavenumbers in either complex.

In the formic acid-water complex, ν_1 and ν_2, corresponding to the antisymmetric and symmetric water stretching modes, are shifted to the lower wavenumbers, by -162 and -124 cm^{-1}, and the ν_3 mode, the acid OH bond stretching, is red shifted by -454 cm^{-1}. The latter shift is quite a large one, consistent with the observation that the formic acid-water complex is the result of the formation of two very strong hydrogen bonds. The ν_5, carbonyl stretching, vibrational mode is red shifted by -68 cm^{-1}. The C1H3 stretching vibration of formic acid is strongly blue shifted even though the C1H3 bond does not directly form part of the 6-membered ring in the formic acid-water complex; such a shift is supported by the fact that the C1H3 bond was shortened by 0.7 pm, as noted earlier in section 9.2.1.

In the acetic acid-water complex a similar pattern of wavenumber shifts is observed. The ν_1 and ν_2 modes, the antisymmeric and symmetric stretching of the water OH bonds, are red shifted by -67 and -150 cm^{-1}, while the ν_3 mode corresponding to the stretching of the OH bond of the acetic acid component is red shifted by -373 cm^{-1}.

Table 9.12. The Symmetry Coordinates of the Complexes of Water with Formic and Acetic Acids

Complex	Symmetry	Coordinate	Description
HCOOH-HOH	S_1	$\{\Delta r_{6,7} - \Delta r_{7,8}\}/\sqrt{2}$	OH_2 a-stretch
	S_2	$\{\Delta r_{6,7} + \Delta r_{7,8}\}/\sqrt{2}$	OH_2 s-stretch
	S_3	$\Delta r_{4,5}$	OH stretch
	S_4	$\Delta r_{1,3}$	CH stretch
	S_5	$\Delta r_{1,2}$	C=O stretch
	S_6	$\Delta\delta_{6,7,8}$	HOH bend
	S_7	$\Delta\delta_{1,4,5}$	COH bend
	S_8	$\{\Delta\delta_{2,1,3} - \Delta\delta_{3,1,4}\}/\sqrt{2}$	CH bend
	S_9	$\Delta r_{1,4}$	C-O stretch
	S_{10}	$\Delta\gamma_{2,1,3,4}$	C=O op bend
	S_{11}	$\Delta\gamma_{5,2,1,4}$	O-H op bend
	S_{12}	$\{\Delta\delta_{2,1,4} - \Delta\delta_{3,1,4}\}/\sqrt{2}$	C-O bend
	S_{13}	$\Delta\delta_{2,6,7}$	O-H...O ip bend
	S_{14}	$\Delta\tau_{1,2,6,7}$	torsion about H...O bond
	S_{15}	$\Delta r_{2,6}$	H...O stretch
	S_{16}	$\Delta\delta_{1,2,6}$	C=O...H ip bend
	S_{17}	$\Delta\gamma_{6,2,1,4}$	OH..O op bend
	S_{18}	$\Delta\tau_{8,7,6,2}$	restricted rotation about H...O bond

Table 9.12 (continued)

CH_3COOH-HOH	S_1	$\{\Delta r_{9,10} - \Delta r_{10,11}\}/\sqrt{2}$	OH_2 a-stretch
	S_2	$\{\Delta r_{9,10} + \Delta r_{10,11}\}/\sqrt{2}$	OH_2 s-stretch
	S_3	$\Delta r_{4,5}$	OH stretch
	S_4	$\{2\Delta r_{1,6} - \Delta r_{1,7} - \Delta r_{1,8}\}/\sqrt{6}$	CH_3 d-stretch
	S_5	$\{\Delta r_{1,7} - \Delta r_{1,8}\}/\sqrt{2}$	CH_3 d-stretch
	S_6	$\{\Delta r_{1,6} + \Delta r_{1,7} + \Delta r_{1,8}\}/\sqrt{6}$	CH_3 s-stretch
	S_7	$\Delta r_{2,3}$	C=O stretch
	S_8	$\Delta \delta_{9,10,11}$	HOH bend
	S_9	$\{2\Delta \delta_{7,1,8} - \Delta \delta_{6,1,7} - \Delta \delta_{6,1,8}\}/\sqrt{6}$	CH_3 d-deformation
	S_{10}	$\{\Delta \delta_{6,1,7} - \Delta \delta_{6,1,8}\}/\sqrt{2}$	CH_3 d-deformation
	S_{11}	$\Delta \delta_{2,4,5}$	COH bend
	S_{12}	$\{\Delta \delta_{6,1,7} + \Delta \delta_{6,1,8} + \Delta \delta_{7,1,8} - \Delta \beta_{6,1,2} - \Delta \beta_{7,1,2} - \Delta \beta_{8,1,2}\}/\sqrt{6}$	CH_3 s-deformation
	S_{13}	$\Delta r_{2,4}$	C-O stretch
	S_{14}	$\{\Delta \beta_{7,1,2} - \Delta \beta_{8,1,2}\}/\sqrt{2}$	CH_3 rock
	S_{15}	$\{2\Delta \beta_{6,1,2} - \Delta \beta_{7,1,2} - \Delta \beta_{8,1,2}\}/\sqrt{6}$	CH_3 rock
	S_{16}	$\Delta \gamma_{5,3,2,4}$	C-O op bend
	S_{17}	$\Delta r_{1,2}$	CC stretch
	S_{18}	$\Delta \delta_{3,9,10}$	O-H...O bend
	S_{19}	$\Delta \delta_{3,2,4}$	O=C-O bend
	S_{20}	$\Delta \tau_{3,2,4,5}$	C=O op bend
	S_{21}	$\Delta \delta_{1,2,3}$	CCO bend
	S_{22}	$\Delta \tau_{10,9,3,2}$	torsion about H...O bond
	S_{23}	$\Delta \tau_{11,10,9,3}$	restricted rotation about H...O bond

Table 9.12 (continued)

S_{24}	$\Delta\delta_{2,3,9}$	C=O...H bend
S_{25}	$\Delta r_{3,9}$	H...O stretch
S_{26}	$\Delta\gamma_{9,1,2,3}$	O-H...O op bend
S_{27}	$\Delta\tau_{6,1,2,3}$	CH op bend

Table 9.13. The Computed Vibrational Wavenumbers of the Acid-Water Complexes and the Differences between the Complex and Monomer Wavenumbers and the %PEDs

		cm^{-1}		
Species	Mode	Wavenumber	Shift	%PED[a]
HCOOH-HOH	ν_1	3868	-162	$81S_1 + 18S_2$
	ν_2	3767	-124	$75S_2 + 19S_1$
	ν_3	3415	-454	$98S_3$
	ν_4	3177	100	$98S_4$
	ν_5	1808	-68	$56S_5 + 14S_8 + 14S_{12}$
	ν_6	1690	8	$67S_6 + 16S_{14}$
	ν_7	1497	27	$44S_7 + 20S_8 + 20S_{12}$
	ν_8	1429	-	$71S_8 + 14S_{12}$
	ν_9	1250	-47	$54S_9 + 22S_{12} + 12S_7$
	ν_{10}	1096	-48	$92S_{10}$
	ν_{11}	981	-71	$77S_{11} + 15S_{10}$
	ν_{12}	715	60	$42S_{12} + 36S_{13} + 10S_{15}$
	ν_{13}	656	IM	$45S_{13} + 28S_{16} + 10S_{12}$
	ν_{14}	380	IM	$61S_{14} + 28S_{11}$
	ν_{15}	305	IM	$50S_{14} + 26S_{18} + 18S_{17}$
	ν_{16}	240	IM	$66S_{16} + 15S_{13}$
	ν_{17}	202	IM	$36S_{17} + 30S_{15} + 12S_{18} + 11S_{11}$
	ν_{18}	193	IM	$35S_{17} + 33S_{15} + 15S_{18}$

Table 9.13 (continued)

CH_3COOH-HOH	ν_1	3963	-67	$78S_1 + 21S_2$
	ν_2	3742	-150	$71S_2 + 21S_1$
	ν_3	3444	-373	$97S_3$
	ν_4	3284	-1	$99S_4$
	ν_5	3245	-1	$100S_5$
	ν_6	3153	-1	$98S_6$
	ν_7	1819	-39	$70S_7$
	ν_8	1694	12	$64S_8 + 18S_{22}$
	ν_9	1537	0	$62S_9 + 28S_{28}$
	ν_{10}	1534	1	$54S_{10} + 24S_{24}$
	ν_{11}	1504	41	$31S_{11} + 13S_{13} + 10S_{12}$
	ν_{12}	1442	62	$71S_{12} + 18S_{11}$
	ν_{13}	1342	111	$32S_{13} + 16S_{11} + 12S_{19}$
	ν_{14}	1098	2	$51S_{14} + 28S_{20}$
	ν_{15}	1054	24	$72S_{15} + 11S_{13}$
	ν_{16}	971	85	$96S_{16}$
	ν_{17}	913	27	$52S_{17} + 26S_{13} + 10S_{19}$
	ν_{18}	713	IM	$59S_{18} + 15S_{24} + 10S_{25}$
	ν_{19}	625	42	$48S_{19} + 23S_{24} + 10S_{21}$
	ν_{20}	598	46	$72S_{20} + 11S_{14} + 10S_{16}$
	ν_{21}	450	25	$67S_{21} + 13S_{15}$
	ν_{22}	368	IM	$74S_{22} + 12S_{16}$
	ν_{23}	310	IM	$46S_{22} + 39S_{23}$
	ν_{24}	212	IM	$64S_{24} + 13S_{25}$

Table 9.13 (continued)

ν_{25}	191	IM	$69S_{25} + 14S_{18}$
ν_{26}	98	8	$47S_{26} + 17S_{27} + 16S_{16}$
ν_{27}	78	IM	$49S_{26} + 20S_{27} + 13S_{20}$

[a] see Table 9.12.

These shifts are somewhat smaller than those of the formic acid-water complex, implying that CH_3COOH-HOH is a slightly weaker complex. The interaction energy of the acetic acid-water complex is also slightly smaller than that of formic acid-water, which is consistent with these wavenumber shifts. The carbonyl stretching mode, ν_7, is red shifted in the CH_3COOH-HOH complex by about half the value of the carbonyl stretching shift of the HCOOH-HOH adduct. The water bending mode is almost unshifted in both the acid-water complexes. The ν_{13} mode of the CH_3COOH-HOH adduct is strongly blue shifted, by 111 cm^{-1}, comparing favourably with the shift experienced by the C1H3 stretching mode in the HCOOH-HOH complex.

The IM modes of HCOOH-HOH are illustrated in Figure 9.3 and these IM mode illustrations are used as prototypes for the rest of the Group 4 complexes. The description of the intermolecular modes in the formic acid-water complex is rather complicated, due to heavy coupling with the two low frequency intramolecular modes. The total sum of the % contributions from intermolecular modes in comparison with that from the intramolecular modes determines whether a particular wavenumber is classified as an inter- or intramolecular mode. Thus the band at 656 cm^{-1}, although it is very close to the band of the formic acid monomer at 655 cm^{-1}, is classified as an intermolecular vibration since 73% of the total motion arises from intermolecular contributions, namely a 45% contribution from the O-H...O in-plane bending mode and a 28% contribution from the C=O...H in-plane bending mode. The band at 380 cm^{-1} is described as a 61% contribution from torsion about the H...O axis and a 28% contribution from the O-H out-of-plane bending mode. The 305 cm^{-1} band is a mixture of the C=O...H in-plane bending and the torsion about the H...O axis, together with some contribution from the out-of-plane O-H...O angle bending.

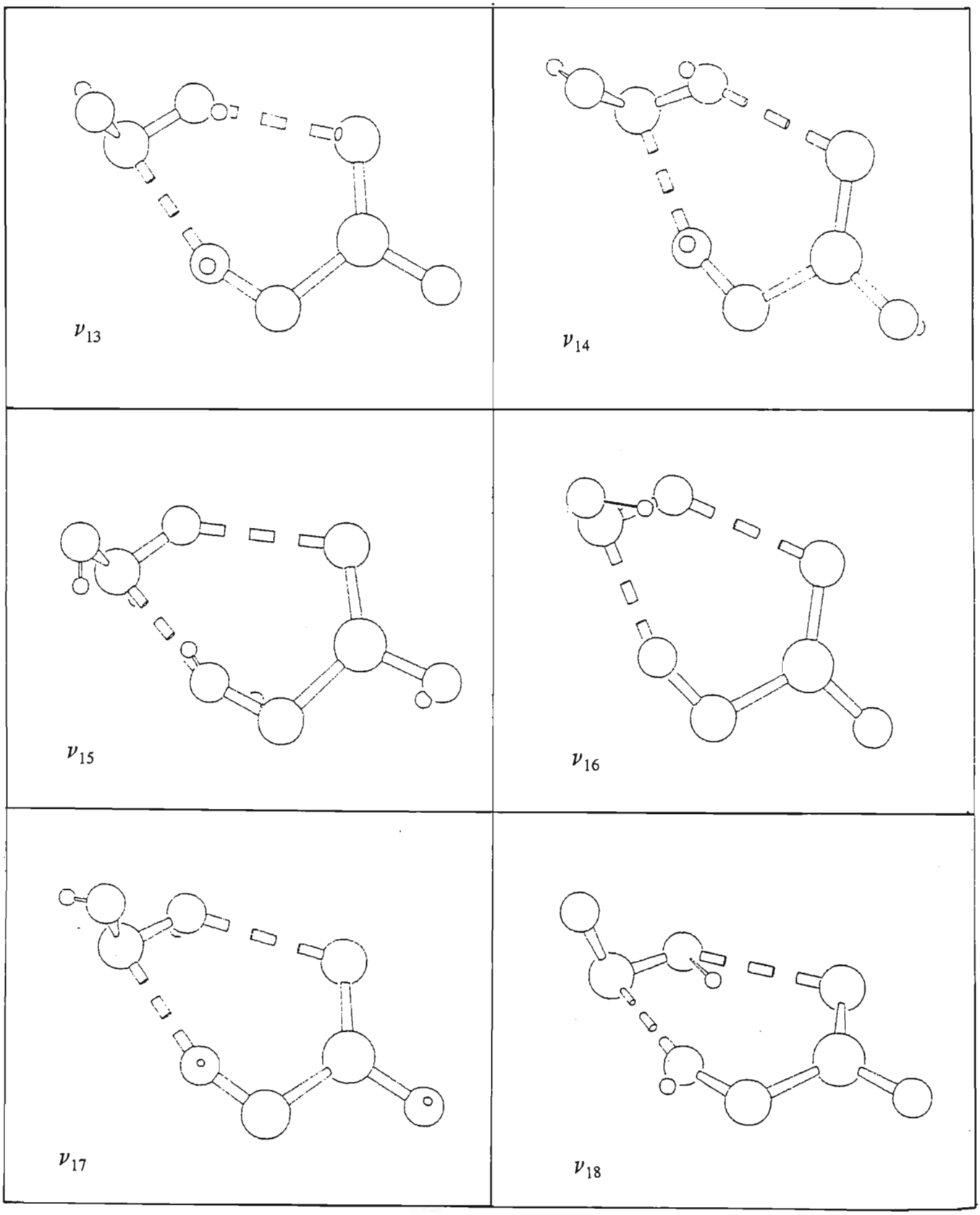

Figure 9.3. Graphical representations of the six intermolecular modes of the HCOOH-HOH complex.

The band at 240 cm^{-1} is a 66% contribution from the C=O...H angle deformation, coupled with a 15% contribution from the intermonomer stretching mode. The remaining intermolecular modes are so heavily coupled that exact assignment is difficult, except by indication of the relative contributions of each mode; it is however important to note that the intermonomer stretching mode occurs at 202 cm^{-1}, with a purity of 30%, with roughly 40% contribution from the out-of-plane bending of the O-H...O angle. The description of the IM modes is further complicated by the low symmetry of the complex.

In the acetic acid-water complex, a vibrational mode described by 59% contribution from the in-plane bending of the O-H...O angle and 15% contribution from the in-plane bending of the C=O...H angle is predicted at 713 cm^{-1}. The torsional motion about the H...O bond occurs at 368 cm^{-1}, comparable with the corresponding motion in the HCOOH-HOH complex which occurs at 380 cm^{-1}. The IM band at 310 cm^{-1} is a mixture of the torsional motion of the C2O3 and O10H9 bonds and the restricted rotation of the water sub-unit. The C=O...H bending, with a contribution of 64%, and with the ν(H...O) mode contributing 13%, occurs at 212 cm^{-1}. The characteristic intermonomer stretching band occurs at 191 cm^{-1}, which compares with 202 cm^{-1} found for the ν(H...O) mode in the HCOOH-HOH complex. The very low vibrational wavenumber is a mixture of a number of intermolecular modes; again a distinctive assignment of this band is complicated by the low complex symmetry, as mentioned above. It is, however, interesting to note that the intermolecular modes in both complexes are very similar.

9.4.2 Intra- and Intermolecular Intensities

The calculated and literature intensities of formic and acetic acids are presented

in Table 9.14, and in keeping with the format used in previous discussions, the ratios of the computed/literature intensities are also shown. The literature intensities cited here were theoretically determined and in general the intensities of formic acid in the literature[176] are higher than those found in this work. This is the effect of basis set on infrared intensities.[67] A similar trend is manifested by the acetic acid intensity ratios, where in general a better agreement between the intensities found in this work and the literature[181] is noted. Again this strong correlation is attributable to the fact that the level of theory used in both cases is the same, although the literature basis set was slightly larger than the one used here.

In Table 9.15 are collected the intensities of the complexes of water with formic and acetic acids along with the ratios of the complex/monomer intensities. The ratio patterns are very similar in both complexes, with a three-fold intensity increase in the $\nu_a(OH_2)$ mode in both the complexes but distinct 40-fold and 60-fold intensity increases for the $\nu_s(OH_2)$ mode of the water sub-unit in the HCOOH-HOH and CH_3COOH-HOH complexes respectively.

The intensity of the ν(OH) mode of the acid is increased to a similar extent, 9 and 10 times higher in the complex than in the monomer for the HCOOH-HOH and CH_3COOH-HOH complexes respectively. The out-of-plane bending of the CO bond is about 160 and 40 times more intense in the formic and acetic acid-water complexes than in the corresponding monomers.

The O4H5 out-of-plane motion in the formic acid-water complex shows a very high intensity ratio on complexation, yet the corresponding motion in the acetic acid-water complex displays no such high intensity ratio.

Table 9.14. The Infrared Intensities of Formic and Acetic Acids Compared with those from the Literature through the Calculated/Literature Intensity Ratios

		A/km mol^{-1}		
Molecule	Mode	Calculated	Literature	$A_{Calc.}/A_{Lit.}$
HCOOH[a]	ν_1	62.1	104.0	0.60
	ν_2	87.5	34.0	2.57
	ν_3	220.7	481.0	0.46
	ν_4	0.7	7.0	0.10
	ν_5	31.7	22.0	1.44
	ν_6	332.9	335.0	0.99
	ν_7	10.9	71.0	0.15
	ν_8	0.9	1.0	0.90
	ν_9	101.2	310.0	0.33
CH_3COOH[b]				
	ν_1	59.6	73.7	0.81
	ν_2	4.0	3.1	1.32
	ν_3	1.5	1.7	0.88
	ν_4	231.2	302.9	0.76
	ν_5	12.0	14.0	0.86
	ν_6	65.8	66.2	0.99
	ν_7	43.3	43.5	1.00
	ν_8	193.8	218.8	0.89
	ν_9	6.2	5.4	1.15
	ν_{10}	66.8	69.7	0.96
	ν_{11}	3.2	6.7	0.48
	ν_{12}	44.1	38.6	1.14
	ν_{13}	4.0	3.9	1.03
	ν_{14}	3.4	3.4	1.00
	ν_{15}	7.8	9.9	0.79
	ν_{16}	6.2	5.4	1.15
	ν_{17}	119.0	82.9	1.44
	ν_{18}	18.1	48.8	0.37
	ν_{19}	0.5	0.6	0.83

[a] Ref. 176. [b] Ref. 181.

Table 9.15. The Computed Intensities of the Acid-Water Adducts, and the Monomers, with the Complex/Monomer Intensity Ratios

		A/km mol^{-1}		
Species	Mode	Complex	Monomer	A_c/A_m
HCOOH-HOH	ν_1	91.7	33.8	2.7
	ν_2	164.7	4.2	39.2
	ν_3	585.8	62.1	9.4
	ν_4	86.0	87.5	1.0
	ν_5	276.5	220.7	1.3
	ν_6	112.6	77.7	1.4
	ν_7	1.9	0.7	2.7
	ν_8	14.0	-	-
	ν_9	210.7	332.9	0.6
	ν_{10}	22.7	31.9	0.7
	ν_{11}	141.7	0.9	157.4
	ν_{12}	141.3	0.9	157.0
	ν_{13}	161.3	IM	IM
	ν_{14}	94.7	IM	IM
	ν_{15}	81.9	IM	IM
	ν_{16}	44.3	IM	IM
	ν_{17}	30.6	IM	IM
	ν_{18}	4.3	IM	IM

Table 9.15 (continued)

CH_3COOH-HOH	ν_1	89.9	33.8	2.7
	ν_2	249.7	4.2	59.5
	ν_3	588.5	59.6	9.9
	ν_4	7.0	4.0	1.8
	ν_5	3.5	3.4	1.0
	ν_6	1.4	1.5	0.9
	ν_7	12.1	231.0	0.1
	ν_8	101.1	77.7	1.3
	ν_9	7.4	7.8	0.9
	ν_{10}	19.5	12.0	1.6
	ν_{11}	46.5	65.8	0.7
	ν_{12}	28.0	43.3	0.6
	ν_{13}	228.1	194.0	1.2
	ν_{14}	6.3	6.2	1.0
	ν_{15}	26.8	66.8	0.4
	ν_{16}	141.6	3.2	44.3
	ν_{17}	6.6	119.0	0.1
	ν_{18}	316.0	IM	IM
	ν_{19}	14.5	0.0	*
	ν_{20}	2.0	44.0	0.0
	ν_{21}	27.9	4.0	7.0
	ν_{22}	85.0	IM	IM
	ν_{23}	105.9	IM	IM
	ν_{24}	19.9	IM	IM
	ν_{25}	18.7	IM	IM
	ν_{26}	3.1	0.5	6.2
	ν_{27}	3.5	IM	IM

* : Division by zero.

The relative intensities of the two binary complexes of water with formic and acetic acids show a similar pattern. The in-plane bending motion of the O-H...O angle coupled with the C=O...H angle is the most intense band and is also heavily coupled in the acid-water adducts. The intensity of the O-H...O bending band is, however, higher in the acetic acid-water complex than in the formic acid-water adduct. The torsional motion about the H...O bond occurs with an

intensity of about 110 km mol^{-1} in the acetic acid-water complex, while the same band occurs with an intensity of about 95 km mol^{-1} in the formic acid-water adduct; again the intensity is the result of a 45% contribution to the total intensity from the restricted rotation about the H...O bond in the acetic acid-water complex but not such a large contribution in the formic acid-water case.

The in-plane bending of the C=O...H angle has an intensity of 44 km mol^{-1} in the formic acid-water adduct while this mode has an intensity of only 20 km mol^{-1} in the acetic acid-water adduct; although in this case the absolute value does not compare that well, the general trend is nevertheless still upheld. The intermonomer stretching mode occurs with an intensity of about 31 km mol^{-1} in the HCOOH-HOH adduct with some small contribution to the intensity from the out-of-plane bending of the O-H...O angle, while in the CH_3COOH-HOH complex, the intermonomer stretching mode occurs with an intensity of about 20 km mol^{-1}, and in this case with a small contribution from the in-plane bending of the O-H...O angle. The band corresponding to the out-of-plane bending of the hydrogen bond angle occurs with intensities of 4 and 3 km mol^{-1} for the formic and acetic acid-water complexes respectively.

9.4.3 Intra- and Intermolecular Force Constants

In Table 9.16 are collected the computed force constants of formic and acetic acids. There is a good agreement with those theoretically[240] determined (e.g. f(C1O2) and f(C1O4) have values of 1369 and 619 N m^{-1} respectively) except for the O-C=O bend, even though the literature computations were carried out using semi-empirical methods.[241]

Table 9.16. Selected Computed Force Constants of Formic and Acetic Acid Monomers

Molecule	Parameter	Calculated
HCOOH	f(C1O2)/N m^{-1}	1413.6
	f(C1O4)/N m^{-1}	676.6
	f(O4H5)/N m^{-1}	526.1
	f(C1H3)/N m^{-1}	521.5
	f(O2C1O4)/N m rad^{-2}	371.0
	f(C1O4H5)/N m rad^{-2}	342.4
CH_3COOH	f(C2O3)/N m^{-1}	1338.2
	f(O4H5)/N m^{-1}	815.9
	f(C1O2)/N m^{-1}	494.3
	f(O3C2O4)/N m rad^{-2}	250.8
	f(C2O4H5)/N m rad^{-2}	77.5

Table 9.17 shows the force constants of the complexes of water with formic and acetic acids, together with the differences between the complex and the monomer force constants. These two complexes show the most dramatic changes in force constants in comparison with the changes of the force constants of the other complexes investigated in this study so far. The C=O stretching force constant is reduced to half its value in the formic acid than in the acetic acid water complex. The stretching force constant, f(C1O4), of the C-O bond is increased by about 90 N m^{-1} on complexation while that of acetic acid, f(C2O4), is reduced by about the same order of magnitude on complexation, moreover the hydroxyl stretching force constant, f(O4H5), is increased by 126.4 N m^{-1} in the formic acid-water complex while its counterpart, f(O4H5), is decreased by 151.1 N m^{-1} in the acetic acid-water complex. These opposite effects in the two acid-water complexes cannot be attributed to the usual wavenumber force constant and mass relationship. A study using a larger basis set would perhaps help to understand the dynamics involved.

Table 9.17. Some Selected Computed Force Constants of the Complexes of Water with Formic and Acetic Acids and the Differences between the Complex and the Monomer Values

		Value	
Complex	Parameter	Calculated	Difference
HCOOH-HOH	f(C1O2)/N m^{-1}	1339.1	-73.6
	f(C1O4)/N m^{-1}	764.5	87.9
	f(O4H5)/N m^{-1}	652.5	126.4
	f(O7H6)/N m^{-1}	863.9	-13.8
	f(C1H3)/N m^{-1}	555.6	34.1
	f(H6...O2)/N m^{-1}	35.8	IM
	f(O7H6...O2)/N m rad^{-2}	33.4	IM
	f(C1O4H5)/N m rad^{-2}	112.7	-229.7
	f(O2C1O4)/N m rad^{-2}	251.2	119.8
	f(O8H7H6)/N m rad^{-2}	68.5	-5.4
CH_3COOH-HOH	f(C2O3)/N m^{-1}	1307.4	-30.8
	f(C2O4)/N m^{-1}	721.4	-94.4
	f(O4H5)/N m^{-1}	664.8	-151.1
	f(O10H9)/N m^{-1}	843.4	-34.3
	f(C1C2)/N m^{-1}	495.2	0.9
	f(H9...O3)/N m^{-1}	36.6	IM
	f(O10H9...O3)/N m rad^{-2}	40.9	IM
	f(O3C2O4)/N m rad^{-2}	349.6	98.7
	f(C2O4H5/N m rad^{-2}	112.8	35.3
	f(H11O10H9)/N m rad^{-2}	67.8	-6.1

The bending force constant, f(C1O4H5), of the COH angle is drastically reduced by 229.7 N m rad^{-2} in the formic acid-water adduct, but increased by 35.3 N m rad^{-2} in the acetic acid-water adduct, implying that in the formic acid-water complex, the bending motion of the COH angle is easily executed compared with the same motion in the acetic acid-water complex. Were it that the mesomeric effect accounted for such changes in the force constant, the CO and OH bond force constants would have increased in CH_3COOH-HOH, but they are reduced. The O-C=O angle bending force constant is increased

in both the formic and acetic acid-water complexes, in accordance with the fact that the opening of this angle is restricted by the two hydrogen bonds in both complexes. The stretching force constant of the bonded water OH bond is reduced by a similar magnitude in both complexes. The large changes in force constants on complexation are consistent with the fact that these are among the strongest interacting systems examined so far.

The intermonomer stretching force constants are 35.8 and 36.6 N m^{-1} for the formic and acetic acid-water complexes respectively; such a close similarity of the characteristic force constants again illustrates the fact that the stabilities of these complexes are fairly close. The force constants of the hydrogen bond angle deformation are 33.4 and 40.9 N m rad^{-2} for the formic and acetic acid-water complexes. The most striking feature is that of the bending force constants having larger magnitudes than the stretching force constants; again this is a unique feature observed only for the acid-water complexes.

9.5 Vibrational Properties of $HCOOCH_3$-HOH and CH_3COOCH_3-HOH Complexes

9.5.1 Intra- and Intermolecular Wavenumbers

The calculated and experimental[193,242] vibrational wavenumbers of the methyl formate and methyl acetate monomers and the ratios of the calculated/experimental wavenumbers are presented in Table 9.18. The calculated/experimental ratios are good indicators of the deviation between the computed and experimental wavenumbers, and are close to unity for most

Table 9.18. The Predicted and Experimental Infrared Spectra of Methyl Formate and Methyl Acetate along with the Calculated/Experimental Wavenumber Ratios

Molecule	Mode	Symmetry species	$\tilde{\nu}$/cm^{-1}		$\tilde{\nu}_{Cal.}/\tilde{\nu}_{Exp.}$
			Calculated	Experimental	
$HCOOCH_3$[a]	a'	ν_1	3288	3045	1.08
		ν_2	3264	2969	1.10
		ν_3	3152	2943	1.07
		ν_4	1815	1754	1.03
		ν_5	1557	1554	1.00
		ν_6	1512	1445	1.05
		ν_7	1434	1371	1.05
		ν_8	1265	1207	1.04
		ν_9	1216	1166	1.04
		ν_{10}	969	925	1.05
		ν_{11}	779	767	1.02
		ν_{12}	311	318	0.98
	a''	ν_{13}	3254	3012	1.08
		ν_{14}	1549	1443	1.07
		ν_{15}	1206	1168	1.03
		ν_{16}	1051	1032	1.02
		ν_{17}	351	332	1.06
		ν_{18}	149	130	1.15

Table 9.18 (continued)

CH_3COOCH_3[b]	a'	ν_1	3281	3035	1.08
		ν_2	3280	3031	1.08
		ν_3	3152	2966	1.06
		ν_4	3149	2964	1.06
		ν_5	1835	1771	1.04
		ν_6	1558	1460	1.07
		ν_7	1533	1440	1.06
		ν_8	1517	1430	1.06
		ν_9	1449	1375	1.05
		ν_{10}	1319	1248	1.06
		ν_{11}	1234	1159	1.06
		ν_{12}	1109	1060	1.05
		ν_{13}	1015	980	1.04
		ν_{14}	875	844	1.04
		ν_{15}	652	639	1.02
		ν_{16}	428	429	1.00
		ν_{17}	291	303	0.96
	a"	ν_{18}	3249	3005	1.08
		ν_{19}	3245	2994	1.08
		ν_{20}	1547	1460	1.06
		ν_{21}	1536	1430	1.07
		ν_{22}	1205	1187	1.02
		ν_{23}	1092	1036	1.05
		ν_{24}	605	607	1.00
		ν_{25}	184	187	1.00
		ν_{26}	150	136	1.10
		ν_{27}	67	110	0.61

[a] Ref. 193. [b] Ref. 242.

wavenumbers. The only exceptions are the very low wavenumbers, due to anharmonicity effects.

Table 9.19 contains the symmetry coordinates of the complexes of water with methyl formate and methyl acetate, while Table 9.20 presents the wavenumbers, and the wavenumber shifts between complex and monomer, the %PEDs and the complex band assignments using the symmetry coordinates.

There are few major wavenumber shifts for either the methyl formate- or methyl acetate-water complexes. The ν_1 and ν_2 modes, ($\nu_s(OH_2)$ and $\nu_a(OH_2)$ vibrational motions of the water component) are red shifted by -40 and -62 cm^{-1} for the methyl formate-water complex respectively and the ν_7 (C1O2 stretching) mode by -27 cm^{-1}. The ν_5 mode is blue shifted by 44 cm^{-1}. A similar value of wavenumber shift was observed for the formaldehyde- and acetaldehyde-water complexes as discussed in sections 7.3.1 and 8.3.1, for a similar type of bond stretching. The significance of this blue shift in these complexes is the fact that it furnishes evidence of a cyclic structure.

In the methyl acetate-water complex, the ν_1 and ν_2 vibrational modes of the water sub-unit are shifted to lower wavenumbers by -47 and -84 cm^{-1} respectively, while the ν_9 mode, corresponding to the carbonyl stretching mode, is red shifted by -26 cm^{-1}. The HOH angle bend is blue shifted by 26 cm^{-1}, compared with the 20 cm^{-1} blue shift in the $HCOOCH_3$-HOH adduct. The shifts are in general not that dramatic, indicating that compared with the carboxylic acid-water complexes, the two ester-water complexes are of lower stability.

Indeed the interaction energies of the two ester complexes are -15.97 kJ mol^{-1} and -20.77 kJ mol^{-1} for $HCOOCH_3$-HOH and CH_3COOCH_3-HOH respectively, while those of the acid complexes are -40.67 kJ mol^{-1} and -40.13 kJ mol^{-1} for HCOOH-HOH and CH_3COOH-HOH respectively.

Table 9.19. The Symmetry Coordinates and the Vibrational Mode Descriptions of the Complexes of Water with Methyl Formate and Methyl Acetate

Complex	Symmetry Coordinate		Description
$HCOOCH_3$-HOH	S_1	$\{\Delta r_{9,10} - \Delta r_{10,11}\}/\sqrt{2}$	OH_2 a-stretch
	S_2	$\{\Delta r_{9,10} + \Delta r_{10,11}\}/\sqrt{2}$	OH_2 s-stretch
	S_3	$\{2\Delta r_{5,8} - \Delta r_{5,7} - \Delta r_{5,6}\}/\sqrt{6}$	CH_3 d-stretch
	S_4	$\{\Delta r_{5,6} - \Delta r_{5,7}\}/\sqrt{2}$	CH_3 a-stretch
	S_5	$\Delta r_{1,3}$	CH stretch
	S_6	$\{\Delta r_{5,6} + \Delta r_{5,7} + \Delta r_{5,8}\}/\sqrt{3}$	CH_3 s-stretch
	S_7	$\Delta r_{1,2}$	CO stretch
	S_8	$\Delta\delta_{9,10,11}$	HOH bend
	S_9	$\{2\Delta\delta_{7,5,8} - \Delta\delta_{6,5,7} - \Delta\delta_{6,5,8}\}/\sqrt{6}$	CH_3 d-deformation
	S_{10}	$\{\Delta\delta_{7,5,8} - \Delta\delta_{6,5,8}\}/\sqrt{2}$	CH_3 d-deformation
	S_{11}	$\{\Delta\delta_{7,5,8} + \Delta\delta_{6,5,7} + \Delta\delta_{6,5,8} - \Delta\beta_{6,5,4} - \Delta\beta_{7,5,4} - \Delta\beta_{854}\}/\sqrt{6}$	CH_3 s-deformation
	S_{12}	$\Delta\delta_{2,1,3}$	O=C-H bend
	S_{13}	$\Delta r_{1,4}$	C-O stretch
	S_{14}	$\{2\Delta\beta_{8,5,4} - \Delta\beta_{7,5,4} - \Delta\beta_{6,5,4}\}/\sqrt{6}$	CH_3 rock
	S_{15}	$\{\Delta\beta_{7,5,4} - \Delta\beta_{8,5,4}\}/\sqrt{2}$	CH_3 rock
	S_{16}	$\Delta\gamma_{3,4,12}$	CH op bend
	S_{17}	$\Delta r_{4,5}$	O-CH_3 stretch
	S_{18}	$\Delta\delta_{4,1,2}$	O=C-H bend
	S_{19}	$\Delta\delta_{2,9,10}$	O-H...O ip bend
	S_{20}	$\Delta\delta_{2,1,4}$	O-C=O bend

Table 9.19 (continued)

	S_{21}	$\Delta\delta_{5,4,1}$	COC bend
	S_{22}	$\Delta\tau_{1,2,9,10}$	torsion about H...O bond
	S_{23}	$\Delta\tau_{11,10,9,2}$	restricted rotation about H...O bond
	S_{24}	$\Delta r_{2,9}$	H...O stretch
	S_{25}	$\Delta\tau_{8,5,4,1}$	torsion about C-O bond
	S_{26}	$\Delta\delta_{1,2,9}$	C=O...H ip
	S_{27}	$\Delta\gamma_{9,4,1,2}$	O-H...O op bend
CH_3COOCH_3-HOH	S_1	$\{\Delta r_{12,13} - \Delta r_{13,14}\}/\sqrt{2}$	OH_2 a-stretch
	S_2	$\{\Delta r_{12,13} + \Delta r_{13,14}\}/\sqrt{2}$	OH_2 s-stretch
	S_3	$\{2\Delta r_{8,9} - \Delta r_{8,11} - \Delta r_{8,10}\}/\sqrt{6}$	CH_3(O) d-stretch
	S_4	$\{2\Delta r_{1,4} - \Delta r_{1,5} - \Delta r_{1,6}\}/\sqrt{6}$	CH_3(C) d-stretch
	S_5	$\{\Delta r_{8,10} - \Delta r_{8,11}\}/\sqrt{2}$	CH_3(O) d-stretch
	S_6	$\{\Delta r_{1,5} - \Delta r_{1,6}\}/\sqrt{2}$	CH_3(C) d-stretch
	S_7	$\{\Delta r_{8,9} + \Delta r_{8,11} + \Delta r_{8,10}\}/\sqrt{3}$	CH_3(O) s-stretch
	S_8	$\{\Delta r_{1,4} + \Delta r_{1,5} + \Delta r_{1,6}\}/\sqrt{3}$	CH_3(C) s-stretch
	S_9	$\Delta r_{2,3}$	CO stretch
	S_{10}	$\Delta\delta_{12,13,14}$	HOH bend
	S_{11}	$\{2\Delta\delta_{10,8,11} - \Delta\delta_{9,8,11} - \Delta\delta_{9,8,10}\}/\sqrt{6}$	CH_3(O) d-deformation
	S_{12}	$\Delta\tau_{14,13,4,1}$	torsion about H...O bond
	S_{13}	$\{\Delta\delta_{10,8,11} + \Delta\delta_{9,8,11} + \Delta\delta_{9,8,10} - \Delta\beta_{987} - \Delta\beta_{10,8,7} - \Delta\beta_{11,8,7}\}/\sqrt{6}$	CH_3(O) s-deformation
	S_{14}	$\{2\Delta\delta_{5,1,6} - \Delta\delta_{4,1,5} - \Delta\delta_{4,1,6}\}/\sqrt{6}$	CH_3(C) d-deformation
	S_{15}	$\{\Delta\delta_{5,1,6} + \Delta\delta_{4,1,5} + \Delta\delta_{4,1,6} - \Delta\beta_{4,1,2} - \Delta\beta_{5,1,2} - \Delta\beta_{6,1,2}\}/\sqrt{6}$	CH_3(C) s-deformation

Table 9.19 (continued)

S_{16}	$\Delta r_{2,7}$	C-O stretch
S_{17}	$\{2\Delta\beta_{9,8,7} - \Delta\beta_{10,8,7} - \Delta\beta_{11,8,7}\}/\sqrt{6}$	CH_3(O) rock
S_{18}	$\Delta r_{7,8}$	O-CH_3 stretch
S_{19}	$\{2\Delta\beta_{4,1,2} - \Delta\beta_{5,1,2} - \Delta\beta_{6,1,2}\}/\sqrt{6}$	CH_3(C) rock
S_{20}	$\Delta r_{1,2}$	CC stretch
S_{21}	$\{\Delta\delta_{1,2,3} - \Delta\delta_{3,2,7}\}/\sqrt{2}$	CCO and O-C=O deformation
S_{22}	$\Delta\delta_{1,2,3}$	CCO deformation
S_{23}	$\Delta\delta_{2,7,8}$	COC deformation
S_{24}	$\{\Delta\delta_{9,8,10} - \Delta\delta_{9,8,11}\}/\sqrt{2}$	CH_3(O) d-deformation
S_{25}	$\{\Delta\delta_{4,1,6} - \Delta\delta_{9,8,10}\}/\sqrt{2}$	CH_3(C) d-deformation
S_{26}	$\{\Delta\delta_{10,8,7} - \Delta\delta_{4,1,5}\}/\sqrt{2}$	CH_3(O) rock
S_{27}	$\{\Delta\delta_{5,1,2} - \Delta\delta_{11,8,7}\}/\sqrt{2}$	CH_3(C) rock
S_{28}	$\Delta\gamma_{2,9,8,7}$	CH(OCH_3) op bend
S_{29}	$\Delta\gamma_{3,8,7,2}$	CO op bend
S_{30}	$\{\Delta\tau_{4,1,2,7} - \Delta\tau_{2,7,8,9}\}/\sqrt{2}$	CC and O-C torsion
S_{31}	$\Delta\tau_{1,2,7,8}$	C-O torsion
S_{32}	$\Delta\gamma_{12,3,2,7}$	O-H...O op bend
S_{33}	$\Delta\delta_{2,3,12}$	C=O...H ip bend
S_{34}	$\Delta\tau_{2,3,12,13}$	torsion about H...O bond
S_{35}	$\Delta\delta_{3,12,13}$	O-H...O ip bend
S_{36}	$\Delta\tau_{14,13,12,3}$	restricted rotation about H...O bond

Table 9.20. The Computed Wavenumbers and Wavenumber Shifts for the $HCOOCH_3$-HOH and CH_3COOCH_3-HOH Complexes and the %PEDs

		$\tilde{\nu}/cm^{-1}$		
Species	Mode	Calculated	Shift	%PED[a]
$HCOOCH_3$-HOH	ν_1	3990	-40	$89S_1 + 10S_2$
	ν_2	3829	-62	$87S_2 + 11S_1$
	ν_3	3292	4	$99S_3$
	ν_4	3257	3	$100S_4$
	ν_5	3208	44	$98S_5$
	ν_6	3255	1	$98S_6$
	ν_7	1789	-27	$80S_7$
	ν_8	1702	20	$88S_8$
	ν_9	1556	-1	$87S_9$
	ν_{10}	1549	0	$92S_{10}$
	ν_{11}	1512	0	$89S_{11}$
	ν_{12}	1431	-3	$93S_{12}$
	ν_{13}	1285	19	$52S_{13} + 15S_{17} + 11S_{14} + 11S_{19}$
	ν_{14}	1221	5	$63S_{14} + 10S_{18} +$
	ν_{15}	1206	0	$94S_{15}$
	ν_{16}	1079	28	$93S_{16}$
	ν_{17}	970	1	$82S_{17}$
	ν_{18}	784	5	$53S_{18} + 19S_{21}$
	ν_{19}	598	IM	$63S_{19} + 14S_{24} + 14S_{26}$

Table 9.20 (continued)

	ν_{20}	375	24	$81S_{20}$
	ν_{21}	329	18	$56S_{21} + 14S_{24}$
	ν_{22}	288	IM	$60S_{22} + 26S_{23}$
	ν_{23}	187	IM	$93S_{23}$
	ν_{24}	159	IM	$85S_{24}$
	ν_{25}	151	2	$96S_{25}$
	ν_{26}	97	IM	$57S_{26} + 20S_{19} + 18S_{24}$
	ν_{27}	53	IM	$69S_{27} + 15S_{23}$
CH_3COOCH_3-HOH	ν_1	3983	-47	$86S_1 + 13S_2$
	ν_2	3807	-84	$84S_2 + 15S_1$
	ν_3	3286	5	$99S_3$
	ν_4	3283	3	$97S_4$
	ν_5	3254	5	$94S_5$
	ν_6	3242	-3	$93S_6$
	ν_7	3152	0	$95S_7$
	ν_8	3149	0	$94S_8$
	ν_9	1809	-26	$75S_9$
	ν_{10}	1708	26	$59S_{10} + 20S_{34}$
	ν_{11}	1558	0	$85S_{11}$
	ν_{12}	1552	5	$53S_{12} + 43S_{13}$
	ν_{13}	1548	11	$55S_{13} + 41S_{19}$
	ν_{14}	1535	2	$74S_{14} + 11S_{13}$
	ν_{15}	1519	2	$73S_{15}$
	ν_{16}	1458	9	$77S_{16}$
	ν_{17}	1345	26	$34S_{17} + 24S_{24} + 17S_{22}$

Table 9.20 (continued)

ν_{18}	1236	2	$74S_{18}$
ν_{19}	1204	-1	$50S_{19} + 32S_{13}$
ν_{20}	1117	8	$40S_{20} + 31S_{21} + 11S_{12}$
ν_{21}	1102	10	$56S_{12} + 16S_{32} + 11S_{19}$
ν_{22}	1022	7	$33S_{21} + 27S_{20} + 18S_{23}$
ν_{23}	888	13	$34S_{22} + 16S_{23} + 13S_{20}$
ν_{24}	660	8	$22S_{24} + 44S_{17} + 12S_{10}$
ν_{25}	620	IM	$70S_{10} + 15S_{35}$
ν_{26}	610	6	$13S_{32} + 66S_{13}$
ν_{27}	443	15	$53S_{24} + 27S_{17}$
ν_{28}	319	IM	$71S_{10} + 10S_{36}$
ν_{29}	309	18	$70S_{10} + 11S_{36}$
ν_{30}	208	IM	$69S_{12} + 11S_{19}$
ν_{31}	179	-5	$49S_{13} + 37S_{19}$
ν_{32}	153	3	$55S_{13} + 44S_{19}$
ν_{33}	146	-3	$57S_{20} + 28S_{19}$
ν_{34}	115	IM	$49S_{13} + 47S_{12}$
ν_{35}	107	40	$39S_{12} + 57S_{13}$
ν_{36}	35	IM	$50S_{32} + 44S_{13}$

[a] see Table 9.19. IM : intermolecular mode.

The in-plane bending of the O-H...O angle is predicted to occur at 598 cm^{-1} in the $HCOOCH_3$-HOH complex, while the torsional motion about the H...O bond occurs at 288 cm^{-1} and is strongly coupled with the C=O...H angle bending, which contributes 26% to the total motion. Restricted rotation of the water sub-unit about the carbonyl bond occurs at 187 cm^{-1}. The ν(H...O) mode occurs at 159 cm^{-1}, with minimal contribution from the other intermolecular modes. The C=O...H in-plane bending mode occurs at 97 cm^{-1} and is heavily coupled with the in-plane O-H...O bending motion and the ν(H....O) mode. The out-of-plane bending motion of the O-H...O angle appears at 53 cm^{-1} and is mixed with the restricted rotation of the water sub-unit about the carbonyl group.

The CH_3COOCH_3-HOH complex displays a similar pattern of intermolecular modes to $HCOOCH_3$-HOH, with the characteristic intermonomer stretching mode occurring at 208 cm^{-1}, while the highest intermolecular mode is observed at 620 cm^{-1}. All the intermolecular modes of the methyl formate-water complex mirror those of the acetic acid-water complex very strongly, both in following a similar pattern as well as in relative magnitudes.

9.5.2 Intra- and Intermolecular Intensities

In Table 9.21 are collected the intensities of the CH_3COOCH_3 molecule,[242] together with the calculated/experimental intensity ratios. The intensities of the $HCOOCH_3$ molecule could not be found in the literature. The ratios appearing in the last column of Table 9.21 indicate that the experimental intensities are larger than the ones computed in this work. Only very few calculated intensities compare favourably with the literature values; ν_1 is such an example.

Table 9.21. The Calculated and Experimental Intensities of Methyl Acetate and the Calculated/Experimental Ratios

		A/km mol^{-1}		
Complex	Mode	Calculated	Experimental[a]	A_c/A_m
CH_3COOCH_3	ν_1	16.3	18.0	0.91
	ν_2	3.2	18.0	0.18
	ν_3	24.3	35.8	0.68
	ν_4	4.4	4.6	0.96
	ν_5	177.3	281.3	0.63
	ν_6	6.6	97.6	0.07
	ν_7	12.7	97.6	0.13
	ν_8	9.6	97.6	0.10
	ν_9	57.6	69.9	0.82
	ν_{10}	331.4	355.8	0.93
	ν_{11}	2.8	3.0	0.93
	ν_{12}	67.9	112.3	0.60
	ν_{13}	2.2	7.6	0.29
	ν_{14}	20.5	38.2	0.54
	ν_{15}	7.2	10.4	0.69
	ν_{16}	6.1	-	-
	ν_{17}	11.8	-	-
	ν_{18}	20.2	27.4	0.74
	ν_{19}	3.9	27.4	0.14
	ν_{20}	5.2	97.6	0.05
	ν_{21}	6.4	97.6	0.07
	ν_{22}	1.7	3.0	0.57
	ν_{23}	5.6	17.6	0.32
	ν_{24}	6.6	-	-
	ν_{25}	6.9	-	-
	ν_{26}	0.4	-	-
	ν_{27}	0.5	-	-

[a] Ref. 242.

Table 9.22 presents the computed intensities of both the $HCOOCH_3$-HOH and CH_3COOCH_3-HOH complexes along with those of the corresponding monomers, together with the complex/monomer ratios. In the methyl formate-water complex, the ν_1 mode shows about a 3-fold increase in intensity while ν_2 shows about a 30-fold increase. It is worth noting that these modes describe the antisymmetric and symmetric water stretching motions. For the methyl acetate-water complex the intensities of the modes corresponding to the antisymmetric and symmetric water stretches are intensified by factors of 3 and 50.

In $HCOOCH_3$-HOH the ν_{19} mode has the highest IM intensity, of 305.8 km mol^{-1}, followed by the ν_{23} mode with an intensity of 119.2 km mol^{-1}, while the ν_{22} mode occurs with an intensity of 105.6 km mol^{-1}. The three remaining IM modes are fairly weak with intensities ranging from 2.1 to 10.6 km mol^{-1}.

The most intense IM mode of the methyl acetate-water complex, ν_{25}, has an intensity of 239.2 km mol^{-1}, which is comparable with 305.8 km mol^{-1} for the corresponding mode in the methyl formate-water complex. The IM modes ν_{28} and ν_{30} have almost half the intensity, 61.1 and 55 km mol^{-1}, of their counterparts in the $HCOOCH_3$-HOH complex, namely 105.6 and 119.2 km mol^{-1} respectively. The remaining IM mode intensities are quite low, a feature also observed for the methyl formate-water complex.

Table 9.22. The Computed Infrared Intensities of $HCOOCH_3$-HOH and CH_3COOCH_3-HOH, and the H_2O, $HCOOCH_3$ and CH_3COOCH_3 Monomer Intensities, together with the Complex/Monomer Intensity Ratios

		Intensity/km mol^{-1}		
Species	Mode	Complex	Monomer	A_c/A_m
$HCOOCH_3$-HOH	ν_1	85.8	33.8	2.5
	ν_2	115.8	4.2	27.6
	ν_3	11.3	12.3	0.9
	ν_4	16.4	18.2	0.9
	ν_5	14.2	46.2	0.3
	ν_6	21.7	31.8	0.7
	ν_7	264.0	231.0	1.1
	ν_8	71.4	77.8	0.9
	ν_9	8.2	7.7	1.1
	ν_{10}	6.2	5.6	1.1
	ν_{11}	5.0	3.1	1.6
	ν_{12}	3.3	1.1	3.3
	ν_{13}	284.8	255.2	1.1
	ν_{14}	332.4	71.4	4.7
	ν_{15}	2.1	1.9	1.1
	ν_{16}	0.1	0.2	0.5
	ν_{17}	20.0	22.8	0.9
	ν_{18}	9.8	9.0	1.1
	ν_{19}	305.8	IM	IM
	ν_{20}	39.8	27.3	1.5
	ν_{21}	31.1	14.5	2.1
	ν_{22}	105.6	IM	IM
	ν_{23}	119.2	IM	IM
	ν_{24}	2.1	IM	IM
	ν_{25}	0.8	0.0	*
	ν_{26}	10.6	IM	IM
	ν_{27}	2.1	IM	IM

Table 9.22 (continued)

CH_3COOCH_3-HOH	ν_1	92.7	33.8	2.7
	ν_2	198.1	4.2	47.2
	ν_3	12.8	16.3	0.8
	ν_4	7.0	3.2	2.2
	ν_5	6.9	20.2	0.9
	ν_6	3.3	3.9	0.8
	ν_7	23.9	4.4	3.9
	ν_8	7.2	24.3	0.3
	ν_9	240.9	177.3	1.4
	ν_{10}	63.4	77.7	0.8
	ν_{11}	7.4	6.6	0.9
	ν_{12}	7.4	5.2	1.1
	ν_{13}	4.4	6.4	0.7
	ν_{14}	10.9	12.7	0.9
	ν_{15}	14.0	9.6	1.4
	ν_{16}	52.0	57.8	0.9
	ν_{17}	345.3	331.4	1.0
	ν_{18}	3.2	2.8	1.1
	ν_{19}	1.8	1.7	1.1
	ν_{20}	66.1	67.9	1.0
	ν_{21}	5.1	5.6	0.9
	ν_{22}	4.2	2.2	1.9
	ν_{23}	12.3	20.5	0.6
	ν_{24}	12.3	7.2	1.7
	ν_{25}	239.2	IM	IM
	ν_{26}	7.8	6.6	1.1
	ν_{27}	5.7	6.1	0.9
	ν_{28}	61.1	IM	IM
	ν_{29}	76.1	11.8	6.4
	ν_{30}	55.0	IM	IM
	ν_{31}	41.7	6.9	6.0
	ν_{32}	3.6	0.4	9.0
	ν_{33}	0.7	IM	IM
	ν_{34}	16.1	IM	IM
	ν_{35}	14.4	0.5	28.4
	ν_{36}	2.5	IM	IM

9.5.3 Intra- and Intermolecular Force Constants

The list of computed force constants is given in Table 9.23, together with some force constants from the literature[187,242] and the ratios of the computed/literature force constants for the $HCOOCH_3$-HOH and CH_3COOCH_3-HOH complexes. The ratio column indicates a good correlation between the force constants calculated in this work and those from the literature. In Table 9.24 are shown the force constants of the complexes of water with methyl formate and methyl acetate and the complex-monomer force constant differences. It is interesting to note the significant deviations in force constants for the acid- and the ester-water complexes. The carbonyl force constant is for instance reduced by nearly 40 N m^{-1} in the methyl formate-water complex, but hardly perturbed at all in the methyl acetate-water complex. The stretching force constant of the C1H3 bond in methyl formate is the most significantly reduced, by 63.4 N m^{-1}.
The H_2O bending force constants are reduced by 4 and 5 N m^{-1} in the $HCOOCH_3$-HOH and CH_3COOCH_3-HOH complexes respectively. The bonded water OH force constants are reduced by 14.6 and 29.0 N m^{-1} respectively (Table 9.24).

The range of characteristic intermolecular force constants of the two ester-water complexes is quite small, as mentioned above, the implication of which is that the complexes have strongly similar structural properties.

The intermonomer stretching mode has a force constant of 21.5 and 19.6 N m^{-1} for the methyl formate- and methyl acetate-water complexes respectively. These values are almost half those of their counterparts in the formic and acetic acid-water complexes, again implying that the latter complexes are less stable than the former ones, a fact consistent with the interaction energies.

Table 9.23. Some Selected Computed Force Constants of the Methyl Formate and Methyl Acetate Monomers with the Literature Values and the Ratios of the Computed/Literature Force Constants

Molecule	Parameter	Value		Ratio
		Calc.	Lit.	
$HCOOCH_3$[a]	f(C1O2)/N m^{-1}	1348.6	1290.8	1.0
	f(C1H3)/N m^{-1}	578.7	464.4	1.2
	f(O2C1H3)/N m rad^{-2}	134.8	60.8	2.2
CH_3COOCH_3[b]	f(C2O3)/N m^{-1}	1318.1	1100.9	1.2
	f(C1C2)/N m^{-1}	488.5	404.6	1.2
	f(C1H4)/N m^{-1}	578.3	485.2	1.2
	f(C1C2O3)/N m rad^{-2}	65.1	129.0	0.5

Calc. : calculated. Lit. : literature. [a] Ref. 187. [b] Ref. 242.

Table 9.24. Some Selected Computed Force Constants of the Methyl Formate-Water and Methyl Acetate-Water Complexes together with the Complex - Monomer Differences

Complex	Parameter	Calculated	Difference
$HCOOCH_3$-HOH	f(C1O2)/N m^{-1}	1312.1	-36.5
	f(C1H3)/N m^{-1}	515.3	-63.4
	f(O10H9)/N m^{-1}	863.1	-14.6
	f(H9...O2)/N m^{-1}	21.5	IM
	f(O10H9...O2)/N m rad^{-2}	11.6	IM
	fO2C1H3)/N m rad^{-2}	132.9	-1.9
	f(H11O10H9)/N m rad^{-2}	70.0	-3.9
CH_3COOCH_3-HOH	f(C2O3)/N m^{-1}	1291.8	1.0
	f(O13H12)/N m^{-1}	848.7	-29.0
	f(H12...O3)/N m^{-1}	19.6	IM
	f(O13H12..O3)/N m rad^{-2}	12.3	IM
	f(C1C2O3)/N m rad^{-2}	65.1	0.0
	f(H14O13H12)/N m rad^{-2}	19.4	-4.5

CHAPTER 10

Summary and Conclusions

In this chapter some correlations between the various parameters are sought, e.g. the interaction energy, ΔE, and the H...B distance, ΔE and the A-H...B angle, the wavenumber shift, $\Delta\tilde{\nu}$, and r(H...B), and $\Delta\tilde{\nu}$ and the A...B distance. Some relationships between ΔE and the force constants, and between the force constants and r(H...B) are also reported. The Morokuma ΔE corrected for BSSE are compared with the RHF ΔE also corrected for BSSE. The computed gas phase enthalpies are discussed and compared with the experimental ones for the related systems.

10.1 Correlation of the Characteristic Geometrical Properties and Interaction Energies

Table 10.1 below presents a summary of both the primary and secondary hydrogen bond lengths, H...B, and the associated primary and secondary A-H...B bond angles, together with the intermolecular potential energies evaluated at the second order Møller-Plesset perturbation theory level. A plot of the primary H...B distance against the interaction energy (see Figure 10.1) shows that at short H...B distances the stability is high, but the stability is decreased as the separation distance is increased. The high stability end of the potential energy curve in Figure 10.1, while reflecting the expected trend, illustrates that the carboxylic acid-water complexes studied here present a unique property, that of very high stability compared with the rest of the complexes; due to the two strong hydrogen bonds formed. It is noted that NCCN-OH_2 does not follow the observed pattern in that, even though the separation distance, O...π, is the

Table 10.1. Summary of the Characteristic Geometrical Parameters and the Intermolecular Potential Energies for all Complexes

Complex	H...B/pm		A-H...B/deg		MP2 Intermolecular Potential Energy /kJ mol^{-1}
	Primary	Secondary	Primary	Secondary	
$NCH\text{-}OH_2$	202.5	-	176.6	-	-22.29
$C_2H_2\text{-}OH_2$	220.5	-	170.1	-	-10.26
$C_2N_2\text{-}OH_2$	273.4	-	-	-	-12.22
$CH_3CN\text{-}HOH$	214.2	-	173.1	-	-15.41
$H_2CO\text{-}HOH$	203.3	255.3	147.3	97.3	-15.04
$CH_2NH\text{-}HOH$	201.5	261.2	149.7	99.2	-21.00
$C_2H_4\text{-}HOH$	244.7	-	178.5	-	-6.85
$CH_3CHO\text{-}HOH$	199.7	258.1	150.0	98.4	-16.60
$(CH_3)_2CO\text{-}HOH$	198.1	243.2	163.4	114.9	-16.48
$HCOOH\text{-}HOH$	176.4	202.4	158.6	136.5	-40.67
$CH_3COOH\text{-}HOH$	177.7	197.1	158.9	139.5	-40.13
$HCOOCH_3\text{-}HOH$	203.8	257.1	147.0	96.9	-15.97
$CH_3COOCH_3\text{-}HOH$	198.5	243.9	161.7	112.9	-20.77

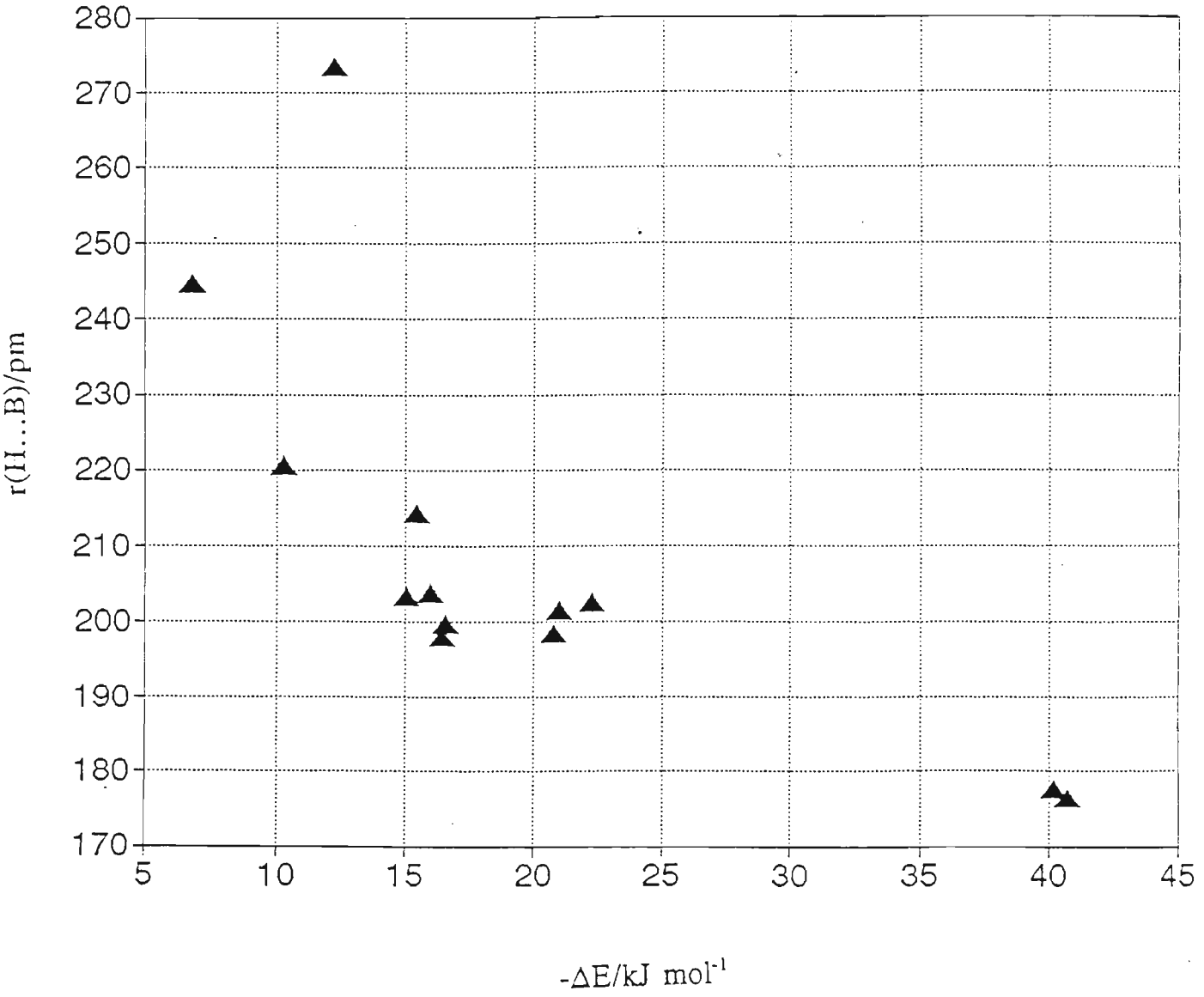

Figure 10.1. A plot of primary H...B distance against interaction energy.

longest of all the complexes, the stability is nevertheless still higher than those of some complexes with shorter A...B distances. Not all the complexes display a secondary H...B distance as depicted in Table 10.1 since they contain only a single interaction. A plot of the primary A-H...B bond angle against the interaction energy is shown in Figure 10.2. There is no apparent correlation between these two parameters but for the A-H...B angles greater than 145° the interaction energies are distributed in the range -10.26 to -22.29 kJ mol^{-1}, with the exception of the C_2H_4-H_2O adduct. For the carbonyl acceptors, the C=O...H angle is normally[233] around 120°. This is true for the complexes containing the C=O group, with the angle ranging from 97.3 to 114.9° for all the complexes studied in this project.

Figure 10.3 shows the plot of the R(A...B) distances against the interaction energies (see Tables 10.1 and 10.2). As noted in Figure 10.1, the greater the intermolecular separation, the lower is the stabilisation energy. The plot of R(A...B) vs ΔE, however, is closer to an inverse linear relationship than the plot of r(H...B) vs ΔE. Hence for the types of complex studied here, the R(A...B) distance predicts complex stability more successfully than the H...B distance.

Interaction energies may be converted into enthalpies in accordance with Del Bene[243] as follows: $\Delta H_{298}=\Delta E_{298} + \Delta(pV)$, where ΔE_{298} is the total energy change of complex formation at 298 K and pV is pressure-volume work. In order to estimate ΔH_{298} for the reaction by ab initio quantum mechanical methods, the energies of both the reactants and products, calculated at their optimised geometries, together with the differences in zero-point vibrational, rotational and translational energies at 298 K are required.[195] The total internal energy change, ΔE_{298}, is given by:

$$\Delta E_{298}=\Delta E_e^{\,0} + \Delta(\Delta E_e)_{298} + \Delta E_v^{\,0} + \Delta(\Delta E_v)_{298} + \Delta E_{r,298} + \Delta E_{t,298}$$

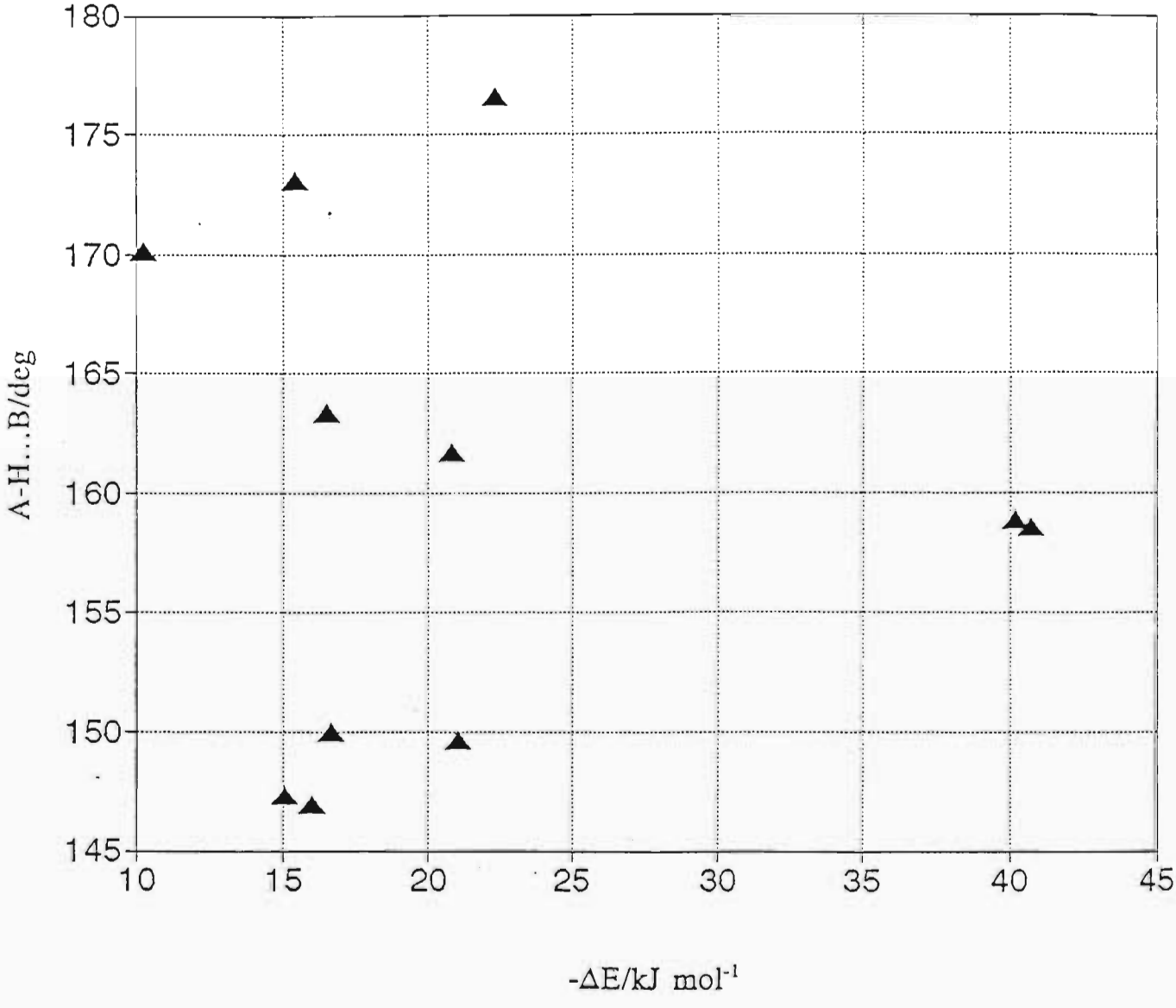

Figure 10.2. A plot of primary hydrogen bond angle A-H...B against interaction energy.

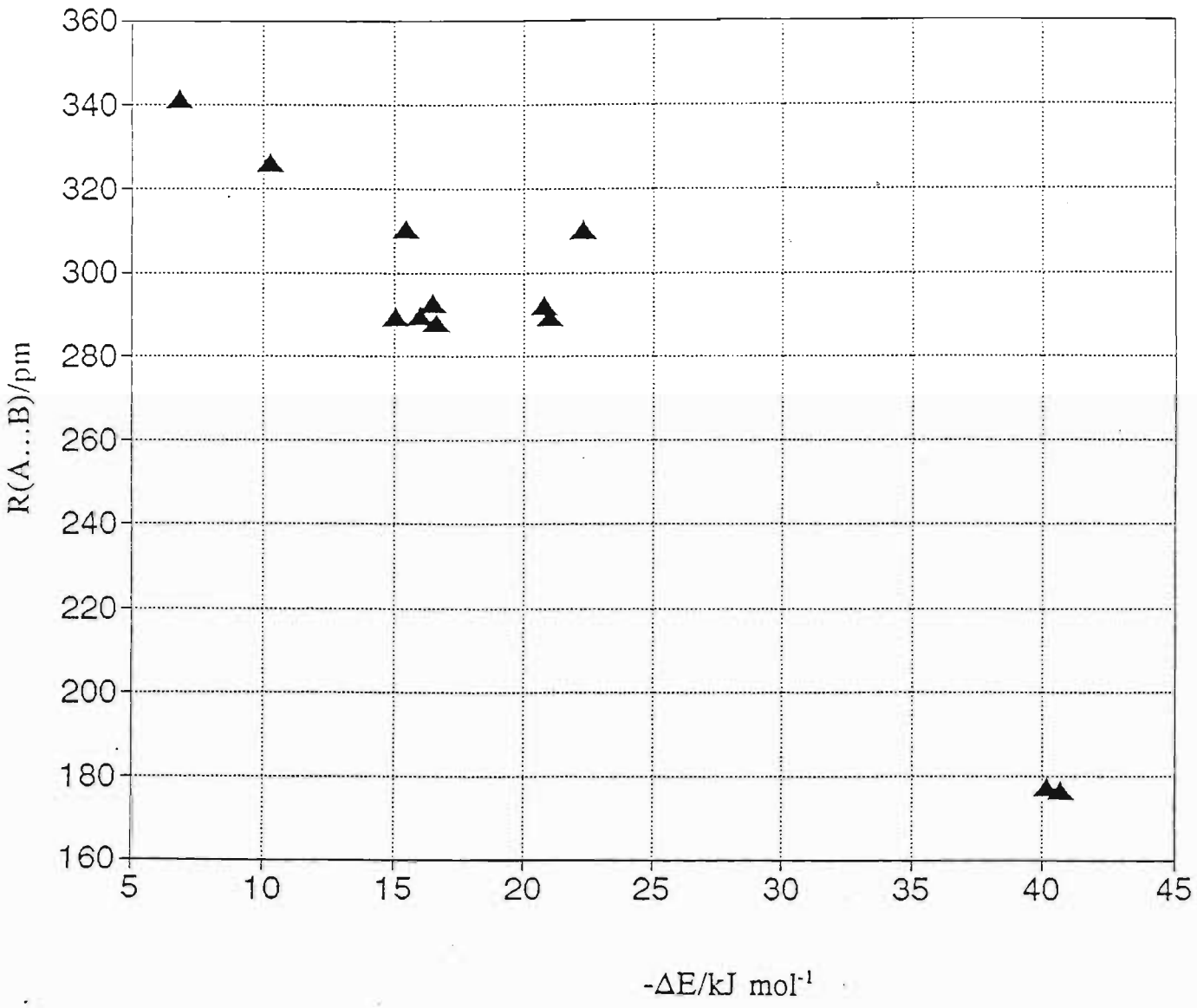

Figure 10.3. A plot of the A...B distance against the interaction energy.

where ΔE_e^0 is the difference in ground state electronic energies of reactants and products at 0 K, including electron correlation effects; $\Delta(\Delta E_e)_{298}$ is the change in electronic energy difference between 298 and 0 K (this term is negligible for reactions at 298 K, since reactants and products remain in their ground electronic states); ΔE_v^0 is the difference between the zero-point energies of reactants and products at 0 K; $\Delta(\Delta E_v)_{298}$ is the change in vibrational energy difference between reactants and products from 0 to 298 K; ΔE_r is the difference in rotational energies between reactants and products at 298 K; and ΔE_t is the difference in translational energies between reactants and products at 298 K.

The zero-point vibrational energy, E_v°, of any substance is given by: $E_v^0=(1/2)Nhc\Sigma\tilde{\nu}_i$, where N is Avogadro's constant, h is Planck's constant, c is the speed of light and $\tilde{\nu}_i$ are vibrational wavenumbers, the summation is taken over all 3n-6 (or 3n-5) normal modes of vibration. The FREQ option routinely calculates E_v^0 in Gaussian-92[63].

The contribution of thermally populated harmonic vibrational modes to internal energy at 298 K is given by[243] $\Delta E_{v,298}=298.R\Sigma(u_i/[\exp(u_i)-1])$ where R is the gas constant, and $u_i=4.826 \times 10^{-3}\tilde{\nu}_i$ with $\tilde{\nu}_i$ the wavenumber of the i^{th} normal mode and the summation is over all normal modes.

The rotational energy contribution to the internal energy is RT/2 for each degree of rotational freedom, by the classical approach, where T is the temperature. In the case of the complexation reactions considered here, there is a loss of three rotational degrees of freedom and the contribution to the internal energy change is -3.72 kJ mol^{-1} at 298 K. The translational energy change contribution is also -3.72 kJ mol^{-1}. Finally, ΔH_{298} differs from ΔE^{298} by the pV term. Assuming ideal

gas behaviour $\Delta(pV)=\Delta nRT$ where Δn is the change in the number of moles of gas and for these complexation reactions, ΔnRT=-2.48 kJ mol^{-1} at 298 K, since Δn=-1 in all cases.

A comparison of the order of stability of the thirteen complexes as determined by their respective ΔH values and that based on the BSSE-corrected electronic energies is given in Table 10.2. The order of the ΔH values follows that of the ΔE_e fairly well except for the C_2N_2-OH_2 and acid-water complexes. In the former case the enthalpy increases in conflict with the rest of the ΔH trend, while for the acid-water complexes, the stabilities are exchanged. These anomalies are subject for further investigation, but perhaps this, together with the large BSSE values, is indicative of a need to study the systems using larger basis sets,[64-69] perhaps including diffuse functions.

The extent to which the ΔE_v^0 and $\Delta(\Delta E_v)$ terms contribute to the ΔH values is apparently non-predictive. A similar pattern was observed in the studies by Del Bene[243] and by Yeo and Ford.[195] In the absence of experimental gas phase enthalpies, the computed ΔH values will be compared with the experimental ΔH values of the related systems. These experimental ΔH energies will thus be used as models for the computed ΔH values.

Mettee determined the enthalpy of the dimerisation of HCN by means of infrared spectroscopy,[244] and reported a value of -17.8 kJ mol^{-1}, while Wofford et al.[245] reported a value of -22.1 kJ mol^{-1} using high resolution FTIR spectroscopy for the HCN-HF complex. Adebayo et al.[246] measured a value of -20.8 kJ mol^{-1} for the HCN-HF complex. The computed NCH-OH_2 ΔH value, in Table 10.2, is fairly close to the reported range,[244-246] although HF is a stronger proton donor than HCN in the NCH-OH_2 complex.

Table 10.2. Components of the Calculated Gas Phase Enthalpies of Interaction, at 298K, of the Complexes of the Groups 1, 2, 3 and 4

	Energy Components/ kJ mol^{-1}						
Complex	ΔE_e	ΔE_v^0	$\Delta(\Delta E_v)$	$-\Delta E_r$	$-\Delta E_t$	$-\Delta(pV)$	$-\Delta H$
$NCH\text{-}OH_2$	-22.29	6.54	4.43	3.72	3.72	2.48	21.24
$HCCH\text{-}OH_2$	-10.26	5.88	5.32	3.72	3.72	2.48	8.98
$C_2N_2\text{-}OH_2$	-12.22	2.93	6.10	3.72	3.72	2.48	13.11
$CH_3CN\text{-}HOH$	-15.41	5.13	8.15	3.72	3.72	2.48	12.05
$H_2CO\text{-}HOH$	-15.04	10.00	4.21	3.72	3.72	2.48	10.75
$H_2CNH\text{-}HOH$	-21.00	10.04	4.33	3.72	3.72	2.48	16.55
$C_2H_4\text{-}HOH$	-6.88	4.87	6.46	3.72	3.72	2.48	5.47
$CH_3CHO\text{-}HOH$	-16.60	9.13	3.56	3.72	3.72	2.48	13.83
$(CH_3)_2CO\text{-}HOH$	-16.48	9.12	7.30	3.72	3.72	2.48	9.98
$HCOOH\text{-}HOH$	-40.67	13.16	3.12	3.72	3.72	2.48	34.31
$CH_3COOH\text{-}HOH$	-40.13	11.70	3.58	3.72	3.72	2.48	38.33
$HCOOCH_3\text{-}HOH$	-15.97	8.52	4.49	3.72	3.72	2.48	12.68
$CH_3COOCH_3\text{-}HOH$	-20.77	8.96	3.50	3.72	3.72	2.48	18.23

The enthalpy of formation of CH_3CN-HF has been reported[246] as -28.8 kJ mol^{-1}, this is twice as large as the computed ΔH value, as shown in Table 10.3, of CH_3CN-HOH. HF is a much better PD than H_2O; although the experimental and computed values, ΔH, of CH_3CN-HF and CH_3CN-HOH are different, the magnitudes of the ΔH values confirm the fact that HF forms a stronger complex with CH_3CN than H_2O justifying the comparisons. The experimental gas phase enthalpy of $(CH_3)_2CO$-I_2 was measured by IR spectroscopy[247,248] and a value of -15.5 kJ mol^{-1} was obtained, while a ΔH value of -22.6 kJ mol^{-1} for the $(CH_3)_2CO$-HCl complex has been reported by Mettee et al.[249] using the same method. The $(CH_3)_2CO$-HCl complex is stronger than the $(CH_3)_2CO$-I_2 adduct, according to these ΔH values. The computed enthalpy for the $(CH_3)_2CO$-HOH adduct is -10.0 kJ mol^{-1}, in accordance with the fact that water is a weaker PD compared with HCl; furthermore, water forms a weaker complex with acetone than the charge transfer complex formed between iodine and acetone.

The enthalpy of dimerisation of HCOOH has been determined by the Fourier transform infrared (FTIR) technique[250] and a value of -48.9 kJ mol^{-1} was reported, which compares very closely with -48.4 kJ mol^{-1} determined theoretically by Turi[251] at the MP2 level of theory using the 6-31G(d) basis set. By FTIR spectroscopy, Jaffe and Rose[252] determined the enthalpy of the CH_3COOH dimer, and reported a value of -60.3 kJ mol^{-1}. These data demonstrate that acetic acid dimer is stronger than formic acid dimer other factors being constant. The computed ΔH values confirm this pattern, again justifying the assumption that the computed ΔH values can be compared with those of related systems.

10.2 Correlation of the Geometrical and Vibrational Properties

Table 10.3 presents the A-H bond extensions, Δr(A-H), the intermolecular distances, R(A...B), the wavenumber shifts of the A-H stretching and A-H...B bending modes together with the complex/monomer intensity ratios of the A-H stretching mode for all the complexes. The wavenumber shift of the ν(A-H) mode is directly proportional to the extension of the A-H bond length, as depicted in Figure 10.4. Moreover, a plot of complex/monomer intensity ratio against r(A-H) shows an approximate proportionality relationship, as shown in Figure 10.5. The correlations are consistent with the observation that for the weak and normal hydrogen bonds the A-H stretching wavenumbers are red shifted by hydrogen bond formation and larger integrated infrared intensities of the corresponding absorption bands are found.[8b,9a,10b]

Table 10.4 shows the high level of consistency in the patterns of the energy components; for example, electrostatic interaction constitutes at least 40% of the total interaction energy for all the complexes, with the exception of the C_2H_4-H_2O (where the electrostatic component is about 36%).

The charge transfer component accounts for about 10% of the total stabilisation energy and hence plays a secondary role in stabilising these complexes. In all the complexes, the exchange and coupling terms are repulsive with the former exerting a stronger effect.

Table 10.3. The Bond Extensions, Δr(A-H), the Intermolecular Distances, R(A...B), and the A-H Bond Stretching and Angle Bending Wavenumber Shifts together with the Complex/Monomer Intensity Ratios of the A-H Bond

	Length/pm		Wavenumber shift/cm^{-1}		
Complex	Δr(A-H)	R(A...B)	A-H Stretch	A-H...B Bend	Intensity Ratio
$NCH-OH_2$	1.0	310.0	-143	147	5.56
$C_2H_2-OH_2$	0.6	326.2	-69	89	2.83
$C_2N_2-OH_2$	-	-	-	-	-
$CH_3CN-HOH$	0.4	310.2	-23	27	38.4
$H_2CO-HOH$	0.6	289.4	-61	21	23.3
$CH_2NH-HOH$	1.0	289.5	-122	22	51.1
C_2H_4-HOH	0.2	341.0	-12	11	15.5
$CH_3CHO-HOH$	0.7	288.1	-80	25	35.5
$(CH_3)_2CO-HOH$	0.8	292.7	-94	30	50.9
$HCOOH-HOH$	1.1	281.0	-124	8	39.2
$CH_3COOH-HOH$	1.3	278.4	-150	12	59.5
$HCOOCH_3-HOH$	0.6	289.7	-62	20	27.6
CH_3COOCH_3-HOH	0.8	292.1	-84	26	47.2

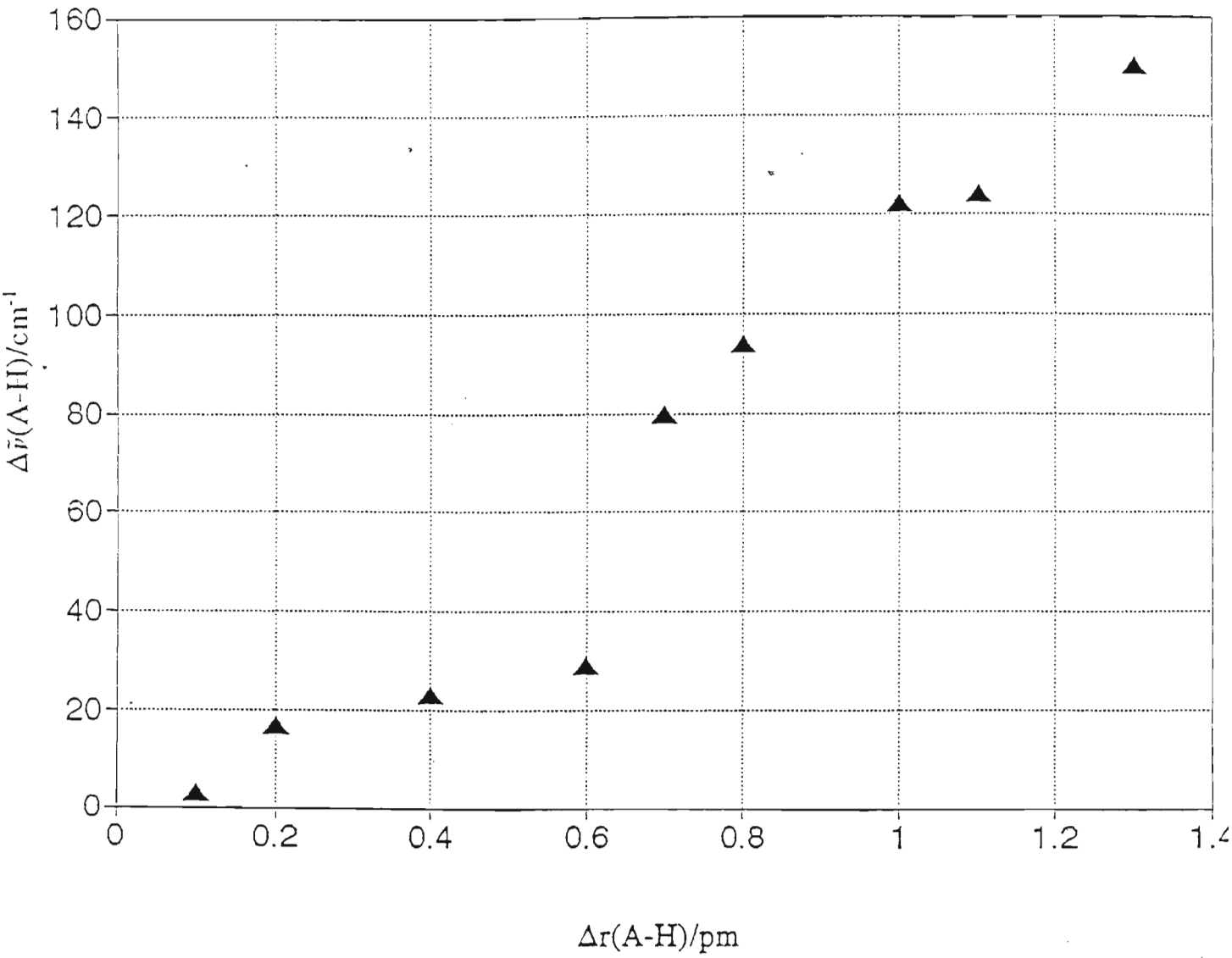

Figure 10.4. A plot of $\Delta\tilde{\nu}$(A-H) against Δr(A-H).

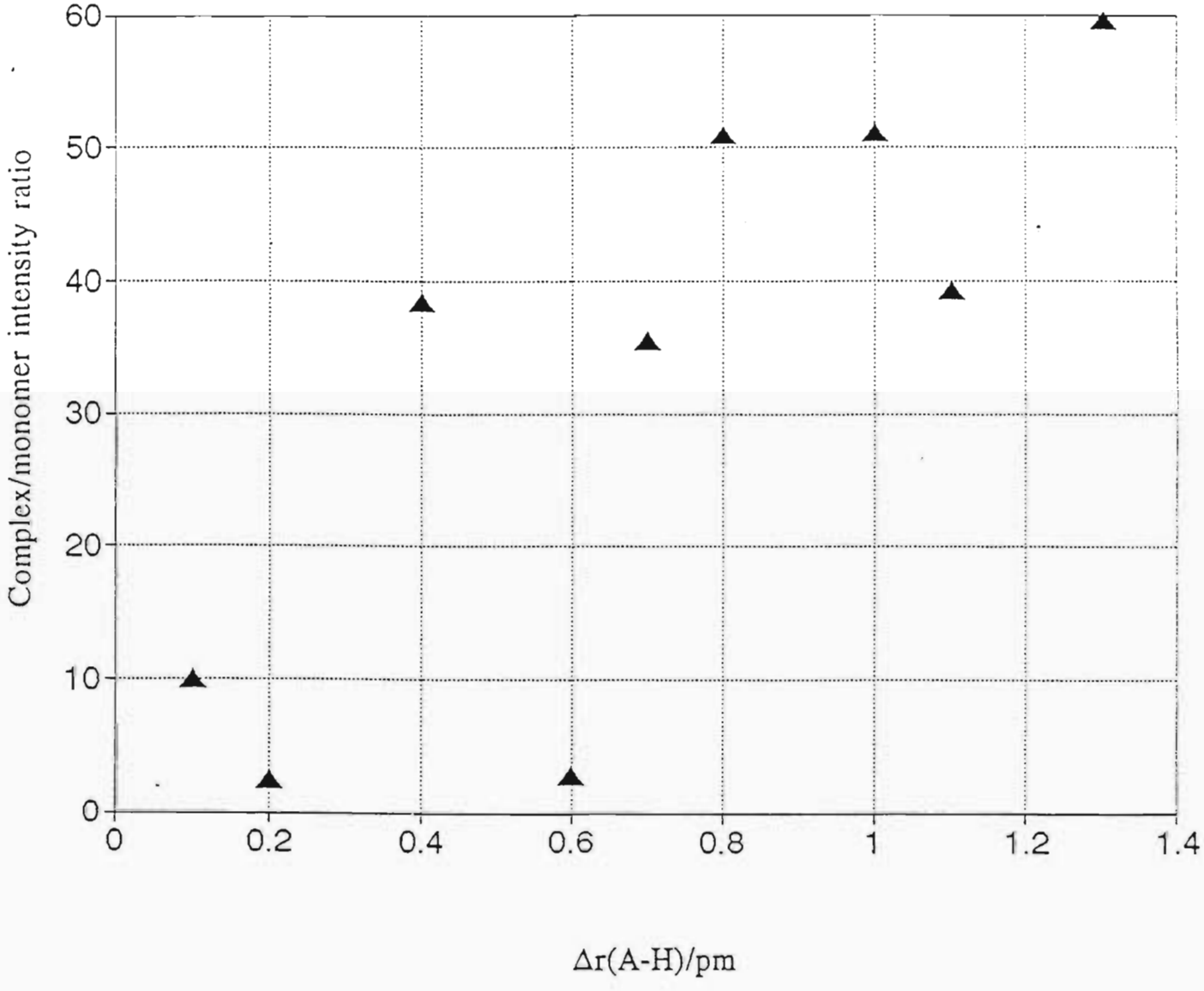

Figure 10.5. A plot of complex/monomer A-H stretching mode intensity ratio against Δr(A-H).

In Table 10.5 are collected the characteristic intermolecular vibrational properties, including the ν(H...B) and the δ(A-H...B) mode vibrational wavenumbers, their infrared intensities and the force constants. For all the complexes in which the A-H bond is the water O-H bond, the intermonomer stretching wavenumber, ν(H...B), is consistently lower than the intermonomer in-plane bending wavenumber, δ(A-H...B).

The intermolecular intensities show a similar pattern to the case of the vibrational wavenumbers discussed above, with the intensity of the hydrogen bond stretching mode being consistently lower than the intensity of the bending mode. The bending of the A-H...B angle results in a greater charge displacement and thus a corresponding marked increase in the intensity of this vibrational mode.

10.3 Correlation of the Atomic Charge of the Bridging Hydrogen and the Interaction Energy

Table 10.6 is a collection of the net atomic charges on the bridging hydrogen atoms for all the complexes investigated in this project along with the corresponding interaction energies at the MP2 level. The bridging hydrogen invariably loses charge on hydrogen bond formation, in the case of the medium to strongly hydrogen bonded complexes (those with interaction energies in the range -15.04 to -22.29 kJ mol^{-1}), losing on average 0.041 e. A notable observation on the net charge of the bridging hydrogen is that of the HCCH-OH_2 adduct, which is comparable with that of $(CH_3)_2CO$-HOH, but which has a remarkably lower interaction energy. Furthermore, the net charge on the bridging hydrogen atom of the C_2H_4-HOH complex is remarkably low in comparison with most of the complexes.

Table 10.4. The RHF Interaction Energies and the Morokuma Interaction Energy Components Corrected for BSSE

	Energy/kJ mol^{-1}					
Complex	ΔE_{CPC}	Es	Pl	Ex	Ct	Mix
$NCH\text{-}OH_2$	-22.82	-36.58	-3.08	22.01	-7.13	1.96
$C_2H_2\text{-}OH_2$	-9.35	-17.98	-1.24	12.11	-5.15	1.91
$C_2N_2\text{-}OH_2$	-7.62	-21.03	-2.05	17.02	-3.61	2.05
$CH_3CN\text{-}HOH$	-15.41	-26.12	-2.88	16.07	-3.83	1.36
$H_2CO\text{-}HOH$	-15.46	-31.93	-2.94	25.07	-8.90	3.24
$CH_2NH\text{-}HOH$	-18.52	-41.57	-4.83	33.86	-9.14	3.16
$C_2H_4\text{-}HOH$	-4.72	-12.82	-1.14	13.01	-5.87	2.10
$CH_3CHO\text{-}HOH$	-17.10	-39.27	-3.90	32.00	-10.45	2.69
$(CH_3)_2CO\text{-}HOH$	-18.93	-34.91	-3.33	27.43	-9.29	3.00
HCOOH-HOH	-38.01	-85.72	-10.72	76.94	-20.77	1.96
$CH_3COOH\text{-}HOH$	-37.20	-87.00	-10.39	79.74	-21.48	1.92
$HCOOCH_3\text{-}HOH$	-16.31	-33.84	-2.92	25.99	-8.41	2.87
$CH_3COOCH_3\text{-}HOH$	-18.24	-38.84	-3.77	31.42	-10.45	2.69

ΔE_{CPC}: Interaction energy from the Morokuma decomposition scheme corrected for BSSE.

Table 10.5. The Intermolecular Wavenumbers of the ν(H...B) and δ(A-H...B) modes, their Corresponding Intensities, A(H...B)and A(A-H...B), and the Force Constants, f(H...B) and f(A-H...B)

Complex	$\tilde{\nu}$/cm^{-1}		Intensity/km mol^{-1}		Force Constants	
	ν(H...B)	δ(A-H...B)	A(H...B)	A(A-H...B)	f(H...B) /N m^{-1}	f(A-H...B) /N m rad^{-2}
$CH\text{-}OH_2$	165	118	7.0	44.2	17.2	5.2
$C_2H_2\text{-}OH_2$	131	91	22.4	42.4	10.2	4.0
$C_2N_2\text{-}OH_2$	-117	-	0.0	-	6.6	
$CH_3CN\text{-}HOH$	131	254	2.3	89.7	12.2	3.2
$H_2CO\text{-}HOH$	195	592	50.0	224.4	20.6	10.6
$H_2NH\text{-}HOH$	206	680	21.8	204.1	22.7	11.1
$C_2H_4\text{-}HOH$	-					
$CH_3CHO\text{-}HOH$	183	629	49.2	236.7	22.2	10.9
$(CH_3)_2CO\text{-}HOH$	160	634	4.2	229.6	19.6	12.2
HCOOH-HOH	202	656	81.9	161.3	35.4	43.4
$CH_3COOH\text{-}HOH$	191	713	18.7	316.0	36.6	40.9
$HCOOCH_3\text{-}HOH$	159	598	2.1	305.8	21.5	11.6
$CH_3COOCH_3\text{-}HOH$	146	620	0.7	239.2	19.5	7.9

Table 10.6. The Net Atomic Charge on the Bridging Hydrogen Atom and the Interaction Energy at the MP2 Level Corrected for BSSE

Complex	Bridging Hydrogen Atomic Charge/e		MP2 Interaction Energy/kJ mol^{-1}
	Primary	Secondary	
$NCH-OH_2$	0.0423	-	-22.29
$HCCH-OH_2$	0.0419	-	-10.26
$NCCN-OH_2$	-	-	-12.22
$CH_3CN-HOH$	0.0422	-	-15.41
$H_2CO-HOH$	0.0326	0.0403	-15.04
$CH_2NH-HOH$	0.0472	0.0323	-21.00
C_2H_4-HOH	0.0053	-	-6.88
$CH_3CHO-HOH$	0.0364	0.0414	-16.60
$(CH_3)_2CO-HOH$	0.0413	0.0329	-16.48
$HCOOH-HOH$	0.0512	0.0603	-40.67
$CH_3COOH-HOH$	0.0540	0.0499	-40.13
$HCOOCH_3-HOH$	0.0350	0.0331	-15.97
CH_3COOCH_3-HOH	0.0430	0.0347	-20.77

The formaldehyde- and acetaldehyde-water complexes have significant net charges on the secondary bridging hydrogens, but their interaction energies are still in the medium range. The acid-water complexes, however, show distinctly larger net charges on the bridging hydrogens and are indeed the most stable complexes encountered in this study. Thus the Mulliken atomic charge analysis does indicate the degree of interaction to a certain extent.

The structures, interaction energies, atomic charge distributions and vibrational properties of the complexes of water with thirteen small molecules were investigated and characterised by ab initio molecular orbital theory. Four types

of hydrogen bonds were identified, namely, C-H...O, O-H...O, O-H...N and O-H...π. Overall, both the geometrical and vibrational properties established from this study are consistent with the corresponding experimentally determined properties.

References

1. M.D. Newton, Chem. Rev., **91**, 767 (1991).
2. J.M. Hutson, Ann. Rev. Phys. Chem., **41**, 123 (1990).
3. A.E. Reed, L.A. Curtiss and F. Weinhold, Chem. Rev., **88**, 899 (1988).
4. G. Nàray-Szabò and G.G. Ferenczy, Chem. Rev., **95**, 829 (1995).
5. B. Friedrich, Intern. Rev. Phys. Chem., **14,** 113 (1995).
6. M.J. Ondrechen, Intern. Rev. Phys. Chem., **14**, 1 (1995).
7. G. Chalasinski and M.M. Szczęśniak, Chem. Rev., **94**, 1723 (1994).
8. G.C. Pimentel and A.L. McClellan, "The Hydrogen Bond", W.H. Freeman and Company, San Francisco, 1960, (a) p. 9, (b) pp. 68-71.
9. P. Schuster, G. Zundel, and C. Sandorfy, "The Hydrogen Bond." Vol. I, North-Holland, Amsterdam, 1976, (a) pp. 1-5, (b) p. 28.
10. M.D. Joesten and L.J. Schaad, "Hydrogen Bonding", Marcel Dekker, Inc., New York, 1974, (a) p. 28, (b) p. 42, (c) pp. 1-3, (d) pp. 195-234.
11. J.B. Foresman and A. Frisch, "Exploring Chemistry with Electronic Structure Methods: A Guide to Using Gaussian", Gaussian Inc., Pittsburgh, 1992, (a) p. 4, (b) pp. 215-216, (c) p. 11.
12. K. Morokuma, Acc. Chem. Res., **10**, 294 (1977).
13. M. Born and J.R. Oppenheimer, Ann. Physik, **84**, 457 (1927).
14. D.M Hirst, "A Computational Approach to Chemistry", Blackwell Scientific Publications, London, 1990, (a) pp. 15-22, (b) pp. 39-62.
15. N.C. Handy, in "Physical Chemistry Series Two, Vol. 1, Theoretical Chemistry" (editors A.D. Buckingham and C.A. Coulson), Butterworths, London, 1975, pp. 79-106.

16. W.J. Hehre, L. Radom, P. von R. Schleyer and J.A. Pople, "*Ab initio* Molecular Orbital Theory", John Wiley & Sons, New York, 1985, pp. 10-41.

17. P.S.C. Matthews, "Quantum Chemistry of Atoms and Molecules", Cambridge University Press, Cambridge, 1986, p. 46.

18. G.G. Hall, Proc. Roy. Soc. (London), **A205**, 541 (1951).

19. C.C.J. Roothaan, Rev. Mod. Phys., **23**, 69 (1951).

20. E.B. Wilson, J.C. Decius and P.C. Cross, "Molecular Vibrations. The Theory of Infrared and Raman Vibrational Spectra", McGraw-Hill Book Company, Inc., New York, 1955, pp. 11-74.

21. E. Knözinger and O. Schrems, in " Vibrational Spectra and Structure, A Series of Advances", Vol. 16 (editor J.R. Durig), Elsevier Scientific Publishing Company, New York, 1987, pp. 141-225.

22. M. Spoliti, L. Bencivenni and F. Ramondo, J. Mol. Structure (Theochem), **303**, 185 (1994).

23. S. Scheiner, Ann. Rev. Phys. Chem., **45**, 23 (1994).

24. S. Dapprich and G. Frenking, J. Phys. Chem., **99**, 9352 (1995).

25. A.E. Reed, L.A. Curtiss and F. Weinhold, Chem. Rev., **88**, 899 (1988).

26. J.N. Murrell, S.F.A. Kettle and J.M. Tedder, "The Chemical Bond", John Wiley & Sons, London, 1978, p. 286.

27. D. Feller and E.R. Davidson, in "Reviews in Computational Chemistry" (editors K. B. Lipkowitz and D. Boyd), VCH Publishers, New York, 1990, pp. 1-43.

28. A.C. Legon and D.J. Millen, Faraday Discuss. Chem. Soc., no. 73, 71 (1982).

29. J.K. Burdett, J. Chem. Phys., **73**, 2825 (1980).

30. J.T. Brobjer and J.N. Murrell, J. Chem. Soc., Faraday Trans. II, **79**, 1455 (1983).
31. A.C. Legon and D.J. Millen, Acc. Chem. Res., **20**, 39 (1987).
32. J.B.O. Mitchell and S.L. Price, Chem. Phys. Lett., **154**, 267 (1989).
33. A.D. Buckingham and P.W. Fowler, Can. J. Chem., **63**, 2018 (1984).
34. D.J. Millen, Intern. J. Quantum Chem., **29**, 191 (1986).
35. J.E. Del Bene, J. Chem. Phys., **58**, 3139 (1973).
36. M. Hargittai and I. Hargittai, Intern. J. Quantum Chem., **44**, 1057 (1992).
37. B. Liu and A.D. McLean, J. Chem. Phys., **59**, 4557 (1973).
38. S.F. Boys and F. Bernardi, Mol. Phys., **19**, 553 (1970).
39. G.A. Yeo, Ph D Thesis, University of the Witwatersrand, Johannesburg, 1991, p. 40.
40. M.J. Frisch, J.E. Del Bene, J.S. Binkley and H.F. Schaefer III, J. Chem. Phys., **84**, 2279 (1986).
41. M.M. Szczęśniak, Z. Latajka and S. Scheiner, J. Chem. Phys., **84**, 6328 (1986).
42. A. Johansson, Theoret. Chim. Acta, **29**, 167 (1973).
43. J.P. Daudey, J.P. Malrieu and O. Rojas, Intern. J. Quantum Chem., **8**, 17 (1974).
44. D.W. Schwenke and D.G. Truhlar, J. Chem. Phys., **82**, 2418 (1985).
45. J.R. Collins and G.A. Gallup, Chem. Phys. Lett., **123**, 56 (1986).
46. A. Alagona, C. Ghio, R. Cammi and J. Tomasi, Intern. J. Quantum Chem., **32**, 227 (1987).
47. M. Gutowski, F.B. van Duijneveldt, G. Chalasinski and L. Piela, Mol. Phys., **61**, 233 (1987).
48. C.E. Dykstra, Acc. Chem. Res., **10**, 355 (1988).

49. I.G. Kaplan, "Theory of Molecular Interactions", Elsevier Scientific Publishing Company, Amsterdam, 1986, pp. 22-23.

50. A.D. Buckingham, Adv. Chem. Phys., **12**, 107 (1967).

51. I.N. Levine, "Quantum Chemistry, Vol. I: Quantum Mechanics and Molecular Electronic Structure" Allyn and Bacon, Boston, 1970, pp. 209-234.

52. H. Umeyama and K. Morokuma, J. Am. Chem. Soc., **99**, 1316 (1977).

53. P. Hobza and R. Zahradnik, Chem. Rev., **88**, 871 (1988).

54. G. Chalasinski and M. Gutowski, Chem. Rev., **88**, 943 (1988).

55. R.S. Mulliken, J. Chem. Phys., **23**, 2343 (1955).

56. Gaussian-70, W.J. Hehre, W.A. Lathan, R. Ditchfield, M.D. Newton and J.A. Pople, QCPE 237, Quantum Chemistry Program Exchange, Indiana University, Bloomington, 1970.

57. Gaussian-76, J.S. Binkley, R.A. Whiteside, P.C. Hariharan, R. Seeger, J.A. Pople, W.J. Hehre and M.D. Newton, Carnegie-Mellon University, Pittsburgh, 1976.

58. Gaussian-80, J.S. Binkley, R.A. Whiteside, R. Krishnan, R.Seeger, D.J. DeFrees, H.B. Schegel, S. Topiol, L.R. Kahn and J.A. Pople, Carnegie-Mellon Quantum Chemistry Publishing Unit, Pittsburgh, 1980.

59. Gaussian-82, J.S. Binkley, M.J. Frisch, D.J. DeFrees, R. Krishnan, R.A. Whiteside, H.B. Schegel, E.M. Fluder and J.A. Pople, Carnegie-Mellon Quantum Chemistry Publishing Unit, Pittsburgh, 1982.

60. Gaussian-86, M.J. Frisch, J.S. Binkley, H.B. Schegel, K. Raghavachari, C.F. Melius, R.L. Martin, J.J.P. Stewart, F.W. Bobrowicz, C.M. Rohlfing, L.R. Kahn, D.J. DeFrees, R. Seeger, R.A. Whiteside, D.J. Fox, E.M. Fluder and J.A. Pople, Carnegie-Mellon Quantum Chemistry Publishing Unit, Pittsburgh, 1984.

61. Gaussian-88, M.J. Frisch, M. Head-Gordon, H.B. Schlegel, K. Raghavachari, J.S. Binkley, C. Gonzalez, D.J. DeFrees, D.J. Fox, R.A. Whiteside, R. Seeger, C.F. Melius, J. Baker, L.R. Kahn, J.J.P. Stewart, E.M. Fluder, S. Topiol and J.A. Pople, Gaussian, Inc., Pittsburgh, 1988.

62. Gaussian-90, M.J. Frisch, M. Head-Gordon, J.B. Foresman, G.W. Trucks, K. Raghavachari, H.B. Schlegel, M. Robb, J.S. Binkley, C. Gonzalez, D.J. DeFrees, D.J. Fox, R.A. Whiteside, R. Seeger, C.F. Melius, J.Baker, L.R. Kahn, J.J.P. Stewart, E.M. Fluder, S. Topiol and J.A. Pople, Gaussian, Inc., Pittsburgh, 1990.

63. Gaussian-92, M.J. Frisch, G.W. Trucks, M. Head-Gordon, P.M.W. Gill, M.W. Wong, J.B. Foresman, B.G. Johnson, H.B.Schegel, M.A.Robb, E.S. Replogle, R. Gomperts, J.L. Andres, K. Raghavachari, J.S. Binkley, C. Gonzalez, R.L. Martin, D.J. Fox, D.J. DeFrees, J. Baker, J.J.P. Stewart and J.A. Pople, Gaussian, Inc. Pittsburgh, 1992.

64. D.J. Swanton, G.B. Bacskay and N.S. Hush, Chem. Phys., **83**, 69 (1984).

65. C. Sosa and B.Schlegel, J. Chem. Phys., **86**, 6937 (1987).

66. Y. Yamaguchi, M. Frisch, J. Gaw, H. Schaefer III and J.S. Binkley, J. Chem. Phys., **84**, 2262 (1986).

67. M.D. Miller, F. Jensen, O.L. Chapman and K. N. Houk, J. Phys. Chem., **93**, 4495 (1989).

68. H.L. Williams, E.M. Mas, K. Szalewicz and B. Jeziorski, J. Chem. Phys., **103**, 7374 (1995).

69. B. Jeziorski, R. Moszynski and K. Szalewicz, Chem. Rev., **94**, 1887 (1994).

70. J.E. Del Bene, J. Phys. Chem., **86**, 2110 (1987).

71. J. Langlet, J. Caillet and M. Caffarel, J. Chem. Phys., **103**, 8083 (1995).

72. K.S. Kim, B.J. Mhin, U-S. Choi and K. Lee, J. Chem. Phys., **97**, 6649 (1992).

73. R.A. Kumpf and J.R. Damewood, Jr, J. Phys. Chem., **93**, 4478 (1989).

74. L.A. Curtiss and D.J. Blander, J. Chem. Phys., **71**, 2703 (1979).

75. J. Reimer, R. Watts and M. Klein, Chem. Phys., **64**, 95 (1982).

76. L.A. Curtiss and M. Blander, Chem. rev., **88**, 827 (1988).

77. M.R. Peterson and R.A. Poirier, Monstergauss, University of Toronto, 1991.

78. J.A. Ellwood, D. Steele and D. Gerrard, Spectrochim. Acta, **50A**, 913 (1994).

79. L.H. Jones, "Inorganic Vibrational Spectroscopy", Vol. 1, Marcel Dekker, Inc., New York, 1971, pp. 25-45.

80. S.J. Cyvin, "Molecular Vibrations and Mean Square Amplitudes", Elsevier Publishing Company, Inc., Amsterdam, 1968, pp. 54-66.

81. F.A. Cotton, "Chemical Applications of Group Theory", John Wiley & Sons, New York, 1990, pp. 317-322.

82. E. Keller, Schakal-92, Kristallographisches Institut der Universität, Freiburg, 1992.

83. S.B.H. Bach and B.S. Ault, J. Phys. Chem., **88**, 3600 (1984).

84. G.A. Yeo and T.A. Ford, Struct. Chem., **3**, 75 (1992).

85. M.J. Bräsler, V.C.E. Carr, M.G. Gerazounis, N.R. Jugga, G.A. Yeo and T. A. Ford, J. Mol. Structure (Theochem), **180**, 241 (1988).

86. S. Chin and T.A. Ford, J. Mol. Structure (Theochem), **133**, 193 (1985).

87. S. Chin and T. A. Ford, J. Mol. Structure (Theochem), **152**, 363 (1987).

88. T.D. Mokomela, I.Rencken, G.A. Yeo and T.A. Ford, J. Mol. Structure, **275**, 33 (1992).

89. G.A. Yeo and T.A. Ford, Can. J. Chem., **69**, 632 (1991).

90. S. Iwata and K. Morokuma, J. Am. Chem. Soc., **95**, 7563 (1973).

91. T.A. Ramelot, C. Hu, J.E. Fowler, B.J. Deleeuw and H.F. Schaefer III, J. Chem. Phys., **100**, 4347 (1994).

92. T.K. Ha, J. Makarewicz and A. Bauder, J. Phys. Chem., **97**, 11415 (1993).

93. B. Nelander, J. Chem. Phys., **72**, 77 (1980).

94. Y. Dimitrova and S.D. Peyerimhoff, J. Phys. Chem., **97**, 12731 (1993).

95. H. Fukunaga and K. Morokuma, J. Chem. Phys., **97**, 59 (1993).

96. O.N. Ventura, E.L. Coitino, K. Irving and A. Iglesias, J. Mol. Structure (Theochem), **210**, 427 (1990).

97. X.Q. Lewell, I.H. Hillier, M.J. Field, J.J. Morris and R.J. Taylor, J. Chem. Soc., Faraday Trans. II, **84**, 893 (1988).

98. D.G. Evans, G.A. Yeo and T.A. Ford, Faraday Disc. Chem. Soc., no. 86, 55 (1988).

99. A.J. Cox, T.A. Ford and L. Glasser, in "Structures and Conformations of Non-Rigid Molecules" (editors J. Laane, M. Dakkouri, B. van der Veken and H. Oberhammer), Kluwer Academic Publishers, Dordrecht, 1993, pp. 391-408.

100. A.J. Cox, T.A. Ford and L. Glasser, J. Mol. Structure (Theochem), **312**, 101 (1994).

101. S. Lee, I.I. Suni and W. Klemperer, J. Chem. Phys., **96**, 5577 (1992).

102. A.J. Gordon and R.A. Ford, "The Chemist's Companion", John Wiley & Sons, New York, 1972, pp. 58-62.

103. A.J. Fillery-Travis, A.C. Legon and L.C. Willoughby, Proc. Roy. Soc. (London), Ser. A, **396**, 405 (1984).

104. H.S. Gutowsky, T.C. Germann, J.D. Augspurger and C.E. Dykstra, J. Chem. Phys., **96**, 5808 (1992).

105. S. Vishveshwara, Chem. Phys. Lett., **59**, 26 (1978).

106. A. Hinchliffe, J. Mol. Structure (Theochem), **136**, 193 (1986).

107. L. Turi and J. J. Dannenberg, J. Phys. Chem., **97**, 7899 (1993).

108. K.I. Peterson and W. Klemperer, J. Chem. Phys., **81**, 3842 (1984).

109. P.A. Block, M.D. Marshall, L.G. Pedersen and R.E. Miller, J. Chem. Phys., **96**, 7321 (1992).

110. A. Engdahl and B. Nelander, Chem. Phys. Lett., **100**, 129 (1983).

111. M.J. Frisch, J.A. Pople and J.E. Del Bene, J. Chem. Phys., **78**, 4063 (1983).

112. E. Knözinger and R. Wittenbeck, J. Chem. Phys., **80**, 5979 (1984).

113. J.W. Bevan, A.C. Legon, D.J. Millen and S.C. Rogers, J. Chem. Soc., Chem. Commun., 130 (1975).

114. A.C. Legon, D.J. Millen and S.C. Rogers, J. Mol. Structure, **67**,35 (1980).

115. N.W. Howard and A.C. Legon, J. Chem. Soc., Faraday Trans. II, **83**, 991 (1987).

116. A.F. Jayaraj and S. Singh, J. Mol. Structure, **327**, 108 (1994).

117. K. Morokuma and L. Pedersen, J. Chem. Phys., **48**, 3275 (1968).

118. P.A. Kollman and L.C. Allen, J. Chem. Phys., **51**, 3286 (1969).

119. K. Morokuma and J.R. Winick, J. Chem. Phys., **52**, 1301 (1970).

120. J.E. Del Bene and J.A. Pople, J. Chem. Phys., **52**, 4858 (1970).

121. J.E. Del Bene, J. Chem. Phys., **62**, 1314 (1975).

122. O.N. Ventura, E.L. Coitino, A. Lledos and J. Bertran, J. Comput. Chem., **13**, 1037 (1992).

123. T.A. Blake and S.E. Novick, J. Mol. Spectrosc., **154,** 72 (1992).

124. F.A. Baiocchi and W. Klemperer, J. Chem. Phys., **78**, 3509 (1982).

125. F.J. Lovas, R.D. Suenram, S. Ross and M. Klobukowski, J. Mol. Spectrosc., **123**, 167 (1987).

126. G.T. Fraser, C.W. Gillies, J. Zozom and F.J. Lovas, J. Mol. Spectrosc., **123**, 200 (1987).

127. R. Honig, Ann. Rev. Phys. Chem., **29**, 31 (1978).

128. R.R. Birge, Ann. Rev. Biophys. Bioeng., **10**, 315 (1981).

129. R. Uhl and E.W. Abrahamson, Chem. Rev., **81**, 291 (1981).

130. W. Stoeckenius and R. Bogomolni, Ann. Rev. Biochem., **51**, 587 (1982).

131. P. Migchels, T. Zeegers-Huyskens and D. Peeters, J. Phys. Chem., **95**, 7599 (1991).

132. N. Sreenama and S. Vishveshwara, J. Mol. Structure, **212**, 53 (1989).

133. J.W. Lewis and C. Sandorfy, Can. J. Chem., **60**, 1727 (1982).

134. K.I. Peterson and W. Klemperer, J. Chem. Phys., **85**, 725 (1986).

135. R.D. Suenram, G.T. Fraser, F.J. Lovas and Y. Kawashima, J. Chem. Phys., **101**, 7230 (1994).

136. J.E. Del Bene, Chem. Phys. Lett., **24**, 203 (1974).

137. A. Engdahl and B. Nelander, J. Chem. Phys., **90**, 4982 (1986).

138. A.M. Andrews and R.L. Kuczkowski, J. Chem. Phys., **98**, 791 (1993).

139. P.D. Aldrich, A.C. Legon and W.H. Flygare, J. Chem. Phys., **75**, 2126 (1981).

140. J.A. Shea and W.H. Flygare, J. Chem. Phys., **76**, 4857 (1982).

141. A.J. Barnes, H.E. Hallam and G.F. Scrimshaw, Trans. Faraday Soc., **65**, 3172 (1969).

142. A.J. Barnes, J. Mol. Structure, **100**, 259 (1983).

143. A.J. Barnes, J.B. Davies, H.E. Hallam and J.D.R. Howells, J. Chem. Soc., Faraday Trans. II, **69**, 246 (1973).

144. A.J. Barnes, J. Mol. Structure, **60**, 343 (1980).

145. R.M. Bentwood, A.J. Barnes and W.J. Orville-Thomas, J. Mol. Spectrosc., **84**, 391 (1980).

146. A.J. Barnes, R.M. Bentwood and M.P. Wright, J. Mol. Structure, **118**, 97 (1984).

147. A.J. Barnes, T.M. Beech and Z. Mielke, J. Chem. Soc., Faraday Trans. II, **80**, 455 (1984).

148. P. Hobza and R. Zahradnik, Intern. J. Quantum. Chem., **42**, 581 (1992).

149. H. Hollenstein and H. Günthard, Spectrochim. Acta, **27A**, 2027 (1971).

150. H. Hollenstein and F. Winter, J. Mol. Spectrosc., **71**, 118 (1978).

151. L. Andrews and G.L. Johnson, J. Phys. Chem., **88**, 5887 (1984).

152. J.G. Baker and G.C. Petty, J. Mol. Structure, **189**, 227 (1988).

153. L. Schriver, J. Chem. Soc., Faraday Trans. II, **85**, 607 (1989).

154. I. Kleiner, J.T. Hougen, R.D. Suenram and F.J. Lovas, J. Mol. Spectrosc., **148**, 38 (1991).

155. A. Engdahl, Chem. Phys., **178**, 305 (1993).

156. X.K. Zhang, E.G. Lewar, R.E. March and J.M. Parnis, J. Phys. Chem., **97**, 4320 (1993).

157. K.B. Wiberg, V. Walters and S.D. Colson, J. Phys. Chem., **88**, 4723 (1984).

158. E.P.F. Lee and J.M. Dyke, J. Chem. Soc., Faraday Trans. II, **88**, 2111 (1992).

159. V. Aviyente and T.Vernali, J. Mol. Structure (Theochem), **277**, 285 (1992).

160. O. Setokuchi and Y. Shimizu, J. Mol. Structure (Theochem), **281**, 67 (1993).

161. S. Scheiner, J. Mol. Structure, **177**, 79 (1988).

162. R.T. Morrison and R.N. Boyd, "Organic Chemistry", Allyn and Bacon, Inc., Boston, 1977, p. 600.

163. C.A. Coulson, Research (London), **10**, 149 (1957).

164. S. Hayashi, J. Umemura, S. Kato and K. Morokuma, J. Phys. Chem., **88**, 1330 (1988).

165. F. Graf, R. Meyer, T.K. Ha and R.R. Ernst, J. Chem. Phys., **75**, 2914 (1981).

166. T. Solmajer, M. Hodoscek and D. Hadzi, Intern. J. Quantum Chem., **23**, 945 (1983).

167. J. Keller, M. Hodoscek and D. Hadzi, J. Mol. Structure (Theochem), **106**, 301 (1984).

168. S. Scheiner and T. Das, Intern. J. Quantum Chem., Quantum Biol. Symp., **45**, 137 (1988).

169. R.W. Williams and A.H. Lowrey, J. Comput. Chem., **12**, 761 (1992).

170. C.H. Reynolds, J. Am. Chem. Soc., **112**, 7903 (1990).

171. L. Pauling and L.O. Brockway, Proc. Nat. Acad. Sci. U.S.A., **20**, 336 (1934).

172. J. Karle and L.O. Brockway, J. Am. Chem. Soc., **66**, 574 (1944).

173. A. Almenningen, O. Bastiansen and T. Motzfelt, Acta Chem. Scand., **23**, 2848 (1969).

174. T. Wachs, D. Borchadt and S.H. Bauer, Spectrochim. Acta, **43A**, 965 (1987).

175. T. Miyazawa and K.S. Pitzer, J. Chem. Phys., **30**, 1076 (1959).

176. Y. Chang, Y. Yamaguchi, W.H. Miller and H.F. Schaefer III, J. Am. Chem. Soc., **109**, 7245 (1987).

177. D. Berkmans, H. Figeys, Y. Marechal and P. Geerlings, J. Phys. Chem., **92**, 66 (1988).

178. J. Lundell, M. Räsänen and Z. Latajka, J. Phys. Chem., **97**, 1152 (1993).

179. D. Peeters, J. Mol. Structure, **332,** 9 (1994).

180. K.B. Borisenko, C.W. Bock and I. Hargittai, J. Mol. Structure (Theochem), **332**, 161 (1995).

181. L. Turi and J.J. Dannenberg, J. Phys. Chem., **97**, 12197 (1993).

182. G.I.L. Jones and N.L. Owen, J. Mol. Structure, **18**, 1 (1973).

183. W.C. Harris, D.A. Coe and W.O. George, Spectrochim. Acta, **32A**, 1 (1976).

184. R.F. Curl, Jr., J. Chem. Phys., **30**, 1529 (1959).

185. H. Wennerström, S. Forsen and B. Roos, J. Phys. Chem., **76**, 2430 (1972).

186. B.J. van der Veken, S. Truyen, W.A. Herrebout and G. Watkins, J. Mol. Structure, **293**, 55 (1993).

187. M.P. Muller, H. Hollenstein and J.R. Huber, J. Mol. Spectrosc., **100**, 95 (1983).

188. L. Vanderheyden, G. Maes and T. Zeegers-Huyskens, J. Mol. Structure, **114**, 145 (1984).

189. G. Maes and T. Zeegers-Huyskens, J. Mol. Structure, **100**, 305 (1983).

190. M.D. Harmony, V.W. Laurie, R.L. Kuczkowski, R.H. Schwendeman, D.A. Ramsay, F.J. Lovas, W.J. Lafferty and A. G. Maki, J. Phys. Chem. Ref. Data, **8**, 619 (1979).

191. K. Morokuma, J. Chem. Phys., **55**, 1236 (1971).

192. K. Kitaura and K. Morokuma, Intern. J. Quantum Chem., **10**, 325 (1976).

193. T. Shimanouchi, "Tables of Molecular Vibrational Frequencies", Consolidated Volume 2, NSRDS-NBS-39, Washington, 1972.

194. T. Shimanouchi, J. Phys. Chem. Ref. Data, **1**, 189 (1972).

195. G.A. Yeo and T.A. Ford, J. Chem. Soc., Faraday Trans. II, **86**, 3067 (1990).

196. G.A. Yeo and T.A. Ford, Chem. Phys. Lett., **178**, 266 (1991).

197. L.M. Nxumalo and T.A. Ford, J. Mol. Structure (Theochem), **236**, 135 (1991).

198. G.A. Yeo and T.A. Ford, Theoret. Chim. Acta, **81**, 255 (1992).

199. G.A. Yeo and T.A. Ford, J. Mol. Structure, **266**, 183 (1992).

200. T.A. Ford, S.F. Agnew and B.I. Swanson, J. Mol. Structure, **297**, 255 (1993).

201. T.A. Ford, S.F. Agnew and B.I. Swanson J. Mol. Structure, **297**, 265 (1993).

202. L.M. Nxumalo and T.A. Ford, J. Mol. Structure, **300**, 325 (1993).

203. L.M. Nxumalo, A.J. Cox and T.A. Ford, J. Mol. Structure (Theochem), **307**, 153 (1994).

204. J. Dillen, Vibram 1.5, Department of Chemistry, University of Pretoria, SA, 1984.

205. G.A. Yeo and T. A. Ford, Spectrochim. Acta, **50A**, 5 (1994).

206. S.A. Clough, Y. Beers, G.P. Klein and L.S. Rothman, J. Chem. Phys., **59**, 2554 (1973).

207. I.W.M. Smith, J. Chem. Soc., Faraday Trans. II, **77**, 2337 (1981).

208. K. Kim and K.T. Kim, J. Chem. Phys., **71**, 1967 (1979).

209. C.P. Rinsland, A. Baldacci and K.N. Rao, Astrophys. J. Suppl. Ser., **49**, 487 (1982).

210. K. Kim and W.T. Kim, J. Mol. Structure, **57**, 201 (1979).

211. K. Kim and W.T. Kim, J. Chem. Phys., **80**, 974 (1984).

212. Y. Koga, S. Kondo, S. Saëki and W.B. Person, J. Phys. Chem., **88**, 3152 (1984).

213. W.B. Person and J.D. Rogers, Analytiktreffen 1980, Schwingungsspektroskopie, Theorie und Anwendungen, Karl Marx Universität, Leipzig, 1980, pp. 262-300.

214. B. Crawford, Jr., in "Vibrational Intensities in Infrared and Raman Spectroscopy" (editors W. B. Person and G. Zerbi), Elsevier Scientific Publishing Company, Amsterdam, 1982, pp. 3-13.

215. P. Pulay, G. Fogarasi, G. Pongor, J.E. Boggs and A.V. Vargha, J. Am. Chem. Soc., **105**, 7037 (1983).

216. G. Herzberg, "Molecular Spectra and Molecular Structure. II. Infrared and Raman Spectra of Polyatomic Molecules", Van Nostrand, New York, 1945, (a) p. 180, (b) p. 174.

217. T.J. Lee, C.E. Daeto, B. Gazdy and J.M. Bowman, J. Phys. Chem., **97**, 8937 (1993).

218. W.B. De Almeida and A. Hinchliffe, J. Mol. Structure (Theochem), **206**, 77 (1990).

219. I.J. Kurnig, M.M. Szczęśniak and S. Scheiner, J. Chem. Phys., **87**, 2214 (1987).

220. A. Fillery-Travis, J. Chem. Phys., **85**, 3180 (1986).

221. A.C. Legon and D.J. Millen, Chem. Rev., **86**, 635 (1986).

222. R.J. Bemish, P.A. Block, L.G. Pedersen and R.E. Miller, J. Chem. Phys., **103**, 7788 (1995).

223. M.E. Jacox and D.E. Milligan, J. Mol. Spectrosc., **56**, 333 (1975).

224. L. Halonen and G. Duxbury, J. Chem. Phys., **83**, 2091 (1985).

225. G. Duxbury, H. Kato and M.L. Le Lerre, Faraday Disc. Chem. Soc., no. 71, 97 (1980).

226. G. Duxbury and M.L. Le Lerre, J. Mol. Spectrosc., **92**, 326 (1982).

227. L. Halonen and G. Duxbury, J. Chem. Phys., **83**, 2078 (1985).

228. J. Kwiatkowski and J. Leszczynski, J. Mol. Spectrosc., **157**, 540 (1993).

229. J. Nakanaga, S. Kondo and S. Saëki, J. Chem. Phys., **76**, 3860 (1982).

230. A. Komornicki and J. W. McIver, Jr., J. Chem. Phys., **70**, 2014 (1979).

231. D.G. Lister and P. Palmieri, J. Mol. Structure, **39**, 295 (1977).

232. A. Vijay and D.N. Sathyanarayana, J. Mol. Structure, **328**, 269 (1994).

233. J.D. Rogers, J. Quant. Spectrosc. Radiat. Transfer, **334**, 27 (1985).

234. K.B. Wiberg, V. Walters and S.D. Colson, J. Phys. Chem., **88**, 4723 (1984).

235. G. Dellepiane and J. Overend, Spectrochim. Acta, **22**, 593 (1966).

236. H.C. Urey and C.A. Bradley, Phys. Rev., **36**, 1969 (1931).

237. W.J. Tabor, J. Chem. Phys., **27**, 974 (1957).

238. K.B. Wiberg and K.E. Laidig, J. Am. Chem. Soc., **110**, 1872 (1988).

239. S. Scheiner, J. Mol. Structure, **177**, 79 (1988).

240. R.L. Redington, J. Mol. Spectrosc., **65**, 171 (1977).

241. A. Annamali and S. Singh, Can. J. Chem., **61**, 263 (1983).

242. J. Dybal and S. Krimm, J. Mol. Structure, **189**, 383 (1988).

243. J.E. Del Bene, in "Molecular Structure and Energetics, Vol. 1, Chemical Models" (editors J.F. Liebman and A. Greenberg), VCH, Deerfield Beach, Florida, 1986, pp. 319-349.

244. H.D. Mettee, J. Phys. Chem., **77**, 1762 (1973).

245. B.A. Wofford, M.E. Eliades, S.G. Lieb and J.W. Bevan, J. Phys. Chem., **87**, 5674 (1987).

246. S.L.A. Adebayo, A.C. Legon and D.J. Millen, J. Chem. Soc., Faraday Trans., **87**, 443 (1991).

247. S.N. Bhat and C.N.R. Rao, J. Am. Chem. Soc., **88**, 3216 (1996).

248. P. Klaboe, J. Am. Chem. Soc., **89**, 3667 (1967).

249. H.D. Mettee, J.E. Del Bene and S.I. Hauck, J. Phys. Chem., **86**, 5084 (1982).

250. G. Henderson, J. Chem. Educ., **64**, 88 (1987).

251. L. Turi, J. Phys. Chem., **100**, 11285 (1996).

252. D.A. Jaffe and N.J. Rose, Spectrochim. Acta, **47A**, 1695 (1991).